Novel functions of LUBAC-mediated M1 poly-ubiquitination in TNFR1-mediated necroptosis

Dissertation

zur Erlangung des Doktorgrades der Naturwissenschaften

vorgelegt beim Fachbereich 14 Biochemie, Chemie und Pharmazie

der Goethe-Universität

in Frankfurt am Main

von

Nadine Weinelt

aus Offenbach am Main

Frankfurt am Main, 2023

(D30)

Vom Fachbereich 14 der Goethe-Universität als Dissertation angenommen.

Dekan: Prof. Dr. Clemens Glaubitz, FB14

Gutachter 1: Prof. Dr. Volker Dötsch, FB14

Gutachter 2: Dr. rer. nat. habil. Sjoerd J.L. van Wijk, FB16

Datum der Disputation:

Table of Contents

List of Abbreviations

3D	3-dimensional
4HB	4-helical bundle
aa	Amino acid
ABC-DLBCL	Activated B-cell-like diffuse large B cell lymphoma
ABD	Antibody dilution buffer
ABIN	A20-binding inhibitor of NF-κB
ALIX	Programmed cell death 6-interacting protein (PDCD6IP)
ASC	Apoptosis-associated speck-like protein containing a CARD
ATG13	Autophagy-related protein 13
ATP	Adenosine triphosphate
AURKA	Aurora kinase A
BCA	Bicinchoninic acid
Bcl-2	B cell lymphoma-2
BE	BV6/Emricasan
BH3	Bcl-2 homology 3
BiE	Birinapant/Emricasan
BMDM	Bone marrow-derived macrophages
BME	Basement membrane extract
BMI	Body mass index
BMLS	Buchmann Institute for Molecular Life Sciences
BR	Brace region
BSA	Bovine serum albumine
BZ	BV6/zVAD.fmk
CARD	Caspase-recruitment domain
CCL20	Chemokine (C-C motif) ligand 20
CDC37	Cell division cycle 37
CHMP2A	Charged multivesicular body protein 2A
CHX	Cycloheximide
cIAP1/2	Cellular inhibitor of apoptosis 1 and 2
CK1	Casein kinase 1

CO1	Cytochrome oxidase subunit 1
CO_2	Carbon dioxide
COPS5	COP9 signalosome subunit 5
cpdm	Chronic proliferative dermatitis
CRISPR	Clustered regularly interspaced short palindromic repeats
CRISPRi	CRISPR interference
CSF2	Colony stimulating factor 2
Ctrl	Control
CXCL1	C-X-C motif ligand 1
CXCL10	C-X-C motif ligand 10
CXCL2	C-X-C motif ligand 2
CXCL8	C-X-C motif ligand 8
CYLD	Cylindromatosis
DAMP	Danger-associated molecular pattern
DAPI	4′,6-diamidino-2-phenylindole
DD	Death domain
DMEM	Dulbecco's Modified Eagle's medium
Dox	Doxycycline hydrochloride
DR	Death receptor
DUB	Deubiquitinating enzyme
ECL	Enhanced chemiluminescence
EDTA	Ethylenediaminetetraacetic acid
EGF	Epidermal growth factor
EGFR	EGF receptor
eGFP	Enhanced green-fluorescent protein
ER	Endoplasmic reticulum
ERK	Extracellular-signal-regulated kinase
ESCRT	Endosomal sorting complexes required for transport
FADD	Fas-associated death domain protein
FBS	Fetal bovine serum
FDA	Fluorescein diacetate
FGF	Fibroblast growth factor
FLOT1/2	Flotillin-1/2

GSK3β	Glycogen synthase kinase 3β
GSK'872	RIPK3 inhibitor
HECT	E6-associated protein (E6AP) C-terminus
HEK293T	Human embryonic kidney 293T cell line
HEPES	2-(4-(2-Hydroxyethyl)-1-piperazinyl)-ethansulfonsäure
HMGB1	High mobility group box protein 1
Hoe	Hoechst33342
HOIL-1	Heme-oxidized IRP2 ubiquitin ligase-1
HOIP	HOIL-1-interacting protein
hPOs	Human pancreatic organoids
HRP	Horseradish peroxidase
Hrs	Hepatocyte growth factor-regulated tyrosine kinase substrate
Hsp70	Heat-shock protein 70
Hsp90	Heat-shock protein 90
HT-29	Human colon adenocarcinoma cell line
IBD	Inflammatory bowel disease
ICAM1	Intercellular adhesion molecule 1
IFN	Interferon
IKKα	IκB kinase α
IKKβ	IκB kinase β
IL-1R	Interleukin-1 receptor
IRAK1	IL-1R-associated kinase 1
IRAK4	IL-1R-associated kinase 4
IRI	Ischemia-reperfusion injury
ISG15	Interferon-stimulated gene 15
ITCH	Itchy homolog
JAMM	JAB1/MPN/MOV34 metalloprotease
JNK	cJun NH2-terminal kinase
KD	Kinase domain
KO	Knockout
L-929	Murine fibroblast cell line
LDD	Linear ubiquitin chain determining domain
LDH	Lactate dehydrogenase

LPS	Lipopolysaccharide
LTM	LUBAC-tethering motif
LUBAC	Linear ubiquitin chain assembly complex
LUBEL	Linear ubiquitin E3 ligase
MACE	Massive analyses of cDNA ends
MAPK	Mitogen-activated protein kinase
MDP	Muramyl dipeptide
MEF	Mouse embryonic fibroblasts
MEM	Minimum essential medium
MINDY	Motif interacting with ubiquitin (MIU)-containing novel DUB family
MJD	Machado-Joseph Disease
MK2	MAPK-activated protein kinase-2
MLKL	Mixed lineage kinase domain-like
MST1	Mammalian ste20-like kinase 1
MyD88	Myeloid differentiation primary-response protein 88
N/A	Not applicable
NEAA	Non-essential amino acids
Nec-1s	Necrostatin-1s (RIPK1 inhibitor)
NEDD8	Neural precursor cell expressed, developmentally downregulated 8
NEMO	NF-κB essential modulator
NF-κB	Nuclear factor-κB
NFKBIA	NF-κB inhibitor alpha
nht	Non-human target
NLR	NOD-like receptor
NLRP3	Nucleotide-binding domain, leucine-rich–containing family, pyrin domain–containing-3
NOD2	Nucleotide-binding and oligomerization domain-containing protein 2
NSA	Necrosulfonamide (MLKL inhibitor)
NTD	N-terminal domain
NZF	Nuclear protein localization 4 (Npl4) zinc finger
OGT	*O*-Glc*N*Ac transferase
OPTN	Optineurin
ORAS	OTULIN-related autoinflammatory syndrome

OTU	Ovarian tumor
OTULIN	OTU DUB with linear linkage specificity
PACRG	Parkin-coregulated gene
PAM	Protospacer adjacent motif
PBS	Phosphate-buffered saline
PBS-T	PBS supplemented with Tween20
PCD	Programmed cell death
PFA	Paraformaldehyde
PI	Propidium iodide
PIM	PUB interaction motif
PIP	Phosphatidylinositol phosphate
poly(I:C)	Polycytidylic acid
Ppm1b	Protein phosphatase 1B
PS	Phosphatidylserine
PsKD	Pseudokinase domain
PTM	Post-translational modification
PUB	PNGase/UBA or UBX
qRT-PCR	Quantitative real-time reverse transcription PCR
RAW 264.7	Murine macrophage tumor cell line
RBR	RING-in-between-RING
RHIM	RIP homotypic interaction motif
RIG-I	Retinoic acid-inducible gene I
RING	Really interesting new gene
RIPK1	Receptor-interacting protein kinase 1
RIPK2	Receptor-interacting protein kinase 2
RIPK3	Receptor-interacting protein kinase 3
RPMI 1640	Roswell Park Memorial Institute medium
RSC	Receptor signaling complex
SDS	Sodium dodecyl sulfate
SDS-PAGE	SDS-polyacrylamide gel electrophoresis
Sharpin	Shank-associated RH domain interactor
siRNA	Small interfering RNA
SIRS	Systemic inflammatory respiratory syndrome

Smac	Second mitochondria-derived activator of caspases
SNX27	Sorting nexin 27
SOD1	Superoxide dismutase 1
SPATA2	Spermatogenesis-associated protein 2
SPFH	Stomatin, prohibitin, flotillin, HflK/C
STAM1	Signal-transducing adapter molecule 1
STAT1	Signal transducer and activator of transcription 1
STING	Stimulator of interferon genes
STR	Short tandem repeat
SUMO	Small ubiquitin-related modifier
TAB2	TAK1-binding protein 2
TAB3	TAK1-binding protein 3
TAK1	TGFβ-activated kinase 1
TAM	TYRO3, AXL, and MER receptor kinase
TB	TNFα/BV6
TBK1	TANK binding kinase 1
TBS-T	Tris-buffered saline supplemented with Tween20
TBZ	TNFα/BV6/zVAD.fmk
TCR	T-cell receptor
TDP-43	TAR DNA-binding protein 43
TGFβ	Transforming growth factor β
THP-1	Human acute monocytic leukemia cell line
TLR	Toll-like receptor
TNFα	Tumor necrosis factor α
TNFAIP3	Tumor necrosis factor alpha-induced protein 3 (A20)
TNFR1	TNF receptor 1
TNFR2	TNF receptor 2
TNFR-SF	TNFR superfamily
TRADD	TNF receptor-associated death domain
TRAF2/5	TNF receptor-associated factor 2/5
TRAIL	TNF-related apoptosis-inducing ligand
TRIF	Toll/IL-1 receptor (TIR) domain-containing adaptor inducing IFN-β
Trx1	Thioredoxin-1

TSG101	Tumor susceptibility gene 101
Ub	Ubiquitin
UBA	Ubiquitin-associated
UBAN	Ubiquitin-binding in ABIN and NEMO
UBD	Ubiquitin binding domain
Ubl	Ubiquitin-like
UCH	Ubiquitin C-terminal hydrolase
UEV	Ubiquitin-conjugating enzyme E2 variant
UIM	Ubiquitin-interacting motif
USP	Ubiquitin-specific protease
UT	Untreated
VCP	p97/valosin-containing protein
VHS	Vps27/Hrs/Stam
VPS4	Vacuolar protein sorting 4
WT	Wildtype
ZBP1	Z-DNA binding protein 1
ZnF	Zinc finger
ZUP1	Zinc finger-containing ubiquitin peptidase 1
zVAD.fmk	Carbobenzoxy-valyl-alanyl-aspartyl-[O-methyl]-fluoromethylketone

List of Figures

List of Tables

1 Abstract

Necroptosis is an immunogenic form of programmed cell death characterized by plasma membrane accumulation of activated mixed lineage kinase domain-like (MLKL) that eventually leads to membrane disruption and release of danger-associated molecular patterns (DAMPs). Necroptotic cell death is tightly controlled by checkpoints, including compartmentalization as well as post-translational modifications (PTMs), like phosphorylation and ubiquitination of receptor-interacting protein kinase (RIPK) 1, RIPK3 and MLKL. Removal of plasma membrane-located activated MLKL via endocytosis or exocytosis can counteract necroptosis, but up till now, the exact mechanisms by which necroptosis is regulated downstream of MLKL activation and oligomerization are not fully understood.

Ubiquitination is a key post-translational modification that regulates various cellular processes including cell survival and cell death signaling via ubiquitination of RIPK1, RIPK3 and MLKL. M1-linked (linear) poly-ubiquitination is mediated exclusively by the linear ubiquitin chain assembly complex (LUBAC) which critically regulates cell fate and immune signaling via death receptors such as TNF receptor 1 (TNFR1).

In this study, we demonstrate that M1 poly-Ubiquitin (poly-Ub) increases during necroptosis which can be blocked by inhibition of LUBAC activity with the small-molecule HOIL-1-interacting protein (HOIP) inhibitor HOIPIN-8 or by loss of LUBAC catalytic subunit HOIP. Intriguingly, HOIPIN-8, as well as the HOIP inhibitor gliotoxin, and HOIP knockdown effectively prevent TNFα/smac mimetic/zVAD.fmk-induced necroptotic cell death in cells of human origin, without affecting necroptotic RIPK1 and RIPK3 phosphorylation, necrosome formation and oligomerization of phosphorylated MLKL. We demonstrate that HOIPIN-8 treatment inhibits MLKL translocation to intracellular membranes and accumulation in plasma membrane hotspots as well as MLKL exocytosis. We further confirm that HOIPIN-8 treatment suppresses necroptotic cell death in primary human pancreatic organoids (hPOs). Using time-lapse imaging and live/dead staining, we demonstrate loss of organoid structure and hPO cell death induced by smac mimetics and caspase inhibitors, thus providing a novel platform to investigate necroptosis in near physiological settings. Inhibition of LUBAC activity with HOIPIN-8 prevents hPO collapse and extends cell viability. Of note, loss of the M1 Ub-

targeting deubiquitinating enzymes (DUBs) OTU DUB with linear linkage specificity (OTULIN) and cylindromatosis (CYLD) in human cell lines does not affect necroptosis induction and HOIPIN-8-mediated rescue of necroptosis. Intriguingly, inhibition of LUBAC activity with HOIPIN-8 does not block necroptotic cell death in murine cell lines.

Using massive analyses of cDNA ends (MACE)-seq-based global transcriptome analysis we confirm that necroptosis induces a pro-inflammatory cytokine profile which is dependent on LUBAC function and necroptotic signaling. Loss of LUBAC activity prevents the MLKL-dependent production and release of pro-inflammatory cytokines and chemokines.

Finally, we identify Flotillin-1 and -2 (FLOT1/2) as putative targets of necroptosis-induced M1 poly-Ub. Ubiquitin-binding in ABIN and NEMO (UBAN)-based pulldowns of M1 poly-ubiquitinated proteins revealed enrichment of FLOTs after necroptosis induction which is dependent on LUBAC activity and can be blocked with necroptosis inhibitors Nec-1s, GSK'872 and NSA, targeting RIPK1, RIPK3 and MLKL, respectively. Of note, loss of FLOT1/2 potentiates necroptosis suppression induced by LUBAC inhibition with HOIPIN-8.

Together, these findings identify LUBAC-mediated M1 poly-Ub as an important mediator of necroptosis and identify FLOTs as novel putative targets of LUBAC-mediated M1 poly-Ub during necroptosis. In addition, by modeling necroptosis in primary human organoids, we further expand the spectrum of experimental models to study necroptosis in human cellular settings.

2 Introduction

2.1 TNFR1-mediated signaling

Tumor necrosis factor α (TNFα) is a master pro-inflammatory cytokine which plays major roles in immunologic processes such as infection and autoimmunity by controlling innate immune responses through TNF receptor 1 (TNFR1)-mediated production of pro-inflammatory cytokines and chemokines as well as regulation of cell death [1]. The death receptor (DR) TNFR1 is ubiquitously expressed on most cell types and belongs to the TNFR superfamily (TNFR-SF) of innate immune receptors that comprises 29 receptors, including TNFR2 (TNFRSF1B), whose expression is restricted to certain cell types such as myeloid cells and T-and B-cell subsets, CD40, TNF-related apoptosis-inducing ligand receptor 1 (TRAIL-R1) (DR4,TNFRSF10A), TRAIL-R2 (DR5, TNFRSF10B) and FAS [2]. In general, TNFR1-mediated signaling underlies cell survival, activation of extrinsic apoptosis or necroptosis (Figure 1). Activation of TNFR1 by TNFα does not lead to programmed cell death (PCD) in most cell lines but induces pro-survival and pro-inflammatory signaling, and PCD is only triggered when these signaling events are suppressed [3].

2.1.1 TNFR1-mediated pro-survival NF-κB signaling

Upon activation of TNFR1, a receptor signaling complex (RSC), termed complex I, composed of TNF receptor-associated death domain (TRADD), receptor-interacting protein kinase 1 (RIPK1) and TNF receptor-associated factor 2/5 (TRAF2/5) forms and recruits the E3 ubiquitin (Ub) ligases cellular inhibitor of apoptosis 1/2 (cIAP1/2) [4-6] which mediate K63, K48 and K11-linked ubiquitination of TNFR1 complex-associated proteins [7-12]. These ubiquitination events are a prerequisite for the recruitment of the linear ubiquitin chain assembly complex (LUBAC) which mediates M1-linked ubiquitination of receptor-associated proteins, including RIPK1, and pre-existing K63 Ub chains, thereby stabilizing the TNFR1 complex I [6, 12, 13]. K63 and M1 poly-Ubiquitin (poly-Ub) chains facilitate the recruitment of the transforming growth factor β (TGFβ)-activated kinase 1 (TAK1) complex via TAK1-binding protein 2 (TAB2) and TAB3 as well as the IκB kinase α (IKKα)/IKKβ complex via nuclear factor-κB (NF-κB) essential modulator (NEMO) [14-17]. Activated TAK1 triggers mitogen-activated protein

kinase (MAPK) signaling via cJun NH_2-terminal kinases (JNKs), extracellular-signal-regulated kinases (ERKs) and p38 MAPK [18]. TAK1-mediated phosphorylation of IKKβ and subsequent *trans*-phosphorylation of IKKα/IKKβ results in IKKβ-mediated phosphorylation of the NF-κB inhibitor IκBα [19]. Following phosphorylation, IκBα is ubiquitinated and targeted for proteasomal degradation which leads to the release and translocation of NF-κB to the nucleus, where it mediates transcription of NF-κB target genes [20] (Figure 1).

2.1.2 TNFR1-mediated apoptosis

Apoptosis can be initiated via the intrinsic pathway in response to cellular stress stimuli or via activation of DRs such as TNFR1, FAS and TRAIL-R1/2 (extrinsic apoptosis), all of which ultimately lead to the activation of effector caspases that mediate apoptosis execution [4, 21-24]. Activation of TNFR1 by TNFα results in pro-survival signaling via TNFR1 complex I, however, upon cIAP1/2 depletion, TNFR1-mediated signaling can switch to apoptosis via formation of the cytosolic complex IIa, consisting of TRADD, the adaptor protein Fas-associated death domain protein (FADD), and caspase-8 [25-27] or via complex IIb which comprises RIPK1, RIPK3, FADD and caspase-8 [27-30] (Figure 1). Activation of caspase-8 mediates cleavage and thus activation of effector caspases-3 and -7 which induce apoptotic cell death [31].

Apoptosis plays an important role during embryogenesis and in maintaining tissue homeostasis as it regulates clearance of damaged cells in a highly coordinated manner [32-34]. Accordingly, dysregulation of apoptosis is involved in various diseases including cancer and neurodegenerative diseases [32-38].

2.2 Necroptosis

Necroptosis is a form of regulated necrosis, characterized by plasma membrane perforation, ultimately leading to the release of danger-associated molecular patterns (DAMPs) and cytokines to elicit a robust immune response [39, 40]. This is in contrast to apoptosis which was generally considered to be an immunologically inert form of programmed cell death since apoptosis results in the formation of ‘apoptotic bodies’ that contain cellular contents and are regularly engulfed by phagocytes, thus allowing no or only limited release of DAMPs [40]. Apart from necroptosis, other types of regulated necrosis have been described, such as pyroptosis, ferroptosis,

NETosis/ETosis and parthanatos, which employ distinct signaling pathways, however, the necroptosis pathway is one of the best-studied PCD pathways [39]. Necroptosis can be induced by a variety of stimuli that induce signaling cascades ultimately leading to activation of the so-called necrosome, an amyloid-like structure consisting of RIP homotypic interaction motif (RHIM) domain-containing proteins RIPK1, RIPK3 and the necroptosis executor mixed lineage kinase domain-like (MLKL) [41-43] (Figure 1).

Pathways leading to necroptotic cell death include activation of the TNFR-SF DRs TNFR1 by its ligand TNFα [44], FAS by FASL [45, 46] or TRAIL-R1/2 by TRAIL [46-48]. Necroptosis can also occur during infection or cellular stress through stimulation of cytosolic nucleic acid sensors, such as retinoic acid-inducible gene I (RIG-I)-like receptors (RGRs) and stimulator of interferon genes (STING), that activate type I interferon (IFN) and TNFα production thereby creating feedback loops that promote necroptosis [49-51], or via Toll-like receptors (TLRs) [52-54]. Activation of TLR3 by polycytidylic acid (poly(I:C)) or TLR4 by lipopolysaccharide (LPS) can result in formation of the necrosome when caspases are blocked, through interactions of Toll/IL-1 receptor (TIR) domain-containing adaptor inducing IFN-β (TRIF) with RIPK1 and RIPK3 via their RHIM domains [52, 53]. Similarly, the RHIM-domain-containing Z-DNA binding protein 1 (ZBP1; DAI), a cytosolic sensor of double-stranded DNA, can recruit RIPK3, via RHIM/RHIM interactions, and MLKL to induce necroptosis [51, 55, 56].

Necrosome formation and necroptosis induction can be modelled *in vitro* through stimulation of RIPK3- and MLKL-expressing cells with a combination treatment of TNFα, second mitochondria-derived activator of caspases (smac) mimetics, which block cIAP1/2, and pan-caspase inhibitors such as zVAD.fmk (carbobenzoxy-valyl-alanyl-aspartyl-[O-methyl]-fluoromethylketone) (Figure 1) or by treatment of the cells with TNFα, zVAD.fmk and the protein synthesis inhibitor cycloheximide (CHX) [39, 43, 57].

2.2.1 The role of necroptosis in diseases

Necroptotic cell death results in the release of DAMPs and inflammatory cytokines which elicit a potent inflammatory response [39, 58, 59]. By doing so, necroptosis plays a role in various inflammatory diseases such as ischemia-reperfusion injury (IRI) [60], systemic inflammatory respiratory syndrome (SIRS) [61, 62] and hepatitis [63].

Increased expression of RIPK3 and MLKL have been reported in inflammatory bowel disease IBD [64] and multiple sclerosis [65], whereas downregulation of these proteins was described in several types of cancer including ovarian cancer [66], gastric cancer [67], cervical squamous cell carcinoma [68], colon carcinoma [69] as well as acute myeloid and chronic lymphocytic leukemia [69, 70]. Since apoptosis resistance is a hallmark of cancer, therapeutic approaches that exploit necroptosis and its immunogenic properties may be beneficial in anti-tumor therapy by activating the antitumor response and thus eliminating apoptosis-resistant tumor cells [71, 72].

2.2.2 The necroptotic core machinery: RIPK1, RIPK3 and MLKL

TNFα-mediated necroptosis is induced upon destabilization of TNFR1 complex I, via deubiquitinating enzyme (DUB) cylindromatosis (CYLD)-mediated removal of K63 Ub chains from complex I proteins, including RIPK1, or via cIAP1/2 depletion [73-77], when caspase-8 activity is reduced or blocked, which leads to activation of RIPK1 and formation of the necrosome [78, 79]. RIPK1 has a pivotal role in the regulation of cell fate as it interacts with complex I members such as TNFR1 and TRADD via their death domains (DD) and serves as a molecular signaling platform during pro-survival signaling thereby enabling NF-κB and MAPK signaling [80-85], but also mediates apoptotic and necroptotic cell death through its catalytic activity [86, 87]. During TNFR1-mediated pro-survival signaling, RIPK1 is targeted by cIAP1/2 [8, 10, 11] and LUBAC [12, 88, 89] that mediate the formation of K63 and M1 Ub chains which are targeted by CYLD [73-75] and the M1 Ub-binding protein A20 (TNFAIP3) [73, 90, 91]. Upon depletion of cIAPs, human RIPK1 undergoes autophosphorylation at S14/S15, S20, S161 and S166 (S14/S15, S161, S166 and T169 in murine RIPK1) [43, 84, 86, 87, 92] leading to its activation. Phosphorylation of RIPK1 S161 is a prerequisite for the recruitment of RIPK3 [87]. Both RIPK1 and RIPK3 contain an N-terminal kinase domain (KD) [93, 94] which mediates auto- and transphosphorylation, and a RHIM domain, responsible for RIPK1-RIPK3 interactions [39, 43, 57, 95] and the formation of hetero-oligomeric amyloid-like necrosomes [41-43, 57, 96]. Phosphorylation of human RIPK3 at S227 (T231/S232 in murine RIPK3) and subsequent RHIM-dependent oligomerization results in the recruitment and phosphorylation of MLKL [97-100].

MLKL is composed of an N-terminal 4-helical bundle (4HB) domain, responsible for the killing activity of MLKL [101-105], an auto-inhibitory brace region (BR) containing two α-helices [106] and the C-terminal pseudokinase domain (PsKD) with an activation loop that contains the phosphorylation sites T357 and S358 (in human MLKL; S345, S347, and T349 in murine MLKL) [101-105]. RIPK3-mediated phosphorylation of dormant MLKL induces a conformational change of the PsKD resulting in the exposure of the 4HB domain and release from RIPK3 [101, 107, 108]. Interestingly, activation of murine MLKL seems to only require a transient interaction with RIPK3 for full activation [109], while in humans a more stable complex between the RIPK3 KD and MLKL PsKD is required [79, 98, 110, 111]. In addition, several studies revealed that murine and human MLKL are not able to complement necroptotic signaling when expressed in the cells of the opposing species, thus confirming fundamental specific-specific differences in the activation modes of human and murine MLKL and highlighting functional and mechanistic differences in human and murine necroptotic signaling pathways [79, 104, 110, 112]. Activation and 4HB exposure trigger MLKL oligomerization and mediate MLKL plasma membrane recruitment via interaction of MLKL with phosphatidylinositol phosphates (PIPs) or interaction with cardiolipin [105, 113]. MLKL is considered the most downstream effector molecule responsible for execution of necroptosis. However, the exact mechanisms that lead to necroptotic cell death remain under debate. Upon activation, phosphorylated murine MLKL oligomerizes into trimers [101, 114] while human MLKL forms tetramers [110]. Additional higher order structures, including hexamers [102], octamers [115] and amyloid-like polymers [116], have been described for MLKL as well. Oligomeric MLKL forms hotspots at the plasma membrane and induces pore formation, thereby compromising cellular integrity [102, 105, 117]. Additionally, plasma membrane-located MLKL has been shown to induce Ca^{2+} and Na^{+} influx via ion channels, leading to a rise of cytosolic cation levels [103, 118]. MLKL-mediated plasma membrane disruption ultimately results in cell swelling and release of intracellular contents, including DAMPs, such as high mobility group box protein 1 (HMGB1), ATP and lactate dehydrogenase (LDH) [119-122], that trigger a robust immune response by recruiting phagocytes and other immune cells [39]. Intriguingly, recent studies revealed that the necroptosis-dependent pro-inflammatory response is not solely a result of the passive release of DAMPs, but is mediated by a cell-intrinsic pathway that includes both NF-κB- and necroptosis-dependent signaling [59]. Necroptotic signaling induces NF-κB- and MLKL-dependent transcription and release

of cytokines and chemokines, such as C-X-C motif ligand 1 (CXCL1), CXCL10, CXCL2 and colony stimulating factor 2 (CSF2), in a cell-autonomous manner, thereby promoting inflammation [59, 123].

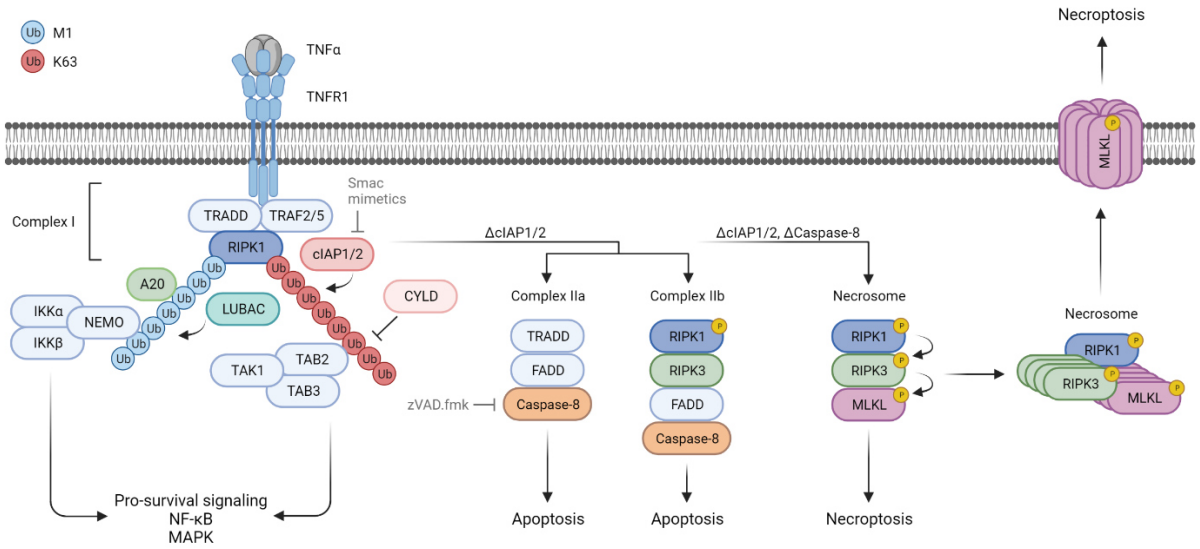

Figure 1. Schematic overview of TNFR1-mediated signaling.

Activation of tumor necrosis factor receptor 1 (TNFR1) by TNFα results in the formation of the TNFR complex I consisting of TNF receptor-associated death domain (TRADD), receptor-interacting protein kinase 1 (RIPK1) and TNF receptor-associated factor 2/5 (TRAF2/5), and subsequent recruitment of the E3 Ub ligases cellular inhibitor of apoptosis 1/2 (cIAP1/2) which mediate K63-linked poly-ubiquitination of RIPK1 and TNFR1-associated proteins (not shown). K63 ubiquitination of complex I components results in the recruitment of the linear ubiquitin chain assembly complex (LUBAC) which induces M1-linked poly-ubiquitination of RIPK1 and TNFR1-associated proteins (not shown). Following these ubiquitination events, transforming growth factor β (TGFβ)-activated kinase 1 (TAK1) complex is recruited via TAK1-binding protein 2 (TAB2) and TAB3-mediated binding to K63 poly Ub, and IκB kinase α (IKKα)/IKKβ complex via nuclear factor-κB (NF-κB) essential modulator (NEMO)-mediated binding to M1 poly-Ub, leading to activation of pro-survival signaling via mitogen-activated protein kinase (MAPK) and NF-κB activation. Depletion of cIAPs (for example via smac mimetic-induced inhibition of cIAPs) and cylindromatosis (CYLD)-mediated removal of K63 Ub result in destabilization of complex I and formation of the cytosolic complex IIa, consisting of TRADD, Fas-associated death domain protein (FADD), and caspase-8, or complex IIb, composed of activated RIPK1, RIPK3, FADD and caspase-8, which induce caspase-dependent apoptosis. The necrosome forms upon depletion of cIAPs and concomitant inhibition of caspase-8 (for example with zVAD.fmk). Activated RIPK1 recruits RIPK3, resulting in auto- and transphosphorylation of RIPK1 and RIPK3 and subsequent RIPK3 oligomerization followed by recruitment of MLKL. RIPK3-mediated phosphorylation of MLKL leads to MLKL oligomerization, plasma membrane translocation and ultimately necroptotic cell death. Created with BioRender.com.

2.2.3 Regulation of necroptosis

Necroptosis is controlled by various checkpoints that comprise compartmentalization and post-translational modifications (PTMs), including phosphorylation and ubiquitination, of the necroptotic key players RIPK1, RIPK3 and MLKL [124-126].

2.2.3.1 Post-translational modifications of RIPK1 and RIPK3

The ubiquitination and phosphorylation status of RIPK1 determines whether RIPK1 serves pro-survival scaffolding functions or pro-death functions [78] (see section 2.2.2). In addition to the cIAPs- and LUBAC-mediated ubiquitination, K11- and K48-linked poly-Ub formation have been described to negatively regulate RIPK1-mediated cell death through both non-degradative and degradative functions [11, 127-130]. In contrast, ubiquitination of human RIPK1 at K627 [131], as well as c-Cbl-mediated- [132] and Pellino1 (PELI1)-mediated K63 ubiquitination of RIPK1 [133, 134] have been recently described to promote necroptosis. Ubiquitination of RIPK1 is further regulated by the DUBs CYLD [73-75] and presumably OTU DUB with linear linkage specificity (OTULIN) [88], while A20 prevents removal of M1 poly-Ub likely by binding to M1 poly-Ub on RIPK1 [73, 91]. RIPK1 kinase activity and its death-inducing function is controlled by inhibitory phosphorylation of RIPK1 via kinases such as MAPK-activated protein kinase-2 (MK2) [135-137], IκB kinase α/β (IKKα/β) [92, 138], TAK1 [139], TANK binding kinase 1 (TBK1) and IKKε [140, 141].

The execution of necroptosis is controlled by extensive modification of RIPK3 with different types of poly-Ub that regulate the RIPK1-RIPK3 interaction, necrosome formation and RIPK3 kinase activity [124, 125]. Cytosolic RIPK3 levels are regulated by K48-linked poly-ubiquitination at K55, K89, K363 and K501 by carboxy terminus of HSC70-interacting protein (CHIP), leading to lysosomal degradation [128], and at K363 by PELI1 which results in proteasomal degradation [142]. Necrosome formation is negatively regulated by Parkin-mediated K33-linked ubiquitination of RIPK3 at K197, K302 and K364 [143] and the tripartite motif E3 ligase TRIM25 has been described to ubiquitinate RIPK3 at K501, thereby inhibiting TNFα-induced necroptosis [144]. In addition, A20 suppresses RIPK1-RIPK3 interactions by removing K63 poly-Ub from RIPK3 at K5 [145] and the DUB USP22 has recently been reported to target necroptosis-induced RIPK3 poly-Ub at K42, K351 and K518, of which K518 has been shown to modulate RIPK3 ubiquitination status, necrosome formation and MLKL

phosphorylation [146]. Phosphorylation of RIPK3 at S227 by members of the casein kinase 1 (CK1) family, which are recruited to the necrosome, promotes necroptosis [147, 148] and this is counteracted by protein phosphatase 1B (Ppm1b) [149]. Recently, *O*-Glc*N*Ac transferase (OGT)-mediated *O*-Glc*N*Acylation of RIPK3 at T476 has been identified which results in inhibition of homotypic interaction via the RHIM domain [150]. Besides these PTMs, RIPK1-RIPK3 interactions and necrosome formation is also controlled by RIPK3-interacting proteins such as Aurora kinase A (AURKA), glycogen synthase kinase 3β (GSK3β) [151], MYC [152], and heat-shock protein 90 (Hsp90)-cell division cycle 37 (CDC37) complex [153].

2.2.3.2 Post-translational modifications and regulatory mechanisms of MLKL

Besides the beforementioned early checkpoints that regulate RIPK1 and RIPK3 activation, several regulatory mechanisms that directly target MLKL have been reported recently. Under basal conditions, MLKL has been shown to interact with TRAF2 which inhibits recruitment of MLKL to the necrosome and RIPK3-mediated MLKL phosphorylation [154]. In the necrosome, MLKL activation is counteracted by the anti-apoptotic protein B cell lymphoma-2 (Bcl-2) which interacts with MLKL via a Bcl-2 homology 3 (BH3)-like motif located at K165 to K177 in MLKL, thereby reducing MLKL phosphorylation and oligomerization [155]. RIPK3-mediated phosphorylation of MLKL at T357 and S358 and subsequent exposure of the MLKL 4HB domain drives MLKL oligomerization, however, several MLKL-interacting proteins have been described recently that modulate oligomerization downstream of MLKL activation. The autophagic core protein Beclin 1 reportedly interacts with the 4HB domain of phosphorylated MLKL in the necrosome and regulates MLKL oligomerization without affecting necrosome formation [156]. In addition, TYRO3, AXL, and MER receptor (TAM) kinases promote MLKL oligomerization by phosphorylating MLKL at Y376 [157]. Importantly, loss of these kinases did not alter phosphorylation of RIPK1, RIPK3 and MLKL at S358, indicating that TAM-mediated MLKL phosphorylation regulates necroptosis downstream of MLKL activation [157]. MLKL oligomerization is further controlled by the molecular chaperones heat shock protein 90 (Hsp90) [158, 159] and Hsp70 [160] which interact with MLKL to promote assembly of MLKL into high molecular weight complexes, plasma membrane localization and induction of necroptotic cell death.

Ubiquitination of MLKL and its relevance for necroptosis has been elucidated only recently and the functional relevance for the control of MLKL killing potential remains a matter of debate. Murine MLKL undergoes ubiquitination at K51, K77, K172 and K219 which is dependent on the kinase activity of RIPK1 and RIPK3 and occurs during the onset of necroptosis prior to MLKL oligomerization and membrane translocation [161]. Of the four Ub acceptor sites, K219, which is conserved in human MLKL (K230), plays a particular role in necroptosis as it keeps MLKL in an inactive state via binding to MLKL Q343, and becomes K63-ubiquitinated during necroptosis upon phosphorylation of MLKL, thereby boosting the cytotoxic potential of MLKL [161]. In contrast, another study points towards a model where necroptosis-mediated ubiquitination of murine MLKL K9, K51, K69 and K77 occurs at the plasma membrane, following MLKL activation and oligomerization, and regulates MLKL proteasome- and lysosome-dependent turnover, thus antagonizing necroptosis [162]. Necroptosis-dependent K63 ubiquitination of MLKL was confirmed in yet another study which identified the E3 Ub ligase itchy homolog (ITCH)-mediated K50/K51 ubiquitinated MLKL to be targeted to endosomal membranes followed by release of MLKL within exosomes (see also section 2.2.3.3) [163]. Intriguingly, MLKL K50/K51 poly-Ub correlated with the lysosome-mediated clearance of intracellular bacteria [163], consistent with previous findings demonstrating MLKL-dependent suppression of intracellular *Listeria* replication [164].

2.2.3.3 Regulation of necroptosis by compartmentalization of MLKL

Formation of oligomerized MLKL hotspots at the plasma membrane is considered the final step of necroptosis, ultimately leading to loss of membrane integrity and cell death. However, prior to plasma membrane disruption, MLKL associates with internal cell membranes including those of the endoplasmic reticulum (ER), mitochondria [102], endosomes [165], (autophago)lysosomes [54, 102, 166, 167], nucleus [168, 169] as well as exosomes [123, 165, 166, 170], followed by translocation to the plasma membrane via trafficking events likely involving the Golgi, microtubule and actin machinery [117]. Although the proteins that are involved in MLKL trafficking have not been identified yet, several studies demonstrated that mutations in the 4HB domain of MLKL prevent MLKL plasma membrane translocation, suggesting that the 4HB domain acts as an interaction site for auxiliary proteins that mediate trafficking [101, 110, 171]. Intriguingly, plasma membrane association of MLKL already occurs before cell lysis

[102, 103, 115, 117, 118, 123, 166] and progression of necroptotic plasma membrane disruption correlates with increasing amount of MLKL located at the plasma membrane, indicating that a certain lytic threshold has to be surpassed to induce cell death [117, 172]. MLKL assembly into higher molecular structures, termed MLKL hotspots, preferentially occurs at intercellular junctions, where MLKL colocalizes with tight junction proteins [117].

Membrane hotspot formation of MLKL is considered the final regulatory checkpoint in necroptosis, however, subthreshold amounts of MLKL residing in the plasma membrane can be removed via endocytosis [166] or via release of MLKL in exosomes [163, 165, 166, 170]. Exocytosis of MLKL is mediated by endosomal sorting complexes required for transport (ESCRT) and ESCRT-associated proteins such as ALIX (PDCD6IP, programmed cell death 6-interacting protein), syntenin-1 and/or Rab27 [165, 166, 173]. Moreover, ESCRT-III has been recently implicated in the repair of the plasma membrane after necroptosis induction [123]. Following MLKL plasma membrane translocation, cells have been shown to expose phosphatidylserine (PS) [117, 123, 170, 174] spatially correlating with MLKL accumulation and the appearance of ESCRT-III-induced plasma membrane bubbles [123]. Subsequent ESCRT-III-mediated shedding of damaged plasma membrane leads to cellular resuscitation [123].

Interestingly, necroptosis-induced exosomes contain phosphorylated MLKL along with ESCRT proteins and flotillin-1 and -2 (FLOT1/2) [165], and FLOTs have been reported to interact with MLKL upon necroptosis induction [166]. FLOTs are lipid raft-residing proteins that associate with the inner leaflet of intracellular membranes, including the plasma membrane, the ER, the Golgi apparatus and endocytic compartments [175, 176] and MLKL has been reported to localize to lipid rafts as well [103]. Lipid rafts, also known as microdomains, are highly ordered membrane structures that are enriched in sphingolipids, cholesterol and gangliosides [177, 178]. FLOTs interact with cholesterol-rich membrane domains via their N-terminal stomatin, prohibitin, flotillin, HflK/C (SPFH) domain and oligomerize to hetero-tetramers through the C-terminal flotillin domain, thereby creating FLOT platforms [179, 180]. Importantly, FLOTs play a role in the establishment of protein complexes at the plasma membrane [181, 182], and also control cytoskeleton-membrane interactions [183-185], cell-cell contacts [186, 187] as well as clathrin-independent endocytosis [188, 189] and generation of exosomes [190]. Intriguingly, in addition to the release of MLKL via exosomes, FLOT1/2-mediated

lysosomal degradation of MLKL has been proposed to regulate MLKL plasma membrane abundance [166].

The abovementioned mechanisms control MLKL abundance at the plasma membrane and highlight the role of compartmentalization events in necroptosis execution. Although the exact mechanisms of necroptosis regulation downstream of MLKL activation still need further investigation, these data demonstrate that translocation of activated MLKL to the plasma membranes is not a “point of no return” for cell survival [123, 172].

2.3 The Ubiquitin code

2.3.1 Ubiquitination

Ubiquitination, like other PTMs, serves important roles in the regulation of cellular signaling processes [191]. Ub is an evolutionary highly conserved 8.5 kDa protein of 76 amino acids, encoded by the four genes *UBB*, *UBC*, *UBA52* and *UBA80* [192-194], which can be covalently attached to substrates and assembled into distinct chain types by an enzymatic cascade that involves E1 Ub-activating enzymes [195], E2 Ub-conjugating enzymes [196] and E3 Ub ligases [197]. The Ub protein itself adopts a globular structure with compact β-grasp fold and a flexible C-terminus [198]. Recognition of Ub by Ub binding domains (UBDs) is mediated through its hydrophobic surfaces, via the I44 patch (consisting of L8, I44, H68 and V70) [199], the I36 patch (consisting of I36, L71 and L73) [200-202], the F4 patch (consisting of Q2, F4 and T14) [14, 202, 203] or the TEK box (consisting of T12, T14, E34, K6, K11) [204] (Figure 2A).

The ubiquitination process is initiated by the E1 enzyme which activates the Ub in an ATP-dependent manner by adenylation of the Ub C-terminus resulting in the formation of a highly reactive E1-Ub thioester. The activated Ub moiety is then transferred to the active site cysteine of an E2 enzyme which is subsequently recruited by an E3 ligase that catalyzes the isopeptide bond of the Ub C-terminus with a lysine residue of the target protein [205]. E3 ligases are divided into three groups which differ in their mechanism of action. The really interesting new gene (RING)-type E3 ligases mediate Ub transfer by bringing the Ub-loaded E2 enzyme in close proximity to the target residue of the substrate protein. In contrast, E6-associated protein (E6AP) C-terminus (HECT)-type and RING-in-between-RING (RBR)-type E3 ligases catalyze a two-step

reaction in which the activated Ub is transferred to the active site cysteine on the E3 ligase and subsequently to the substrate [197] (Figure 2B).

Modification of a protein with Ub can result in mono- or multi-monoubiquitination and can generate homotypic Ub chains, heterotypic (mixed) Ub chains and branched Ub chains [191] (Figure 2C). The Ub code relies on the seven lysine residues K6, K11, K27, K29, K33, K48 and K63, and the N-terminal M1 residue which serve as attachment sites for Ub chain assembly to generate the eight different homotypic Ub chain types [191, 206] (Figure 2C-D). The Ub linkage type determines the structure and conformation of the Ub chain resulting in distinct functions and outcomes in the cell. In addition, crosstalk between the Ub system and ubiquitin-like (Ubl) modifiers like small ubiquitin-related modifier (SUMO) [207], interferon-stimulated gene 15 (ISG15) [208] or neural precursor cell expressed, developmentally downregulated 8 (NEDD8) [209] can result in Ub/Ubl hybrid chains [210, 211] and Ub itself can be modified by PTMs including acylation [212], ribosylation [213-215] and phosphorylation [216-218], making the Ub code even more complex (Figure 2C).

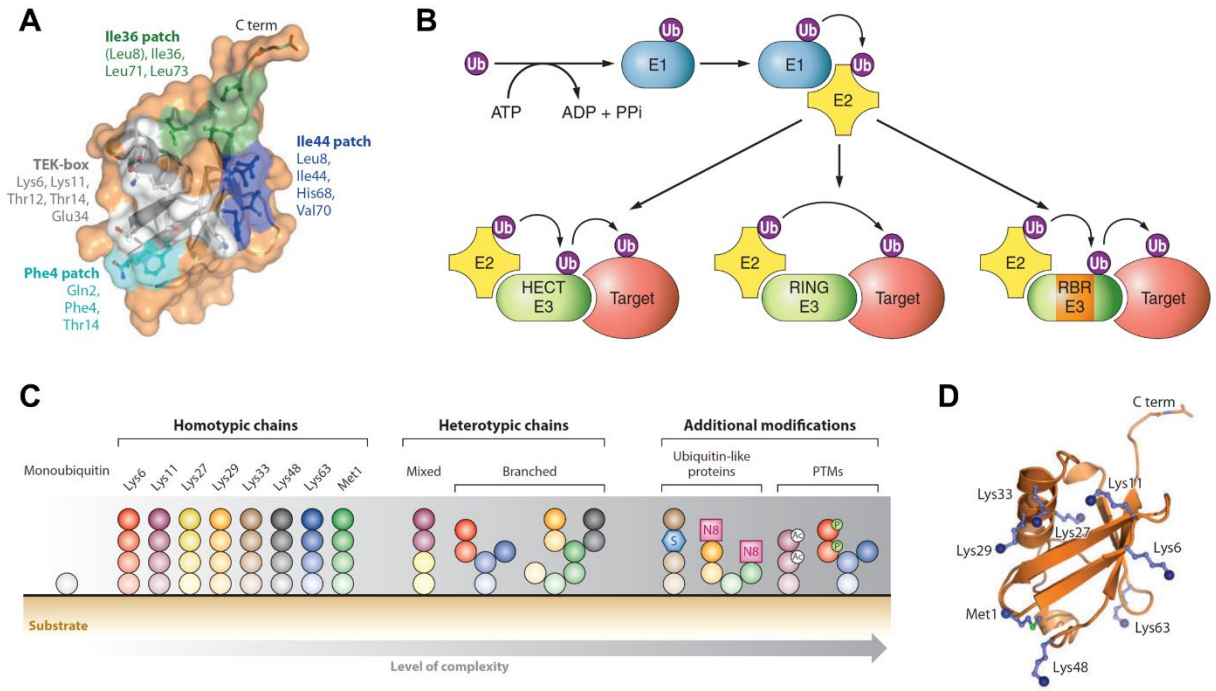

Figure 2. The complexity of the ubiquitin code.

A Recognition of the Ub surface by UBDs is mediated through the hydrophobic I44 patch (consisting of L8, I44, H68 and V70), I36 patch (consisting of I36, L71 and L73), F4 patch (consisting of Q2, F4 and T14) and TEK box (consisting of T12, T14, E34, K6, K11) of Ub. Adapted from [191]. **B** Ubiquitination is initiated by an E1 Ub-activating enzyme which, under consumption of one ATP molecule, mediates the

Figure 2. Continued.

transfer of the activated Ub to the E2 Ub-conjugating enzyme. The three groups of E3 Ub ligase comprise the really interesting new gene (RING)-type E3 ligases, the E6-associated protein (E6AP) C-terminus (HECT)-type and the RING-in-between-RING (RBR)-type E3 ligases. RING-type E3 ligases mediate Ub transfer by bringing the Ub-loaded E2 enzyme in close proximity to the target residue of the substrate protein, while HECT and RBR E3 ligases catalyze a two-step reaction by transferring the activated Ub to the E3 ligase active site cysteine and subsequently to the substrate. Adapted from [219]. **C** Ub modification can result in mono-ubiquitination, generation of homotypic or heterotypic Ub chains (e.g. mixed or branched chains). Ub chains can be further modified by PTMs such as acylation, ribosylation or phosphorylation and through integration of ubiquitin-like (Ubl) modifiers like small ubiquitin-related modifier (SUMO), interferon-stimulated gene 15 (ISG15) or neural precursor cell expressed, developmentally downregulated 8 (NEDD8). Adapted from [191]. **D** Structure of Ub showing the seven lysine residues K6, K11, K27, K29, K33, K48 and K63, and the N-terminal M1 residue. Adapted from [220].

Translation of the Ub code triggers specific cellular outcomes and is mediated by effector proteins through non-covalent binding to Ub signals via UBDs. Approximately 20 families of UBDs with distinct modes of interaction have been reported, such as the single or multiple α-helices (including ubiquitin-associated (UBA) domain, ubiquitin-interacting motif (UIM) and ubiquitin-binding in A20-binding inhibitor of NF-κB (ABIN) and NEMO (UBAN)) and zinc fingers (including nuclear protein localization 4 zinc finger (NZF) and zinc-finger in A20 protein (ZnF A20)) [199, 221]. The cellular functions of Ub comprise proteasomal and lysosomal degradation (e.g. K48, K11) [204, 222-224], DNA damage response and repair (K6, K27) [225-228], cell cycle regulation (K11) [204, 222, 229], kinase modification (K29, K33) [230-232], regulation of trafficking and endocytosis (K33, K63) [233, 234] as well regulation of NF-κB and innate immune signaling (K63, M1) [12, 235-238].

2.3.2 Deubiquitinating enzymes

Ubiquitination is a reversible PTM which is counteracted by DUBs, specialized proteases which cleave peptide or isopeptide bonds between Ub and the modified protein or between conjoined Ub molecules [239]. Up till now, 99 DUBs have been identified which can be divided into seven DUB families. The ubiquitin-specific proteases (USPs), the ovarian tumor (OTU) proteases, the ubiquitin C-terminal hydrolases (UCHs), the Machado-Joseph Disease (MJD) DUBs, the motif interacting with ubiquitin (MIU)-containing novel DUB family (MINDY) and the recently discovered zinc finger-containing ubiquitin peptidase 1 (ZUP1) are classified as cysteine proteases while the JAB1/MPN/MOV34 metalloprotease DUBs (JAMMs) are zinc-dependent

metalloproteinases [239]. Since ubiquitination plays a role in virtually all cellular signaling processes, the balance between ubiquitination and deubiquitination needs to be tightly controlled. DUBs regulate cell signaling networks by removing non-degradative Ub modifications from target proteins. In addition, 'housekeeping' DUBs, such as USP14, UCH37/UCHL5 and RPN11/POH1, control cellular Ub levels by cleaving Ub from proteins that are targeted for proteasomal or lysosomal degradation [223] and by processing newly synthesized Ub precursors [240]. DUBs can either be substrate-specific or display specificity towards Ub chain architecture, e.g. the Ub linkage type. Members of the USP family of DUBs, such as USP2 and USP21, show no or only limited preference for specific chains types [241], with the exception of a subset of USP DUBs including CYLD and USP30 [242-245], and can also hydrolyze mono-Ub from substrate proteins [239]. Thus, their specificity lies within their ability to be recruited to and interact with their target substrate protein through distinct protein interaction domains. In contrast, linkage-specific DUBs prefer one or few Ub chain types. Examples of DUBs with preference for one linkage type are OTULIN (M1 Ub) [88, 246], Cezanne (K11 Ub) [247, 248] and USP30 (K6 Ub) [243-245], as well as COP9 signalosome subunit 5 (COPS5) for the Ubl modifier NEDD8 [249], USPL1 for SUMO [250] and USP18 for ISG15 [251]. Moreover, DUBs may show preference for chain length, cleave intact Ub chains ('en bloc' cleavage) or mono-Ub, or distinguish between cleavage from the distal end of an Ub chain (exo-DUB activity) or cleavage within chains (endo-DUB activity) [239]. The process of deubiquitination relies on the interaction of the DUB with the Ub moieties via at least one Ub binding site within the surface of the DUB enzyme, termed S1 site, which orientates the Ub C-terminus and scissile bond towards the catalytic center, resulting in hydrolysis of the peptide bond and release of the distal Ub [220]. The catalytic center of cysteine protease DUBs is formed by a catalytic triad composed of a cysteine, a histidine and an asparagine or aspartate residue, while the active site of metalloprotease DUBs (JAMMs) contains a Zn atom that is coordinated by conserved catalytic residues [220].

2.4 M1-linked (linear) ubiquitination

2.4.1 LUBAC

M1-linked ubiquitination is a non-degradative form of Ub specifically generated by the ~600 kDa linear ubiquitin chain assembly complex (LUBAC) [252, 253] which is

composed of the subunits heme-oxidized IRP2 ubiquitin ligase-1 (HOIL-1, RBCK1) [254], HOIL-1-interacting protein (HOIP, RNF31) [252] and shank-associated RH domain interactor (Sharpin) [12, 235, 253] (Figure 3A). HOIP interacts with Ubl domains and LUBAC-tethering motifs (LTMs) in HOIL-1 and Sharpin via its UBA1 and UBA2 domain [255] and possesses a PNGase/UBA or UBX (PUB) domain which mediates binding to the M1-Ub-editing DUBs OTULIN [256, 257] and CYLD (via the CYLD-spermatogenesis-associated protein 2 (SPATA2) complex) [258-261] (Figure 3A) as well as to the AAA ATPase p97/valosin-containing protein (VCP) [256, 257, 262]. In addition, HOIP contains two NZF domains, one of them being responsible for binding to NEMO [263]. NZF domains are also found in HOIL-1 and Sharpin, mediating interaction with M1 Ub [264] and K63 Ub [265], respectively.

Both HOIL-1 and HOIP are RBR-type E3 Ub ligases, however, HOIP is the E3 ligase responsible for M1 poly-Ub chain generation [17, 252, 266]. HOIP mediates M1 poly-Ub generation through a RING-HECT hybrid reaction whereby the activated donor Ub is transferred to the HOIP active site C885 and subsequently conjugated to the acceptor Ub captured in the HOIP linear ubiquitin chain determining domain (LDD) [267-269]. In contrast to poly-Ub chains of other linkage types which form isopeptide bonds, M1 poly-Ub chains are formed by true peptide bonds as a consequence of conjugation of the C-terminal carboxyl group with the α-amino group of the N-terminal methionine (M1) of the substrate-bound Ub [252]. It has been initially proposed that HOIP catalyzes mono-ubiquitination of target proteins [263, 270, 271], however, other studies revealed that LUBAC mediates M1 ubiquitination of existing K63 Ub chains, thus generating K63/M1 Ub hybrid chains [16, 17].

Although HOIL-1 and Sharpin are redundant for the LUBAC catalytic activity, they may play important roles in the control of LUBAC localization and substrate specificity [272]. Moreover, loss of any of the LUBAC subunits results in destabilization of the other two, leading to impaired LUBAC function [12, 235, 236, 253, 270, 273, 274]. Recent studies revealed regulation of LUBAC activity after recruitment to TNFR1 via mammalian ste20-like kinase 1 (MST1)-induced inhibitory phosphorylation of HOIP [275] and parkin-coregulated gene (PACRG)-mediated LUBAC stabilization [276]. LUBAC catalytic function is further regulated through its interaction with OTULIN, as OTULIN prevents HOIP auto-ubiquitination, thereby promoting LUBAC function [277]. In

addition, LUBAC is targeted by caspases which cleave the N-terminus of HOIP during apoptosis, thereby suppressing LUBAC-mediated activation of NF-κB [278, 279].

LUBAC catalytic activity can be blocked *in vitro* with small molecule chemical inhibitors such as BAY11-7082 [280], bendamustine [281], gliotoxin [282], compound (5) [283, 284] and the recently developed HOIPINs [285, 286]. However, although BAY-11-7082, bendamustine and gliotoxin show some inhibitory effects on LUBAC, they lack selectivity when used in non-toxic concentrations [286]. HOIPIN-8 is the most potent LUBAC inhibitor reported so far, capable of inhibiting *in vitro* M1 ubiquitination activity of recombinant LUBAC with an IC_{50} value of 11 nM [285]. HOIPIN-8 inhibits the RING-HECT hybrid reaction of HOIP by covalently binding to the HOIP catalytic C885 located in the RING2 domain and by masking several residues, including R935 and D936 which are responsible for acceptor-Ub binding, in the LDD of HOIP [285, 286] (Figure 3B). So far, specific inhibitors of LUBAC have not been used *in vivo*, however, the development of potent therapeutics to target LUBAC-mediated M1 poly-Ub may be beneficial for the treatment of inflammatory diseases.

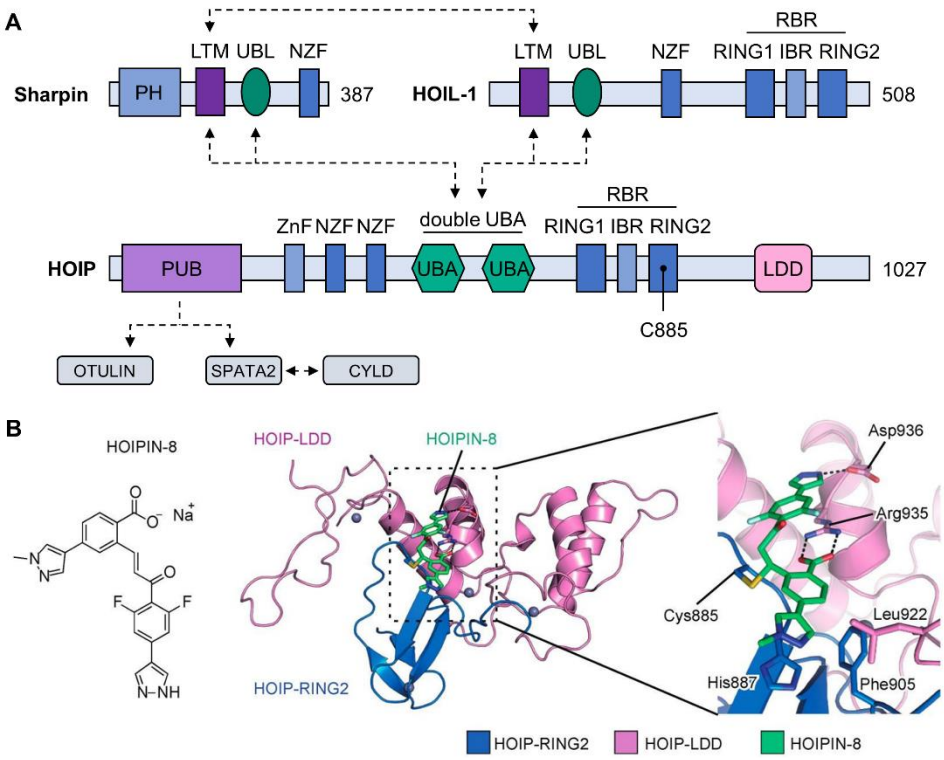

Figure 3. Structural and mechanistical characteristics of LUBAC and LUBAC inhibitor HOIPIN-8.

A Schematic representation of the domain structure of HOIP, HOIL-1 and Sharpin. HOIP belongs to the RING-in between-RING (RBR)-type E3 ligases and generates M1 Ub via its two really interesting new

Figure 3. Continued.

gene (RING) domains, with RING2 containing the active site C885. HOIP contains a C-terminal linear ubiquitin chain determining domain (LDD), two ubiquitin-associated (UBA) domains, two Npl4-type zinc finger (NZF) domains and a zinc-finger (ZnF) domain. HOIP interaction with OTULIN or SPATA2-CYLD is mediated via its N-terminal PNGase/UBA or UBX (PUB) domain. HOIP interacts via its UBA domains with Ub-like (UBL) domains and LUBAC-tethering motifs (LTM) of Sharpin and the RBR E3 ligase HOIL-1. Sharpin and HOIL-1 interact with each other via their LTMs. IBR, in-between RING; PH, Pleckstrin-homology. Adapted from [272, 287]. **B** Left panel: Chemical structure of HOIPIN-8. Right panel: Crystal structure of HOIPIN-8 bound to the HOIP-LDD. HOIPIN-8 inhibits HOIP-mediated M1 Ub generation by covalently binding to the HOIP catalytic C885 located in the RING2 domain and by masking several residues in the HOIP-LDD, including R935 and D936, thereby inhibiting the RING-HECT hybrid reaction. Adapted from [288].

2.4.2 M1 Ub-specific DUBs

M1 ubiquitination is counteracted by the DUBs OTULIN (FAM105B, Gumby) and CYLD. Up till now, OTULIN is the only DUB described to exclusively cleave M1 poly-Ub, while CYLD hydrolyzes both M1 and K63 poly-Ub with similar activity [88, 242, 246, 289]. Both OTULIN and CYLD are important mediators of inflammatory signaling, which is in line with the role of LUBAC and M1 Ub in the regulation of immune receptor signaling and NF-κB activation. Another DUB that has been shown to regulate LUBAC-mediated NF-κB activation is A20 (TNFAIP3), however, A20 shows no DUB activity towards M1 Ub but inhibits NF-κB activation by binding to the M1 poly-Ub chain through its seven-zinc finger (ZF7) domain [90, 91].

2.4.2.1 OTULIN

The high specificity of OTULIN for M1-linked poly-Ub is mediated by the Ub binding site, which discriminates between M1 Ub and the structurally similar K63 Ub, and by a mechanism termed substrate-assisted catalysis, whereby the Ub moiety directly contributes to DUB activation [88, 246]. OTULIN contains a highly conserved OTU domain with a catalytic triad consisting of C129/H339/N341 and an N-terminal PUB interaction motif (PIM), including the phosphorylation site Y56, through which OTULIN selectively interacts with the HOIP PUB domain [88, 246, 256]. Through its interaction with HOIP, OTULIN counteracts LUBAC auto-ubiquitination, thereby promoting LUBAC function [277, 290-293]. In addition, OTULIN deficiency results in cell type-specific degradation of LUBAC subunits [290, 294, 295], indicating a role of OTULIN in LUBAC homeostasis.

OTULIN counteracts LUBAC-mediated M1 Ub and NF-κB activation [88, 246, 256, 257, 290, 292, 293, 295-297], and accordingly, OTULIN deficiency or overexpression of catalytically inactive OTULIN mutants such as OTULIN C129A results in an increase of total cellular M1 Ub levels [73, 88, 246, 257, 292, 295, 296, 298]. OTULIN is involved in immune receptor signaling pathways including TNFR1 signaling [88, 256, 261] and nucleotide-binding and oligomerization domain-containing protein 2 (NOD2) signaling [292, 293], however whether OTULIN plays active roles at RSCs has been under debate [73, 299]. Importantly, loss of OTULIN or expression of OTULIN C129A sensitizes cells towards TNFα/CHX-induced apoptosis and TNFα/CHX/zVAD-induced necroptosis [290, 291] and similarly, knock-in mice expressing OTULIN C129A show increased apoptotic and necroptotic cell death [277]. During necroptosis, OTULIN becomes hyper-phosphorylated at Y56, leading to reduced interaction with LUBAC, whereby it promotes necroptosis supposedly due to altered RIPK1 M1 Ub levels [291]. In addition, OTULIN deficiency in hepatocytes increases apoptotic cell death, and accordingly OTULIN has important functions in liver pathogeneses such hepatitis and hepatocellular carcinoma [294, 300]. Genetic mutations in human *OTULIN* result in the severe inflammatory disease called OTULIN-related autoinflammatory syndrome (ORAS) [290, 294-296, 301, 302] (see section 2.4.4).

Apart from its role in inflammatory signaling, OTULIN-mediated regulation of M1 poly-Ub is involved in the control of autophagy [298, 303], degradation of protein aggregates [262], Wnt signaling [88, 246, 256, 292, 293, 297, 304], and regulation of IFN-mediated antiviral signaling via signal transducer and activator of transcription 1 (STAT1) [305]. Furthermore, recent data link OTULIN to the regulation of endosomal trafficking via sorting nexin 27 (SNX27), revealing a novel Ub-independent function of OTULIN [306].

2.4.2.2 CYLD

CYLD interacts via its USP domain with the PUB domain of the adapter SPATA2, which in turn associates via its PIM with the PUB domain of HOIP [258-260]. Therefore, OTULIN and SPATA2/CYLD interaction with HOIP is mutually exclusive [73, 256-258]. Unlike OTULIN, CYLD is not involved in regulating LUBAC auto-ubiquitination [293]. However, a recent report demonstrated that SPATA2, independently of CYLD, competes with OTULIN for binding to HOIP, thus promoting HOIP auto-ubiquitination and inhibition of LUBAC-mediated pro-inflammatory signaling [307]. CYLD is recruited

to immune receptors such as TNFR1 and NOD2 via LUBAC where it antagonizes M1 and K63 Ub, leading to RSC destabilization [73, 260, 293, 308]. The lack of M1 Ub at RSCs is decisive for cell fate as it results in inhibition of NF-κB activation and pro-survival gene expression [309]. In the case of TNFR1 signaling, the M1 and/or K63 Ub-antagonizing role of CYLD is responsible for the induction of cell death signaling via formation of complex IIa/b or the necrosome, leading to apoptotic or necroptotic cell death, respectively [73-76, 310].

2.4.3 Cellular functions of M1 poly-Ub

M1-linked Ub is involved in a variety of signaling pathways and critically regulates cell fate and immune signaling via TNFR1, interleukin-1 receptor (IL-1R), CD40, NOD-like receptors (NLRs) and TLRs (Figure 4). In addition, LUBAC-mediated M1 poly-Ub has been implicated in the regulation of interferon signaling, inflammasome signaling and selective autophagy [288].

In order to 'read' the M1 Ub code, M1 Ub-specific binding proteins utilize UBDs such as the UBAN domain [311] and the ZF7 domain in A20 (A20 ZF7) [90, 91]. As the name implies, the UBAN domain can be found in NEMO, ABIN-1, ABIN-2 and ABIN-3 as well as in optineurin (OPTN), all of which are critical regulators of NF-κB signaling. The NEMO-UBAN plays a critical role for the recruitment of the IKK complex to M1 poly-Ub chains, thus inducing NF-κB activation [263]. In contrast, ABINs function as inhibitors of NF-κB signaling [311, 312]. The OPTN-UBAN shares high sequence homology with the NEMO-UBAN domain and was identified as a negative regulator of NF-κB signaling as well, as it competes with NEMO for M1 Ub binding [313]. However, OPTN also has multiple functions in other cellular pathways including selective autophagy, vesicular transport and antiviral signaling pathways [314-316].

2.4.3.1 Immune receptor-mediated canonical NF-κB signaling

LUBAC-mediated M1 poly-Ub plays a major role in the control of immune receptor-activated canonical NF-κB signaling [237]. In general, engagement of immune receptors such as TNFR1, NLRs, IL-1R, TLRs and CD40 by their respective ligands results in the formation of RSCs, composed of receptor-associated adaptor proteins and E3 ligases, in which ubiquitination events regulate stabilization of RSCs and thus control cellular outcomes. Recruitment of LUBAC is dependent on Ub modifications

within RSCs and is presumably mediated via its NZF domains [6, 12, 17, 235, 265, 317].

During TNFR1 signaling, LUBAC is recruited to the complex I in response to cIAP1/2/TRAF2/5-mediated K63 ubiquitination of RSC components such as RIPK1 [6, 89, 318]. LUBAC conjugates M1-linked Ub to RIPK1 [12, 88], NEMO and FADD [12, 270, 278], resulting in stabilization of complex I, recruitment of the TAK1 complex via TAB2/3 (through binding to K63 Ub) [15] and IKKα/β complex via NEMO (through binding to M1 Ub) [14] and subsequent activation of NF-κB and MAPK signaling.

Similarly, following stimulation of the NOD2 receptor with bacterial muramyl dipeptide (MDP), LUBAC is recruited to and conjugates M1 Ub to K63 ubiquitinated RIPK2 and thus plays a role in the innate immune response to intracellular bacteria [16, 317, 319]. Furthermore, LUBAC conjugates M1 Ub to myeloid differentiation primary-response protein 88 (MyD88), IL-1R-associated kinase 1 (IRAK1) and IRAK4 during IL-1β-mediated signaling [17, 320, 321]. LUBAC is also implicated in the regulation of TLR1/2 and TLR4 signaling [17, 235, 322] which share the same molecules involved in IL-β signaling. M1 Ub has been shown to play a role in CD40-mediated NF-κB signaling in B-cells and during B-cell development [12, 323] and is involved in the T-cell receptor (TCR)-mediated NF-κB activation pathway [324] (Figure 4). These studies demonstrate that LUBAC-mediated M1 poly-Ub acts as major regulator of canonical NF-κB signaling and controls pro-inflammatory immune responses via various pathways. Accordingly, loss of LUBAC expression or impaired LUBAC function results in deregulated NF-κB activity and decreased gene-activator signaling, leading to inflammatory disorders in both humans and mice [12, 235, 236, 253, 270, 273, 325, 326].

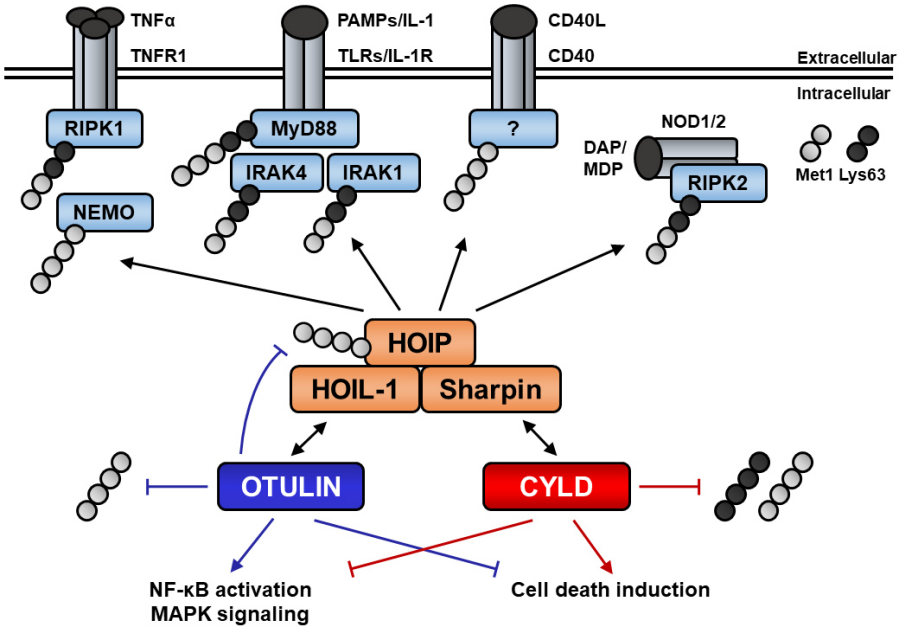

Figure 4. LUBAC-mediated M1 poly-Ub regulates immune receptor signaling.

The linear ubiquitin chain assembly complex (LUBAC), consisting of the heme-oxidized IRP2 ubiquitin ligase-1 (HOIL-1), HOIL-1-interacting protein (HOIP) and shank-associated RH domain interactor (Sharpin) subunits, mediates M1-linked ubiquitination at immune receptors including tumor necrosis factor receptor 1 (TNFR1), toll-like receptors (TLRs), the interleukin-1 receptor (IL-1R), CD40 and nucleotide-binding and oligomerization domain-containing protein 1/2 (NOD1/2). LUBAC targets receptor-associated proteins such as receptor-interacting protein kinase 1 (RIPK1) and NF-κB essential modulator (NEMO) at TNFR1, myeloid differentiation primary-response protein 88 (MyD88) and IL-1R-associated kinase 1/4 (IRAK1/4) at TLRs and IL-1R, RIPK2 at NOD1/2 and yet unspecified proteins at CD40. M1 ubiquitination is counteracted by the DUBs OTU DUB with linear linkage specificity (OTULIN) and cylindromatosis (CYLD). OTULIN specifically targets M1 poly-Ub and counteracts LUBAC auto-ubiquitination, whereby it promotes pro-survival signaling via NF-κB and mitogen-activated kinase (MAPK) activation. CYLD cleaves M1 and K63 poly-Ub, thereby inducing destabilization of receptor signaling complexes, thus inhibiting NF-κB and MAPK signaling and promoting cell death. Met1, M1 Ub; Lys63, K63 Ub. Reprinted from [299].

2.4.3.2 Cell death

TNFR1-mediated signaling via NF-κB activates pro-survival gene expression and thus functions as an important regulator of cell fate. However, under certain conditions, when NF-κB activation is blocked, TNFR1-mediated signaling results in apoptotic cell death via formation of the complex IIa/b or necroptosis via activation of the necrosome. LUBAC deficiency in genetic mouse models not only impairs NF-κB activity but also sensitizes towards TNFR1- and RIPK1-dependent cell death [12, 235, 274, 327-330]. In *Sharpin*-deficient mice (*cpdm* mice), cell death can be suppressed through deletion of *Tnf* [12], *Tnfr* [328], *Ripk3* or *Caspase-8* [327]. Similarly, introduction of a kinase-dead mutant of RIPK1 rescues the *cpdm* phenotype [84]. Complete genetic loss of

HOIP in mice leads to embryonic lethality due to TNFR1-mediated cell death [274] and HOIP or HOIL-1 deficiency in results in TNFR1-mediated cell death, which can be rescued through combined deletion of *Caspase-8*, *Ripk3* or *Mlkl* [274, 330, 331].

Of note, the abovementioned effects of LUBAC deficiency on cytokine-induced canonical NF-κB signaling can be mimicked *in vitro* by LUBAC inhibitors such as HOIPIN-1 and -8 [285, 286] (Figure 3B). HOIPINs have been demonstrated to increase TNFα/CHX-induced cell death in *cpdm* MEFs and apoptotic cell death in the human cell lines A549 and HeLa [286]. HOIPIN-8 also induced loss of cell viability in WT MEFs upon combined treatment with TNFα and zVAD.fmk, indicating a role of LUBAC in necroptosis [286]. In addition, treatment of activated B-cell-like diffuse large B cell lymphoma (ABC-DLBCL) cell lines with HOIPINs effectively induced apoptotic cell death [286].

2.4.3.3 Inflammasome activation

Apart from NF-κB signaling and cell death, LUBAC has been implicated in the regulation of inflammasomes, multiprotein complexes consisting of adaptor proteins and inflammatory caspases which upon activation induce secretion of pro-inflammatory cytokines IL-1β and IL-18, as well as apoptotic or pyroptotic cell death [332]. LUBAC has been demonstrated to conjugate M1 poly-Ub to the caspase-recruit domain (CARD) of adapter protein apoptosis-associated speck-like protein containing a CARD (ASC) and caspase-1, components of the nucleotide-binding domain, leucine-rich–containing family, pyrin domain–containing-3 (NLRP3) inflammasome, thereby inducing caspase-1 activation [333, 334].

2.4.3.4 Autophagy

LUBAC has been shown to regulate selective autophagy by conjugating M1-linked poly-Ub onto the surface of cytosolic *Salmonella*, resulting in the recruitment of autophagy receptors, such as p62 and OPTN, and formation of local NF-κB signaling platforms to restrict bacterial proliferation [298, 335]. In addition, a recent report describes a role for LUBAC in the regulation of autophagy initiation and maturation via M1 ubiquitination and stabilization of the autophagy-related protein 13 (ATG13) [303].

2.4.3.5 Interferon signaling

LUBAC has been linked to the regulation of IFN-mediated antiviral signaling and RIG-I-dependent IFN production [336, 337]. Interestingly, virus infection induces an upregulation of HOIP expression which leads to increased M1 ubiquitination of STAT1, thereby blocking the interaction of STAT1 with the type-I IFN receptor IFNAR2 and thus inhibiting STAT1 activation and the IFN antiviral response [305].

2.4.4 LUBAC and M1 Ub in diseases

Deregulated M1 ubiquitination due to loss of LUBAC expression is well described in mouse models lacking *Hoip*, *Hoil-1* or *Sharpin* and results in inflammatory phenotypes linked to impaired NF-κB activation and increased cell death [12, 274, 327-331]. Sharpin deficiency in *Sharpin*^{cpdm} mice leads to the development of chronic proliferative dermatitis (cpdm) at 3-6 weeks age, due to aberrant TNFR1-mediated cell death, characterized by highly inflamed skin lesions, keratinocyte apoptosis and infiltration of eosinophils, neutrophils, and macrophages, as well as inflammation in other organs [12, 84, 326-328, 338-344]. In contrast, homozygous deletion of *Hoip* or *Hoil-1* in mice results in embryonic lethality due to defective vascularization and increased TNFR1-mediated cell death in the yolk sac [274, 331].

Only a few cases of genetic LUBAC deficiencies in human patients have been described thus far. Up till now, only one patient with Sharpin deficiency has been reported [325]. Unexpectedly, this patient showed no signs of dermatologic manifestations but multi-organ inflammation and impaired cellular NF-κB activation [325]. Patients with genetic mutations in the HOIL-1 gene suffer from systemic auto-inflammation and invasive bacterial infections supposedly due to impaired LUBAC stability and deregulated TNFα- and IL-1β-induced NF-κB activation [273]. Furthermore, HOIL-1 deficiency has been linked to glycogen storage disease (amylopectinosis), muscular weakness and cardiomyopathy [273, 345, 346]. Of note, the clinical phenotypes of HOIL-1 and HOIP deficiency in patients largely overlap [236]. A recent case of a patient with *HOIP* mutations additionally links HOIP deficiency to the regulation of type I IFN-mediated gene expression [347].

Interestingly, two polymorphisms in the HOIP gene, which lead to enhanced HOIP-HOIL-1 interaction and increased LUBAC enzymatic activity, are associated with the constitutively elevated NF-κB activation in ABC-DLBCL [348, 349] and inhibition of

HOIP expression as well as treatment with LUBAC inhibitors have been demonstrated to reduce viability of ABC-DLBCL cell lines [286, 350, 351].

The pathophysiological relevance of M1 Ub regulation is further highlighted in patients with rare mutations in the OTULIN gene which cause the ORAS, a TNFα-driven inflammatory disease characterized by sterile systemic inflammation with fever, panniculitis and liver pathologies [290, 294-296, 301, 302]. OTULIN deficiency in ORAS patients results in cell-type-specific LUBAC degradation and enhanced M1 Ub levels, leading to deregulated NF-κB and MAPK activation [290, 295, 296].

Furthermore, LUBAC and OTULIN play a role in neurodegenerative diseases as they control recognition and processing of misfolded proteins such as mutated Huntingtin, superoxide dismutase 1 (SOD1) and TAR DNA-binding protein 43 (TDP-43) [262, 352].

3 Aim of the study

The ability of mammalian cells to undergo PCD, such as apoptosis or necroptosis, is a crucial feature that enables tissue homeostasis during embryonic development as well as clearance of damaged cells in adult organisms. Consequently, dysregulation of PCD affects inflammatory processes in the cellular microenvironment and thus is implicated in various inflammatory diseases and in cancer [39, 353].

In this study, we aimed to characterize how LUBAC-mediated M1-linked poly-Ub controls cell fate decisions downstream of TNFR1. Using CRISPR/Cas9-mediated genetic knockout of OTULIN and CYLD in HT-29 colon carcinoma cells and THP-1 monocytes, we intended to investigate the roles of these DUBs during TNFR1-mediated NF-κB signaling and cell death induction. In addition, we used the small molecule chemical HOIP inhibitor HOIPIN-8 to study the effect of LUBAC inhibition on TNFR1-mediated signaling, which led to an interesting finding, i.e., that inhibition of LUBAC activity with HOIPIN-8 delayed TNFα/BV6/zVAD.fmk (TBZ)-induced necroptosis.

TNFR1-mediated necroptosis is critically regulated by cellular compartmentalization events and post-translational modifications such as phosphorylation or ubiquitination of the key necroptotic proteins RIPK1, RIPK3 and MLKL [124-126]. Activated MLKL mediates plasma membrane disruption ultimately resulting in necroptotic cell death, however, although emerging concepts of MLKL compartmentalization suggest intricate regulatory mechanisms of MLKL membrane availability, how necroptosis is regulated downstream of MLKL oligomerization remains largely unknown. Therefore, in the second part of this study, we focused on the role of LUBAC-mediated M1 poly-Ub during necroptosis. Our aim was to determine how LUBAC and M1 poly-Ub affect necroptotic signaling, MLKL oligomerization and MLKL plasma membrane localization in human and mouse cell lines. Finally, in cooperation with our partners at the Buchmann Institute for Molecular Life Sciences (BMLS), we intended to study necroptosis and the effect of LUBAC inhibition in more physiological settings by using human primary pancreatic organoids (hPOs).

4 Materials and Methods

4.1 Materials

4.1.1 Cell lines

Table 1. Human and murine cell lines.

Cell line	Source	Identifier
HT-29	DSMZ	RRID: CVCL_0320
HT-29 CRISPR/Cas9 control (nht)	Roedig et al. [146]	N/A
HT-29 CRISPR/Cas9 control 2 (nht)	This study	N/A
HT-29 RIPK3 KO	Roedig et al. [146]	N/A
HT-29 RIPK3 KO re-expressing PAM-mutated Dox-inducible Strep-tagged WT RIPK3	Roedig et al. [146]	N/A
HT-29 MLKL KO	This study (Jens Roedig/Birte Jeiler)	N/A
HT-29 OTULIN KO	This study	N/A
HT-29 CYLD KO	This study	N/A
HT-29 OTULIN/CYLD KO	This study	N/A
HT-29 HOIP KO	This study	N/A
THP-1	Gift from Thomas Oellerich	RRID: CVCL_0006
THP-1 CRISPR/Cas9 control (nht)	This study	N/A
THP-1 CRISPR/Cas9 control 2 (nht)	This study	N/A
THP-1 OTULIN KO	This study	N/A
THP-1 CYLD KO	This study	N/A
THP-1 OTULIN/CYLD KO	This study	N/A
THP-1 HOIP KO	This study	N/A
HEK293T	ATCC	RRID: CVCL_0063
MEF	Gift from Joanne Hildebrand	N/A
MEF CRISPR/Cas9 control (nht)	This study	N/A

Cell line	Source	Identifier
MEF HOIP KO	This study	N/A
MEF *Tnf*$^{-/-}$	Gift from Henning Walczak	N/A
MEF *Tnf*$^{-/-}$ *Hoip*$^{-/-}$	Gift from Henning Walczak	N/A
L-929	ATCC	RRID: CVCL_0462
L-929 CRISPR/Cas9 control (nht)	This study	N/A
L-929 HOIP KO	This study	N/A
RAW 264.7	Gift from Stefan Müller	RRID: CVCL_0493
Primary human pancreatic organoids	Gift from Lorenza Lazzari	N/A

4.1.2 Cell culture media and supplements

Table 2. Cell culture media and supplements.

Cell culture media and supplements	Source	Identifier
McCoy's 5A Medium +GlutaMAX™-I	Thermo Fisher Scientific	Cat#36600-021
RPMI1640 Medium +GlutaMAX™-I	Thermo Fisher Scientific	Cat#61870-010
DMEM +GlutaMAX™-I	Thermo Fisher Scientific	Cat#32430-027
Penicillin/streptomycin	Thermo Fisher Scientific	Cat#15140-122
Fetal bovine serum (FBS)	Thermo Fisher Scientific	Cat#10270-106
Sodium pyruvate	Thermo Fisher Scientific	Cat#11360-039
MEM Non-Essential Amino Acids (NEAA) Solution	Thermo Fisher Scientific	Cat#11140-035
Cultrex Reduced Growth Factor BME, Type 2 (BME-2)	R&D Systems	Cat#3533-005-02
Advanced DMEM/F-12	Thermo Fisher Scientific	Cat#12634010

Cell culture media and supplements	Source	Identifier
GlutaMAX™ Supplement	Thermo Fisher Scientific	Cat#35050038
HEPES	Thermo Fisher Scientific	Cat#15630080
B-27™ Supplement, minus vitamin A	Thermo Fisher Scientific	Cat#12587010
N-2 Supplement	Thermo Fisher Scientific	Cat#17502048
N-acetylcysteine	Merck Sigma	Cat#A9165-5g
Recombinant human R-Spondin1	PeproTech	Cat#120-38
Nicotinamide	Merck Sigma	Cat#N0636
Recombinant human EGF	PeproTech	Cat#AF-100-15
Recombinant human FGF-10	PeproTech	Cat#100-26
Noggin	PeproTech	Cat#120-10C
[Leu15]-Gastrin I	Merck Sigma	Cat#G9145
A83-01	Tocris Bioscience	Cat#2939
Forskolin	Tocris Bioscience	Cat#1099
Prostaglandin E2	Tocris Bioscience	Cat#2296

4.1.3 Chemicals, peptides and recombinant proteins

Table 3. Chemicals, peptides and recombinant proteins.

Chemicals, peptides and recombinant proteins	Source	Identifier
HOIPIN-8	Axon Medchem	Cat#2972
Gliotoxin	Tocris Bioscience	Cat#2637
Recombinant human TNFα	PeproTech	Cat#300-01A
BV6	Genentech	N/A
Birinapant	Selleckchem	Cat#S7015
zVAD.fmk	Bachem	Cat#4027403
Emricasan (IDN-6556)	Selleckchem	Cat#S7775

Chemicals, peptides and recombinant proteins	**Source**	**Identifier**
Nec-1s	MerckMillipore	Cat#480065
GSK'872	MerckMillipore	Cat# 530389
NSA	MerckMillipore	Cat#480073
Bafilomycin A1 (BafA1)	Selleckchem	Cat#S1413
Doxycycline hydrochloride	Sigma-Aldrich	Cat#D3447
Propidium iodide	Merck Sigma	Cat#P4170
Hoechst33342	Thermo Fisher Scientific	Cat#H1399
Fluorescein diacetate (FDA)	Merck Sigma	Cat#F7378
DAPI	Carl Roth	Cat#6335.1
OptiMEM	Thermo Fisher Scientific	Cat#31985062
Lipofectamine™ RNAiMAX Transfection Reagent	Thermo Fisher Scientific	Cat#13778030
FuGENE HD Transfection Reagent	Promega	Cat#E2311
Polybrene	Merck Sigma	Cat#TR-1003
Puromycin dihydrochloride	Thermo Fisher Scientific	Cat# A1113803
Blasticidin S hydrochloride	Carl Roth	Cat#CP14.4
cOmplete™ Protease Inhibitor Cocktail	Roche/Merck Sigma	Cat#04693116001
Pierce Universal Nuclease	Thermo Fisher Scientific	Cat#88701
Pierce™ ECL Western Blotting-Substrate	Thermo Fisher Scientific	Cat#32106
Total Exosome Isolation Reagent (from cell culture media)	Thermo Fisher Scientific	Cat#4478359
Triton™ X-114	Merck Sigma	Cat#X114
SYBR Green PCR Master Mix	Thermo Fisher Scientific	Cat#4312704
Ponceau S	Merck Sigma	Cat#P7170
MagStrep "type3" XT beads	IBA Lifesciences	Cat#2-4090-002

Chemicals, peptides and recombinant proteins	Source	Identifier
Glutathione MagBeads	Genscript	Cat#L00895

4.1.4 Buffers and solutions

Table 4. Buffers and solutions.

All chemicals were purchased from Carl Roth or Merck Sigma.

Buffer	Composition
RIPA lysis buffer	50 mM Tris-HCl pH 8, 150 mM NaCl, 1%, Nonidet P-40 (NP-40), 2 mM MgCl2, 0.5% sodium deoxycholate
1% NP-40 lysis buffer	20 mM Tris-HCl pH 7.5, 50 mM NaCl, 5 mM EDTA, 10% glycerol, 1% NP-40
Triton-X114 lysis buffer	150 mM NaCl, 20 mM HEPES pH 7.4, 2% Triton X-114
Basal buffer	150 mM NaCl, 20 mM HEPES pH 7.4
6x SDS loading buffer	350 mM Tris Base pH 6.8, 38% glycerol, 10% SDS, 93 mg/mL dithiothreitol (DTT), 120 mg/mL bromophenol blue
6x SDS loading buffer (non-reducing)	350 mM Tris Base pH 6.8, 38% glycerol, 10% SDS, 120 mg/mL bromophenol blue
5x SDS-PAGE running buffer	30.2 g Tris-HCl, 188 g glycine, 100 mL 10% SDS, filled up to 2 L of ddH_2O
Blotting buffer	11.6 g Tris-HCl, 5.8 g glycine, 7.5 mL 10% SDS, 400 mL methanol, filled up to 2 L of ddH2O
Blocking buffer	5% milk powder in PBS-T
Stripping buffer	0.4 M NaOH
5% polyacrylamide gel	5% polyacrylamide, 375 mM Tris/HCl pH 6.8, 0.1% SDS, 0.1% APS, 0.1% TEMED
10%/12% polyacrylamide gel	10%/12% polyacrylamide, 125 mM Tris/HCl pH 8.8, 0.1% SDS, 0.1% APS, 0.04% TEMED
BSA solution	2% BSA, 0.1% ProClin™ 150 in PBS
TBS-T	20 mM Tris, 150 mM NaCl, 0.1%Tween 20, pH 8.0
PBS-T	0.1% Tween 20 in PBS
Antibody dilution buffer (ABD)	0.9% NaCl, 10 mM Tris/HCl pH 7.5, 5 mM EDTA, 1 mg/mL BSA

4.1.5 Antibodies

Table 5. Primary and secondary antibodies.

Primary antibodies for Western blotting were prepared 1:1,000 in BSA solution unless stated otherwise. Secondary antibodies were prepared 1:10,000 in 5% milk in PBS-T.

Antibody	Source	Identifier
human anti-linear poly-Ub (1F11/3F5/Y102L)	Genentech	N/A
rabbit polyclonal anti-RNF31/HOIP	Abcam	Cat#ab46322; RRID: AB_945269
mouse monoclonal anti-HOIL-1	Merck Millipore	Cat#MABC576; RRID: AB_2737058
rabbit monoclonal anti-Sharpin (D4P5B)	Cell Signaling Technology	Cat#12541; RRID: AB_2797949
mouse monoclonal anti-phospho-IκBα (S32/S36) (5A5)	Cell Signaling Technology	Cat#9246; RRID: AB_2267145
rabbit polyclonal anti-IκBα	Cell Signaling Technology	Cat#9242; RRID: AB_331623
mouse monoclonal NF-κB p65 (F-6)	Santa Cruz Biotechnology	Cat#sc-8008, RRID: AB_628017
rabbit monoclonal anti-phospho-NF-κB p65 (Ser536) (93H1)	Cell Signaling Technology	Cat#3033, RRID: AB_331284
rabbit monoclonal anti-phospho-RIPK1 (S166) (D1L3S)	Cell Signaling Technology	Cat#65746; RRID: AB_2799693
rabbit polyclonal anti-phospho-RIPK1 (S166) (rodent specific)	Cell Signaling Technology	Cat#31122; RRID: AB_2799000
mouse monoclonal anti-RIPK1	BD Biosciences	Cat#551041; RRID: AB_394014
mouse monoclonal anti-RIPK1	BD Biosciences	Cat#610459; RRID: AB_397832
rabbit monoclonal anti-phospho-RIPK3 (S277)	Abcam	Cat#ab209384; RRID: AB_2714035
rabbit monoclonal anti-RIPK3 (E1Z1D)	Cell Signaling Technology	Cat#13526; RRID: AB_2687467
rabbit monoclonal anti-phospho-MLKL (S358) (D6H3V)	Cell Signaling Technology	Cat#91689; RRID: AB_2732034

Antibody	Source	Identifier
rabbit monoclonal anti-phospho-MLKL (S345)	Abcam	Cat#ab196436; RRID: AB_2687465
rabbit monoclonal anti-MLKL (D2I6N)	Cell Signaling Technology	Cat#14993; RRID: AB_2721822
rabbit monoclonal anti-MLKL (mouse specific)	Biorbyt	Cat#orb32399; RRID: AB_10927389
rabbit monoclonal anti-phospho-MLKL (S358)	Abcam	Cat#ab187091; RRID: AB_2619685
mouse monoclonal anti-ALIX	BioLegend	Cat#634502; RRID: AB_2162471
mouse monoclonal anti-CD9 (C-4)	Santa Cruz Biotechnology	Cat#sc-13118; RRID: AB_627213
rabbit polyclonal anti-CHMP2A	Proteintech	Cat#10477-1-AP; RRID: AB_2079470
mouse monoclonal anti-VPS4 (E-8)	Santa Cruz Biotechnology	Cat#sc-133122; RRID: AB_2304400
mouse monoclonal anti-Flotillin-1 (clone 18)	BD Biosciences	Cat#610820; RRID: AB_398139
mouse monoclonal anti-Flotillin-2 (clone 29)	BD Biosciences	Cat#610383; RRID: AB_397766
mouse monoclonal anti-GAPDH	Hytest	Cat#5G4cc-6C5cc; RRID: AB_2858176
mouse monoclonal anti-Vinculin	Sigma-Aldrich	Cat#V9131; RRID: AB_477629
mouse monoclonal anti-β-actin	Sigma-Aldrich	Cat#A5441; RRID: AB_476744
HRP-conjugated polyclonal goat anti-mouse IgG H&L	Abcam	Cat#ab6789; RRID: AB_955439
HRP-conjugated polyclonal goat anti-rabbit IgG H&L	Abcam	Cat#ab6721; RRID: AB_955447
HRP-conjugated goat anti-human IgG	Merck Millipore	Cat#AP309P; RRID: AB_92684
Cy3-AffiniPure polyclonal donkey anti-rabbit IgG (H+L)	Jackson ImmunoResearch	Cat#711-165-152; RRID: AB_2307443

4.1.6 qPCR primer

Table 6. qPCR primer.

Target	Primer sequence (5'-3')
CXCL1 forward	AACCGAAGTCATAGCCACAC
CXCL1 reverse	GTTGGATTTGTCACTGTTCAGC
CXCL10 forward	CTGAGCCTACAGCAGAGGAAC
CXCL10 reverse	GATGCAGGTACAGCGTACAGT
TNFA forward	ACAACCCTCAGACGCCACAT
TNFA reverse	TCCTTTCCAGGGGAGAGAGG
ICAM1 forward	CTTCCTCACCGTGTACTGGAC
ICAM1 reverse	GGCAGCGTAGGGTAAGGTTC
HOIP forward	ACCCCCTATTGAGAGAGATTGCT
HOIP reverse	TGGAGCCTGGGACAGAGG
HOIL-1 forward	GTGCCAGATCATGGAGGCCC
HOIL-1 reverse	GAGCATCCTCCACGCTCACC
SHARPIN forward	GAAGCCTCCACACTCAAG
SHARPIN reverse	TTCTCTCTCCGTCAAGTTTC
NFKBIA forward	GTCAAGGAGCTGCAGGAGAT
NFKBIA reverse	ATGGCCAAGTGCAGGAAC
CXCL8 forward	CTCTTGGCAGCCTTCCTGATT
CXCL8 reverse	TATGCACTGACATCTAAGTTCTTTAGCA
TNFAIP3 forward	GTGGCCTTTTGTGATGGTTT
TNFAIP3 reverse	GCTTTTGCTGTCCCAATACC
18S forward	CGCAAATTACCCACTCCCG
18S reverse	TTCCAATTACAGGGCCTCGAA
RPII forward	GCACCACGTCCAATGACAT
RPII reverse	GTGCGGCTGCTTCCATAA

4.1.7 siRNA

Table 7. siRNA.

siRNA	Source	Identifier
Silencer™ Select RNF31/HOIP siRNA #1 s30108	Thermo Fisher Scientific	Cat#4392420
Silencer™ Select RNF31/HOIP siRNA #2 s30109	Thermo Fisher Scientific	Cat#4392420
Silencer™ Select RNF31/HOIP siRNA #3 s30110	Thermo Fisher Scientific	Cat#4392420
Silencer™ Select Negative Control No. 1 siRNA	Thermo Fisher Scientific	Cat#4390843
ON-TARGETplus Human CHMP2A siRNA SMART POOL	Horizon Discovery	Cat#L-020247-01-0010
ON-TARGETplus Human VPS4A siRNA SMART POOL	Horizon Discovery	Cat#L-013092-00-0010
ON-TARGETplus Human PDCP6IP siRNA SMART POOL	Horizon Discovery	Cat#L-004233-00-0010
ON-TARGETplus Human FLOT1 siRNA SMART POOL	Horizon Discovery	Cat#L-010636-00-0010
ON-TARGETplus Human FLOT2 siRNA SMART POOL	Horizon Discovery	Cat#L-003666-01-0010

4.1.8 Plasmids and guide RNA sequences for CRISPR/Cas9-mediated KO

Table 8. Plasmids and guide RNA sequences for CRISPR/Cas9-mediated KO.

Plasmid, guide RNA	Source	Identifier
Plasmid plentiCRISPR v2	Sanjana et al. [354]	RRID:Addgene_52961
Plasmid pMD2.G	Gift from Didier Trono	RRID:Addgene_12259
Plasmid psPAX2	Gift from Didier Trono	RRID:Addgene_12260
Guide RNA sequence for eGFP #1 (nht): GGAGCGCACCATCTTCTTCA	from Brunello library Doench et al. [355]	RRID:Addgene_73178

Plasmid, guide RNA	Source	Identifier
Guide RNA sequence for eGFP #2 (nht): GGCCACAAGTTCAGCGTGTC	from Brunello library Doench et al. [355]	RRID:Addgene_73178
Guide RNA sequence for eGFP #3 (nht): GGGCGAGGAGCTGTTCACCG	from Brunello library Doench et al. [355]	RRID:Addgene_73178
Guide RNA sequence for human MLKL #1: ATGACAATGGAGAATTGAGG	from Brunello library Doench et al. [355]	RRID:Addgene_73178
Guide RNA sequence for human MLKL #2: CCTGTTTCACCCATAAGCCA	from Brunello library Doench et al. [355]	RRID:Addgene_73178
Guide RNA sequence for human MLKL #3: TTCCCTTAGCAGAATCCACG	from Brunello library Doench et al. [355]	RRID:Addgene_73178
Guide RNA sequence for human OTULIN #1: ACCACGGACTCGCCGTATGG	from Brunello library Doench et al. [355]	RRID:Addgene_73178
Guide RNA sequence for human OTULIN #2: ATTGCTTATACATGAAAGAG	from Brunello library Doench et al. [355]	RRID:Addgene_73178
Guide RNA sequence for human OTULIN #3: TGAACTATTCACAAATGAGG	from Brunello library Doench et al. [355]	RRID:Addgene_73178
Guide RNA sequence for human CYLD #1: GATGGGAAGGACGATTCTGC	This study	N/A
Guide RNA sequence for human CYLD #2: AGAGTGGAATCTGTTCTCGG	This study	N/A
Plasmid pLCV2-sgRNF31-2 blast Guide RNA sequence for human HOIP #1: CACCGCCCAACCCCTTACAGCCTCG	Gift from Zhengkui Zhang	N/A
Plasmid pLCV2-sgRNF31-4 blast Guide RNA sequence for human HOIP #2: CACCGGGATCATGCTCACTAGCTGG	Gift from Zhengkui Zhang	N/A
Plasmid pLCV2-sgRNF31-1 blast mouse Guide RNA sequence for murine HOIP #1: CACCGGATGGATTGAGTTTCCCCGA	Gift from Zhengkui Zhang	N/A
Plasmid pLCV2-sgRNF31-2 blast mouse Guide RNA sequence for murine HOIP #2: CACCGGAACTATGAGTTGTTGGACG	Gift from Zhengkui Zhang	N/A

Plasmid, guide RNA	Source	Identifier
Plasmid pLentiCRISPRv2-sgNTC 141-Blast Guide RNA sequence for non-targeting control: AGCTTTCGAAATTGAGTGTC	Gift from Daniel Peeper from Brunello library Doench et al. [355]	RRID:Addgene_73178

4.1.9 Commercial assays and kits

Table 9. Commercial assays and kits.

Assay or kit	Source	Identifier
Pierce™ BCA Protein Assay Kit	Thermo Fisher Scientific	Cat#23227
peqGOLD total RNA isolation kit	VWR Life Science	Cat#13-6834-02
RevertAid H Minus First Strand cDNA Synthesis Kit	Thermo Fisher Scientific	Cat#K1632
Human CXCL1/GROα DuoSet® ELISA kit	R&D Systems	Cat#DY275

4.1.10 Plastic ware and consumables

Table 10. Plastic ware and consumables.

Plastic ware, consumables	Source
CELLSTAR® 96-well suspension culture plates	Greiner Bio-One
CELLSTAR® 48-well suspension culture plates	Greiner Bio-One
CELLSTAR® 96-well tissue culture plates	Greiner Bio-One
CELLSTAR® 6-well tissue culture plates	Greiner Bio-One
Cellstar® cell culture flasks T-25, T-75, T-175	Greiner Bio-One
Cell culture dishes 100 mm	Greiner Bio-One
Cell culture dishes 150 mm	Greiner Bio-One
15 ml and 50 ml conical tubes, polypropylene	Greiner Bio-One
Combitips advanced (0.5 ml, 1 ml, 2.5 ml, 5 ml, 10 ml)	Eppendorf
TipOne Graduated Tip (10 µl, 200 µl, 1000 µl)	Starlab
Sterile pipettes (2 ml, 5 ml, 10 ml, 25 ml, 50 ml)	Greiner Bio-One

Plastic ware, consumables	Source
Microcentrifuge tubes (0.5 ml, 1.5 ml, 2 ml)	Starlab
Cryogenic vials (1.8 ml)	Starlab
Syringes (5 mL)	B. Braun
Millex-HA Filter, 0.45 µm	Merck
Filter paper	Carl Roth
Amersham Hyperfilm™ (High performance chemiluminescence film)	GE Healthcare
Amersham™ Protran™ 0.2 µm Nitrocellulose Membrane	GE Healthcare

4.1.11 Equipment and instruments

Table 11. Equipment and instruments.

Equipment and instruments	Source
ARE heating magnetic stirrer	VELP Scientifica
BioRAD Mini Protean® Tetra Cell	BioRAD Laboratories
BioRAD Power-Pac HC	BioRAD Laboratories
BioRAD Trans-Blot SD Semi-Dry Transfer Cell	BioRAD Laboratories
CASY® cell counter	OMNI Life Science
Centrifuge MIKRO 200 R	Hettich
Centrifuge ROTANTA 460 R	Hettich
Centrifuge ROTIXA 50 RS	Hettich
Easypet 3	Eppendorf
Freezer (-20°C)	EWALD Innovationstechnik
Freezer (-80°C)	Sanyo Electric Co. Ltd.
Fridge (4°C)	EWALD Innovationstechnik
HERAsafe class II biological safety cabinet	Kendro
ImageXpress Micro XLS Imaging System	Molecular Devices
inCUsafe CO2 incubator model: MCO-20AIC	Sanyo Electric Co. Ltd.
Infinite M200 microplate reader	Tecan
MM-Separator M12+12, MD90001	MagnaMedics

Equipment and instruments	Source
Multipette® M4	Eppendorf
NanoDrop 1000	PeqLab
Odyssey® Imaging System	LI-COR Biosciences
Olympus CKX41 Microscope	Olympus
Peqlab PerfectBlue™ Vertical Double Gel System	VWR Life Science
Pipettes Research Plus (2.5 µl, 10 µl, 20 µl, 100 µl, 200 µl, 1000 µl)	Eppendorf
QuantStudio™ 7 Flex Real-Time PCR System	Applied Biosystems
Rocking shaker	MS-L GmbH
Roller mixer	Ratek
Rotator	MS-L GmbH
Steam pressure autoclave Systec VX-150	Systec GmbH
Vapo.Protect Mastercycler® Pro	Eppendorf
ThermoMixer® comfort	Eppendorf
Vortex (ZX classic, wizard X)	VELP Scientifica
Water bath SWB20	Medingen
Zeiss AxioObserver Z1	Carl Zeiss Microscopy GmbH

4.1.12 Software and algorithms

Table 12. Software and algorithms.

Software/algorithm	Source	Identifier
MetaXpress® 6.7.2	Molecular Devices	https://www.moleculardevices.com/products/cellular-imaging-systems/acquisition-and-analysis-software/metaxpress
ZEN lite 2.6	Carl Zeiss Microscopy	https://www.zeiss.de/mikroskopie/produkte/mikroskopsoftware/zen-lite.html
ImageJ	Schneider et al. [356]	https://imagej.nih.gov/ij/

Software/algorithm	Source	Identifier
GraphPad Prism 9	GraphPad	https://www.graphpad.com/scientific-software/prism/
Endnote™ 20	Clarivate	https://endnote.com/
MS Office 2019	Microsoft	https://www.microsoft.com/de-de/microsoft-365
Paint.net 4.3	dotPDN LLC	https://www.dotpdn.com/downloads/pdn.html
Magellan™ Data Analysis Software Version 7.2	Tecan Life Sciences	N/A
i-control Version 1.10	Tecan Life Sciences	N/A
Cutadapt	Martin [357]	https://cutadapt.readthedocs.io/en/stable/
FastQC	Babraham Bioinformatics	https://www.bioinformatics.babraham.ac.uk/projects/fastqc/
STAR	Dobin et al. [358]	https://github.com/alexdobin/STAR
DESeq2	Love et al. [359]	https://bioconductor.org/packages/release/bioc/html/DESeq2.html
deepTools	Ramírez et al. [360]	https://deeptools.readthedocs.io/en/develop/
R	N/A	https://www.R-project.org/

4.2 Methods

4.2.1 Cell culture

All cell lines used in this study were regularly monitored for mycoplasma infection. Cell line authentication of HT-29, THP-1, HEK293T and L-929 cells was performed by the Leibniz-Institute DSMZ GmbH (Braunschweig, Germany). HT-29, THP-1 and HEK293T were authenticated by DNA profiling using 8 different highly polymorphic short tandem repeat (STR) loci. L-929 were subjected to DNA barcoding of Cytochrome oxidase subunit 1 (CO1) to confirm *Mus musculus* origin [361].

4.2.1.1 Culturing of cell lines

All cell lines were cultured in humidified incubators at 37°C with 5% carbon dioxide (CO_2)-atmosphere. HT-29 cell lines were cultured in McCoy's 5A Medium, GlutaMAX™-I, supplemented with 10% fetal bovine serum (FBS) and 1% penicillin/streptomycin. HEK293T and MEF cell lines were cultured in DMEM GlutaMAX™-I medium supplemented with 10% FBS, 1% penicillin/streptomycin and 1% sodium pyruvate and THP-1 in RPMI 1640 medium supplemented with 10% FBS, 1% penicillin/streptomycin and 1% sodium pyruvate. L-929 cells were maintained in DMEM GlutaMAX™-I supplemented with 1% sodium pyruvate, 1% penicillin/streptomycin, 1% MEM Non-Essential Amino Acids (NEAA) Solution and 10% FBS. RAW 264.7 cells were maintained in DMEM GlutaMAX™-I (Thermo Fisher Scientific) supplemented with 10% FBS. All cell lines were cultivated in cell culture flasks and passaged two to three times per week. Adherent cell lines were cultivated until 80-90% confluency. For passaging, the cells were washed with pre-warmed PBS and then incubated with trypsin/EDTA until the cells detached. Trypsin activity was blocked by addition of fresh cell culture medium. The cells were passaged into new cell culture flasks with fresh medium. After a maximum of 30 passages, the cells were discarded and freshly thawed.

4.2.1.2 Freezing and thawing of cell lines

For long-term storage, cryostocks of the cell lines were stored in a liquid nitrogen tank. Cryostocks were prepared by resuspending the cells in FBS supplemented with 10% DMSO followed by overnight freezing at -80°C and subsequent transfer of the

cryogenic vials to a liquid nitrogen tank. Thawing of the cells was performed by thawing the cryogenic vials in a water bath at 37°C and immediate transfer of the cell suspension into prewarmed medium. After 5 min centrifugation at 1800 rpm, the cell pellet was resuspended in fresh prewarmed cell culture medium and transferred into a cell culture flask.

4.2.1.3 Seeding and treatment of cell lines

The cells were seeded in fresh cell culture medium the day before the treatment at an appropriate cell density ranging from $0.4x10^5$ cells/cm^2 to $0.8x10^5$ cells/cm^2 for adherent cells and $0.2\text{-}0.3x10^6$ cells/mL for suspension cells. Adherent cells were trypsinized from the cell culture flask as described previously. The cell number was determined using a Casy cell counter (OMNI Life Science, Bremen, Germany) according to the manufacturer's instructions. Compound solutions were prepared in fresh cell culture medium as 20x concentrated solutions and applied directly to the cell culture dishes.

4.2.2 Induction and quantification of necroptotic cell death

For necroptosis induction, cells were seeded in 96-well dishes the day before the treatment, pre-treated with 1 µM BV6 and 20 µM zVAD.fmk for 30 min, followed by treatment with 10 ng/mL recombinant human TNFα for the indicated time (TBZ). Cell death inhibitors Nec-1s (30 µM), GSK'872 (20 µM) and NSA (10 µM) as well as HOIPIN-8 (30 µM) and Gliotoxin (1 µM) were added 1 h prior to TBZ treatment. Cell death measurement was performed using combined Hoechst 33342 (Hoe) and propidium iodide (PI) staining (working concentrations: 10 µg/mL Hoe and 1 µg PI). Fluorescence-based quantification of non-viable (PI-positive) cells compared the total cell number (Hoe-positive cells) was performed using the ImageXpress Micro XLS Widefield High-Content Analysis System and MetaXpress® Software (Molecular Devices, Sunnyvale, CA, USA).

4.2.3 Maintenance of primary organoids

Primary human pancreatic organoids (hPOs) were provided by Lorenza Lazzari (Policlinico di Milano, Milan, Italy) and their use is approved by the Institutional Review Board and the Pancreatic Islet Processing Unit, a National Transplant Center

accredited facility (IT000679, https://webgate.ec.europa.eu/eucoding/reports/te/index.xhtml). hPOs are derived from the pancreatic duct of a male patient (age: 60, BMI: 26.3) and were maintained in an incubator at 37°C in a humidified atmosphere with 5% CO_2, embedded in Cultrex Reduced Growth Factor Basement Membrane Extract, Type 2 (BME-2) droplets (R&D Systems, Minneapolis, MN, USA) and covered under medium.

The organoid culture protocol is adapted from Broutier et al. [362]. In brief, hPOs were cultured in basal medium composed of Advanced DMEM/F-12 (Thermo Fisher Scientific) with 1x GlutaMAX™ Supplement (Thermo Fisher Scientific), 100 U/mL penicillin/streptomycin (Thermo Fisher Scientific) and 10 mM HEPES (Thermo Fisher Scientific), supplemented with 1x B-27™ (minus vitamin A, Thermo Fisher Scientific), 1x N-2 (Thermo Fisher Scientific), 2,5 mM N-acetylcysteine (MilliporeSigma, St. Louis, US), 1 µg/mL recombinant human R-Spondin1 (PeproTech, Rocky Hill, US), 10 mM nicotinamide (MilliporeSigma), 50 ng/mL recombinant human EGF (PeproTech), 100 ng/mL recombinant human FGF-10 (PeproTech), 25 ng/mL Noggin (PeproTech), 10 nM [Leu15]-Gastrin I (MilliporeSigma), 5 µM A83-01 (Tocris Bioscience, Minneapolis, US), 10 µM Forskolin (Tocris Bioscience) and 3 µM Prostaglandin E2 (Tocris Bioscience) (hPO medium). The hPO medium was changed every 2-3 days. and hPOs were passaged every 7-14 days depending on the proliferation rate and organoid size. For passaging, BME droplets were disrupted by pipetting, followed by centrifugation in ice-cold hPO medium. Organoids were sheared into fragments, resuspended in ice-cold liquified BME-2 and subsequently seeded as droplets in pre-warmed CELLSTAR® 48-well suspension culture plates (Greiner Bio-One GmbH, Kremsmünster, Austria). After polymerization for 15 min at 37°C, the organoid-containing BME-2 droplets were covered with hPO medium.

Culturing and experimentation on hPOs were performed by Kaja Nicole Wächtershäuser and Francesco Pampaloni of the Physical Biology Group at the Buchmann Institute for Molecular Life Sciences (BMLS) (Goethe University Frankfurt, Frankfurt am Main).

4.2.4 Induction and imaging of necroptotic cell death in primary hPOs

For necroptosis induction, hPOs were seeded in 5 µL BME-2 droplets in CELLSTAR® 96-well suspension culture plates (Greiner Bio-One) covered with 100 µL hPO medium

and cultured for 3-5 days prior to treatment to allow organoid formation and growth. For pre-treatment with inhibitors HOIPIN-8 or NSA, the hPO medium was exchanged to medium containing the indicated concentration of the respective inhibitors. After 30 min incubation at 37°C, the medium was replaced with medium supplemented with the indicated treatments and the plates were placed in the Zeiss AxioObserver Z1 microscope (Carl Zeiss Microscopy GmbH, Oberkochen, Germany). 24 h time lapse imaging of the hPOs was performed at 37°C and 5% CO_2 in 30 min intervals. Each well was imaged as tiles of two x two with eleven Z-slices of 60 µm thickness.

Following time-lapse imaging, hPOs were subjected to live/dead staining using 10 µg/mL PI (Millipore Sigma), 0.5 µg/mL FDA (Millipore Sigma) and 200 µg/mL Hoe (ThermoFisher Scientific). After 30 min incubation with PI//FDA/Hoe, the dyes were removed and the wells were washed with pre-warmed PBS. Imaging of hPOs was performed with the Zeiss AxioObserver Z1 microscope as described above and images were analyzed and processed using the ZEN 2.6 lite software (Carl Zeiss Microscopy GmbH) and FiJi/ImageJ software.

4.2.5 Generation of CRISPR/Cas9-mediated genetic knockout cell lines

CRISPR/Cas9-mediated stable genetic knockout (KO) of OTULIN, CYLD, OTULIN/CYLD, MLKL and HOIP in HT-29, THP-1, MEF or L-929 cells was generated using two or three gene-specific guideRNAs and control guideRNAs for the control cell lines (Table 8). The guide RNAs were cloned into the LentiCRISPR v2 plasmid (Addgene plasmid #52961) using standard cloning techniques and verified by Sanger DNA sequencing [146]. Plasmids containing guideRNAs targeting human or murine HOIP, as well as a non-targeting control, were kindly provided by Daniel Peeper and Zhengkui Zhang.

4.2.5.1 Production of lentiviral particles and transduction of target cell lines

Lentiviral particles for the transduction of the target cell lines were generated by co-transfection of HEK293T cells with the respective guide RNA-containing vectors and the packaging plasmids pMD2.G (Addgene plasmid #12259) and psPAX2 (Addgene plasmid #12260) using FuGENE HD Transfection Reagent (DNA/transfection reagent ratio 1:3) according to the manufacturer's instructions in DMEM without penicillin/streptomycin. After 24 h, the medium was changed to full DMEM. The viral

supernatant was collected 48 h and 72 h after transfection, sterile filtered through a 0.45 µm filter and either used directly for transduction or stored at -80°C.

The target cell lines were transduced by adding 500 µL of the viral supernatant to the cell culture medium which was supplemented with 8 g/mL polybrene. The medium was exchanged with fresh medium containing 8-12.5 µg/mL puromycin or 10-20 µg/mL blasticidin S 72 h after transduction and the cells were cultured in the selection medium for at least 14 days. The KO efficiency was tested by western blotting and the cells were either subjected to single clone selection or the bulk culture was used for further experiments. For single clone selection, the cells were seeded at 0.5 cells/well in 96-well plates and expanded. The KO was confirmed by western blotting.

4.2.6 RNAi-mediated silencing

Transient knockdown of HOIP, FLOT1 and FLOT2, ALIX (PDCD6IP), charged multivesicular body protein 2A (CHMP2A) and VPS4A in HT-29 cells was performed using the following siRNAs: human siHOIP (RNF31) (Silencer® Select siRNA #1 s30108, #2 s30109, #3 s30110, 40 nM) (Thermo Fisher Scientific), human FLOT1 (ON-TARGETplus Human FLOT1 siRNA SMART POOL, L-010636-00-0010) (Horizon Discovery, Waterbeach, UK), human FLOT2 (ON-TARGETplus Human FLOT2 siRNA SMART POOL, L-003666-01-0010) (Horizon Discovery), human ALIX (PDCD6IP) (ON-TARGETplus Human PDCP6IP siRNA SMART POOL, L-004233-00-0010) (Horizon Discovery), human VPS4A (ON-TARGETplus Human VPS4A siRNA SMART POOL, L-013092-00-0010) (Horizon Discovery), human CHMP2A (ON-TARGETplus Human CHMP2A siRNA SMART POOL, L-020247-01-0010) (Horizon Discovery), non-targeting control siRNA (#4390843, 40 nM) (Thermo Fisher Scientific) (Table 7). For siRNA transfection, siRNA was prepared in Lipofectamine™ RNAiMAX Transfection Reagent (Thermo Fisher Scientific) according to the manufacturer's instructions and mixed with the target cells which were seeded at $0.3x10^5$ cells/cm^2 in medium without penicillin/streptomycin. The medium was exchanged with fresh growth medium 6-8 h after the transfection. After 48 h, the cells were reseeded at $0.4x10^5$ cells/cm^2 and the experiment was performed on the following day.

4.2.7 Western blot analysis

4.2.7.1 Cell lysis and determination of protein concentration

The cells were seeded and treated according to the experiment setup in 6-well, 10 cm or 15 cm cell culture dishes (Greiner BioOne). After treatment, the cells were washed with ice-cold PBS and then lysed in RIPA lysis buffer (supplemented with protease inhibitor complex (PIC), 1 mM sodium orthovanadate, 5 mM sodium fluoride, 1 mM β-glycerophosphate, 1 mM phenylmethylsulfonyl fluoride and Pierce™ Universal Nuclease) or 1% NP-40 lysis buffer (supplemented with PIC, 1 mM sodium orthovanadate, 5 mM sodium fluoride, 1 mM β-glycerophosphate and Pierce™ Universal Nuclease) using a cell scraper. The lysates were incubated on ice for 20-30 min and then centrifuged for 20 min at 18,000 x *g* at 4°C. The supernatant was transferred in a new tube and the protein concentration was determined using the Pierce™ BCA Protein Assay kit (Thermo Scientific) according to the manufacturer's instructions. The quantification was done by measuring absorbance at 550 nm with a Tecan Sunrise™ microplate reader.

4.2.7.2 SDS-PAGE and Western Blotting

For SDS-polyacrylamide gel electrophoresis (SDS-PAGE), 40-50 µg protein were mixed with 6x SDS loading buffer (or non-reducing 6x SDS loading buffer) and incubated for 5 min at 96°C. The samples were loaded onto a polyacrylamide gel and run at 80-150 V for 2-3 h in running buffer. The proteins were transferred to a nitrocellulose membrane by semi-dry blotting. For this purpose, the gel was placed on a blotting buffer-soaked membrane between blotting buffer-soaked filter papers and run at 1-1.5 mA/cm^2 for 1 h and 45 min. The membrane was blocked in 5% milk powder in PBS-T (blocking buffer) for 1 h and then incubated with the respective primary antibodies over night at 4°C. The following day, the membrane was washed three times in PBS-T and then incubated with HRP-coupled secondary antibodies in blocking buffer for 1.5 h at room temperature. After three washing steps with PBS-T, signals were detected in a dark room using Pierce™ ECL Western Blotting Substrate (Thermo Fisher Scientific) or Thermo Scientific™ SuperSignal™ West Femto Chemiluminescent Substrate (Thermo Fisher Scientific) according to the manufacturer's instructions. Stripping of primary antibodies was performed by

incubation of the membrane in a 0.4 M NaOH solution (stripping buffer) for 10 min at room temperature. After three washing steps with PBS-T and 1 h incubation in blocking buffer the membrane was incubated with fresh primary antibodies over night at 4°C. All antibodies used in this study are listed in Table 5. Representative blots of at least two independent experiments are shown unless stated otherwise. If the samples of one experiment are detected on multiple Western blotting membranes, only one representative loading control is shown for clarity.

4.2.8 RIPK3 immunoprecipitation

For RIPK3 immunoprecipitation, RIPK3 expression in HT-29 RIPK3 KO cells re-expressing PAM-mutated doxycycline (Dox)-inducible Strep-tagged RIPK3 WT was induced by adding 1 µg/mL Dox 6 h after seeding. Before treatment, the medium was exchanged to fresh medium. Cells were lysed in 1% NP-40 lysis buffer (as described above) and immunoprecipitation of Strep-RIPK3 was performed using MagStrep "type3" XT beads (IBA Lifesciences GmbH, Göttingen, Germany). The beads were washed twice in 1% NP-40 lysis buffer and incubated with 1.8-2 mg protein over night at 4°C on a rotating wheel and subsequently washed five times with TBS-T using a magnetic separator, followed by incubation in 2x SDS loading buffer for 5 min at 96°C and western blotting.

4.2.9 UBAN pulldown

For enrichment of M1-ubiquitinated proteins, $0.8x10^5$ cells/cm^2 were seeded in full medium in 10 m cell culture dishes (Greiner BioOne) the day before treatment. After treatment, the cells were washed in ice-cold PBS and lysed using 1% NP-40 lysis buffer (supplemented with PIC, 1 mM sodium orthovanadate, 5 mM sodium fluoride, 1 mM β-glycerophosphate and Pierce™ Universal Nuclease). For the pulldown, 100 µL GST-tagged UBAN-coupled [363] Glutathione MagBeads (Genscript, Piscataway, NJ, USA) were washed twice with 1% NP-40 lysis buffer and then incubated with 1.5-2 mg protein over night at 4°C on a rotating wheel. On the next day, the beads were washed 5 times with TBS-T buffer and then incubated in 2x SDS loading buffer for 5 min at 96°C followed by western blot analysis.

4.2.10 RNA isolation, cDNA synthesis and quantitative real-time PCR

Relative gene expression levels were determined using quantitative real-time reverse transcription (qRT)-PCR. For this purpose, the cells were seeded at $0.4x10^5$ cells/cm^2 in 6-well cell culture dishes (Greiner BioOne) the day before the treatment. After treatment, the cell culture medium was removed and RNA isolation was performed using the peqGOLD Total RNA Kit (VWR Life Science, Radnor, PA, USA) according to the manufacturer's instructions. RNA concentration and purity were determined with a NanoDrop 1000 Spectrometer. cDNA synthesis was performed with 1 µg RNA using The RevertAid H Minus First Strand cDNA Synthesis Kit (Thermo Scientific) according to the manufacturer's protocol. The cDNA samples were analyzed by SYBR green-based qRT-PCR with the QuantStudio™ 7 Flex Real-Time PCR System (Applied Biosystems, Waltham, MA, USA). At least three independent experiments were performed in triplicates. Relative gene expression was determined using the ΔΔct-method and expression levels of the target genes were normalized against *18S* or *RPII* gene expression.

4.2.11 Massive Analysis of cDNA Ends (MACE-seq)

Massive Analyses of cDNA Ends (MACE-Seq) was performed by GenXPro GmbH (Frankfurt am Main) using the MACE-Seq kit according to the manufacturer's protocol. cDNA generation from fragmented RNA was performed using barcoded poly-A primers during reverse transcription. Following second-strand synthesis and 5' adapter integration, a library was produced by PCR with minimum number of cycles and subsequently sequenced on an Illumina NextSeq500 machine with 1x 75 bps [364].

For MACE seq analysis, raw data were pre-processed using Cutadapt [357] in order to eliminate bad-quality base reads and poly-A-tails. FastQC was used to assess the quality of sequencing after trimming and cleaned reads were mapped and quantified with a reference genome using STAR [358]. ENSEMBL-GTF data were used to provide genomic locations for quantification as well as additional data for annotation (gene name, gene description, Gene Ontology (GO) terms, etc.) and DESeq2 [359] was used to perform differential expression analysis. The final results table was generated that includes significance parameters (P value, FDR) and log2FoldChanges and significantly expressed and differentially regulated genes were visualized using custom R scripts.

4.2.12 Immunofluorescence staining

For immunofluorescence staining, the cells were seeded at 0.6x10^5 cells/cm^2 in 96-well black clear-bottom plates (Greiner BioOne) the day before the treatment. After stimulation, prewarmed 8% paraformaldehyde solution (PFA) was added to the cells (EC 4% PFA) and incubated for 15 min at room temperature for fixation. The PFA solution was removed and the cells were permeabilized by incubation in 0.1% TritonX in PBS for 15 min at room temperature. The cells were then washed three times with PBS, followed by 30 min incubation in antibody dilution buffer (ADB). The primary antibody against phospho-MLKL was prepared in ADB (1:100) and incubated with the cells over night at 4°C. After five washing steps with PBS, the cells were incubated with secondary antibodies (1:800) and DAPI (1:5,000) prepared in ADB for 1.5 h at room temperature in the dark, followed by three washing steps with PBS. IF analysis was performed using the ImageXpress Micro XLS Widefield High-Content Analysis System (Molecular Devices) and analyzed using the MetaXpress® Software (Molecular Devices). Image formatting was performed using ImageJ.

4.2.13 Isolation of exosomes

For the isolation of exosomes from the cell culture supernatant, 0.6x10^5 cells/cm^2 were seeded in 10 cm cell culture dishes (Greiner BioOne) in 10 mL full medium the day before the treatment. The following day, the cell culture medium was removed, cells were washed with PBS and 2.5 mL FBS-free medium was added. The cells were treated by adding 20x solution of the respective compounds or the respective volume of medium as a control. After treatment, the cell culture supernatant was centrifuged at 2,000 x *g* for 30 min at 4°C in order to remove cell debris. The supernatant was then divided and transferred into three 1.5 mL tubes, mixed with Total Exosome Isolation Reagent (from cell culture media) (Thermo Scientific) according to the manufacturer's instructions and incubated overnight at 4°C. The samples were centrifuged for 1 h at 10,000 x *g* at 4°C. The supernatant was discarded and the pellet of the first tube was resuspended in RIPA lysis buffer and subsequently transferred into the second tube and third tube. The pooled lysate was incubated on ice for 30 min. An appropriate amount of 6x SDS loading buffer was added and the samples were incubated at 96°C for 5 min. The whole samples were loaded onto a polyacrylamide gel followed by western blot analysis.

4.2.14 Cell fractionation

Cell fractionation by phase separation was performed using Triton X-114 (Merck Sigma) lysis buffer. The cells were seeded in 15 cm cell culture dishes (Greiner BioOne) at $0.8x10^5$ cells/cm^2 the day before treatment. For cell lysis, cells were incubated in Triton X-114 lysis buffer (supplemented with PIC, 1 mM sodium orthovanadate, 5 mM sodium fluoride and 1 mM β-glycerophosphate) for 30 min on ice, followed by centrifugation at 15,000 x *g* and 4°C. 40-50 µg of the cleared lysate was incubated with 6x SDS loading dye and boiled for 5 min at 96°C (input). The remaining lysate was warmed at 30°C for 4 min and centrifuged at 1,500 x *g* for 5 min. The aqueous layer was transferred into a new tube and centrifuged at 1,500 x *g* for 5 min in order to remove contamination from the detergent-enriched phase. The detergent-enriched phase was washed twice with basal buffer by centrifugation at 1,500 x *g* for 5 min followed by dilution in basal buffer. The protein concentration of both the aqueous and detergent-enriched fraction was determined and 40-60 µg protein were mixed with an appropriate amount of 6x SDS loading dye, incubated for 5 min at 96°C and then analyzed by western blotting.

4.2.15 Statistical analysis

Statistical analysis was performed using the GraphPad Prism 9 Software (GraphPad Software, La Jolla CA, USA). Statistical significance was determined using ordinary one-way ANOVA or 2-way ANOVA followed by Dunnett's, Tukey's or Sidak's multiple comparisons test. *P* values < 0.05 are considered significant and depicted as follows: $P \leq 0.05$: *, $P \leq 0.01$: **, $P \leq 0.001$: ***, $P \leq 0.0001$: ****, ns: not significant.

5 Results

Parts of the following work are described in the manuscript “Species-specific LUBAC-mediated M1 ubiquitination regulates necroptosis by segregating the cellular distribution and fate of activated MLKL” (bioRxiv 2022.12.08.519265; doi: https://doi.org/10.1101/2022.12.08.519265) [365]. Experimentation on hPOs and data analyses were performed by Kaja Nicole Wächtershäuser and Francesco Pampaloni of the Physical Biology Group at the Buchmann Institute for Molecular Life Sciences (BMLS) (Goethe University Frankfurt, Germany). MACE-seq-based transcriptome analysis was performed by Leonard Feist and Björn Rotter from GenXPro GmbH (Frankfurt am Main, Germany) and further data analyses and visualization were performed by Geoffroy Andrieux, Tonmoy Das and Melanie Börries at the Institute of Medical Bioinformatics and Systems Medicine of the Medical Center-University of Freiburg (Faculty of Medicine, University of Freiburg, Germany). Sonja Smith provided support with qPCR and ELISA experiments.

5.1 Roles of the DUBs OTULIN and CYLD in TNFR1-mediated cell fate control

5.1.1 OTULIN and CYLD KO result in increased levels of M1 poly-Ub

Cell fate decisions are critically regulated by DRs such as TNFR1 and the balance of ubiquitination and de-ubiquitination of proteins by E3 ligases and DUBs plays a critical role in death receptor-induced cell fate control [366]. Since both CYLD and the M1 Ub-specific DUB OTULIN interact with LUBAC, which mediates M1 poly-ubiquitination of several proteins at the TNFR1 RSC resulting in pro-survival gene-activation signaling via NF-κB and MAPKs [237, 288, 366], we aimed to characterize how the interplay of these DUBs affects the balance between M1/K63 Ub and cell fate decisions. For this purpose, we used the HT-29 human colon carcinoma cell line to generate stable OTULIN KO, CYLD KO and combined OTULIN/CYLD KO cell lines as well as a non-human target (nht) control cell line using CRISPR/Cas9-mediated genome editing (Figure 5A). Loss of OTULIN lead to a marked increase of total M1 poly-Ub levels (Figure 5B), which is in accordance with previous findings [73, 295, 296], while depletion of CYLD only slightly increased M1 poly-Ub levels (Figure 5B). Combined

deletion of OTULIN and CYLD resulted in even higher levels of M1 poly-Ub compared to OTULIN KO (Figure 5B). K63 poly-Ub and total Ub levels remained unchanged in OTULIN KO, CYLD and OTULIN/CYLD KO cell lines as compared to the control cells (Figure 5C-D). Of note, loss of OTULIN lead to a reduction of HOIP and HOIL-1 protein levels and combined KO of OTULIN and CYLD resulted in undetectable levels of HOIP and HOIL-1 and strongly reduced levels of Sharpin (Figure 5E), while mRNA levels of all three LUBAC subunits remained relatively stable (Figure 5F).

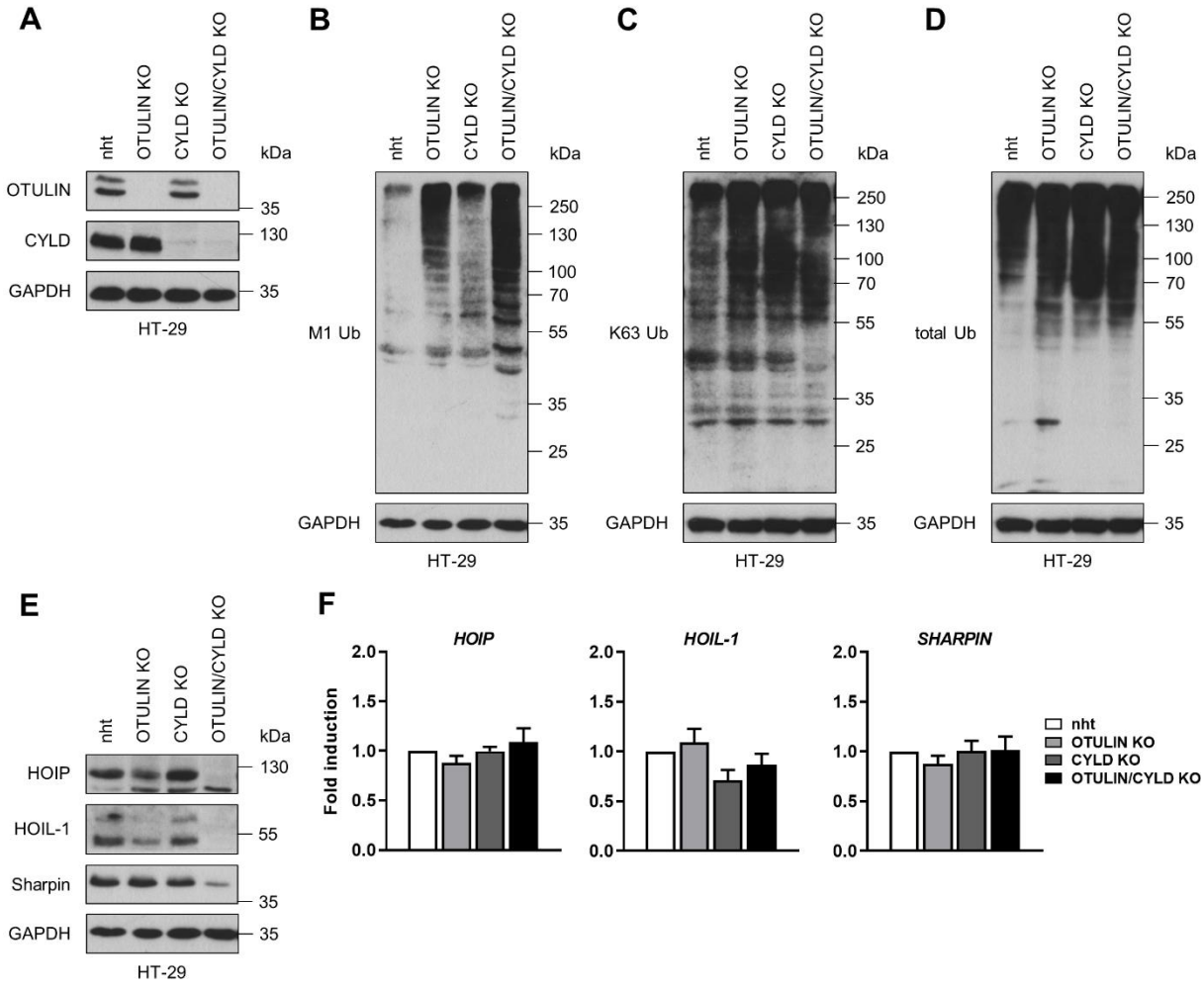

Figure 5. CRISPR/Cas9-mediated KO of OTULIN and CYLD and combined OTULIN/CYLD KO in HT-29 result in increased M1 poly-Ub levels.

A Expression of OTULIN an CYLD in control (nht), OTULIN KO, CYLD KO and combined OTULIN/CYLD KO HT-29 cell lines. GAPDH was used as loading control. Representative blots of two independent experiments are shown. **B-D** M1 poly-Ub (B), K63 poly-Ub (C) and total Ub (D) levels in control (nht), OTULIN KO, CYLD KO and combined OTULIN/CYLD KO HT-29 cell lines. GAPDH was used as loading control. C and D share the same loading control since both signals were detected on one membrane. Representative blots of two independent experiments are shown. **E** HOIP, HOIL-1 and Sharpin

Figure 5. Continued.

expression in control (nht), OTULIN KO, CYLD KO and combined OTULIN/CYLD KO HT-29 cell lines. GAPDH was used as loading control. Representative blots of two independent experiments are shown. **F** mRNA expression levels of *HOIP*, *HOIL-1* and *SHARPIN* in control (nht), OTULIN KO, CYLD KO and combined OTULIN/CYLD KO HT-29 cell lines. Gene expression was normalized against *28S* mRNA expression and is presented as x-fold mRNA expression compared to the control (nht). Mean and SEM of at least three independent experiments are shown.

Several studies have found that LUBAC subunits are differentially expressed in different cell types that are deficient of OTULIN. Loss of OTULIN leads to decreased levels of HOIP and Sharpin in fibroblasts of ORAS patients [290, 296] as well as in MEFs with catalytic inactive OTULIN (OTULIN C129A) [277] and murine OTULIN-deficient B and T cells [295]. Interestingly, LUBAC levels remain stable in murine myeloid OTULIN KO cells [295] and after stable shRNA-mediated knockdown of OTULIN in human THP-1 monocytes [290], suggesting a cell type-specific regulation of LUBAC expression. We therefore generated stable CRISPR/Cas9-mediated OTULIN KO, CYLD KO and combined OTULIN/CYLD KO THP-1 cell lines (Figure 6A) and evaluated the expression levels of M1 poly-Ub and LUBAC subunits. Similar to the HT-29 KO cell lines, OTULIN and combined OTULIN/CYLD KO lead to strong increases in M1 poly-Ub, but CYLD KO alone did not alter M1 poly-Ub levels in THP-1 cells (Figure 6B). Surprisingly and in contrast to the abovementioned findings [290], HOIP, HOIL-1 and Sharpin protein expression levels were strongly reduced in OTULIN KO and combined OTULIN/CYLD KO THP-1 cells (Figure 6C), which resembled the effects of OTULIN and OTULIN/CYLD KO in HT-29 cell lines (Figure 5E).

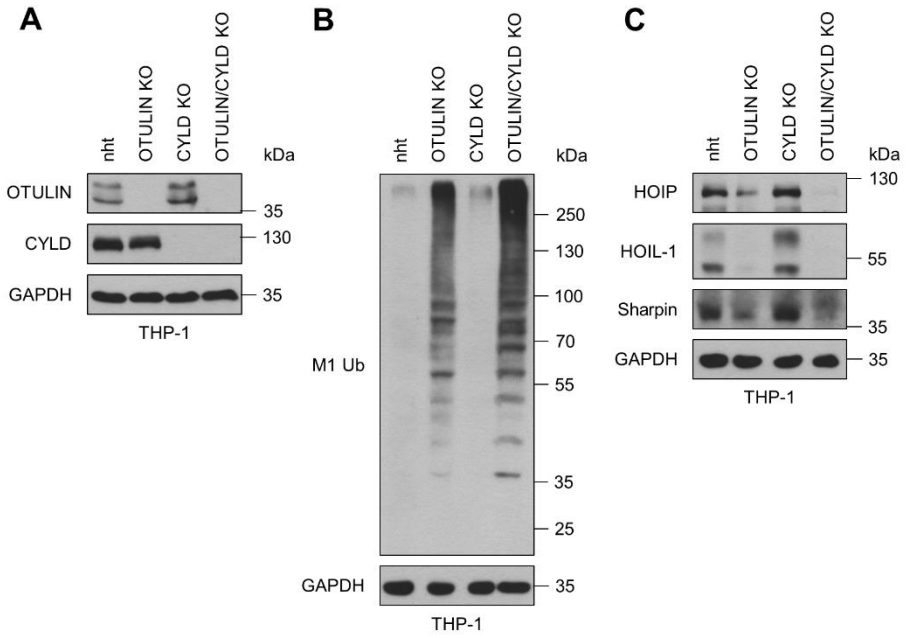

Figure 6. CRISPR/Cas9-mediated KO of OTULIN and CYLD and combined OTULIN/CYLD KO in THP-1 cells results in increased M1 poly-Ub levels.

A Expression of OTULIN an CYLD in control (nht), OTULIN KO, CYLD KO and combined OTULIN/CYLD KO THP-1 cell lines. GAPDH was used as loading control. Representative blots of two independent experiments are shown. **B** M1 poly-Ub expression in control (nht), OTULIN KO, CYLD KO and combined OTULIN/CYLD KO THP-1 cell lines. GAPDH was used as loading control. Representative blots of two independent experiments are shown. **C** HOIP, HOIL-1 and Sharpin expression in control (nht), OTULIN KO, CYLD KO and combined OTULIN/CYLD KO THP-1 cell lines. GAPDH was used as loading control. Representative blots of two independent experiments are shown.

5.1.2 Combined OTULIN/CYLD KO results in impaired TNFα-induced NF-κB signaling

To investigate the effects of OTULIN and/or CYLD KO on NF-κB activation, the basal and phosphorylated levels of IκBα and NF-κB p65 subunit were determined by western blotting after stimulation of HT-29 and THP-1 cell lines with human recombinant TNFα. OTULIN counteracts LUBAC-mediated M1 poly-Ub generation and NF-κB activation [299] and accordingly, OTULIN deficiency in HT-29 lead to slightly increased levels of phosphorylated IκBα and NF-κB p65 as compared to the control cells after stimulation with TNFα (Figure 7A), however in THP-1 OTULIN KO cells, no overt effects were visible (Figure 7D). Loss of CYLD resulted in decreased expression of IκBα and slightly increased phosphorylation of NF-κB p65 compared to the control cells after stimulation with TNFα (Figure 7B and D). Interestingly, combined deletion of OTULIN and CYLD lead to defective NF-κB activation characterized by stabilization of IκBα levels and delayed phosphorylation of IκBα and NF-κB p65 (Figure 7C-D).

Of note, loss of OTULIN in HT-29 cells did not affect basal mRNA expression levels of NF-κB target genes *TNFA*, *NFKBIA* (NF-κB inhibitor alpha), *CXCL8* and *TNFAIP3* (Figure 7E). In line with its role in the regulation of Ub levels of key NF-κB signaling molecules, loss of CYLD lead to an increased expression of *TNFA*, *NFKBIA*, *CXCL8* and *TNFAIP3* mRNA (Figure 7E), consistent with previous data showing that CYLD deficiency results in pro-inflammatory gene expression through constitutive NF-κB activation [74-76]. Interestingly, combined loss of OTULIN/CYLD also increased basal *CXCL8* mRNA expression levels (Figure 7E).

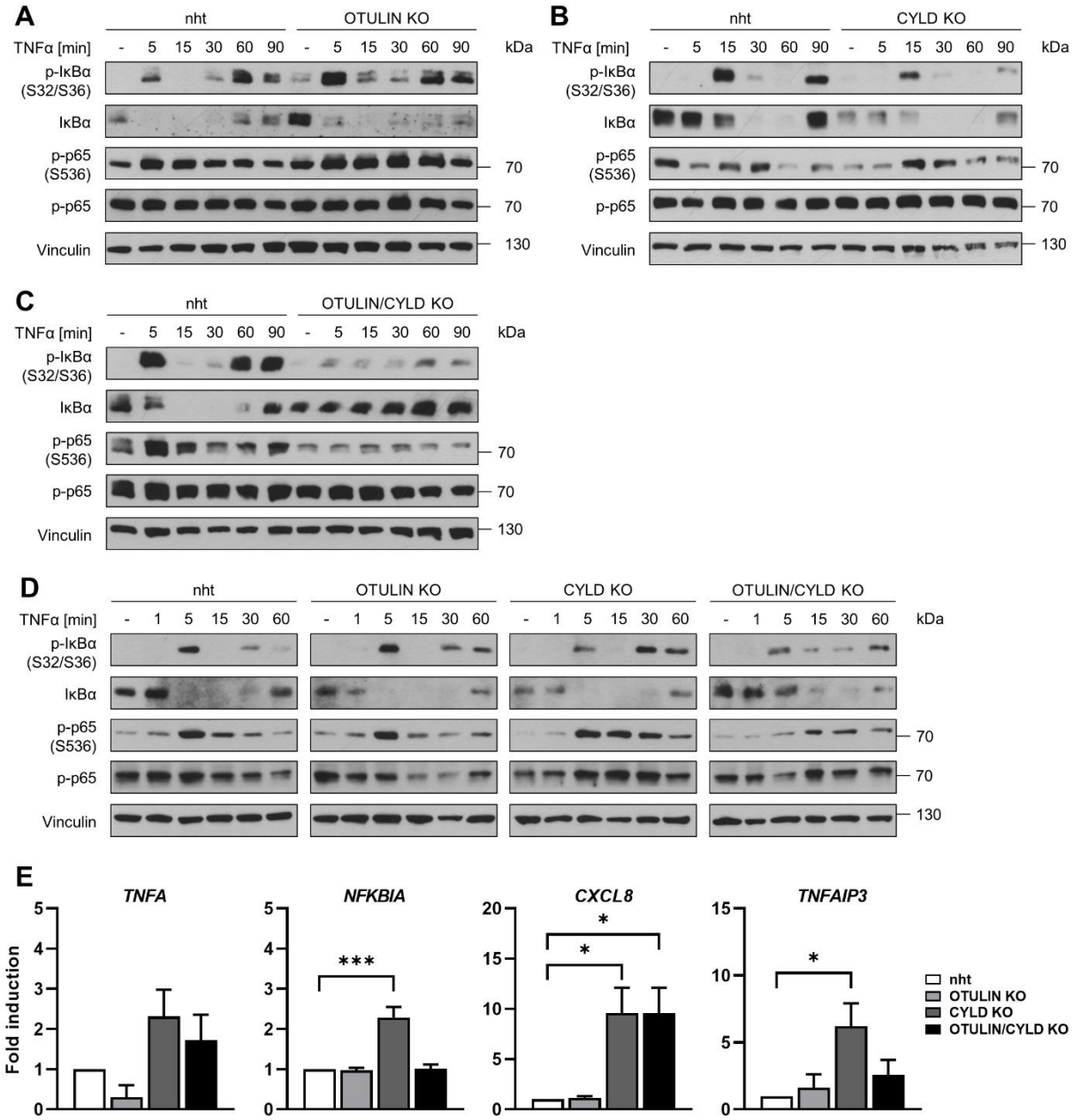

Figure 7. NF-κB activation in OTULIN KO, CYLD KO and combined OTULIN/CYLD KO cell lines.

Figure 7. Continued.

A-C Expression of total and phosphorylated IκBα and NF-κB p65 subunit in control (nht), OTULIN KO (A), CYLD KO (B) and combined OTULIN/CYLD KO (C) HT-29 cell lines after treatment with 10 ng/mL TNFα for the indicated time points. Cells were starved in cell culture medium containing 1% FBS for 2 h prior to treatment. Vinculin was used as loading control. Representative blots of at least two independent experiments are shown. **D** Expression of total and phosphorylated IκBα and NF-κB p65 subunit in control (nht), OTULIN KO, CYLD KO and combined OTULIN/CYLD KO THP-1 cell lines after treatment with 10 ng/mL TNFα for the indicated time points. Cells were starved in cell culture medium containing 1% FBS overnight prior to treatment. Vinculin was used as loading control. Representative blots of at least two independent experiments are shown. **E** mRNA expression levels of *TNFA* (A), *NFKBIA* (B), *CXCL8* (C) and *TNFAIP3* (D) in control (nht), OTULIN KO, CYLD KO and combined OTULIN/CYLD KO HT-29 cell lines. Gene expression was normalized against *28S* mRNA expression and is presented as x-fold mRNA expression compared to the control (nht). Mean and SEM of at least three independent experiments are shown. **P*<0.05; ****P*<0.001.

5.1.3 Combined OTULIN/CYLD KO sensitizes cells towards TNFα-induced cell death

Although OTULIN has been shown to counteract NF-κB signaling and its deletion increases NF-κB activation, several studies suggest a role of OTULIN in the regulation of cell death as loss of OTULIN or expression of catalytic inactive OTULIN sensitizes cells towards TNFα-induced apoptotic and necroptotic cell death [277, 290, 291, 294, 300]. CYLD controls cell death induction, e.g., through deubiquitination of RIPK1 at TNFR1 complex I, thereby inducing the formation of the cell death-inducing complexes IIa/b or the necrosome [73, 310, 367]. Interestingly, OTULIN or CYLD deletion in HT-29 cells did not affect TBZ (TNFα/BV6/zVAD.fmk)-induced necroptosis or TB (TNFα/BV6)-induced apoptosis (Figure 8A-B) as determined by high-content imaging-based quantification of PI-positive cells. However, combined deletion of OTULIN and CYLD sensitized HT-29 cells towards TB-induced apoptosis and induced cell death in cells treated with TNFα (10 ng/mL) alone (Figure 8B-C).

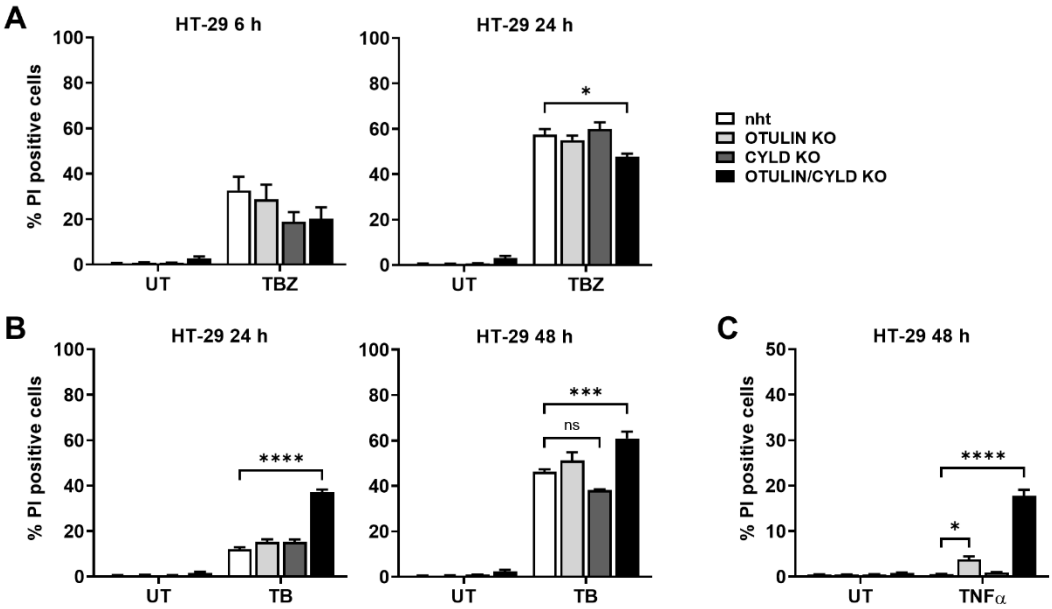

Figure 8. Effects of OTULIN KO, CYLD KO and combined OTULIN/CYLD KO on TNFα-, TB or TBZ-induced cell death in HT-29 cells.

A Quantification of cell death in control (nht), OTULIN KO, CYLD KO and combined OTULIN/CYLD KO HT-29 cell lines after treatment with TBZ (10 ng/mL TNFα, 1 µM BV6, 20 µM zVAD.fmk) for the indicated time points. Mean and SEM of n=3 independent experiments are shown. **B** Quantification of cell death in control (nht), OTULIN KO, CYLD KO and combined OTULIN/CYLD KO HT-29 cell lines after treatment with TB (10 ng/mL TNFα, 5 µM BV6) for the indicated time points. Mean and SEM of n=3 independent experiments are shown. **C** Quantification of cell death in control (nht), OTULIN KO, CYLD KO and combined OTULIN/CYLD KO HT-29 cell lines after treatment with TNFα (10 ng/mL) for 48 h. Mean and SEM of n=3 independent experiments are shown.

**P*<0.05; ****P*<0.001; *****P*<0.0001; ns: not significant.

In THP-1 cells, CYLD KO resulted in slightly decreased levels of cell death compared to the control cells after treatment with TBZ, TB or TNFα (Figure 9A-C) while OTULIN KO had no effect on cell death induction. In contrast to HT-29 cell lines, combined OTULIN/CYLD depletion only slightly increased cell death in THP-1 cells (Figure 9A-C).

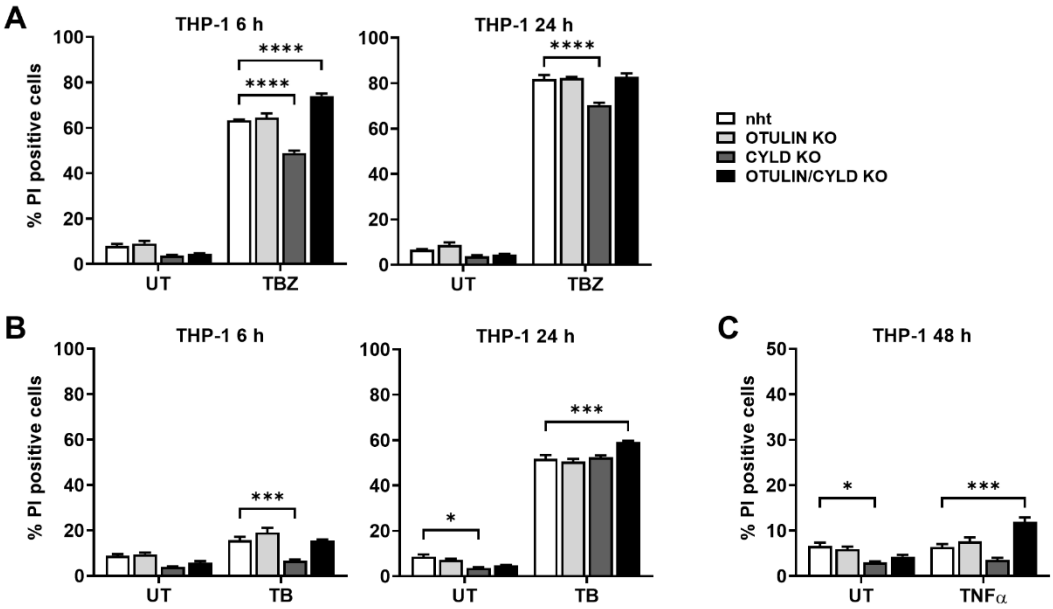

Figure 9. Effects of OTULIN KO, CYLD KO and combined OTULIN/CYLD KO on TNFα-, TB or TBZ-induced cell death THP-1 cells.

A Quantification of cell death in control (nht), OTULIN KO, CYLD KO and combined OTULIN/CYLD KO THP-1 cell lines after treatment with TBZ (10 ng/mL TNFα, 1 µM BV6, 20 µM zVAD.fmk) for the indicated time points. Mean and SEM of n=3 independent experiments are shown. **B** Quantification of cell death in control (nht), OTULIN KO, CYLD KO and combined OTULIN/CYLD KO THP-1 cell lines after treatment with TB (10 ng/mL TNFα, 5 µM BV6) for the indicated time points. Mean and SEM of n=3 independent experiments are shown. **C** Quantification of cell death in control (nht), OTULIN KO, CYLD KO and combined OTULIN/CYLD KO THP-1 cell lines after treatment with TNFα (10 ng/mL) for 48 h. Mean and SEM of n=3 independent experiments are shown.

*P<0.05; ***P<0.001; ****P<0.0001.

5.2 Roles of LUBAC-mediated M1 poly-Ub in the regulation of necroptosis

5.2.1 The effect of LUBAC deficiency on necroptotic cell death

5.2.1.1 Inhibition of LUBAC with HOIP inhibitors prevents necroptotic cell death in human cell lines

Since M1 poly-Ub is exclusively generated by the E3 Ub ligase complex LUBAC, we used the small molecule inhibitor HOIPIN-8 [285, 368] to assess the effect of LUBAC inhibition on TNFR1-mediated signaling. HOIPIN-8 has been shown to effectively suppress M1 poly-Ub generation and TNFα-induced NF-κB signaling by inhibiting the catalytic activity of HOIP [285, 286] without inducing cytotoxicity. Indeed, 24 h treatment of HT-29 OTULIN KO, CYLD KO and OTULIN/CYLD KO cell lines with 30 µM HOIPIN-8 completely suppressed M1 poly-Ub generation (Figure 10A). HOIPIN-8 pre-treatment also effectively blocked TNFα-induced NF-κB signaling, characterized by delayed phosphorylation of IκBα and stabilization of IκBα levels (Figure 10B).

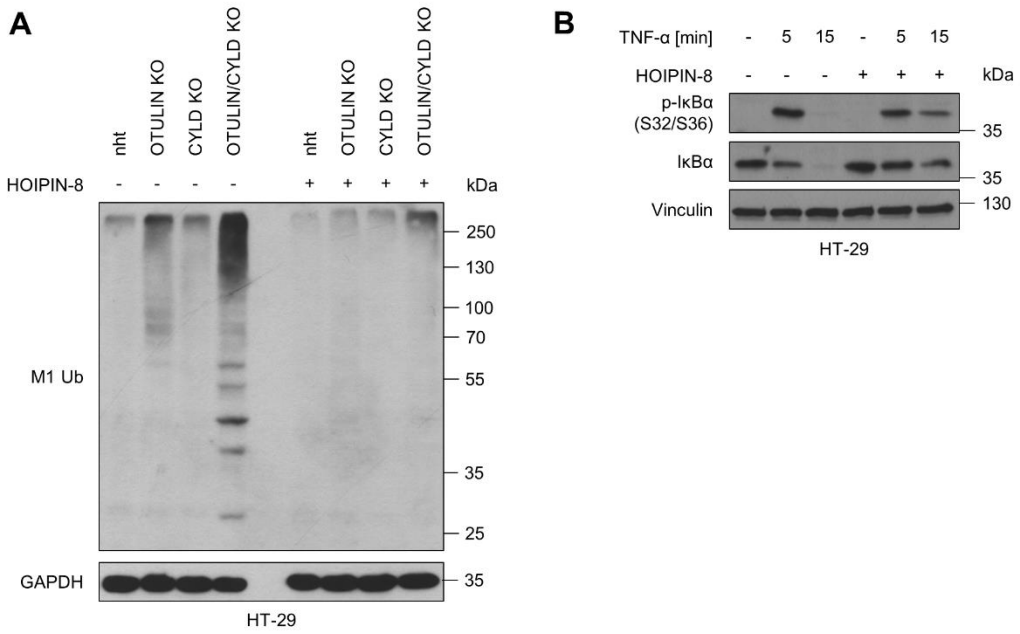

Figure 10. HOIPIN-8 inhibits LUBAC-induced M1 poly-Ub and TNFα-induced NF-kB activation in HT-29 cells.

A Expression of M1 poly-Ub in control (nht), OTULIN KO, CYLD KO and combined OTULIN/CYLD KO HT-29 cell lines after treatment with HOIPIN-8 (30 µM) for 24 h. GAPDH was used as loading control.

Figure 10. Continued.

n=1 is shown. **B** Expression of phosphorylated and total IκBα levels in control and HOIPIN-8 (30 µM)-pre-treated HT-29 WT cells after treatment with TNFα (10 ng/mL) for the indicated time points. Vinculin was used as loading control. Representative blots of two independent experiments are shown.

Intriguingly, inhibition of LUBAC activity with HOIPIN-8 not only blocked TNFα-induced NF-κB activation but also rescued TBZ-induced necroptotic cell death in HT-29 and THP-1 cells in a time-dependent manner (Figure 11A-B). In line with these results, chemical inhibition of LUBAC with the mycotoxin gliotoxin [282] also effectively rescued necroptosis in both HT-29 and THP-1 cells (Figure 11C-D).

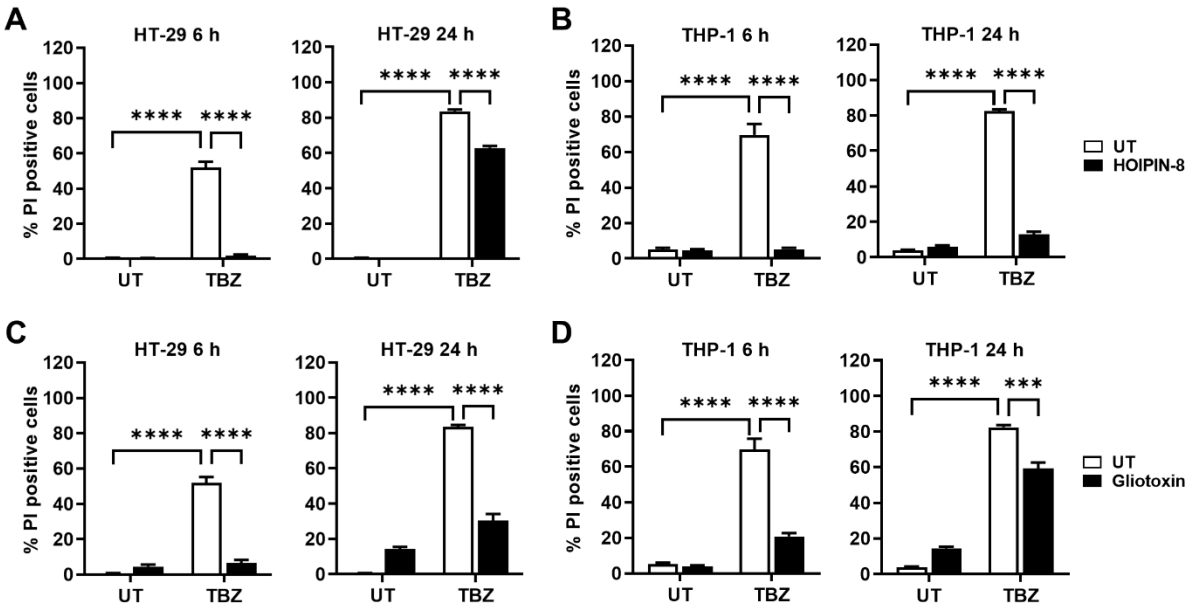

Figure 11. LUBAC inhibition with HOIPIN-8 or gliotoxin blocks TBZ-induced necroptosis in HT-29 and THP-1 cells.

A-B Quantification of cell death in control (UT) or HOIPIN-8 (30 µM)-pre-treated HT-29 (A) or THP-1 (B) cells after treatment with TBZ (10 ng/mL TNFα, 1 µM BV6, 20 µM zVAD.fmk) for the indicated time points. Mean and SEM of n=3 independent experiments are shown. **C-D** Quantification of cell death in control (UT) or gliotoxin (1 µM)-pre-treated HT-29 (C) or THP-1 (D) cells after treatment with TBZ (10 ng/mL TNFα, 1 µM BV6, 20 µM zVAD.fmk) for the indicated time points. Mean and SEM of n=3 independent experiments are shown.

***P<0.001; ****P<0.0001.

In agreement with the effects of HOIPIN-8 on necroptotic cell death, total cellular M1 poly-Ub levels increased upon induction of necroptosis in both HT-29 and THP-1 cells and this increase could be efficiently blocked by LUBAC inhibition with HOIPIN-8 (Figure 12A-B). Importantly, M1 poly-Ub levels were even higher in cells treated with

TBZ as compared to cells treated with TB or TNFα alone (Figure 12C), suggesting that necroptosis-induced increases of M1 poly-Ub are not solely the consequence of TNFα-induced NF-κB signaling. To exclude the possibility that alterations in LUBAC abundance are responsible for the increased M1 poly-Ub levels during necroptosis, the expression levels of LUBAC subunits HOIP, HOIL-1 and Sharpin were determined by western blotting. Intriguingly, LUBAC protein levels did not change upon induction of necroptosis with TBZ or after LUBAC inhibition with HOIPIN-8 (Figure 12D), indicating that neither induced expression nor selective loss of LUBAC is the cause of the observed effects on M1 poly-Ub levels during necroptosis and upon treatment with HOIPIN-8.

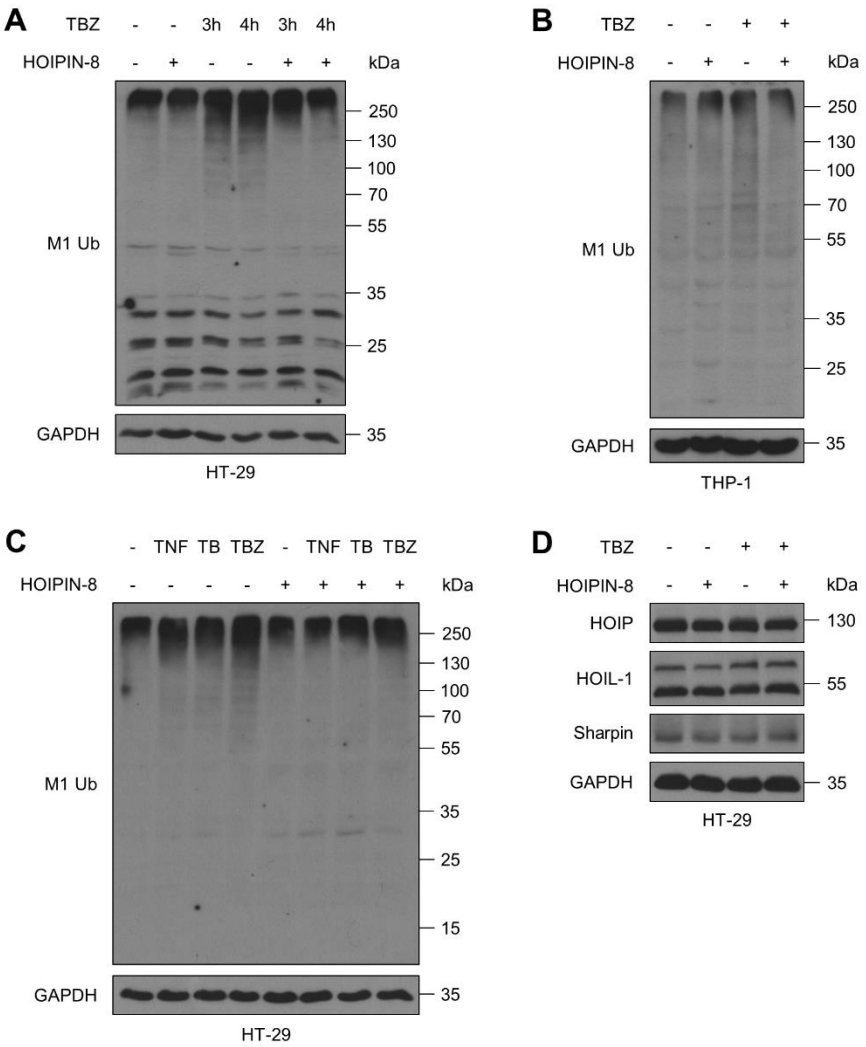

Figure 12. TBZ-induced necroptosis results in increased M1 poly-Ub levels which can be prevented by LUBAC inhibition with HOIPIN-8.

A Expression of M1 poly-Ub in control and HOIPIN-8 (30 µM)-pre-treated HT-29 cells after treatment with TBZ (10 ng/mL TNFα, 1 µM BV6, 20 µM zVAD.fmk) for the indicated time points. GAPDH was used

Figure 12. Continued.

as loading control. Representative blots of at least two independent experiments are shown. **B** Expression of M1 poly-Ub in control and HOIPIN-8 (30 µM)-pre-treated THP-1 cells after treatment with TBZ (10 ng/mL TNFα, 1 µM BV6, 20 µM zVAD.fmk) for 3 h. GAPDH was used as loading control. Representative blots of at least two independent experiments are shown. **C** Expression of M1 poly-Ub in control or HOIPIN-8 (30 µM)-pre-treated HT-29 cells treated with TNFα (10 ng/mL), TB (10 ng/mL TNFα, 5 µM BV6) or TBZ (10 ng/mL TNFα, 1 µM BV6, 20 µM zVAD.fmk) for 4 h. GAPDH was used as loading control. Representative blots of at least two independent experiments are shown. **D** Expression of LUBAC subunits HOIP, HOIL-1 and Sharpin in control and HOIPIN-8 (30 µM)-pre-treated HT-29 cells after treatment with TBZ (10 ng/mL TNFα, 1 µM BV6, 20 µM zVAD.fmk) for 4 h. GAPDH was used as loading control. Representative blots of at least two independent experiments are shown.

To confirm the effects of HOIPIN-8 and gliotoxin on necroptosis induction, we performed siRNA-mediated knockdown of HOIP expression in HT-29 cells. Depletion of HOIP expression resulted in decreased necroptotic cell death (Figure 13A-B) and blocked necroptosis-induced increases of M1 poly-Ub levels (Figure 13C).

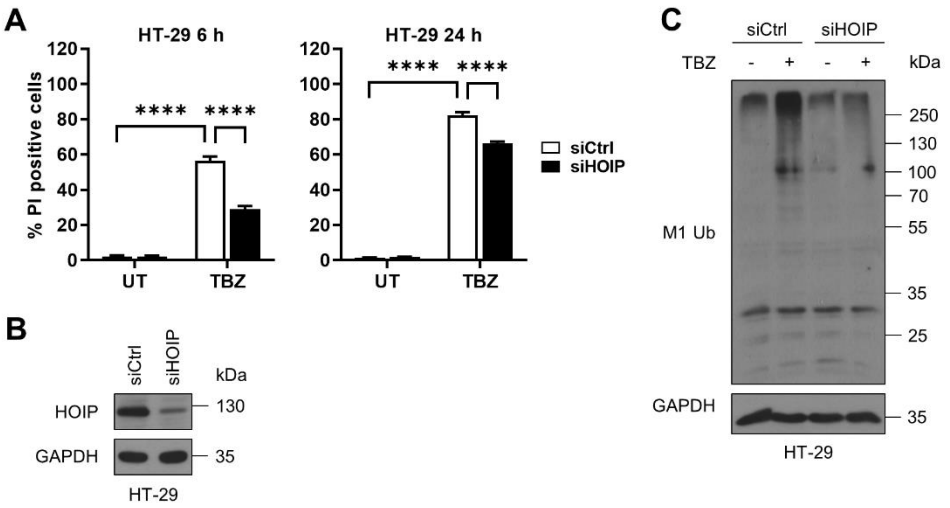

Figure 13. siRNA-mediated HOIP knockdown blocks TBZ-induced cell death and M1 poly-Ub levels in HT-29 cells.

A Quantification of cell death in control (siCtrl) and HOIP knockdown (siHOIP) HT-29 cells after treatment with TBZ (10 ng/mL TNFα, 1 µM BV6, 20 µM zVAD.fmk) for the indicated time points. Mean and SEM of n=3 independent experiments are shown. ****P<0.0001. **B** Expression of HOIP in control (siCtrl) and HOIP knockdown (siHOIP) HT-29 cells. GAPDH was used as loading control. Representative blots of at least two independent experiments are shown. **C** Expression of M1 poly-Ub in control (siCtrl) and HOIP knockdown (siHOIP) HT-29 cells after treatment with TBZ (10 ng/mL TNFα, 1 µM BV6, 20 µM zVAD.fmk) for 4 h. GAPDH was used as loading control. Representative blots of at least two independent experiments are shown.

5.2.1.2 Inhibition of LUBAC with HOIPIN-8 does not affect necroptotic signaling

To further understand how LUBAC-mediated M1 poly-Ub regulates necroptosis, the effect of LUBAC inhibition on necroptotic signaling was determined. TBZ induces necroptosis via activation of RIPK1 and RIPK3 which form the amyloid-like necrosome to recruit MLKL. Surprisingly, inhibition of LUBAC activity with HOIPIN-8 in HT-29 and THP-1 cells did not reduce necroptosis-induced phosphorylation of RIPK1 at S166, RIPK3 at S277 or MLKL at S358, all of which represent major checkpoints in necroptosis signaling (Figure 14A-B). In contrast, treatment with HOIPIN-8 induced a slight accumulation of phosphorylated RIPK1, RIPK3 and MLKL (Figure 14A-B, see also Figure 16), suggesting alternative effects of LUBAC on the core necroptotic machinery. Similar to the effects observed with HOIPIN-8, siRNA-mediated knockdown of HOIP expression did not affect necroptotic signaling as well (Figure 14C).

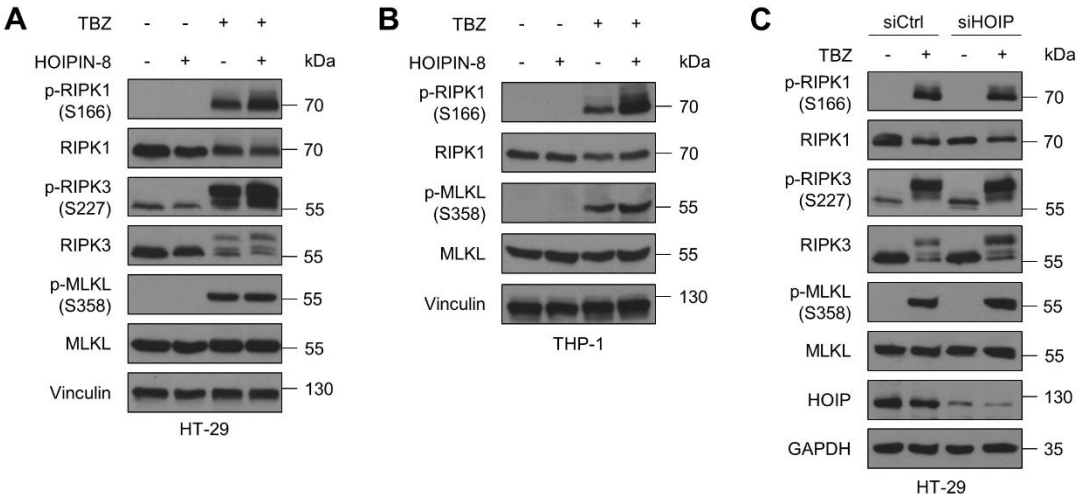

Figure 14. Loss of LUBAC function does not reduce TBZ-induced phosphorylation of RIPK1, RIPK3 and MLKL.

A Western blot analysis of phosphorylated and total expression levels of RIPK1, RIPK3 and MLKL in control versus HOIPIN-8 (30 µM)-pre-treated HT-29 cells upon treatment with TBZ (10 ng/mL TNFα, 1 µM BV6, 20 µM zVAD.fmk) for 4 h. Vinculin was used as loading control. Representative blots of at least two independent experiments are shown. **B** Western blot analysis of expression levels of phosphorylated and total RIPK1 and MLKL upon 4 h TBZ (10 ng/mL TNFα, 1 µM BV6, 20 µM zVAD.fmk) treatment of THP-1 cells pre-treated with HOIPIN-8 (30 µM). Vinculin was used as loading control. Representative blots of at least two independent experiments are shown. **C** Western blot analysis of expression levels of phosphorylated and total RIPK1, RIPK3 and upon 4 h TBZ (10 ng/mL TNFα, 1 µM BV6, 20 µM zVAD.fmk) treatment of control (siCtrl) and HOIP knockdown (siHOIP) HT-29 cells. GAPDH was used as loading control. Representative blots of at least two independent experiments are shown.

In order to investigate how HOIPIN-8-mediated LUBAC inhibition affects necrosome formation, we used RIPK3 KO HT-29 cells re-expressing PAM-mutated doxycycline (Dox)-inducible Strep-tagged RIPK3 wild-type (WT) [146]. Intriguingly, loss of LUBAC activity did not affect necrosome formation, as determined by co-immunoprecipitation of phosphorylated RIPK1 S166 and MLKL S358 with Strep-tagged RIPK3 from untreated and HOIPIN-8-pre-treated cells after induction of necroptosis with TBZ (Figure 15A).

Formation of the necrosome and activation of MLKL ultimately leads to oligomerization of MLKL. Importantly, treatment of HT-29 cells with HOIPIN-8 did not affect necroptosis-induced MLKL oligomerization, while inhibition of RIPK3 with the RIPK3 inhibitor GSK'872 completely abrogated MLKL phosphorylation and oligomerization (Figure 15B). In contrast, the MLKL inhibitor NSA did not block MLKL phosphorylation and only slightly affected MLKL oligomerization (Figure 15B), as NSA only inhibits MLKL membrane translocation [102]. In agreement with the results obtained after treatment with HOIPIN-8, siRNA-mediated knockdown of HOIP expression, also did not affect MLKL oligomerization after induction of necroptosis (Figure 15C).

Together, these data suggest that LUBAC-mediated M1 poly-Ub serves as a novel checkpoint that regulates necroptotic cell death downstream of MLKL activation and oligomerization.

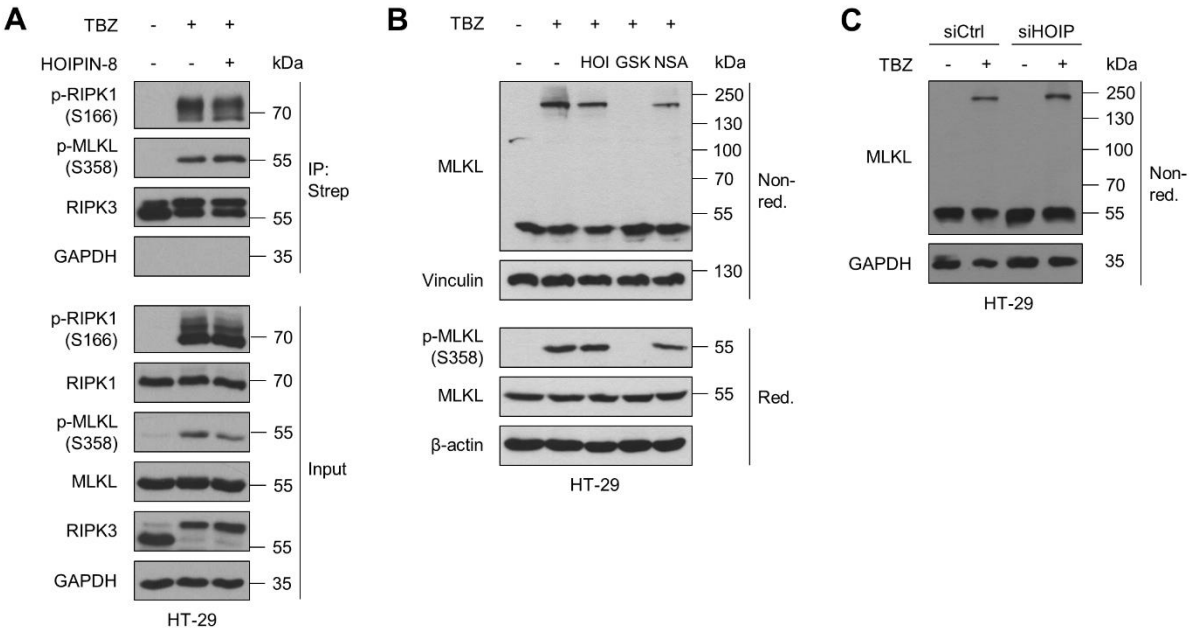

Figure 15. Treatment with HOIPIN-8 does not influence TBZ-induced necrosome formation and MLKL oligomerization.

A Immunoprecipitation of Strep-RIPK3 from control and HOIPIN-8 (30 µM)-pre-treated RIPK3 KO HT-29 cells re-expressing PAM-mutated doxycycline (Dox)-inducible Strep-tagged RIPK3 wild-type (WT) [146] was performed in order to analyze necrosome formation after treatment with TBZ (10 ng/mL TNFα, 1 µM BV6, 20 µM zVAD.fmk) for 3 h. Cells were incubated overnight with 1 µg/mL Dox prior to treatment to induce expression of Strep-RIPK3. GAPDH was used as loading control. Representative blots of at least two independent experiments are shown. **B** Western blot analysis of MLKL oligomerization upon treatment with TBZ (10 ng/mL TNFα, 1 µM BV6, 20 µM zVAD.fmk) for 4 h by non-reducing Western blotting of control, HOIPIN-8 (30 µM), GSK'872 (20 µM) or NSA (10 µM)-pre-treated HT-29 cells. Vinculin or β-actin were used as loading controls. Representative blots of at least two independent experiments are shown. **C** Western blot analysis of MLKL oligomerization upon treatment with TBZ (10 ng/mL TNFα, 1 µM BV6, 20 µM zVAD.fmk) for 4 h by non-reducing Western blotting of control (siCtrl) and HOIP knockdown (siHOIP) HT-29 cells. GAPDH was used as loading control. Representative blots of at least two independent experiments are shown.

In contrast to HOIPIN-8-mediated inhibition of LUBAC activity, inhibition of RIPK1 with Nec-1s or RIPK3 with GSK'872 blocked necroptosis-induced phosphorylation of RIPK1 S166, RIPK3 S227 and MLKL S358, while treatment with NSA, which targets MLKL, did not affect phosphorylation levels (Figure 16A). Of note, in contrast to HOIPIN-8, Nec-1s, GSK'872 or NSA, as well as deletion of RIPK3 or MLKL, did not affect total M1 poly-Ub levels in necroptotic cells, suggesting that regulation of M1 poly-Ub occurs in parallel with necroptosis initiation and progression (Figure 16B).

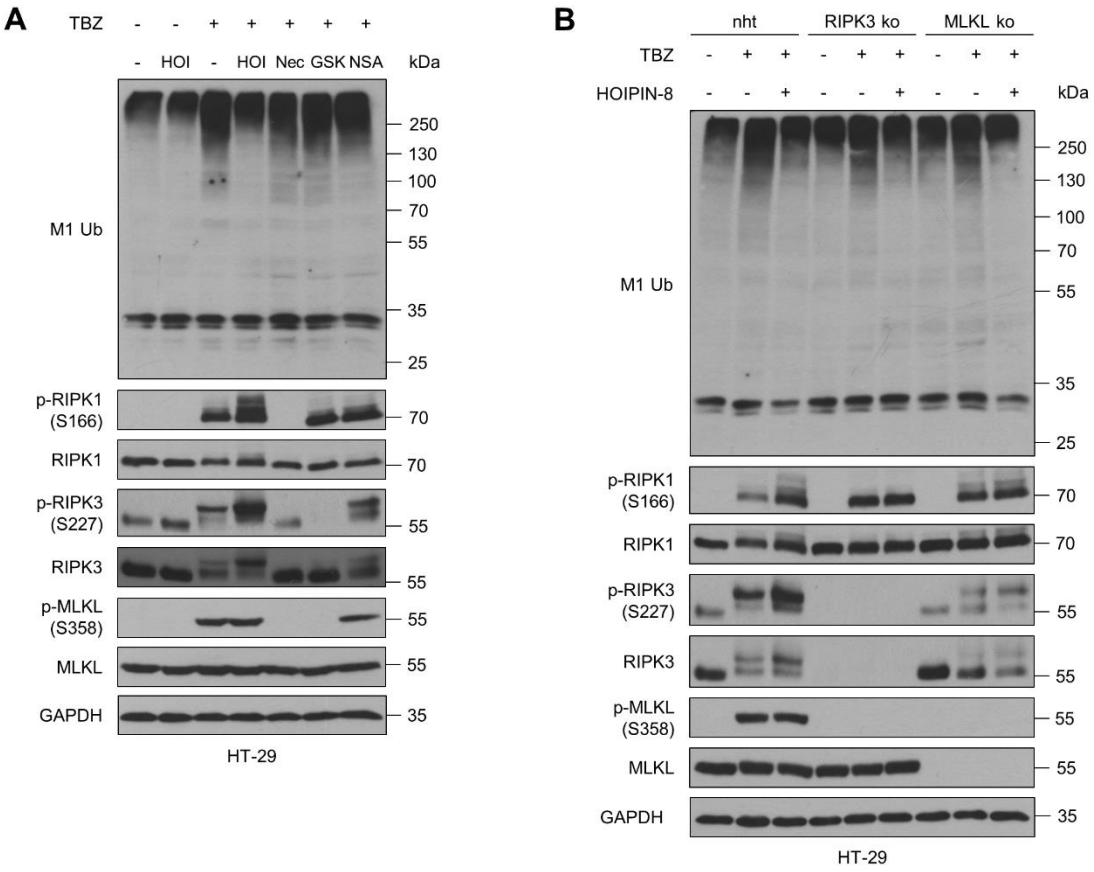

Figure 16. TBZ-induced increases in M1 poly-Ub during necroptosis are not dependent on RIPK3 and MLKL.

A Western blot analysis of expression levels of phosphorylated and total RIPK1, RIPK3, MLKL and M1 Ub upon 4 h TBZ (10 ng/mL TNFα, 1 µM BV6, 20 µM zVAD.fmk) treatment of HT-29 cells pre-treated with HOIPIN-8 (30 µM), Nec-1s (30 µM), GSK'872 (20 µM) or NSA (10 µM). GAPDH was used as loading control. Representative blots of at least two independent experiments are shown. **B** Western blot analysis of expression levels of phosphorylated and total RIPK1, RIPK3 and MLKL, and of M1 Ub in TBZ-treated (10 ng/mL TNFα, 1 µM BV6, 20 µM zVAD.fmk) control (nht), RIPK3 KO and MLKL KO HT-29 cells pre-treated with HOIPIN-8 (30 µM). GAPDH was used as loading control. Representative blots of at least two independent experiments are shown.

5.2.1.3 Inhibition of LUBAC with HOIPIN-8 prevents necroptotic cell death in primary hPOs

The present data reveal that LUBAC inhibition with HOIPIN-8 or siRNA-mediated knockdown of HOIP rescues necroptotic cell death in the human cancer cell lines HT-29 and THP-1. To exclude artefacts in necroptotic signaling related to the use of cancer cell lines, the effect of HOIPIN-8-mediated loss of M1 poly-Ub during necroptosis was studied in adult stem cell-derived primary human pancreatic organoids (hPOs). Organoids consist of organ-specific cell types that form self-organizing three-

dimensional cellular clusters which exhibit similar functionality and complexity as their tissue of origin [369, 370], thus representing highly physiological models as compared to two-dimensional monolayer cell culture models [371]. Adult stem cell-derived primary hPOs recapitulate the phenotype of the original pancreatic ductal epithelia and retain the pancreatic morphology and the distribution of ductal, acinar, mesenchymal and endothelial cells in a hollow spherical polarized cell monolayer enclosing a central lumen [362, 372-374].

In order to examine cell death, hPOs were grown in matrix for 3-5 days prior to treatment to allow formation of organoid spheres which were composed of a cellular monolayer surrounding a liquid-filled lumen, that expanded over time (Figure 17A and Figure 18A), corresponding with previous reports [375]. Matrix-embedded hPOs were then treated with BV6 (B) and the clinically-applicable pan-caspase inhibitor IDN-6556 (Emricasan; E), followed by time-lapse imaging and subsequent fluorescein diacetate (FDA)- and PI-based live/dead imaging. Combined BV6 and Emricasan treatment resulted in a prominent loss of luminal hPO morphology, characterized by organoid collapse and compaction, with individual cells migrating away from the collapsed organoids (Figure 17A). Subsequent live/dead staining confirmed high levels of PI-positive cells and low levels of FDA-positive cells, demonstrating prominent hPO cell death (Figure 17B). Intriguingly, pre-treatment of hPOs with the LUBAC inhibitor HOIPIN-8 delayed BE-induced organoid collapse, prevented the loss of luminal hPO morphology and extended hPO viability up to 24 h (Figure 17A-B).

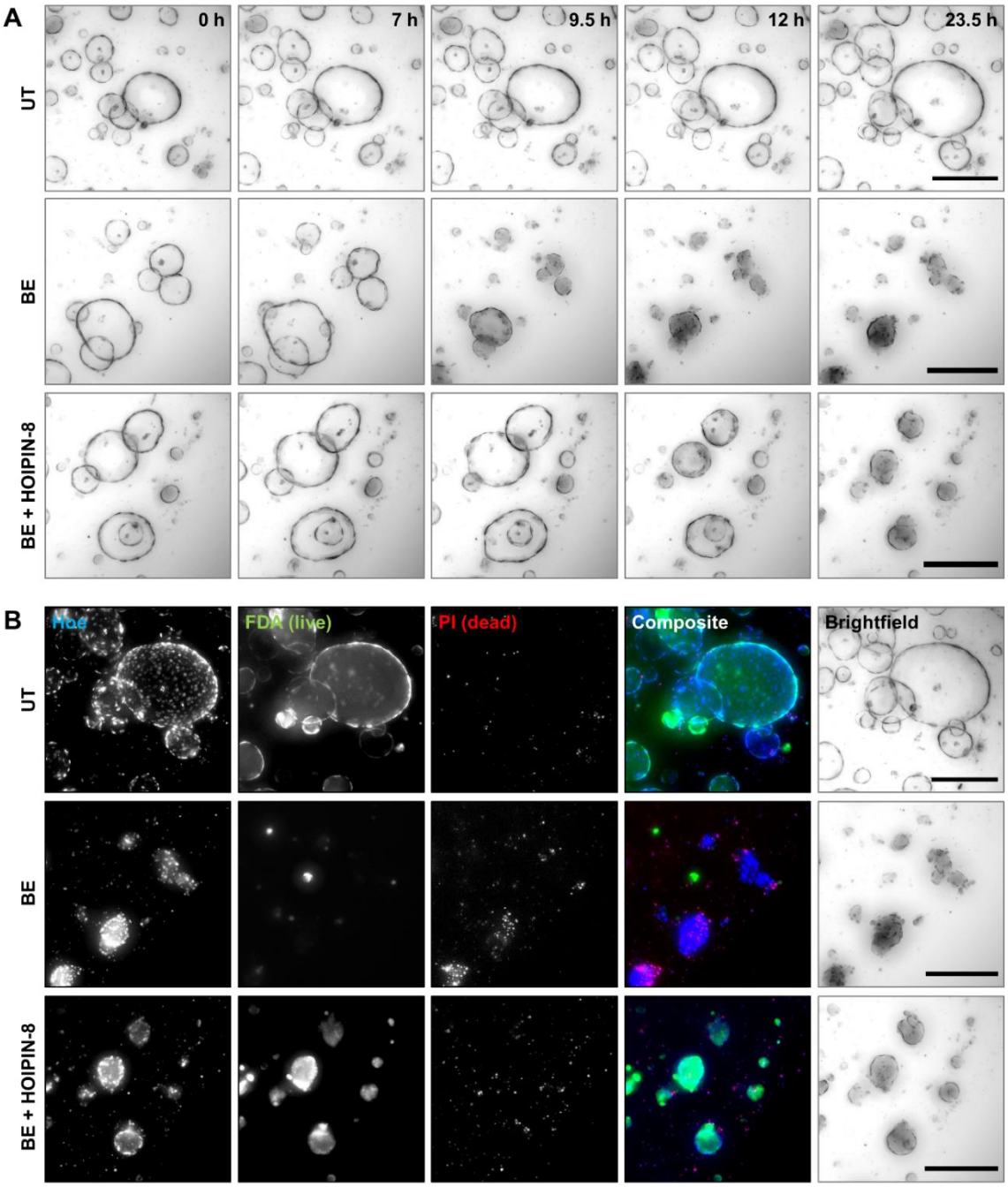

Figure 17. HOIPIN-8 prevents BV6/Emricasan-induced necroptotic cell death in primary hPOs.

A Representative images of time-lapse videos of untreated (UT), BV6 (1 µM) and Emricasan (10 µM) (BE)-treated and HOIPIN-8 (30 µM)-pre-treated and BE (BE+HOIPIN-8)-treated primary hPOs for a total period of 23.5 h. Scalebars: 250 µm. **B** Idem as A, but treated primary hPOs were stained with Hoe (blue), FDA (live; green) and PI (dead; red) after 24 h treatment with BE or BE+HOIPIN-8 prior to imaging. Scalebars: 250 µm. Representative images of at least two independent experiments are shown (A, B).

Experiments and analyses were performed by Kaja Nicole Wächtershäuser and Francesco Pampaloni.

Similar results were obtained upon treatment of hPOs with the smac mimetic Birinapant (Bi) and Emricasan. BiE-induced organoid collapse, loss of luminal morphology and cell death which could be prevented by inhibition of LUBAC with HOIPIN-8 (Figure 18A-B). Of note, organoid collapse and compaction, loss of hPO morphology and cell death triggered by BiE could be blocked by NSA, indicating the occurrence of MLKL-dependent necroptotic cell death (Figure 18A-B). Furthermore, treatment of hPOs with BV6 and zVAD.fmk (BZ) potently triggered cell death as well, which was decreased by LUBAC inhibition with HOIPIN-8 (Figure 19).

By modelling necroptotic cell death in primary hPOs, this study provides a novel experimental platform to study programmed cell death in intact human multicellular systems and further corroborates the abovementioned findings by demonstrating that LUBAC inhibition with HOIPIN-8 prevents necroptosis in primary human cells.

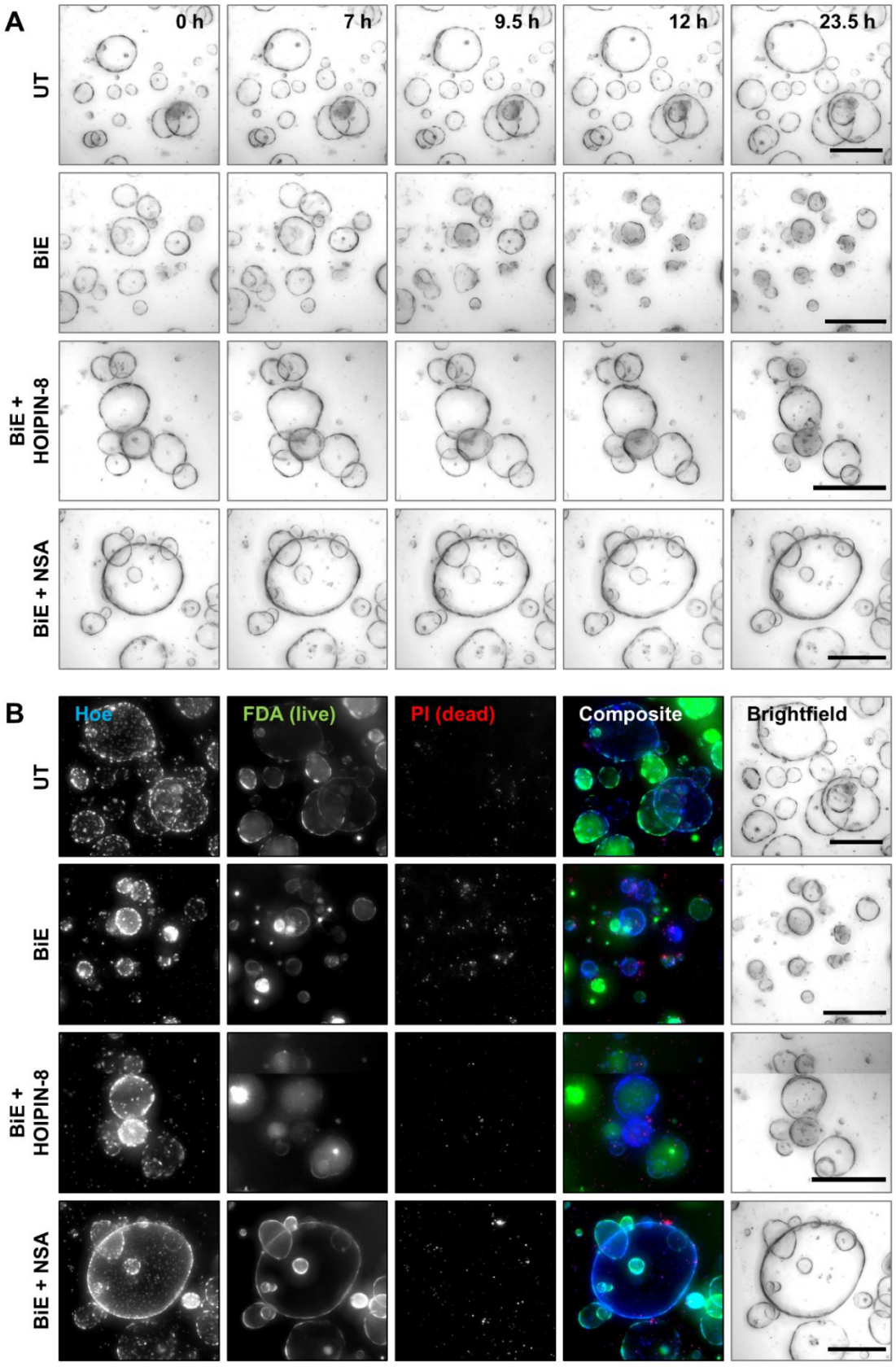

Figure 18. HOIPIN-8 prevents Birinapant/Emricasan-induced necroptotic cell death in primary hPOs.

Figure 18. Continued.

A Representative images of time-lapse videos of untreated (UT), Birinapant (20 µM) and Emricasan (10 µM) (BiE)-treated, HOIPIN-8 (30 µM)-pre-treated and BiE-treated (BiE+HOIPIN-8) and NSA (10 µM)-pre-treated and BiE-treated (BiE+NSA) primary hPOs for a total period of 23.5 h. Scalebars: 250 µm. **B** Idem as A, but treated primary hPOs were stained with Hoe (blue), FDA (live; green) and PI (dead; red) after 24 h treatment with BiE, BiE+HOIPIN-8 or BiE+NSA prior to imaging. Representative images of at least two independent experiments are shown (A, B). Scalebars: 250 µm.

Experiments and analyses were performed by Kaja Nicole Wächtershäuser and Francesco Pampaloni.

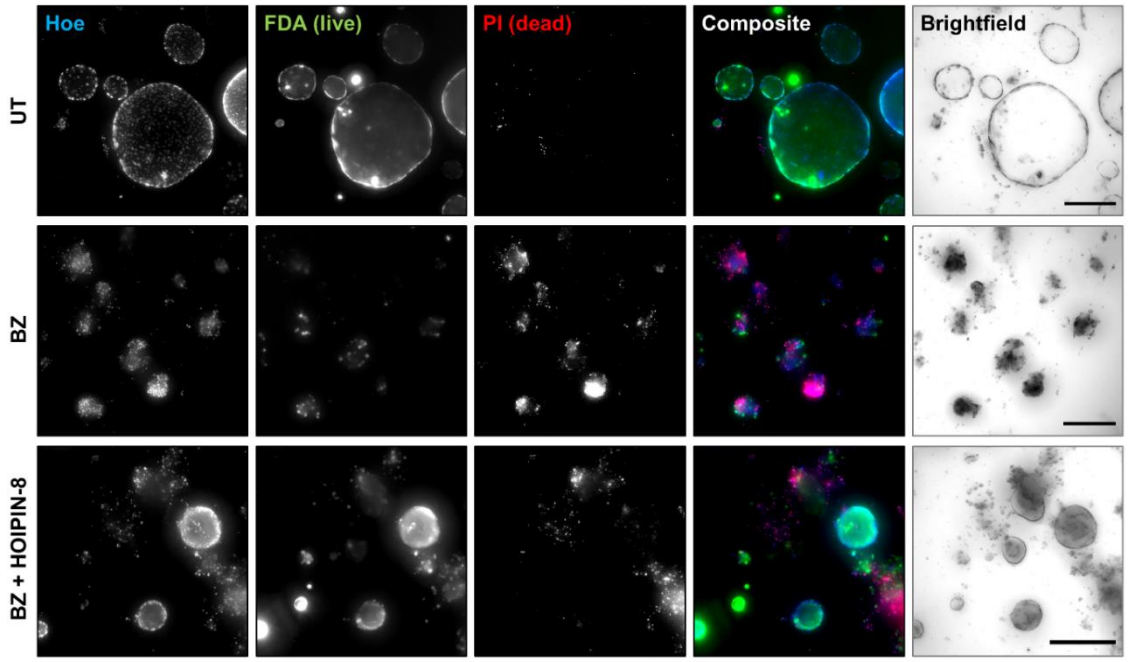

Figure 19. HOIPIN-8 prevents BV6/zVAD.fmk-induced necroptotic cell death in primary hPOs.

Representative images of untreated (UT), BV6 (5 µM) and zVAD.fmk (20 µM) (BZ)-treated and HOIPIN-8 (30 µM)-pre-treated and BZ-treated (BZ+HOIPIN-8) primary hPOs that were stained with Hoe (blue), FDA (live; green) and PI (dead; red) after 24 h treatment prior to imaging. Representative images of at least two independent experiments are shown. Scalebars: 250 µm.

Experiments and analyses were performed by Kaja Nicole Wächtershäuser and Francesco Pampaloni.

5.2.1.4 OTULIN or CYLD depletion does not affect HOIPIN-8-mediated rescue of necroptotic cell death

Both OTULIN and CYLD cleave M1 poly-Ub and interact with the LUBAC subunit HOIP [256-261]. CYLD has been demonstrated to be recruited to TNFR1 via LUBAC where it cleaves K63 and M1 poly-Ub leading to destabilization of TNFR1 complex I [73, 259, 260, 293]. In contrast, whether OTULIN plays an active role at RSCs has been a matter

of debate [299], however, OTULIN has been shown to counteract HOIP auto-ubiquitination and thus regulates the catalytic activity of LUBAC [277, 290-293]. Although KO of OTULIN and/or CYLD had only minor effects on necroptotic cell death in HT-29 and THP-1 cells (Figure 20A-B, see also Figure 8 and Figure 9), KO of these DUBs led to marked increases of M1 poly-Ub levels (see Figure 5B, Figure 6B and Figure 10A), raising the question as to whether the elevated basal M1 poly-Ub levels could influence the effects of HOIP inhibition during necroptotic cell death. The effect of HOIPIN-8 was therefore evaluated in necroptotic HT-29 and THP-1 control, OTULIN KO, CYLD KO and combined OTULIN/CYLD KO cells. Intriguingly, loss of OTULIN and/or CYLD expression had no effect on HOIPIN-8-mediated rescue of necroptosis in HT-29 and THP-1 cell lines (Figure 20A-B). In line with this, OTULIN KO, CYLD KO and combined OTULIN/CYLD KO did not affect necroptotic signaling, as determined by phosphorylation of RIPK1 S166, RIPK3 S227 and MLKL S358, in HT-29 cell lines (Figure 20C). Of note, induction of necroptosis lead to increased levels of M1 poly-Ub in control, OTULIN KO and CYLD KO HT-29 cells as compared to the respective untreated control cells, but not in the combined OTULIN/CYLD KO cells, and this increase could be effectively blocked by LUBAC inhibition with HOIPIN-8 (Figure 20D).

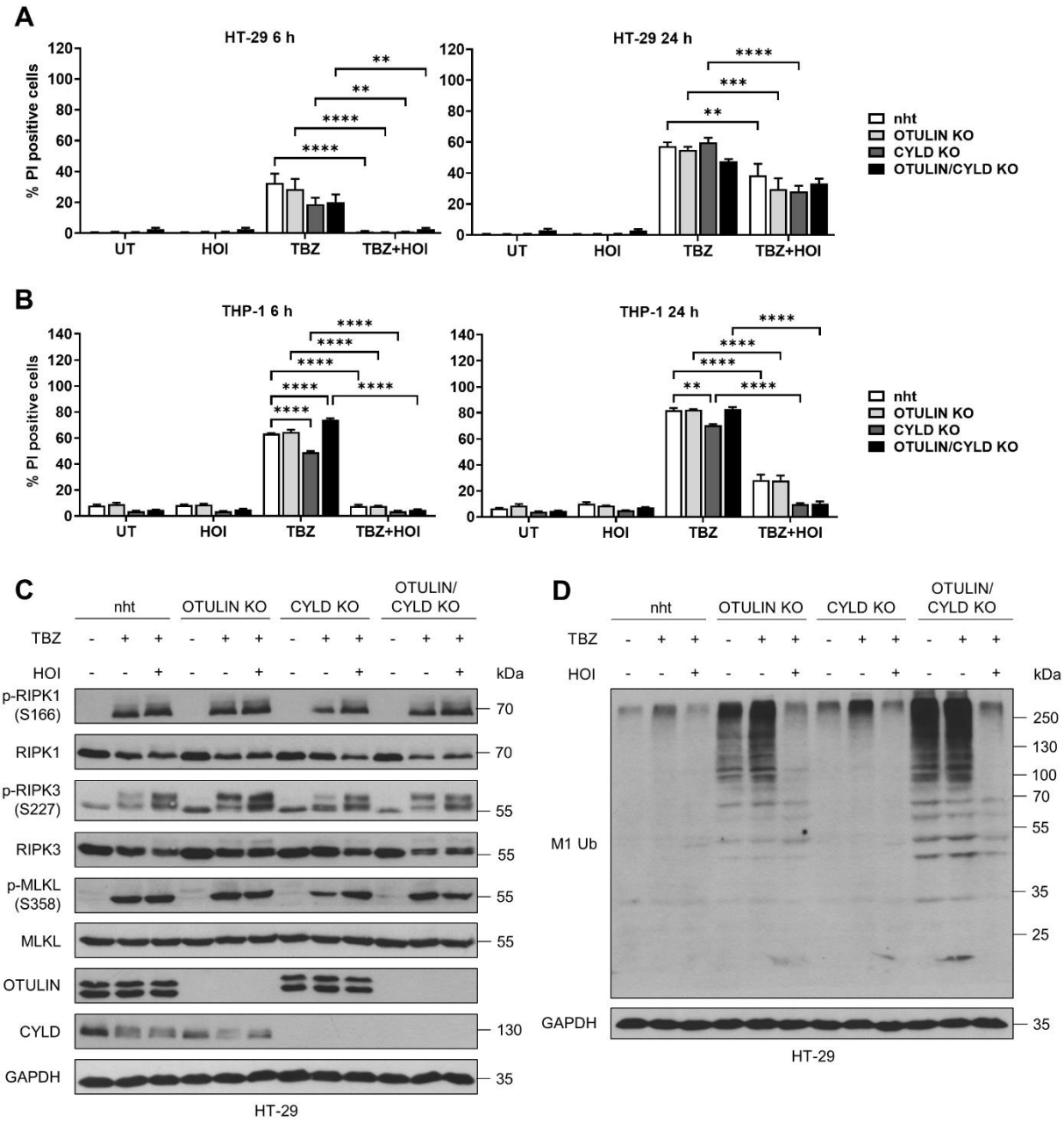

Figure 20. Loss of OTULIN and/or CYLD do not affect the HOIPIN-8-mediated rescue of TBZ-induced necroptosis.

A-B Quantification of cell death in control (UT) or HOIPIN-8 (30 µM)-pre-treated HT-29 (A) or THP-1 (B) control (nht), OTULIN KO, CYLD KO or OTULIN/CYLD KO cells after treatment with TBZ (10 ng/mL TNFα, 1 µM BV6, 20 µM zVAD.fmk) for the indicated time points. Mean and SEM of at least three independent experiments are shown. ***P*<0.01; ****P*<0.001; *****P*<0.0001. **C** Western blot analysis of expression levels of OTULIN, CYLD, and phosphorylated and total RIPK1, RIPK3 and MLKL in control (UT) or HOIPIN-8 (30 µM)-pre-treated control (nht), OTULIN KO, CYLD KO and OTULIN/CYLD KO HT-29 cells upon 4 h TBZ (10 ng/mL TNFα, 1 µM BV6, 20 µM zVAD.fmk). GAPDH was used as loading control. Representative blots of two independent experiments are shown. **D** Western blot analysis of expression levels of M1 Ub in control (UT) or HOIPIN-8 (30 µM)-pre-treated control (nht), OTULIN KO, CYLD KO and OTULIN/CYLD KO HT-29 cells upon 4 h TBZ (10 ng/mL TNFα, 1 µM BV6, 20 µM zVAD.fmk). GAPDH was used as loading control. n=1 is shown.

Similarly, OTULIN KO did not influence the rescue effect of siRNA-mediated knockdown of HOIP in necroptotic HT-29 cells (Figure 21).

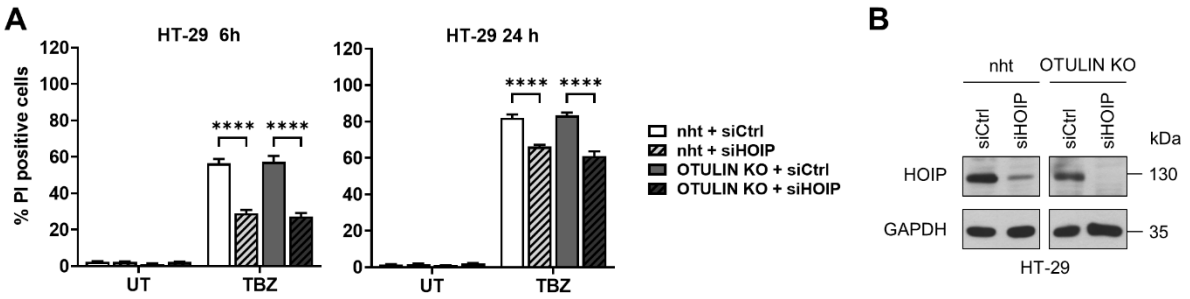

Figure 21. Loss of OTULIN does not affect HOIP knockdown-mediated rescue of TBZ-induced necroptosis.

A Quantification of cell death in control (UT) or HOIPIN-8 (30 µM)-pre-treated HT-29 control (nht + siCtrl), HOIP knockdown (nht + siHOIP), OTULIN KO (OTULIN KO + siCtrl) or OTULIN KO/HOIP knockdown (OTULIN KO + siHOIP) cells after treatment with TBZ (10 ng/mL TNFα, 1 µM BV6, 20 µM zVAD.fmk) for the indicated time points. Mean and SEM of n=3 independent experiments are shown. ****P<0.0001. **B** Expression of HOIP in control (siCtrl) and HOIP knockdown (siHOIP) control (nht) and OTULIN KO HT-29. GAPDH was used as loading control. Representative blots of at least two independent experiments are shown for nht, n=1 is shown for OTULIN KO.

5.2.1.5 Necroptosis in human CRISPR/Cas9-mediated HOIP KO cell lines

In order to further confirm the rescue effect of LUBAC inhibition on necroptotic cell death, we generated HOIP KO HT-29 and THP-1 cells using CRISPR/Cas9-mediated gene editing. To our surprise, HOIP KO did not prevent TBZ-induced necroptotic cell death in both HT-29 (Figure 22A-B) and THP-1 cell lines (Figure 22C-D). This is in contrast to the observed rescue of TBZ-induced cell death in siRNA-mediated HOIP knockdown HT-29 cells (Figure 13 and Figure 21) and HOIPIN-8 or gliotoxin-treated HT-29 and THP-1 cells (Figure 11). Intriguingly, HOIP inhibition with HOIPIN-8 blocked TBZ-induced cell death in control cells but also in HOIP KO cell lines (Figure 22A-B) to a similar extent as in HT-29 WT and THP-1 WT cells (Figure 11). The HOIP KO cell lines used in these experiments are polyclonal bulk cultures that still contain small amounts of HOIP-expressing cells, however, the HOIPIN-8-mediated rescue of cell death in HOIP KO cells may suggest that HOIPIN-8 has additional off-target effects.

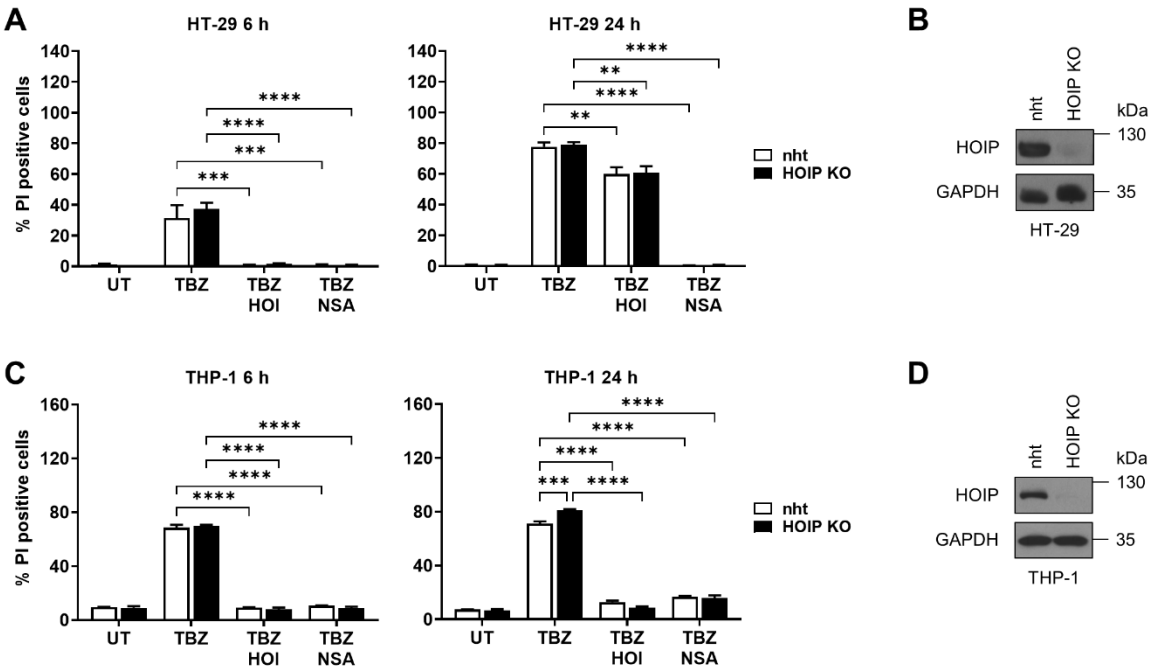

Figure 22. CRISPR/Cas9-mediated knockout of HOIP does not affect necroptosis in HT-29 or THP-1 cell lines.

A,C Quantification of cell death in control (UT), HOIPIN-8 (30 µM) or NSA (10 µM)-pre-treated control (nht) and CRISPR/Cas9-mediated HOIP KO HT-29 (A) and THP-1 (C) cell lines after treatment with TBZ (10 ng/mL TNFα, 1 µM BV6, 20 µM zVAD.fmk) for the indicated time points. Mean and SEM of n=3 independent experiments are shown. **B,D** Expression of HOIP in control (nht) and CRISPR/Cas9-mediated HOIP knockout (HOIP KO) HT-29 (B) and THP-1 (D) cell lines. GAPDH was used as loading control. Representative blots of at least two independent experiments are shown.

P*<0.01; ****P*<0.001;**P*<0.0001.

CRISPR/Cas9-mediated KO of HOIP in HT-29 cells resulted in destabilization of the HOIL-1 higher molecular weight species and decreased Sharpin levels, corresponding with previous data [236, 274, 323], both of which were not affected by treatment with HOIPIN-8 (Figure 23A). As expected, HOIP KO prevented necroptosis-dependent increases of cellular M1 poly-Ub to a similar extent as treatment with HOIPIN-8 (Figure 23A). In addition, KO of HOIP did not affect necroptotic phosphorylation of RIPK1, RIPK3 and MLKL and did not affect oligomerization of MLKL, as determined by non-reducing western blotting (Figure 23B).

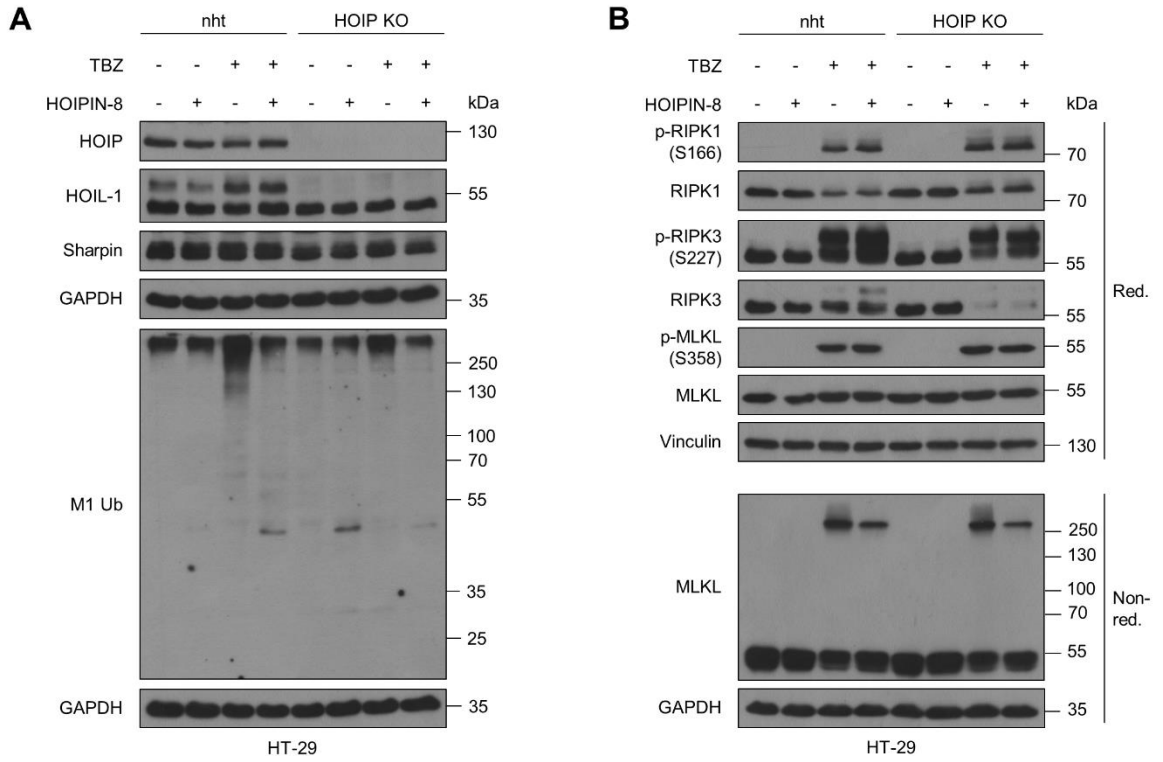

Figure 23. CRISPR/Cas9-mediated KO of HOIP does not affect necroptotic signaling and MLKL oligomerization.

A Expression of LUBAC subunits HOIP, HOIL-1 and Sharpin as well as M1 poly-Ub in control and HOIPIN-8 (30 µM)-pre-treated control (nht) and HOIP KO HT-29 cells after treatment with TBZ (10 ng/mL TNFα, 1 µM BV6, 20 µM zVAD.fmk) for 4 h. GAPDH was used as loading control. Representative blots of at least two independent experiments are shown. **B** Western blot analysis of phosphorylated and total expression levels of RIPK1, RIPK3 and MLKL as well as of MLKL oligomerization (by non-reducing Western blotting) upon treatment with TBZ (10 ng/mL TNFα, 1 µM BV6, 20 µM zVAD.fmk) for 4 h in control versus HOIPIN-8 (30 µM)-pre-treated control (nht) and HOIP KO HT-29 cells. Vinculin and GAPDH were used as loading controls. Representative blots of at least two independent experiments are shown.

5.2.1.6 LUBAC inhibition with HOIPIN-8 does not block necroptosis in murine cell lines

The relevance of LUBAC-generated M1 poly-Ub in TNFα-mediated cell fate signaling has been extensively researched in the context of genetic mouse models that are deficient in *Hoip*, *Hoil-1* (*Rbck1*) or *Sharpin*. Several studies have demonstrated that loss of either of the LUBAC subunits interferes with TNFR1-mediated signaling, resulting in decreased NF-κB activity and elevated TNFR1-mediated cell death [12, 274, 327-331, 376]. Of note, homozygous deletion of *Hoip* in mice results in embryonic lethality at E10.5 due to endothelial cell death and survival of these embryos can be prolonged by concomitant deletion of *Tnf* or *Tnfr1* [274]. In line with this, *Tnf*$^{-/-}$ *Hoip*$^{-/-}$

MEFs were sensitized towards cell death upon TNFα treatment (Figure 24A-B) [274] which could be blocked by inhibition of caspases with zVAD.fmk, but not by inhibition of RIPK3 with GSK'872, suggesting that the cells die mainly by apoptosis (Figure 24A). Similarly, HOIP inhibition with HOIPIN-8 resulted in increased TNFα-mediated cell death in *Tnf*$^{-/-}$ MEFs which could be prevented by zVAD but not GSK'872 treatment (Figure 24A). Surprisingly and in contrast to the data obtained with human cell lines, treatment of *Tnf*$^{-/-}$ *Hoip*$^{-/-}$ MEFs with TBZ resulted in increased necroptotic cell death as compared to *Tnf*$^{-/-}$ MEFs, however, HOIPIN-8 did not affect cell death levels in *Tnf*$^{-/-}$ MEFs (Figure 24C). Interestingly, cell death levels did not further increase in both *Tnf*$^{-/-}$ *and Tnf*$^{-/-}$ *Hoip*$^{-/-}$ MEFs but were strongly reduced after 24 h TBZ treatment as compared to cell death levels after 6 h (Figure 24C), suggesting that autocrine TNFα is a major driver of necroptotic cell death in MEFs.

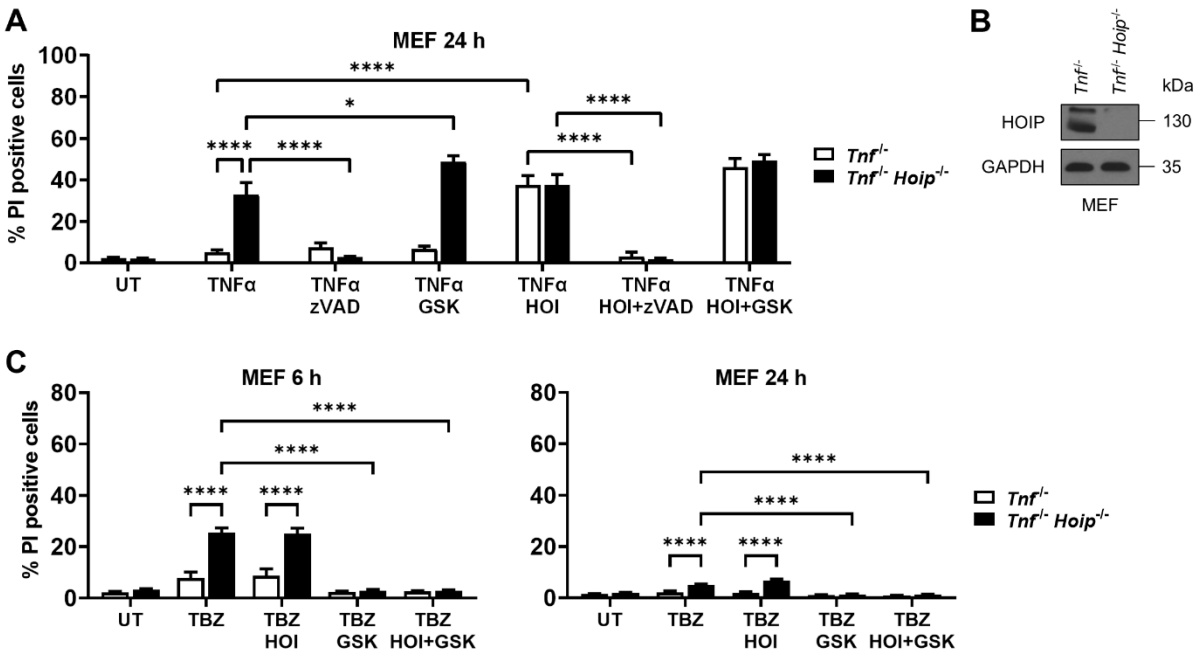

Figure 24. *Tnf*$^{-/-}$ *Hoip*$^{-/-}$ MEFs are sensitized towards TNFα and TBZ-induced cell death

A Quantification of cell death in control (UT), zVAD.fmk (20 µM), GSK'872 (20 µM) or HOIPIN-8 (30 µM)-pre-treated *Tnf*$^{-/-}$ and *Tnf*$^{-/-}$ *Hoip*$^{-/-}$ MEFs after treatment with TNFα (10 ng/mL) for 24 h. Mean and SEM of n=3 independent experiments are shown. **B** Expression of HOIP in *Tnf*$^{-/-}$ and *Tnf*$^{-/-}$ *Hoip*$^{-/-}$ MEFs. GAPDH was used as loading control. Representative blots of at least two independent experiments are shown. **C** Quantification of cell death in control (UT), HOIPIN-8 (30 µM) or GSK'872 (20 µM)-pre-treated *Tnf*$^{-/-}$ and *Tnf*$^{-/-}$ *Hoip*$^{-/-}$ MEFs after treatment with TBZ (10 ng/mL TNFα, 1 µM BV6, 20 µM zVAD.fmk) for the indicated time points. Mean and SEM of n=3 independent experiments are shown.

**P*<0.05; *****P*<0.0001.

To corroborate the abovementioned data, the effect of LUBAC inhibition was further investigated in WT MEFs and other murine cell lines. In line with the data obtained with *Tnf*$^{-/-}$ *Hoip*$^{-/-}$ MEFs, treatment with HOIPIN-8 did not block TBZ-induced necroptotic cell death in WT MEFs (Figure 25A) and necroptosis induced only a minor increase in M1 poly-Ub levels (Figure 25B). Similar to HT-29 cells, induction of necroptosis with TBZ and treatment with HOIPIN-8 did not affect protein expression levels of LUBAC subunits HOIP and HOIL-1 (Figure 25C). HOIPIN-8 interferes with the active site residue C885 and residues H887 and F905 located in the RING2 domain of HOIP, as well as L922, R935 and D936 in the HOIP LDD, thereby inhibiting the RING-HECT hybrid reaction [286]. Importantly, amino acid sequence alignment of human and murine HOIP demonstrated that these residues are conserved in humans and mice (Figure 25D) and treatment of MEFs with HOIPIN-8 effectively blocked TNFα-induced NF-κB activation (Figure 25E). Furthermore, treatment of *Tnf*$^{-/-}$ MEFs with HOIPIN-8 mimicked the effect of HOIP deletion on TNFα-induced cell death in *Tnf*$^{-/-}$ *Hoip*$^{-/-}$ MEFs (Figure 24A). Together, these data demonstrate the effectiveness of HOIPIN-8 in murine cells.

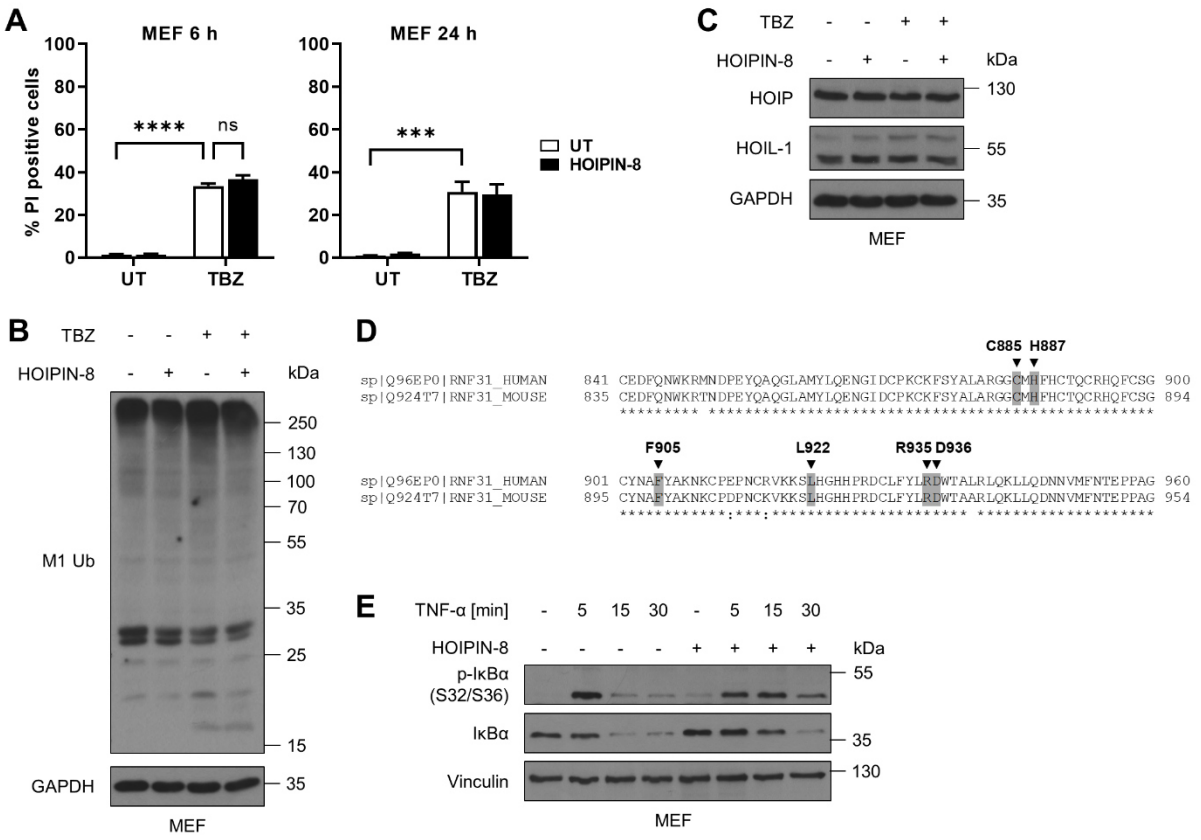

Figure 25. LUBAC inhibition with HOIPIN-8 does not block TBZ-induced cell death in MEFs.

A Quantification of cell death in control (UT) and HOIPIN-8 (30 µM)-pre-treated MEFs after treatment with TBZ (10 ng/mL TNFα, 1 µM BV6, 20 µM zVAD.fmk) for the indicated time points. Mean and SEM of n=4 independent experiments are shown. ****P*<0.001; *****P*<0.0001; ns: not significant. **B** Expression of M1 poly-Ub in control (UT) and HOIPIN-8 (30 µM)-pre-treated MEFs after treatment with TBZ (10 ng/mL TNFα, 1 µM BV6, 20 µM zVAD.fmk) for 3 h. GAPDH was used as loading control. Representative blots of at least two independent experiments are shown. **C** Expression of LUBAC subunits HOIP and HOIL-1 in control and HOIPIN-8 (30 µM)-pre-treated MEFs after treatment with TBZ (10 ng/mL TNFα, 1 µM BV6, 20 µM zVAD.fmk) for 3 h. GAPDH was used as loading control. Representative blots of at least two independent experiments are shown. **D** Amino acid sequence alignment showing conservation of human (aa841-aa960) and murine HOIP (RNF31) (aa835-aa954). Conserved residues interacting with HOIPIN-8 are highlighted and indicated by arrowheads. Sequence alignment was performed using the CLUSTAL O (1.2.4) algorithm. **E** Expression of phosphorylated and total IκBα levels in control and HOIPIN-8 (30 µM)-pre-treated MEFs after treatment with TNFα (10 ng/mL) for the indicated time points. Vinculin was used as loading control. Representative blots of at least two independent experiments are shown.

The consequences of LUBAC inhibition on TNFα-induced necroptosis were further evaluated in L-929 mouse lung fibroblasts and RAW 264.7 mouse macrophages. Inhibition of LUBAC with HOIPIN-8 even enhanced TBZ-induced necroptosis in both L-929 and RAW 264.7 (Figure 26). This is in accordance with previous findings demonstrating that RNAi-mediated silencing of HOIP or HOIL-1 sensitizes L-929 cells to necroptotic cell death [376].

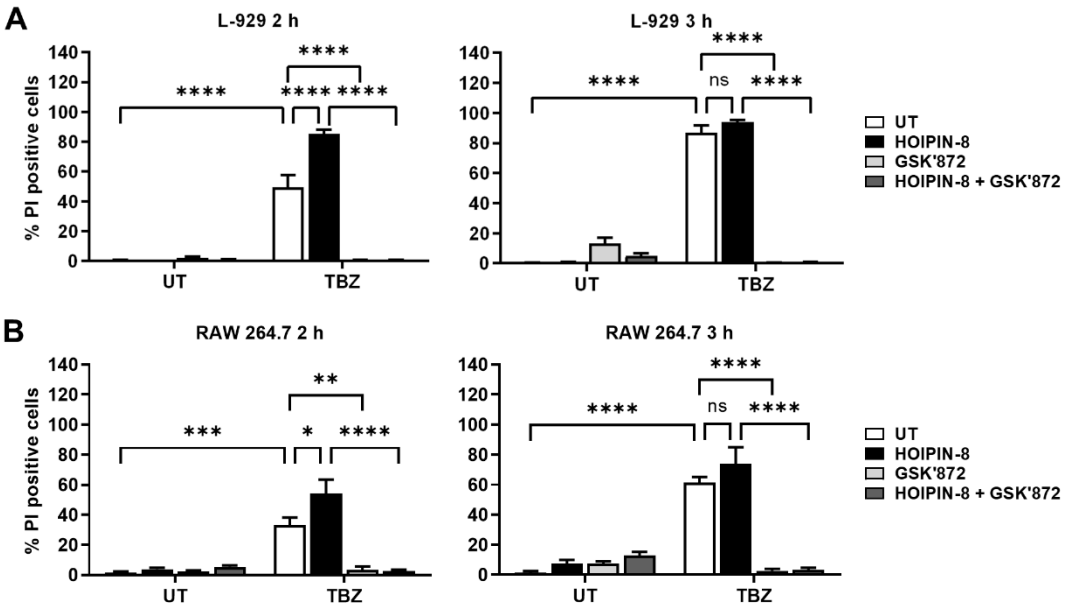

Figure 26. LUBAC inhibition with HOIPIN-8 increases TBZ-induced cell death in mouse L-929 and RAW 264.7 cell lines.

A,B Quantification of cell death in control (UT), HOIPIN-8 (30 µM) or GSK'872 (20 µM)-pre-treated L-929 (A) and RAW 264.7 (B) cells after treatment with TBZ (10 ng/mL TNFα, 0.1 µM BV6, 20 µM zVAD.fmk) for the indicated time points. Mean and SEM of n=3 independent experiments are shown. **P*<0.05; ***P*<0.01; ****P*<0.001; *****P*<0.0001; ns: not significant.

5.2.1.7 CRISPR/Cas9-mediated HOIP KO does not affect necroptosis in murine cell lines

In order to confirm the abovementioned data, CRISPR/Cas9-mediated HOIP KO MEFs and L-929 cell were used to study necroptotic cell death in murine cells. Corresponding with previous data obtained with *Tnf*$^{-/-}$ *Hoip*$^{-/-}$ MEFs (Figure 24A), CRISPR/Cas9-mediated HOIP KO MEFs were sensitized towards TNFα-induced cell death (Figure 27A-B), however, HOIP KO did not lead to increased TBZ-induced cell death (Figure 27C). Similar to *Tnf*$^{-/-}$ *Hoip*$^{-/-}$ MEFs, treatment of HOIP KO MEFs with HOIPIN-8, did not further increase necroptosis (Figure 27C). While HOIP KO in L-929 cells did not result in increased TBZ-induced cell death, HOIPIN-8 treatment increased cell death in both control and HOIP KO L-929 cells (Figure 27D-E) which can be explained by the use of polyclonal bulk cultures that still contain cells expressing HOIP (Figure 27E).

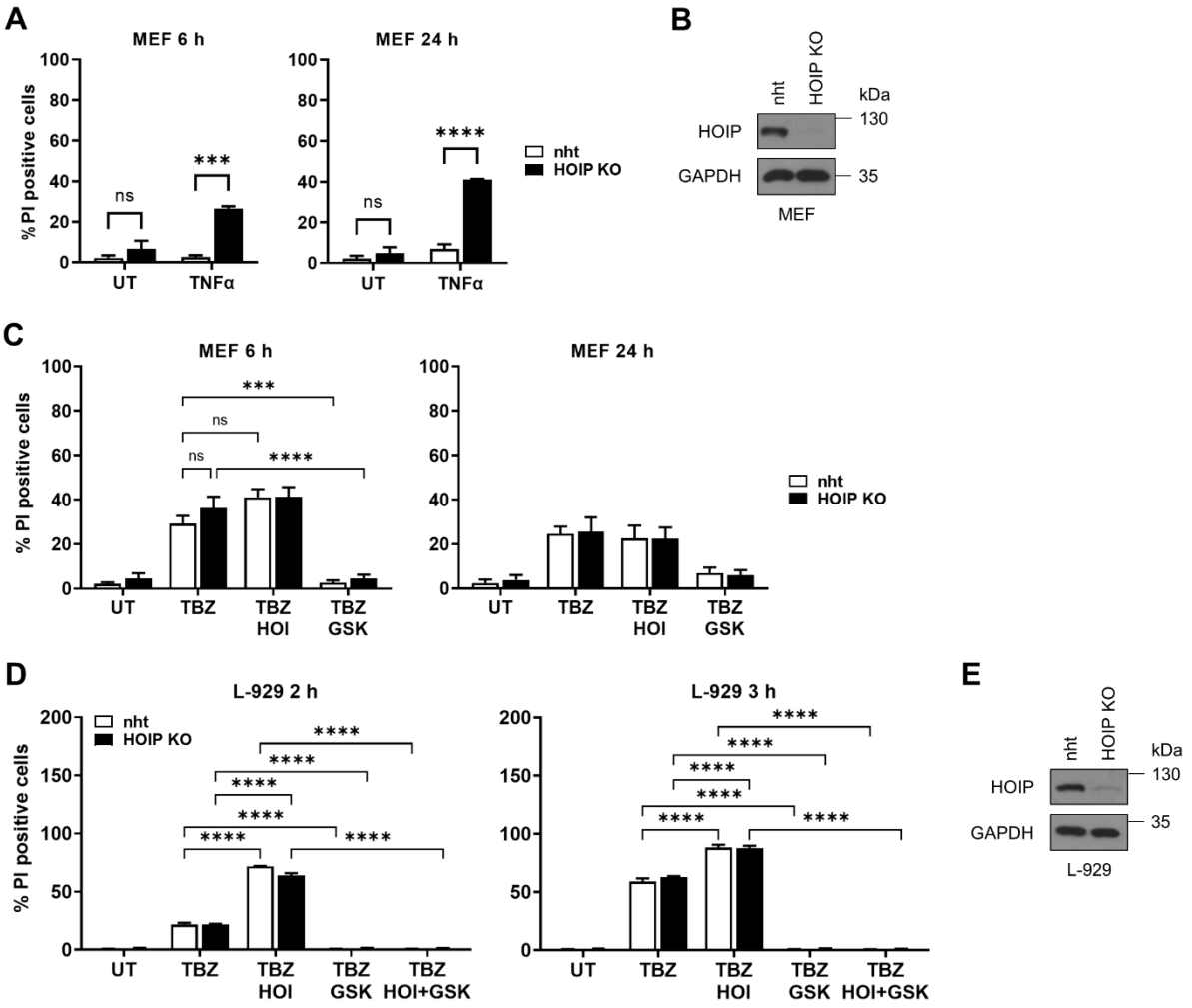

Figure 27. CRISPR/Cas9-mediated HOIP KO does not increase TBZ-induced cell death in MEF and L-929 cell lines.

A Quantification of cell death in control (nht) and HOIP KO MEFs after treatment with TNFα (10 ng/mL) for the indicated time points. Mean and SEM of n=3 independent experiments are shown. **B** Expression of HOIP in control (nht) and HOIP KO MEFs. GAPDH was used as loading control. Representative blots of at least two independent experiments are shown. **C** Quantification of cell death in control (UT), HOIPIN-8 (30 µM) or GSK'872 (20 µM)-pre-treated control (nht) and HOIP KO MEFs after treatment with TBZ (10 ng/mL TNFα, 1 µM BV6, 20 µM zVAD.fmk) for the indicated time points. Mean and SEM of n=3 independent experiments are shown. **D.** Quantification of cell death in control (UT), HOIPIN-8 (30 µM), GSK'872 (20 µM) or HOIPIN-8/GSK'872-pre-treated control (nht) and HOIP KO L-929 cells after treatment with TBZ (10 ng/mL TNFα, 0.1 µM BV6, 20 µM zVAD.fmk) for the indicated time points. Mean and SEM of n=3 independent experiments are shown. **E** Expression of HOIP in control (nht) and HOIP KO L-929 cells. GAPDH was used as loading control. Representative blots of at least two independent experiments are shown.

***P<0.001; ****P<0.0001; ns: not significant.

5.2.1.8 LUBAC inhibition with HOIPIN-8 prevents the translocation of activated MLKL to cellular membranes

After activation of MLKL by RIPK3-mediated phosphorylation, MLKL oligomerizes into higher molecular structures and subsequently translocates to the plasma membrane where it interacts with PIPs to form so-called hotspots, preferentially at cellular junctions [102, 105, 117]. Since our previous data indicated that treatment of human cells with the LUBAC inhibitor HOIPIN-8 blocks necroptosis downstream of MLKL oligomerization, we sought to examine whether HOIPIN-8 affects MLKL translocation to membrane compartments. For this, a non-ionic detergent- and temperature-dependent fractionation of micelle-poor (aqueous) and micelle-rich (detergent-enriched) fractions was performed to isolate membrane-associated proteins from HT-29 cells. As expected, upon TBZ-induced necroptosis phosphorylated MLKL S358 accumulated in the detergent-enriched fractions (Figure 28A), indicating extensive membrane accumulation. Treatment of the cells with the MLKL inhibitor NSA completely abrogated phosphorylated MLKL translocation to crude membrane fractions (Figure 28A), in line with previous findings [102]. Intriguingly, inhibition of LUBAC with HOIPIN-8 prevented accumulation of phosphorylated MLKL in the detergent-enriched fraction (Figure 28A), suggesting that HOIPIN-8 affects MLKL membrane translocation during necroptosis.

Of note, cell fractionation experiments demonstrate a prominent necroptosis-dependent accumulation of M1 poly-Ub in the detergent-enriched fraction which could be blocked by LUBAC inhibition with HOIPIN-8, but not with NSA (Figure 28B). These data indicate that LUBAC-mediated M1 poly-Ub has a yet unidentified necroptosis-dependent function at cellular membranes, however, inhibition of MLKL membrane translocation with NSA did not affect accumulation of M1 poly-Ub at membrane compartments, suggesting that this occurs independently of necroptotic signaling.

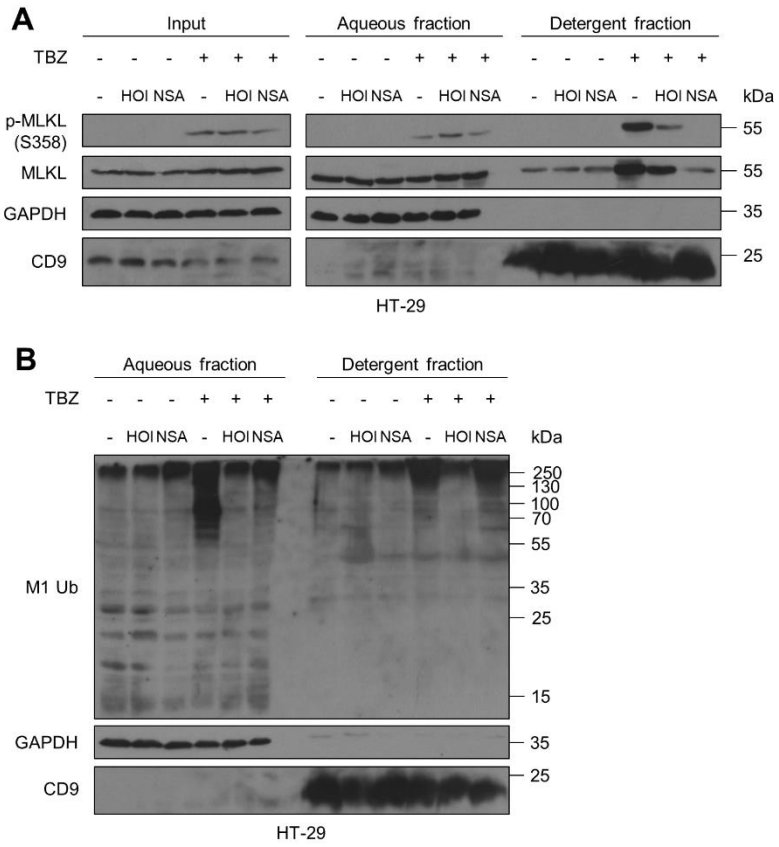

Figure 28. HOIPIN-8 blocks necroptosis-induced translocation of activated MLKL to membrane compartments.

A Fractionation of phosphorylated and total MLKL in the micelle-poor (aqueous) and micelle-rich (detergent) fractions upon phase separation using Triton X-114 lysis buffer in untreated and HOIPIN-8 (30 µM) pre-treated HT-29 cells upon treatment with TBZ (10 ng/mL TNFα, 1 µM BV6, 20 µM zVAD.fmk) for 4 h. GAPDH was used as loading control for soluble proteins and CD9 as loading control for membrane proteins. Representative blots of at least two independent experiments are shown. **B** Distribution of M1 poly-Ub in the micelle-poor (aqueous) and micelle-rich (detergent) fraction after phase separation using Triton X-114 lysis buffer in untreated and HOIPIN-8 (30 µM)-pre-treated HT-29 cells upon treatment with TBZ (10 ng/mL TNFα, 1 µM BV6, 20 µM zVAD.fmk) for 4 h. GAPDH was used as loading control for soluble proteins and CD9 as loading control for membrane proteins. Representative blots of at least two independent experiments are shown.

To further investigate how HOIPIN-8 affects plasma membrane accumulation of MLKL, the distribution of phosphorylated MLKL S358 after necroptosis induction was assessed by immunofluorescence. In necroptotic cells, phosphorylated MLKL translocated to the plasma membrane where it formed large hotspots at intercellular junctions (Figure 29), corresponding with previous data [117]. In accordance with the altered cellular distribution of phosphorylated MLKL in fractionation experiments, treatment with HOIPIN-8 completely prevented phosphorylated MLKL hotspots, but instead led to the formation of diffuse cytoplasmic punctate clusters of phosphorylated

MLKL (Figure 29). As expected [102], treatment with NSA also effectively blocked phosphorylated MLKL plasma membrane translocation (Figure 29).

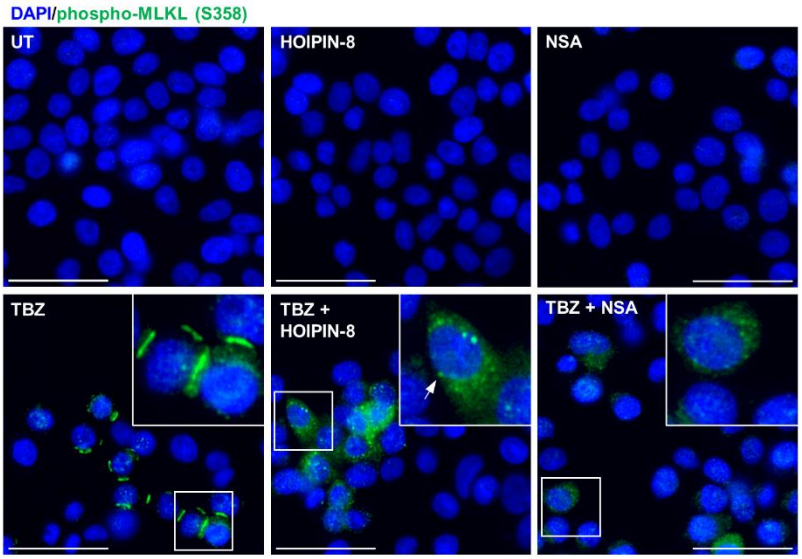

Figure 29. HOIPIN-8 blocks necroptosis-induced plasma membrane translocation of activated MLKL.

Representative fluorescence microscopy demonstrating the cellular distribution of phosphorylated MLKL (green) in untreated (UT), HOIPIN-8 (30 µM) and NSA (10 µM)-pre-treated HT-29 cells and after treatment with TBZ (10 ng/mL TNFα, 1 µM BV6, 20 µM zVAD.fmk) for 3 h. Nuclei were stained with DAPI (blue). Arrows indicate cytoplasmic clusters of phosphorylated MLKL. Representative images of two independent experiments are shown. Scale bar 50 µm.

Necroptosis is tightly controlled by PTMs and by compartmentalization of key players of the necroptosis pathway (see section 2.2.3). MLKL plasma membrane translocation and subsequent loss of membrane integrity are considered the final steps of necroptosis execution, however, activated MLKL already accumulates at the plasma membrane prior to plasma membrane disruption which can be antagonized by exocytosis or endocytosis [163, 165, 166, 170]. In order to examine the effect of HOIPIN-8 treatment on MLKL exocytosis during necroptosis, we performed isolation of extracellular vesicles (exosomes) from the supernatant of necroptotic HT-29 cells. Indeed, TBZ-induced necroptosis resulted in the release of MLKL in ALIX-, CD9- and vinculin-positive extracellular exosomes (Figure 30A). As expected, NSA-mediated inhibition of MLKL blocked TBZ-induced exosome formation and release of MLKL (Figure 30A). Importantly, MLKL release in exosomes was also strongly reduced in

HOIPIN-8-treated cells (Figure 30A), suggesting that HOIPIN-8 blocks MLKL association with the plasma membrane and formation of extracellular vesicles. Of note, HOIPIN-8 triggered a necroptosis-dependent increase of MLKL S358 phosphorylation and only partially affected lysosomal degradation of phosphorylated MLKL upon necroptosis induction, as determined after 18 hours after washout of the necroptotic stimulus in the absence or presence of the lysosomal inhibitor bafilomycin A1 (BafA1) (Figure 30B). Taken together, these data indicate that treatment with HOIPIN-8 affects the availability of activated MLKL at membranes and prevents MLKL hotspot formation at the plasma membrane.

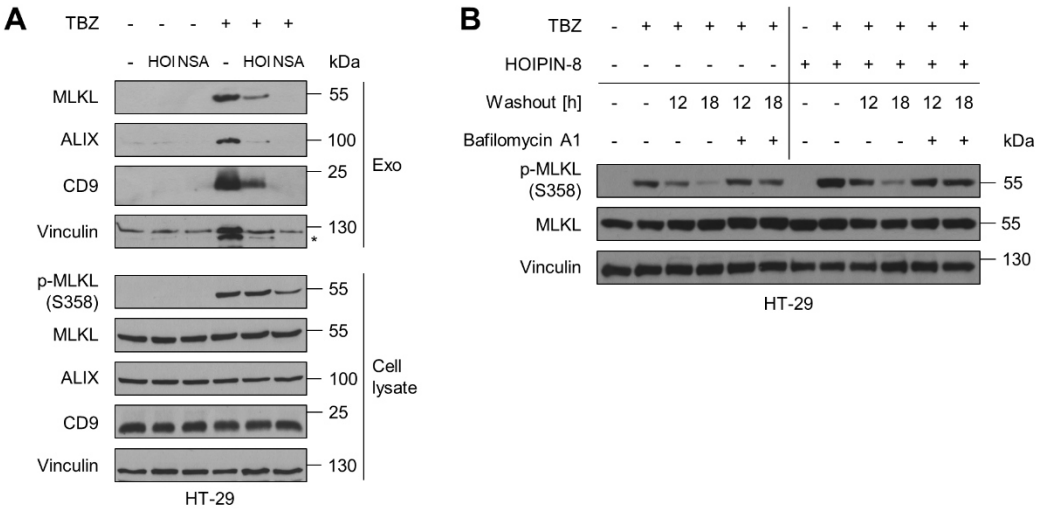

Figure 30. Treatment with HOIPIN-8 affects subcellular segregation of activated MLKL.

A Western blot analysis of TBZ-induced release of MLKL in exosomes, isolated from the supernatants of control, HOIPIN-8 (30 µM) or NSA (10 µM)-pre-treated HT-29 cells after treatment with TBZ (10 ng/mL TNFα, 1 µM BV6, 20 µM zVAD.fmk) for 3 h. Exosome isolation was confirmed with antibodies against ALIX, CD9 and Vinculin. Asterisk marks unspecific band. Expression of phosphorylated and total MLKL was determined by Western blotting of cell lysates from the same experiment. Vinculin was used as loading control. Representative blots of at least two independent experiments are shown. **B** Western blot analysis of lysosomal degradation of phosphorylated MLKL upon TBZ (10 ng/mL TNFα, 0.1 µM BV6, 20 µM zVAD.fmk) treatment of control, HOIPIN-8 (30 µM) or NSA (10 µM)-pre-treated HT-29 cells. HT-29 cells were treated with TBZ for 3 h and either harvested or the medium was exchanged with fresh medium with or without BafA1 (100 nM) after a washing step with PBS. Washed-out cells were harvested 12 h or 18 h after medium exchange. Vinculin was used as loading control. Representative blots of at least two independent experiments are shown.

5.2.1.9 Loss of CHMP2A and ESCRT-associated proteins does not affect HOIPIN-8-mediated rescue of necroptosis

Secretion of exosomes is mediated by the ESCRT-III machinery and ESCRT-associated proteins such as ALIX which cooperate with the ATPase VPS4 to induce membrane scission and exosome biogenesis [377]. Interestingly, ESCRT-III and ESCRT-associated proteins have been implicated in the necroptosis-dependent plasma membrane repair [123] and ESCRT-III was shown to mediate MLKL exocytosis in several studies [173]. In order to investigate whether ESCRT-III or ESCRT-associated proteins affect necroptosis and the HOIPIN-8-mediated rescue of necroptotic cell death, we performed siRNA-mediated knockdown of ESCRT-III protein charged multivesicular body protein 2A (CHMP2A), ALIX and VPS4A in HT-29 cells. Silencing of CHMP2A led to cell death in untreated and HOIPIN-8-treated cells (Figure 31A-B) which is line with a previous report demonstrating that loss of CHMP2A induces cell death [123]. Although basal cell death levels were higher in CHMP2A knockdown cells, TBZ treatment induced prominent cell death which could be reduced to a similar extent as in the control cells by treatment with HOIPIN-8 (Figure 31A). In addition, both siRNA-mediated knockdown of VPS4A and ALIX did not affect TBZ-induced cell death and HOIPIN-8-mediated rescue of necroptosis (Figure 31C-D and Figure 31E-F).

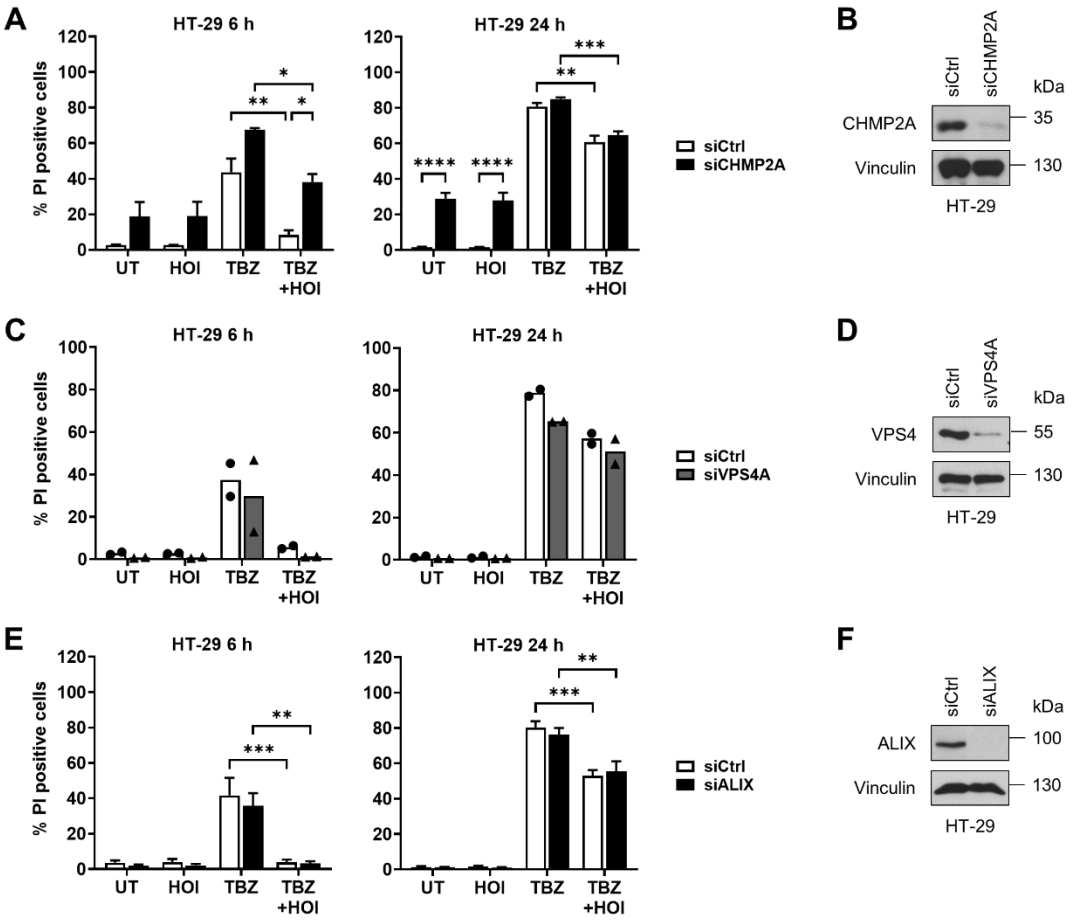

Figure 31. Loss of CHMP2A or ESCRT-associated proteins ALIX and VPS4A does not affect HOIPIN-8-mediated rescue of TBZ-induced necroptosis.

A Quantification of cell death in control (siCtrl) and CHMP2A knockdown (siCHMP2A) HT-29 cells after treatment with TBZ (10 ng/mL TNFα, 1 µM BV6, 20 µM zVAD.fmk) for the indicated time points. Mean and SEM of n=3 independent experiments are shown. **B** Expression of CHMP2A in control (siCtrl) and CHMP2A knockdown (siCHMP2A) HT-29 cells. GAPDH was used as loading control. Representative blots of at least two independent experiments are shown. **C** Quantification of cell death in control (siCtrl) and VPS4A (siVPS4A) knockdown HT-29 cells after treatment with TBZ (10 ng/mL TNFα, 1 µM BV6, 20 µM zVAD.fmk) for the indicated time points. Mean and individual values of n=2 independent experiments are shown. **D** Expression of VPS4 in control (siCtrl) and VPS4A knockdown (siVPS4A) HT-29 cells. GAPDH was used as loading control. n=1 is shown. **E** Quantification of cell death in control (siCtrl) and ALIX knockdown (siALIX) HT-29 cells after treatment with TBZ (10 ng/mL TNFα, 1 µM BV6, 20 µM zVAD.fmk) for the indicated time points. Mean and SEM of n=3 independent experiments are shown. **F** Expression of ALIX in control (siCtrl) and ALIX knockdown (siALIX) HT-29 cells. GAPDH was used as loading control. Representative blots of at least two independent experiments are shown.

*P<0.05; **P<0.01; ***P<0.001.

5.2.2 Necroptosis induces an inflammatory cytokine profile that is dependent on LUBAC function

5.2.2.1 LUBAC-mediated M1 poly-Ub regulates necroptosis-induced and MLKL-dependent production of inflammatory signaling molecules

Necroptosis is an immunogenic form of PCD characterized by the release of cellular contents which promote a pro-inflammatory response [58, 353]. Furthermore, recent studies demonstrated that necroptosis triggers expression of a variety of pro-inflammatory cytokines and chemokines, including CXCL1 and CXCL10, which are dependent on necroptotic signaling and MLKL activation [59, 123]. Indeed, transcriptome profiling using unbiased MACE-seq of necroptotic HT-29 cells confirmed transcriptional upregulation of a highly pro-inflammatory gene expression profile that included upregulation of cytokines and chemokines such as TNFα, CSF1, CXCL2 and chemokine (C-C motif) ligand 20 (CCL20), as well as the intercellular adhesion molecule 1 (ICAM1) (Figure 32). Importantly, expression of these necroptosis-induced cytokines and chemokines could be potently reversed by LUBAC inhibition with HOIPIN-8 (Figure 32). The MACE-seq data obtained in this study have been deposited at GEO (GEO accession GSE220171).

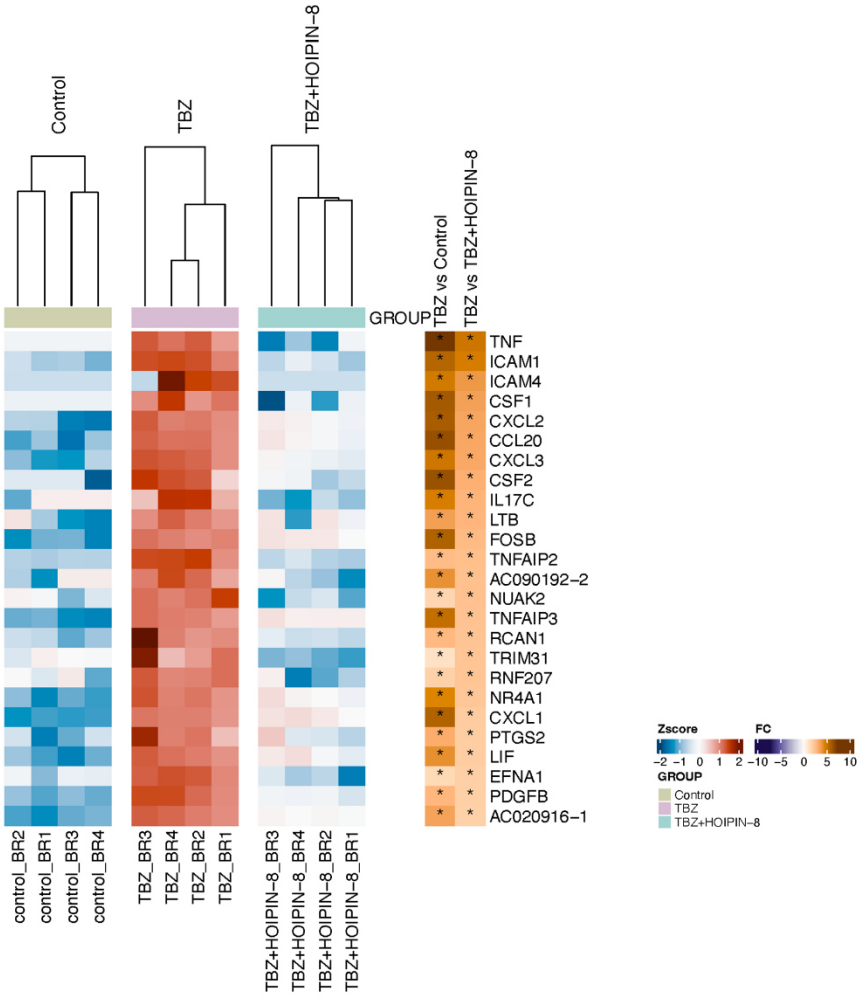

Figure 32. Necroptosis induces an inflammatory cytokine profile which can be blocked by inhibition of LUBAC function with HOIPIN-8.

MACE-seq-determined heatmap showing the row-wise scaled intensity (left panel) of the top-25 upregulated genes in HT-29 cells treated with TBZ (10 ng/mL TNFα, 1 µM BV6, 20 µM zVAD.fmk) for 3 h in comparison to HOIPIN-8 (30 µM)-pre-treated and TBZ-treated HT-29 cells. Genes are sorted according to their log2 fold change values (right panel). *P<0.05.

MACE-seq-based transcriptome analysis was performed by Leonard Feist and Björn Rotter. Geoffroy Andrieux, Tonmoy Das and Melanie Börries analyzed and visualized the MACE-seq data.

Quantitative real-time PCR further demonstrated necroptosis-dependent upregulation of *CXCL1* and *CXCL10* mRNA (Figure 33A) as well as *TNFA* and *ICAM1* mRNA (Figure 33B) in HT-29 cells, consistent with previous findings [59, 123]. In agreement with the abovementioned observations, LUBAC inhibition with HOIPIN-8 in necroptotic cells reduced expression of these cytokines (Figure 33A-B), and siRNA-mediated knockdown of HOIP expression resulted in decreased expression of *CXCL1* and *CXCL10* (Figure 33C).

Of note, previous studies have demonstrated that necroptosis-induced expression of pro-inflammatory cytokine profiles occurs in two waves. The first wave is transient and occurs in response to TNFα alone, whereas the second wave depends on necroptotic signaling [59]. In line with these data, necroptosis-induced expression of *CXCL1* and *CXCL10* could be largely blocked by inhibition of MLKL with NSA and by CRISPR/Cas9-mediated KO of MLKL (Figure 33A and Figure 33D). Similarly, NSA treatment blocked expression of *TNFA* and *ICAM1* mRNA in necroptotic cells (Figure 33B). These results confirm that MLKL is required for necroptosis-induced upregulation of cytokines and chemokines.

Since LUBAC plays a prominent role in the regulation of TNFα-induced NF-κB activation, HT-29 cells were treated with TNFα and TBZ, in order to exclude the possibility that HOIPIN-8-mediated decreases in cytokine production are solely due to the role of LUBAC in the regulation of TNFα-induced signaling. In agreement with previous data [59], TNFα-induced *CXCL1* and *TNFA* mRNA expression was weaker than in cells treated with TBZ (Figure 33E). Importantly, HOIPIN-8-mediated LUBAC inhibition prevented *CXCL1* and *TNFA* upregulation in both TNFα- and TBZ-treated cells, however, inhibition of MLKL with NSA only blocked TBZ-induced *CXCL1* and *TNFA* levels (Figure 33E).

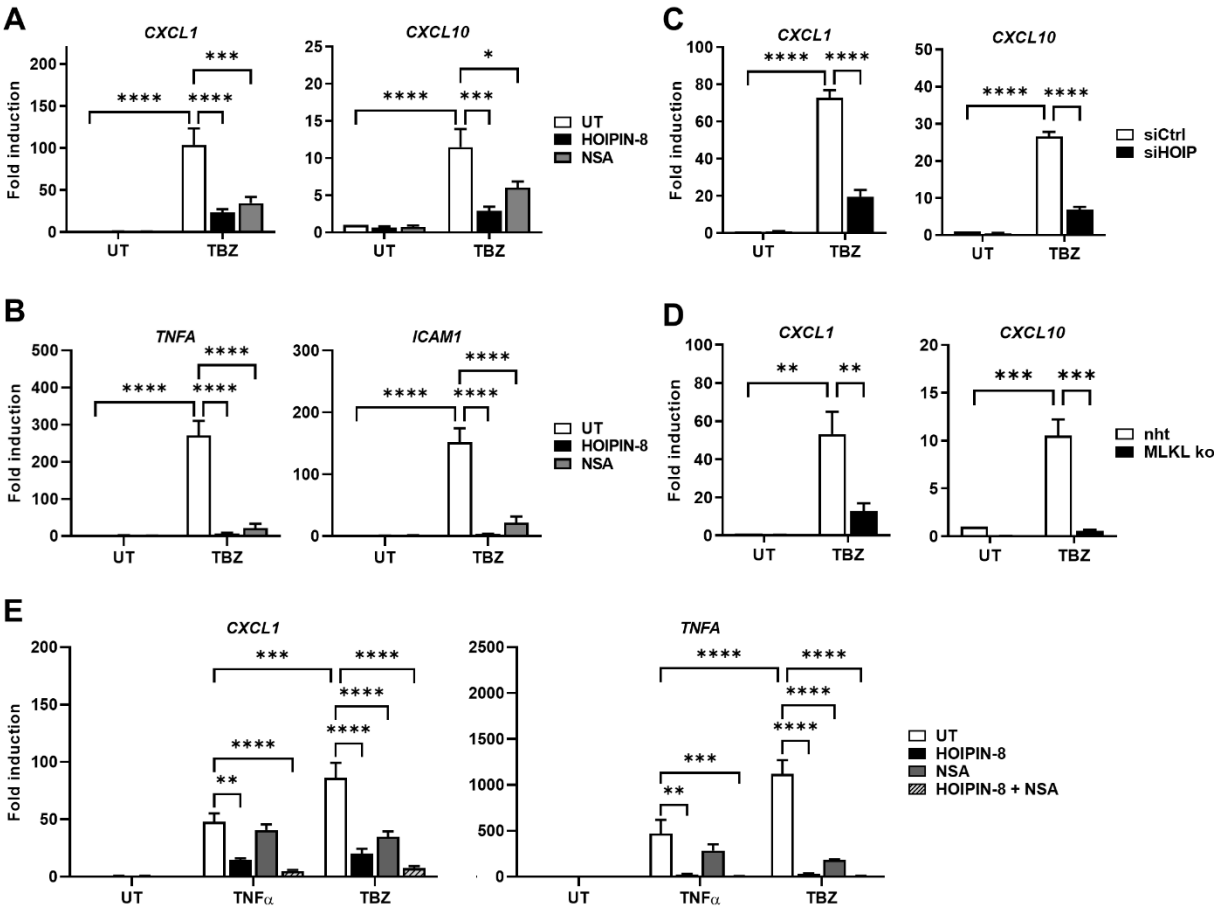

Figure 33. Loss of LUBAC function blocks necroptosis-induced and MLKL-dependent cytokine production.

A mRNA expression levels of *CXCL1* and *CXCL10* of (UT), HOIPIN-8 (30 µM) or NSA (10 µM)-pre-treated HT-29 cells upon treatment with TBZ (10 ng/mL TNFα, 1 µM BV6, 20 µM zVAD.fmk) for 3 h. Gene expression was normalized against *18S* and *RPII* mRNA expression and is presented as x-fold mRNA expression compared to the untreated (UT) control. Mean and SEM of n=4 independent experiments are shown. **B** mRNA expression levels of *TNFA* and *ICAM1* of control (UT), HOIPIN-8 (30 µM) or NSA (10 µM)-pre-treated HT-29 cells upon treatment with TBZ (10 ng/mL TNFα, 1 µM BV6, 20 µM zVAD.fmk) for 3 h. Gene expression was normalized against *18S* and *RPII* mRNA expression and is presented as x-fold mRNA expression compared to the untreated (UT) control. Mean and SEM of n=3 independent experiments are shown. **C** mRNA expression levels of *CXCL1* and *CXCL10* of control (siCtrl) or HOIP knockdown (siHOIP) HT-29 cells treated with TBZ (10 ng/mL TNFα, 1 µM BV6, 20 µM zVAD.fmk) for 4 h. Gene expression was normalized against *18S* and *RPII* mRNA expression and is presented as x-fold mRNA expression compared to the untreated (UT) control cells. Mean and SEM of n=4 independent experiments are shown. **D** mRNA expression levels of *CXCL1* and *CXCL10* of control (nht) or MLKL KO HT-29 cells treated with TBZ (10 ng/mL TNFα, 1 µM BV6, 20 µM zVAD.fmk) for 3 h. Gene expression was normalized against *18S* and *RPII* mRNA expression and is presented as x-fold mRNA expression compared to the untreated (UT) control cells. Mean and SEM of n=3 independent experiments are shown. **E** mRNA expression levels of *CXCL1* and *TNFA* of control (UT), HOIPIN-8 (30 µM), NSA (10 µM) or combined HOIPIN-8 (30 µM) and NSA (10 µM)-pre-treated HT-29 cells upon treatment with TNFα (10 ng/mL) or TBZ (10 ng/mL TNFα, 1 µM BV6, 20 µM zVAD.fmk) for 3 h. Gene expression was normalized against *18S* and *RPII* mRNA expression and is presented as x-fold mRNA expression compared to the untreated (UT) control. Mean and SEM of n=4 independent experiments are shown. qPCR analysis for *CXCL1* in (E) was performed by Sonja Smith.

**P*<0.05; ***P*<0.01; ****P*<0.001; *****P*<0.0001.

In line with the LUBAC-dependent necroptosis-induced upregulation of cytokines, necroptosis-dependent secretion of CXCL1 was strongly reduced upon treatment of HT-29 cells with HOIPIN-8 and in HOIP-deficient HT-29 cells (Figure 34).

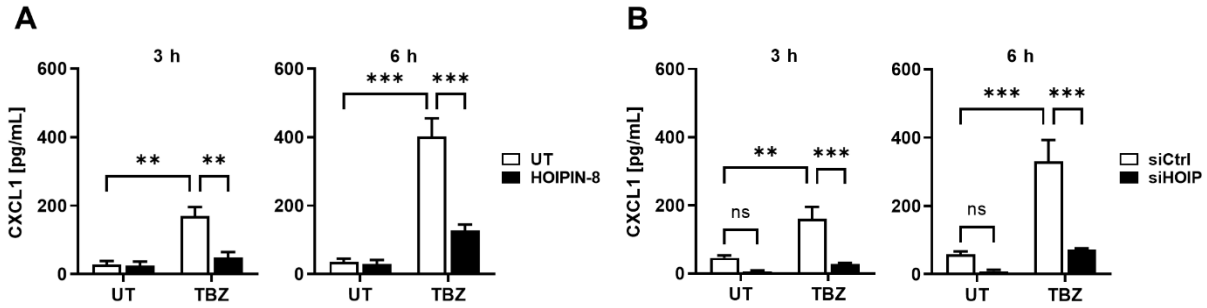

Figure 34. Loss of LUBAC function blocks necroptosis-induced CXCL1 release.

A ELISA-based quantification of CXCL1 secretion in supernatants of control (UT) or HOIPIN-8 (30 µM)-pre-treated HT-29 cells after treatment with TBZ (10 ng/mL TNFα, 1 µM BV6, 20 µM zVAD.fmk) for the indicated time points. Mean and SEM of n=3 independent experiments are shown. **B** ELISA-based quantification of CXCL1 secretion in supernatants of control (siCtrl) or HOIP knockdown (siHOIP) HT-29 cells treated with TBZ (10 ng/mL TNFα, 1 µM BV6, 20 µM zVAD.fmk) for the indicated time points. Mean and SEM of n=4 independent experiments are shown.

$^{**}P<0.01$; $^{***}P<0.001$; ns: not significant.

ELISA analysis was performed by Sonja Smith.

5.2.2.2 CRISPR/Cas9-mediated HOIP KO prevents necroptosis-induced cytokine production

Importantly, CRISPR/Cas9-mediated HOIP KO in HT-29 cells prevented TNFα- as well as TBZ-induced upregulation of *CXCL1* and *TNFA* mRNA (Figure 35). HOIPIN-8 further decreased *CXCL1* and *TNFA* mRNA levels, however, this is likely due to remaining HOIP-expressing cells in the polyclonal HOIP KO bulk culture (Figure 35).

Together, these findings demonstrate that LUBAC-mediated M1 poly-Ub is required for necroptosis-induced and MLKL-dependent production and release of signaling molecules, cytokines and chemokines.

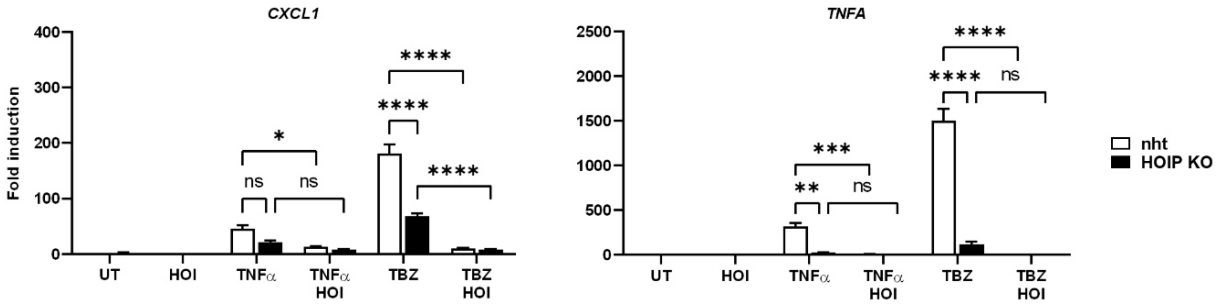

Figure 35. CRISPR/Cas9-mediated KO of HOIP blocks necroptosis-induced *CXCL1* and *TNFA* expression.

mRNA expression levels of *CXCL1* and *TNFA* of control (UT) or HOIPIN-8 (30 µM)-pre-treated HT-29 control (nht) or HOIP KO cells upon treatment with TNFα (10 ng/mL) or TBZ (10 ng/mL TNFα, 1 µM BV6, 20 µM zVAD.fmk) for 4 h. Gene expression was normalized against *18S* and *RPII* mRNA expression and is presented as x-fold mRNA expression compared to the untreated (UT) control cells (nht). Mean and SEM of n=3 independent experiments are shown. **P*<0.05; ***P*<0.01; ****P*<0.001; *****P*<0.0001; ns: not significant.

5.2.3 FLOT1/2 are putative targets of LUBAC-mediated M1 poly-Ub during necroptosis

5.2.3.1 Necroptosis induces LUBAC-dependent enrichment of FLOT1/2 in M1 poly-Ub pulldowns

FLOTs have been recently implicated in the regulation of MLKL endocytosis [165, 166] and interact with MLKL upon necroptosis induction [166]. In order to understand the potential link between M1 poly-Ub and FLOT1/2 during necroptosis, we performed UBAN-based enrichment of M1 poly-Ub chains, substrates and associated proteins from necroptotic HT-29 and THP-1 cells. Intriguingly, high levels of FLOT1 and FLOT2 could be detected in UBAN-based M1 poly-Ub pulldowns upon treatment of HT-29 cells with TBZ, which increased over time (Figure 36A). The M1 poly-Ub-associated necroptosis-dependent enrichment of FLOT1/2 could be effectively blocked by LUBAC inhibition with HOIPIN-8, without affecting total FLOT1/2 cellular expression levels (Figure 36A). Similar results were obtained in necroptotic THP-1 cells (Figure 36B). TBZ induced enrichment of FLOT1 in M1 poly-Ub pulldowns from THP-1 cells which could be completely prevented with HOIPIN-8 (Figure 36B). In order to confirm the LUBAC and M1 poly-Ub-dependent enrichment of FLOT1 upon TBZ treatment, M1 poly-Ub pulldown was performed using CRISPR/Cas9-mediated HOIP KO HT-29 cells.

In line with the abovementioned findings, HOIP deletion effectively prevented necroptosis-induced enrichment of FLOT1 in M1 poly-Ub pulldowns (Figure 36C).

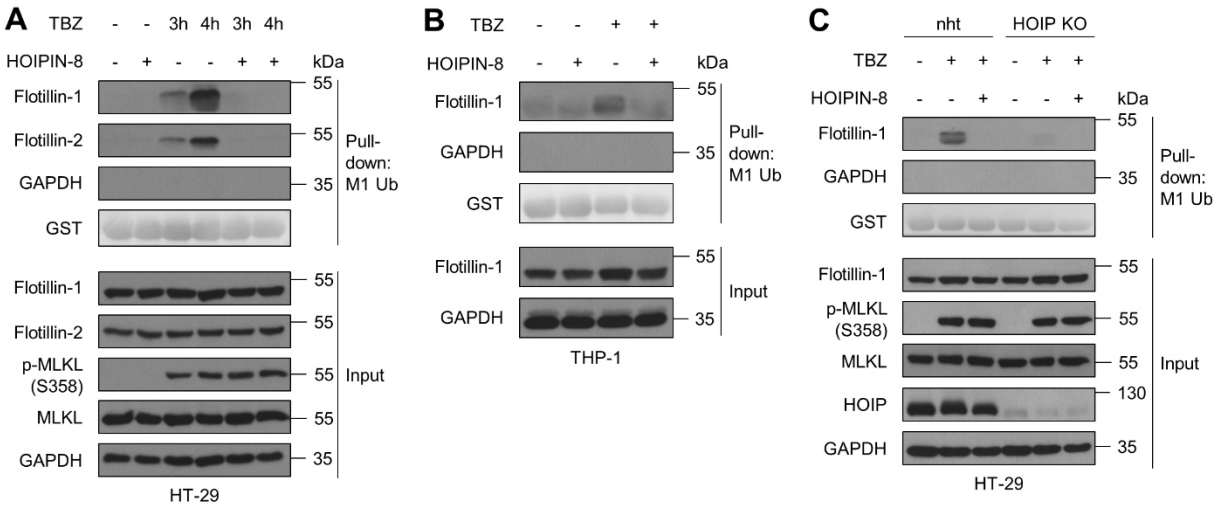

Figure 36. Necroptosis induces LUBAC-dependent FLOT1/2 enrichment in UBAN-mediated M1 Ub pulldowns.

A UBAN-mediated pulldown of M1-ubiquitinated proteins in control or HOIPIN-8 (30 µM)-pre-treated HT-29 cells treated with TBZ (10 ng/mL TNFα, 1 µM BV6, 20 µM zVAD.fmk) for the indicated time points. GST and GAPDH were used as loading controls. Representative blots of at least two independent experiments are shown. **B** UBAN-mediated pulldown of M1-ubiquitinated proteins in control or HOIPIN-8 (30 µM)-pre-treated THP-1 cells treated with TBZ (10 ng/mL TNFα, 1 µM BV6, 20 µM zVAD.fmk) for 4 h. GST and GAPDH were used as loading controls. Representative blots of at least two independent experiments are shown. **C** UBAN-mediated pulldown of M1-ubiquitinated proteins in control or HOIPIN-8 (30 µM)-pre-treated control (nht) or HOIP KO HT-29 cells treated with TBZ (10 ng/mL TNFα, 1 µM BV6, 20 µM zVAD.fmk) for 4 h. GST and GAPDH were used as loading controls. Representative blots of at least two independent experiments are shown.

Importantly, in addition to HOIPIN-8-mediated LUBAC inhibition, TBZ-induced enrichment of FLOT1 in M1 poly-Ub pulldowns could be blocked by treatment of HT-29 cells with the RIPK1 inhibitor Nec-1s, RIPK3 inhibitor GSK'872 and MLKL inhibitor NSA, without affecting basal FLOT1 expression levels (Figure 37A-B). These results demonstrate that the enrichment of FLOT1 in UBAN-based pulldowns is dependent on necroptotic signaling and furthermore suggest that MLKL plasma membrane translocation is a prerequisite for the association of FLOT1 with M1 poly-Ub. However, since FLOT1/2 enrichments in UBAN-based pulldowns of M1 poly-Ub of necroptotic cells may be due to their interaction with other M1 poly-ubiquitinated proteins and since FLOTs have been demonstrated to directly interact with MLKL, levels of MLKL and RIPK3 in UBAN-based pulldowns upon necroptosis induction were further analyzed.

While MLKL could be detected in UBAN-based pulldowns, RIPK3 was completely absent (Figure 37B). Importantly, TBZ-induced necroptosis did not further increase M1 poly-Ub-associated enrichment of MLKL (Figure 37B), it is therefore unlikely that the necroptosis-induced enrichment of FLOT1/2 is due to interactions with M1 Ub-modified MLKL.

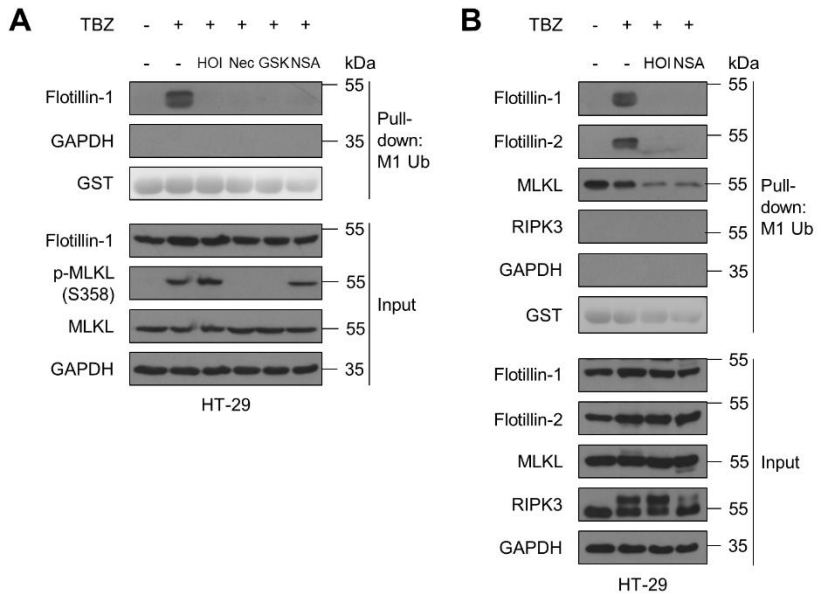

Figure 37. Inhibition of RIPK3 and MLKL restricts necroptosis-dependent FLOT1/2 enrichment in UBAN-mediated M1 Ub pulldowns.

A UBAN-mediated pulldown of M1-ubiquitinated proteins in control, HOIPIN-8 (30 µM), Nec-1s (30 µM), GSK'872 (20 µM) or NSA (10 µM)-pre-treated HT-29 cells treated with TBZ (10 ng/mL TNFα, 1 µM BV6, 20 µM zVAD.fmk) for 4 h. GST and GAPDH were used as loading controls. Representative blots of at least two independent experiments are shown. **B** UBAN-mediated pulldown of M1-ubiquitinated proteins in control, HOIPIN-8 (30 µM) or NSA (10 µM)-pre-treated HT-29 cells treated with TBZ (10 ng/mL TNFα, 1 µM BV6, 20 µM zVAD.fmk) for 4 h. GST and GAPDH were used as loading controls. Representative blots of at least two independent experiments are shown.

5.2.3.2 FLOT1/2 license necroptosis in a M1 poly-Ub-dependent manner

Since FLOTs could be detected in UBAN-based M1 poly-Ub pulldowns upon necroptosis induction, we examined how loss of FLOT expression may affect necroptotic cell death in HT-29 cells. In contrast to previously published data [166], siRNA-mediated knockdown of both FLOT1 and FLOT2 or combined knockdown of FLOT1/2 decreased necroptotic cell death and further potentiated the repressive effects of HOIPIN-8 on necroptosis (Figure 38A-B).

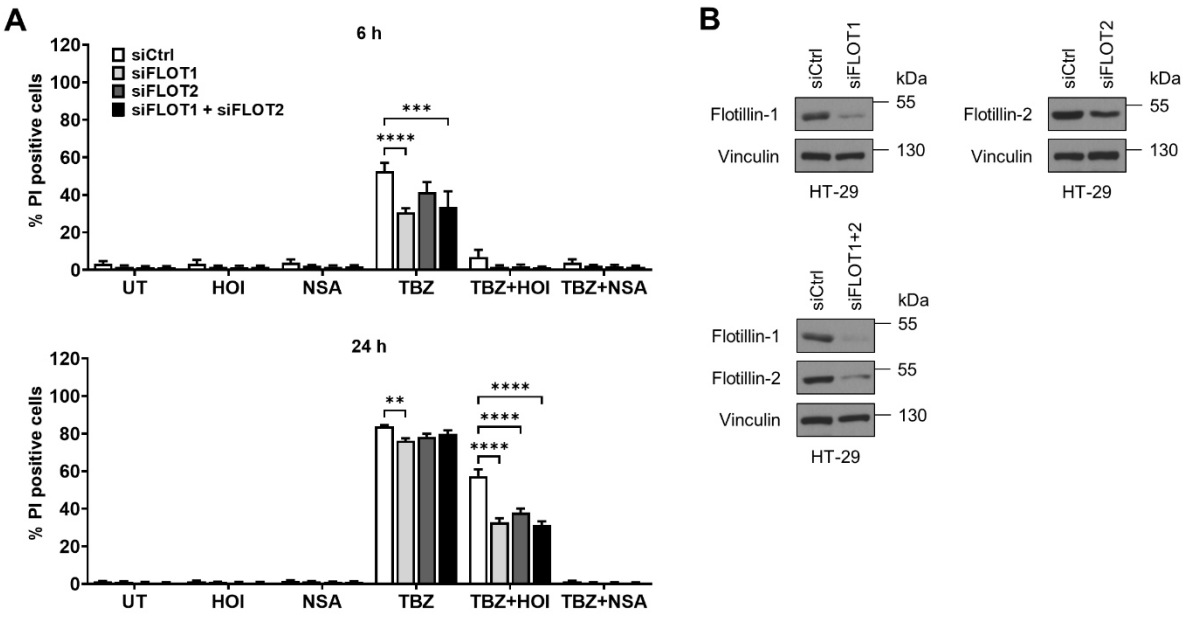

Figure 38. Loss of FLOT1/2 decreases necroptotic cell death and further increases the rescue effect of HOIPIN-8.

A Quantification of cell death in untreated (UT), HOIPIN-8 (30 µM) or NSA (10 µM)-pre-treated control (siCtrl), FLOT1 (siFLOT1), FLOT2 (siFLOT2) or combined FLOT1 and FLOT2 (siFLOT1+siFLOT2) knockdown HT-29 cells after treatment with TBZ (10 ng/mL TNFα, 1 µM BV6, 20 µM zVAD.fmk) for the indicated time points. Mean and SEM of n=3 independent experiments are shown. ***P*<0.001; ****P*<0.001; *****P*<0.0001. **B** Western blot analysis of FLOT1/2 levels in control (siCtrl) and FLOT1 (siFLOT1), FLOT2 (siFLOT2) or combined FLOT1/2 (siFLOT1+2) knockdown HT-29 cells. Vinculin was used as loading control. Representative blots of at least two independent experiments are shown.

To further explore the effects of FLOT1/2 deficiency on necroptosis, the necroptotic signaling pathway was assessed. Importantly, combined loss of FLOT1/2 expression did not affect phosphorylation of RIPK3 S227 and MLKL S358 (Figure 39A-B) and did not influence necrosome formation, as determined by immunoprecipitation of Strep-RIPK3 from control and combined FLOT1/2 knockdown RIPK3 KO HT-29 cells re-expressing PAM-mutated Dox-inducible Strep-tagged RIPK3 WT (Figure 39A). Furthermore, loss of FLOT1/2 did not affect necroptosis-induced MLKL oligomerization (Figure 39B) and necroptosis-induced increases in M1 poly-Ub or HOIPIN-8-mediated decreases in necroptosis-triggered M1 poly-Ub (Figure 39C).

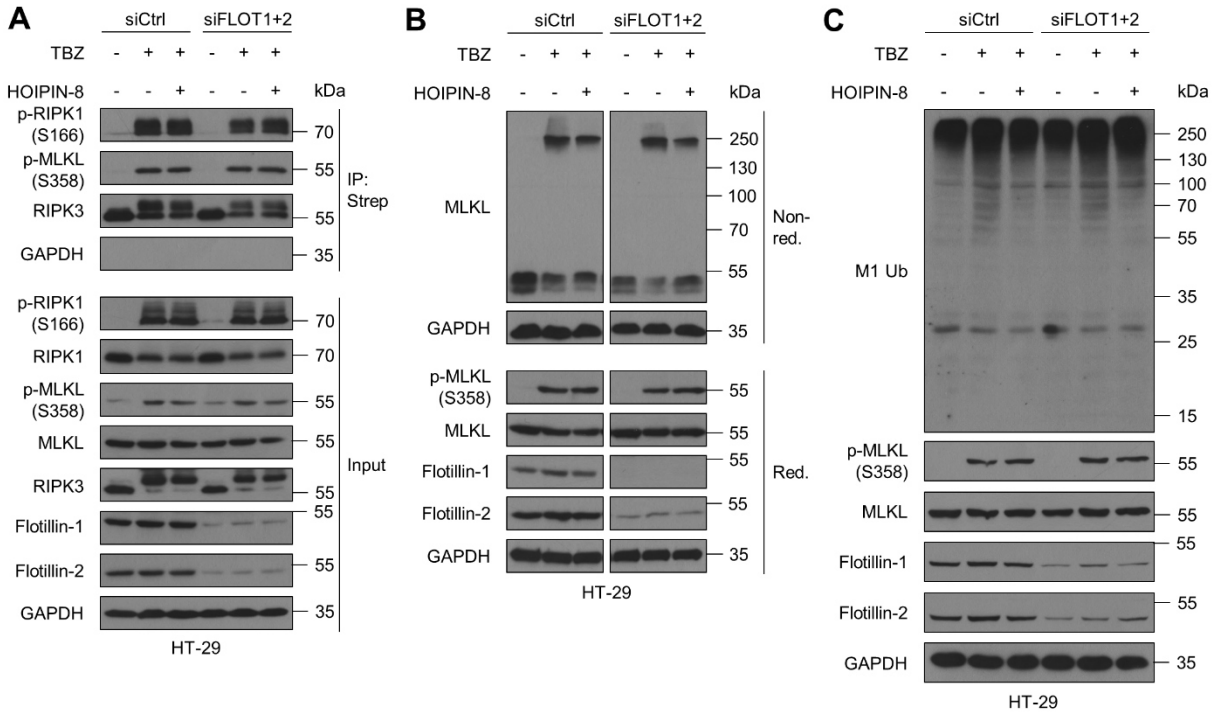

Figure 39. Loss of FLOT1/2 does not affect necrosome formation and MLKL oligomerization.

A Characterization of necrosome formation by immunoprecipitation of Strep-RIPK3 from control and HOIPIN-8 (30 µM)-pre-treated control (siCtrl) and combined FLOT1 and FLOT2 knockdown (siFLOT1+2) RIPK3 KO HT-29 cells re-expressing PAM-mutated Dox-inducible Strep-tagged RIPK3 WT [146] after treatment with TBZ (10 ng/mL TNFα, 1 µM BV6, 20 µM zVAD.fmk) for 3 h. Cell lines were incubated overnight with 1 µg/mL Dox prior to treatment to induce expression of Strep-RIPK3. GAPDH was used as loading control. Representative blots of at least two independent experiments are shown. **B** Western blot analysis of MLKL oligomerization after treatment with TBZ (10 ng/mL TNFα, 1 µM BV6, 20 µM zVAD.fmk) for 4 h by non-reducing Western blotting of control (siCtrl) and combined FLOT1 and FLOT2 knockdown (siFLOT1+2) HT-29 cells. GAPDH was used as loading control. Representative blots of at least two independent experiments are shown. **C** Western blot analysis of total M1 Ub levels of control or HOIPIN-8 (30 µM)-pre-treated control (siCtrl) or FLOT1/2 (siFLOT1+2) knockdown HT-29 cells after treatment with TBZ (10 ng/mL TNFα, 1 µM BV6, 20 µM zVAD.fmk) for 4 h. GAPDH was used as loading control. Representative blots of at least two independent experiments are shown.

In conclusion, this study identifies LUBAC-mediated M1 poly-Ub as a novel mediator in necroptosis. We observed a prominent decrease of necroptotic cell death upon treatment with HOIP inhibitors HOIPIN-8 and gliotoxin, as well as after siRNA-mediated HOIP knockdown, in human cell lines and primary hPOs, but not in murine cells. We provide evidence that HOIPIN-8 affects necroptosis induction downstream of MLKL activation and oligomerization, by blocking MLKL membrane translocation and without affecting upstream necroptotic RIPK1 and RIPK3 phosphorylation and necrosome formation. Furthermore, our data highlight the role of LUBAC-mediated M1 poly-Ub and MLKL in the necroptosis-dependent induction of pro-inflammatory

cytokine and chemokine production. In addition, we identify FLOT1/2 as putative targets of M1 poly-Ub during necroptosis. Finally, by using primary hPOs we provide a novel platform to study necroptosis in near-physiological settings.

6 Discussion

The relevance of LUBAC-generated M1-linked Ub in the regulation of cytokine-induced canonical NF-κB signaling is highlighted in various studies including genetic mouse models of LUBAC deficiency [12, 235, 253, 270, 326] as well as in patients with mutations in either of the LUBAC subunits which cause NF-κB-related autoinflammatory diseases (relopathies) [236, 273, 325, 347, 378]. In line with this, deficiency of the M1 Ub-cleaving DUB OTULIN in ORAS patients also results in severe autoinflammatory disease as a result of dysregulated canonical NF-κB pathway activation [290, 294-296, 301, 302]. In addition to the abovementioned effects on NF-κB signaling, loss of LUBAC subunits also sensitizes some cells towards TNFR1- and RIPK1-dependent cell death [12, 235, 274, 327-330], indicating a central role of M1 poly-Ub in the regulation of TNFR1-mediated cell fate signaling. In this study, we identify LUBAC-mediated M1-poly-Ub as an essential mediator of necroptosis-induced and MLKL-dependent inflammatory cytokine production. In addition, by utilizing UBAN-based M1 poly-Ub pulldowns, we identify FLOT1/2 as a novel putative target of LUBAC-mediated M1 poly-Ub during TNFR1-induced necroptosis. We further demonstrate that inhibition of LUBAC activity with the small molecule chemical HOIP inhibitor HOIPIN-8, or by siRNA-mediated HOIP knockdown, inhibits TBZ-induced cell death in various human but not murine cell lines, without affecting necroptotic signaling, including phosphorylation of MLKL at S358 and MLKL oligomerization. HOIPIN-8 prevents MLKL membrane translocation and hotspot formation at the plasma membrane. In addition to human cell lines, we confirm the rescue effect of HOIPIN-8 on necroptotic cell death in primary human organoids. Intriguingly, the rescue effect of HOIPIN-8 could not be validated in CRISPR/Cas9-mediated HOIP KO cell lines.

6.1 HOIPIN-8-mediated LUBAC inhibition blocks necroptosis in human but not in murine cells

Our data indicate a role of LUBAC-mediated M1-linked poly-Ub in the regulation of necroptotic cell death in human cells, as treatment with the LUBAC inhibitors HOIPIN-8 and gliotoxin, as well as siRNA-mediated knockdown of HOIP prominently blocked TBZ-induced necroptosis. Interestingly, LUBAC is conserved among mammals, where

it regulates innate and acquired immune responses, and an ortholog of HOIP, named linear ubiquitin E3 ligase (LUBEL), has been recently identified to control stress and inflammatory responses in *drosophila* [379, 380], suggesting that the role of M1-linked ubiquitination in maintaining cellular homeostasis is evolutionary conserved [288]. Intriguingly, the observed protective effects of LUBAC inhibition with HOIPIN-8 or siRNA-mediated HOIP knockdown in the context of necroptosis could only be demonstrated in human cells but not in cell lines of murine origin. To exclude the possibility that the observed effects are cell type-specific, we explored the influence of HOIPIN-8 on necroptosis in the human colon carcinoma cell line HT-29, the human leukemic monocyte cell line THP-1 and primary hPOs, as well as in MEFs, L-929 mouse lung fibroblasts and the murine monocyte/macrophage cell line RAW264.7. While all tested human cells showed strongly reduced/delayed necroptotic cell death upon treatment with HOIPIN-8, necroptosis was increased in HOIPIN-8-treated murine cell lines, as compared to the untreated controls. To our surprise, CRISPR/Cas9-mediated HOIP KO in HT-29 and THP-1 did not mirror the rescue of necroptosis mediated by HOIPIN-8 or siRNA-mediated HOIP knockdown and HOIP KO in murine L-929 cells did not reflect the HOIPIN-8-mediated increase of necroptosis. Moreover, HOIPIN-8 also blocked necroptosis in HOIP KO cells. Although the used cell cultures are polyclonal bulk cultures that still contain HOIP-expressing cells, it cannot be excluded that HOIPIN-8 has additional off-target effects.

Of note, HOIPIN-8 effectively inhibits NF-κB activation and IFN antiviral pathways in several human and murine cell lines, including HEK293T, HeLa, A549, Jurkat, MEF, murine bone marrow-derived macrophages (BMDM) [285, 286, 381], as well as in HT-29 (this study). In addition, HOIPIN-8 treatment has been shown to block xenophagy of invading *Salmonella* in HeLa cells, by inhibiting M1 Ub decoration of *Salmonella* and recruitment of LC3-positive membranes, which initiate bacterial clearance [381]. Indeed, amino acid sequence alignment of the catalytic HOIP-RING2 and LDD, which include several residues that interact with HOIPIN-8 [286], revealed high sequence conservation between humans and mice, thus indicating that HOIPIN-8 is effective in both species. Although HOIPIN-8 is reportedly the most effective selective HOIP inhibitor [286], we obtained similar results with gliotoxin, a metabolite of fungal species, which has been demonstrated to inhibit LUBAC-mediated generation of M1 poly-Ub and NF-κB activation by binding to the catalytic center of HOIP at aa699-aa1072 [282].

It has been stated by others that gliotoxin lacks inhibitory effects when used at non-toxic concentrations in HEK293T cells [286, 288], however, our data demonstrate potent inhibition of necroptotic cell death with gliotoxin which resembles the data obtained with HOIPIN-8 in both HT-29 and THP-1 cells.

6.1.1 Species-specific differences of the core necroptotic signaling pathway

Although HOIP inhibition prevented necroptotic cell death in human cells, evaluation of the necroptotic signaling pathway revealed that treatment with HOIPIN-8, similar as siRNA-mediated HOIP knockdown or CRISPR/Cas9-mediated HOIP KO, did not affect necroptotic phosphorylation of RIPK1, RIPK3 and MLKL in both human and murine cell lines. Intriguingly, several important mechanistic differences between necroptotic signaling pathways in cells of human and murine origin have been described, which might underlie the species-specific effects of HOIPIN-8.

The components of the necroptotic core machinery are surprisingly poorly conserved throughout the animal kingdom, however, both humans and mice express RIPK1, RIPK3 and MLKL, and human and murine cell lines, such as HT-29 and MEF, are commonly used model cell lines to study necroptosis *in vitro* [382]. Hence, current knowledge about the molecular mechanisms that underlie necroptosis mostly stems from studies carried out with samples of human or murine origin [382]. Necroptosis is regulated by post-translational modifications of necroptotic key players RIPK1, RIPK3 and MLKL, as well as by compartmentalization events, including necrosome clustering and translocation of MLKL to cellular membranes [124-126]. Although the principles of necroptotic signaling are conserved between mammals, several studies revealed important species-specific differences between human and murine necroptotic pathways [79, 104, 110, 112, 114, 383-386]. Intriguingly, expression of murine and human MLKL orthologs in cells of the opposite species does not reconstitute necroptotic signaling [104, 110, 112]. Moreover, while expression of murine phosphomimic mutant MLKL S345D can induce necroptosis in murine cells [107, 109, 387], it failed do so in human cells [104]. Expression of the human phosphomimic mutant MLKL T357E/S358E could not induce cell death in both murine cells and human cells, however, in human cell lines, forced dimerization of MLKL could overcome this [104]. Together, these data suggest mechanistic differences in the activation modes of murine and human MLKL. Interestingly, while RIPK3-mediated

phosphorylation of MLKL seems to be sufficient to allow activation of murine MLKL [101], several reports indicate that, apart from RIPK3-mediated phosphorylation, human MLKL also requires stable interaction with RIPK3 in order to be fully activated [79, 110, 383-386, 388]. Recent studies also suggest that distinct conformations of the MLKL pseudokinase domain and structural differences in the human RIPK3:MLKL interface may account for the strict species specificity of MLKL activation during necroptosis, indicating divergent regulatory mechanisms among MLKL orthologues and coevolution of the RIPK3:MLKL signaling cassette [110, 112, 126, 383, 384, 388]. Although the key steps of necroptosis signaling are conserved, rapid coevolution of RIPK3 and MLKL led to important mechanistic differences and there are likely more, yet unidentified modulators that control necroptosis both upstream and downstream of MLKL activation in a species- and cell-specific manner [126].

6.1.2 HOIPIN-8 blocks necroptosis downstream of human MLKL oligomerization

Cellular fractionation experiments and immunofluorescence imaging of phosphorylated MLKL in HT-29 cells, as well as analysis of necroptosis-induced release of MLKL in exosomes, strongly suggest that HOIPIN-8 prevents translocation of activated MLKL to cellular membranes including the plasma membrane. Thus, HOIPIN-8 likely affects signaling or trafficking events downstream of MLKL oligomerization. Although the membrane-permeabilization function of the MLKL 4HB domain is evolutionarily conserved, oligomerization of MLKL and execution of necroptosis depend on additional proteins that are poorly conserved and not expressed in all cell types [104, 389]. Several studies indicate that murine MLKL forms trimers [101, 114] while human MLKL assembles into tetramers [110]. Interestingly, while murine MLKL spontaneously oligomerizes into higher molecular weight complexes, human MLKL lacks the intrinsic capacity to oligomerize and requires additional factors [104]. Oligomerization of human MLKL is promoted by several auxiliary interactors such as HSP70 [160], HSP90 [158, 159, 390] as well as inositol phosphate kinases [391, 392] and is tuned by phosphorylation of MLKL Y376 by TAM kinases [157], while thioredoxin-1 (Trx1) has been shown to suppress MLKL polymerization [393]. Oligomerized MLKL complexes are actively trafficked to the plasma membrane via trafficking pathways that include the Golgi, microtubule and actin networks [117, 171], however, in some cell types, blockade of the Golgi,

microtubule and actin machinery did not prevent MLKL trafficking and necroptotic death [117]. Although the proteins that mediate MLKL trafficking have not been identified yet, their interaction site within the 4HB MLKL has been mapped using inhibitory monobodies [171]. Taken together, the abovementioned data demonstrate that necroptotic signaling and MLKL translocation to membranes in human cells is regulated by a network of auxiliary proteins which control activation, oligomerization and trafficking of MLKL [126]. The present study revealed that treatment with HOIPIN-8 blocks TBZ-induced necroptosis in human tumor cell lines and primary hPOs, but not in murine cell lines, without affecting core necroptotic signaling. Instead, HOIPIN-8 treatment prominently prevented translocation of MLKL to the plasma membrane. Therefore, our data suggest that HOIPIN-8 might target regulatory proteins that modulate MLKL trafficking or membrane tethering in a species-specific manner.

6.2 Modelling necroptosis in primary human pancreatic organoids

The 3-dimensional (3D) organoid technology allows researchers to study tissue homeostasis as well as diseases in near-physiological settings and thus serves as an excellent model system for basic research and translational applications [371, 394]. In contrast to 2D monolayer cell cultures, organoids recapitulate the *in vivo* tissue architecture, heterogeneity and cellular functions of the primary tissue [394]. Therefore, organoids represent an important bridge between 2D cell culture and *in vivo* models, such as genetically engineered mouse models or patient-derived xenografts, and their generation and maintenance are relatively easy and thus suitable for high-throughput screening [371, 394]. In this study, we used adult stem cell-derived hPOs which are characterized by a single-layer ductal epithelium surrounding a central liquid-filled lumen [362]. Induction of necroptosis with the clinically applicable smac mimetic Birinapant and the caspase inhibitor Emricasan, as well as with BV6 and zVAD.fmk, lead to prominent organoid collapse and compaction as well as high levels of PI-positive (dead) cells, which could be efficiently blocked with NSA, indicating MLKL-dependent necroptotic cell death. Importantly, we could confirm the results we obtained with 2D monolayer cell culture and could demonstrate that LUBAC inhibition with HOIPIN-8 prevents necroptosis in primary hPOs. This first-time use of human primary organoids to systematically model necroptosis in intact multicellular near-physiological settings provides a novel experimental platform apart from necroptosis-

proficient cell lines. Since necroptosis underlies various diseases, including autoimmune diseases, inflammatory disorders and cancer [39, 395], modeling necroptotic cell death in primary organoids will significantly contribute to gain new fundamental insights and to develop novel therapeutic options.

6.3 The role of OTULIN and CYLD in TNFR1-mediated signaling

LUBAC-mediated M1 poly-Ub is cleaved by the DUBs OTULIN and CYLD, and both DUBs mutually exclusively interact with HOIP [299]. OTULIN directly binds to HOIP to control HOIP autoubiquitination and thus its catalytic activity, while CYLD interacts with HOIP via the adaptor protein SPATA2 [299]. As anticipated [73, 295, 296], deletion of OTULIN lead to a marked increase of cellular M1 poly-Ub levels. Various studies have demonstrated that OTULIN counteracts NF-κB activation [299], while others reported that loss of OTULIN or expression of catalytic inactive OTULIN C129A sensitizes cells towards apoptotic and necroptotic cell death [277, 290, 291]. In the present study, evaluation of CRISPR/Cas9-mediated OTULIN KO HT-29 and THP-1 cell lines revealed no overt changes in NF-κB signaling and did not affect TNFα-induced apoptotic or necroptotic cell death despite high levels of cellular M1 poly-Ub. Unlike OTULIN, whose role at immune receptors is still under debate [299], CYLD is recruited to immune receptors where it cleaves M1 and K63 poly-Ub to inhibit NF-κB activation [73, 260, 293, 308]. Accordingly, CRISPR/Cas9-mediated CYLD KO resulted in enhanced basal expression of NF-κB target genes and slightly decreased TNFα-induced cell death. Interestingly, combined OTULIN/CYLD KO prominently increased TNFα-induced cell death in HT-29 cells and resulted in decreased NF-κB activation, indicating marked defects in TNFR1-mediated signaling. Intriguingly, OTULIN KO or combined OTULIN/CYLD KO lead to the destabilization of the LUBAC complex while mRNA expression of *HOIP*, *HOIL-1* and *SHARPIN* remained stable. This appears to be in contrast to the marked increase in cellular M1 poly-Ub levels in both OTULIN and OTULIN/CYLD KO cell lines, but supports the notion that the main function of OTULIN is to counteract HOIP autoubiquitination, thereby maintaining HOIP in an active state and preventing destabilization of the LUBAC complex [277]. This is supported by a study demonstrating that stimulation of OTULIN-deficient keratinocytes with TNFα results in decreased M1 ubiquitination of RIPK1 and NEMO as well as reduced NF-κB activation [291]. Importantly, elevated M1 poly-Ub levels in OTULIN KO cell lines could

be effectively blocked by HOIPIN-8 and TBZ-induced necroptosis lead to an increase in M1 poly-Ub in OTULIN KO cells, indicating that LUBAC is still active in these cells. Neither OTULIN KO nor CYLD KO or combined OTULIN/CYLD KO had an effect on the HOIPIN-8-mediated inhibition of necroptotic cell death and did not affect necroptotic signaling, suggesting that the elevated cellular M1 poly-Ub levels do not interfere with necroptosis induction. The key substrates of OTULIN, apart from HOIP, remain elusive, however the abovementioned findings suggest that OTULIN regulates cytosolic processes that are dependent on M1 poly-Ub [299]. In the present study, we could demonstrate that LUBAC-mediated M1 poly-Ub regulates production and release of pro-inflammatory cytokines during necroptosis, however, whether OTULIN and CYLD regulate necroptosis-induced cytokine production remains to be established.

6.4 LUBAC-mediated M1 poly-Ub controls necroptosis-dependent pro-inflammatory cytokine production

Necroptotic cell death is characterized by plasma membrane rupture resulting in the passive release of DAMPs, thereby promoting inflammation [39]. Intriguingly, recent studies have revealed that the release of pro-inflammatory mediators is not only a result of membrane damage but are regulated by intracellular signaling mechanisms which lead to expression and release of pro-inflammatory cytokines and chemokines prior to cell death [59, 123, 173]. Although the role of necroptosis in the pathogenesis of inflammatory diseases such as systemic inflammatory respiratory syndrome (SIRS) and IBD is well established [39, 61, 62, 64, 396], it has been a matter of debate whether necroptotic cell death is a result of inflammation or an active mediator of inflammation [39]. The latter is supported by *in vivo* studies demonstrating that loss of RIPK3 expression prevents cell death and inflammation in mouse models of intestinal inflammation, skin inflammation and retinal degeneration [397-400]. Necroptosis can promote inflammation indirectly, e.g. by disrupting epithelial barriers which triggers immune responses via tissue-invading microbes, or directly via passive release DAMPs [39]. In addition, recent data demonstrating the necroptosis-induced and cell autonomous production of pro-inflammatory cytokines provide novel insights into the mechanisms that may underlie acute and chronic inflammation [59, 123, 173]. In the present study, we could corroborate these findings by performing an unbiased MACE-

seq-based transcriptome profiling of necroptotic HT-29 cells. Our data demonstrate the upregulation of a highly pro-inflammatory cytokine profile, including cytokines and chemokines such as TNFα and CXCL1, as well as the adhesion receptor ICAM1, which could be prevented by LUBAC inhibition with HOIPIN-8 as well as by siRNA-mediated and CRISPR/Cas9-mediated deletion of HOIP. Importantly, LUBAC-dependent upregulation of these pro-inflammatory mediators is not solely the result of TNFα-mediated NF-κB signaling, as treatment TNFα alone induces lower levels of *CXCL1* and *TNFA* mRNA as compared to treatment with TBZ, in line with previous findings [59]. Necroptosis-dependent cytokine production relies on NF-κB activation, as inhibition of IKKs and TAK1 blocks upregulation of cytokines [59]. LUBAC is an important mediator of NF-κB activation [237], therefore, our data demonstrating that inhibition or deficiency of HOIP potently inhibits cytokine production and release suggest that necroptosis-induced cytokine expression is dependent on LUBAC-mediated NF-κB signaling. In addition, we demonstrated that inhibition of MLKL membrane translocation with NSA as well as CRISPR/Cas9-mediated MLKL KO inhibited the necroptosis-dependent induction of pro-inflammatory cytokines. Our data further substantiate previous findings [59, 123, 173] showing that cell-intrinsic signaling via the RIPK1-RIPK3-MLKL axis, rather than the passive release of DAMPs, triggers the induction of pro-inflammatory cytokines during necroptosis and further supports the role of MLKL membrane translocation in the control of cytokine production.

Together, the abovementioned findings reveal a novel function of LUBAC-mediated M1 Ub in the regulation of pro-inflammatory cytokine expression during necroptosis and further support the notion that necroptosis actively promotes inflammation. Interestingly, TNFα, a key player in chronic inflammation, is among the most upregulated cytokines during necroptosis and anti-TNFα therapy is a well-established therapeutic tool in the treatment of chronic inflammatory diseases such as IBD [39]. Since necroptosis-dependent inflammation contributes to the pathogeneses and chronicity of various inflammatory diseases [39, 401] and impairment of linear ubiquitination in patients with mutations in *HOIP*, *HOIL-1* or *SHARPIN*, as well as in ORAS patients, results in deregulated NF-κB signaling and autoinflammation [236, 273, 290, 294-296, 325, 347], targeting LUBAC may provide a novel therapeutic option for the treatment of inflammatory and immunological diseases.

6.5 FLOTs and their potential role in LUBAC and M1 Ub-dependent regulation of necroptosis

6.5.1 LUBAC-dependent enrichment of FLOT1/2 in M1 poly-Ub pulldowns of necroptotic cells

In the present study, we identify FLOT1 and FLOT2 as putative targets of LUBAC-mediated M1 poly-Ub. Both FLOT1 and FLOT2 were enriched in UBAN-based M1 poly-Ub pulldowns of necroptotic cells which could be prevented by inhibition of LUBAC with HOIPIN-8 and CRISPR/Cas9-mediated HOIP KO. FLOT1/2 are ubiquitously expressed proteins that reside in lipid rafts, dynamic and transient ordered membrane domains that provide functional platforms for the regulation of numerous cellular processes [178], and are involved in various and partially overlapping cellular processes including protein trafficking, actin cytoskeleton remodeling and endocytosis [402]. Intriguingly, FLOTs have been recently implicated in the endocytosis and subsequent lysosomal degradation of MLKL, thereby protecting the cells against necroptotic cell death [166]. This is in contrast to the findings of this study, demonstrating that siRNA-mediated knockdown of FLOT1/2 decreases necroptotic cell death. Potential explanations for this difference could be acute compensatory mechanisms, as well as variations in the technical and experimental set-up that require future investigation. Moreover, loss of FLOT1/2 partially potentiated the HOIPIN-8-mediated decrease in necroptotic cell death to a certain extent. Evaluation of the necroptotic signaling pathway in FLOT1/2-deficient cells showed no changes in necroptotic phosphorylation of RIPK1, RIPK3 and MLKL, and no alterations in necrosome formation and MLKL oligomerization, indicating that FLOTs might play a role in the control of necroptotic cell death downstream of MLKL oligomerization. Of note, and in addition to HOIPIN-8, necroptotic enrichment of FLOT1 in UBAN-based M1 poly-Ub pulldowns could be prevented by inhibition of necroptosis key players RIPK1 with Nec-1s, RIPK3 with GSK'872 and MLKL with NSA, confirming that FLOT1/2 enrichment is indeed necroptosis-dependent and suggesting that activation and membrane translocation of MLKL is a prerequisite for association of FLOT1 with M1 poly-Ub.

Interestingly, FLOT1 is implicated in the regulation of ubiquitinated cargo transfer between ESCRT-0 and ESCRT-I complexes and has been shown to interact with

ESCRT-0 subunit hepatocyte growth factor-regulated tyrosine kinase substrate (Hrs) and ESCRT-I subunit tumor susceptibility gene 101 (TSG101) [403]. Due to the experimental setup used in the present study, it cannot be excluded that proteins detected in UBAN-based M1 poly-Ub pulldowns are associated with other M1 poly-Ub-modified proteins. Both MLKL and RIPK3 are extensively ubiquitinated during necroptosis [125], however, up till now there are no studies demonstrating M1-linked ubiquitination of these necroptotic key proteins. In the present study, MLKL could be detected in UBAN pulldowns of untreated control and necroptotic cells and treatment with HOIPIN-8 or NSA slightly reduced the amount of UBAN-enriched MLKL, while RIPK3 was completely absent. It remains unclear whether MLKL itself is directly modified with M1 poly-Ub, yet these data indicate that the necroptosis-dependent enrichment of FLOTs in M1 poly-Ub pulldowns is likely not a result of interaction of FLOTs with putative M1-ubiquitinated MLKL or RIPK3, although a previous study has suggested an interaction of FLOTs and MLKL upon necroptosis induction [166].

6.5.2 FLOTs and their potential role in MLKL trafficking plasma membrane localization

Prior to plasma membrane accumulation, activated MLKL is located at internal membranes followed by translocation to the plasma membrane [52, 102, 117, 165-169]. MLKL trafficking mechanisms presumably involve the Golgi, microtubule and actin machinery as pharmacological inhibition of these pathways with Brefeldin A (targeting ER-Golgi transport), Nocodazole (microtubule inhibitor) and Cytochalasin B (targeting actin) prevented MLKL plasma membrane hotspot formation [117]. Inhibition of LUBAC with HOIPIN-8 triggered a similar phenotype, suggesting that LUBAC-mediated M1 poly-Ub might be involved in the regulation of MLKL trafficking. However, the proteins which mediate these trafficking events have not been identified yet. Of note, the M1 poly-Ub-dependent effects on MLKL described in the present study mimic MLKL-specific monobodies that target the 4HB of human MLKL to inhibit necroptosis [171], but without affecting necrosome formation, MLKL activation and MLKL oligomerization, and the 4HB domain of MLKL has been proposed to act as an interaction site for auxiliary proteins that promote MLKL trafficking [101, 110, 171].

FLOTs are implicated in various cellular trafficking events [402] including protein and receptor recycling [404-406], trafficking to lysosomes [166, 403, 407] and trafficking

from the ER to the plasma membrane [408, 409]. FLOT2 has been shown to directly interact with F-actin [183], and various studies indicate a role for FLOTs in actin cytoskeleton remodeling [183, 402, 410, 411]. In addition, FLOTs are involved in the establishment of protein complexes at the plasma membrane by providing a scaffold for protein clustering [181-183, 402]. Interestingly, phosphorylated MLKL associates with FLOT1/2-containing lipid rafts after necroptosis induction [166], corresponding with previous data and the results of the present study demonstrating the accumulation of phosphorylated MLKL in the micelle-rich fraction after cell fractionation [102]. Necroptosis-dependent lipid raft association of phosphorylated MLKL is dependent on the presence of FLOTs, since shRNA-mediated knockdown of FLOT2 resulted in the retention of MLKL in the non-lipid raft fraction [166]. These data suggest that the presence of FLOTs is a prerequisite for the translocation of MLKL to cellular membranes [166]. Although shRNA-mediated knockdown of FLOT2 sensitized cells towards necroptosis in the abovementioned study, which is in line with the notion that FLOTs mediate endocytosis of phosphorylated MLKL [166], our data showed that siRNA-mediated transient knockdown of FLOT1/2 decreased TBZ-induced necroptosis and further enhanced the protective effect of HOIPIN-8. Intriguingly, the present study revealed necroptosis-dependent FLOT1/2 enrichment in UBAN-mediated M1 poly-Ub pulldowns which could be blocked by LUBAC inhibition and HOIP KO. Although the necroptosis-induced increase in cellular M1 poly-Ub levels was not dependent on MLKL, inhibition of MLKL membrane translocation with NSA also blocked the association of FLOTs with M1 poly-Ub, indicating a direct link for FLOT1/2, M1 poly-Ub and MLKL membrane localization and further demonstrating independent LUBAC signaling events during necroptosis.

MLKL membrane accumulation is balanced by both endocytic and exocytic events which involve FLOT1/2 [166], ESCRT complexes, ALIX, syntenin-1 and Rab27 [123, 165, 166, 170, 173]. In line with previous studies demonstrating a function of FLOTs in extracellular vesicle generation [190, 412, 413], phosphorylated MLKL has been found together with FLOTs and certain ESCRT proteins in necroptosis-induced exosomes [165]. Intriguingly, our data showed a marked reduction of MLKL in necroptosis-induced exosomes upon inhibition of LUBAC with HOIPIN-8 which is in accordance with the altered cellular distribution of phosphorylated MLKL observed in fractionation experiments and corresponds with immunofluorescence analysis of necroptotic cells,

further demonstrating that LUBAC inhibition prevents plasma membrane translocation of phosphorylated MLKL. Recognition of ubiquitinated cargo by ESCRT complex subunits, like Hrs, signal-transducing adapter molecule (STAM) 1 and 2 and TSG101 via UBDs, such as the Vps27/Hrs/Stam (VHS) domain, UIM domain and ubiquitin-conjugating enzyme E2 variant (UEV) domain, are important for endo- or exocytosis [414-420]. Although the binding specificity and affinity of these UBD-containing proteins for M1 poly-Ub remain unclear, specific recognition of M1 poly-Ub might serve as docking platform to position activated MLKL in hotspots and to allow necroptosis.

6.6 Limitations and outlook

We demonstrated that LUBAC-mediated M1 poly-Ub is required for the production and release of pro-inflammatory cytokines during necroptosis. Necroptotic cell death is involved in various inflammatory diseases, however, it remains unclear whether and how necroptosis actively mediates inflammation [39]. By releasing inflammatory mediators including cytokines and chemokines, necroptotic cells likely contribute to the activation of immune cells which in turn release cytokines that trigger cell death, thus fueling chronic inflammation [39]. Necroptosis-induced pro-inflammatory cytokine production was dependent on MLKL activation and presumably also on MLKL translocation to membranes. Interestingly, a recent study demonstrated that the ESCRT-III protein CHMP2A is involved in the necroptosis-induced production of cytokines, by limiting necroptotic cell death through plasma membrane repair and removal of activated MLKL from the plasma membrane, thus allowing necroptotic cells to signal to surrounding cells [123]. LUBAC-mediated M1 poly-Ub plays an important role in the control of NF-κB signaling downstream of various immune receptors and necroptosis-induced and MLKL-dependent cytokine production has been shown to be dependent on NF-κB signaling [59]. Importantly, we could demonstrate that inhibition of LUBAC with HOIPIN-8 prevents MLKL membrane translocation which raises the question as to whether LUBAC-mediated M1 poly-Ub mainly regulates pro-inflammatory cytokine production via its role in NF-κB signaling or by regulating the availability of activated MLKL at the membrane. Intriguingly, both RIPK3 and MLKL have also been implicated in the regulation of cytokine production via activation of the NLPR3 inflammasome [421-425] and LUBAC has been linked to the regulation of caspase-1 activity [333, 334]. We focused on the characterization of TNFR1-mediated

signaling in the present study, however, necroptosis can be initiated via various pathways, including TLR signaling, which likely converge to form intricate signaling networks that trigger inflammatory responses. Therefore, the role of LUBAC in the regulation of inflammatory cytokine production during necroptosis needs to be further investigated in the context of other necroptosis-inducing pathways. Nonetheless, our data provide novel insights into the mechanism that underlies necroptosis-dependent cytokine production and inflammation and thus may further contribute to the development of novel therapeutic options for treatment of inflammatory diseases by targeting LUBAC and M1-poly Ub.

In addition to its role in necroptosis-dependent cytokine production, our data indicate that LUBAC-dependent M1 poly-Ub controls the availability of activated MLKL at the plasma membrane and thus critically regulates execution of necroptotic cell death. LUBAC inhibition with HOIPIN-8 blocked necroptosis-induced formation of activated MLKL plasma membrane hotspots without affecting upstream necroptotic signaling and MLKL oligomerization. Furthermore, HOIP inhibition blocked necroptotic cell death in human HT-29 and THP-1 cells as well as in hPOs in a time-dependent manner, and siRNA-mediated knockdown of HOIP also reduced necroptosis to a similar extent. To our surprise, CRISPR/Cas9-mediated HOIP KO in both HT-29 and THP-1 cell lines did not affect TNFα-induced necroptosis, raising the question as to whether there are additional mechanisms that compensate for the loss of M1 poly-Ub during necroptosis. To address this and to rule out any sequence-based off-target effects of siRNAs, future experiments should be carried out using siRNAs that target different sequences or alternative methods, such as shRNA-based stable knockdown or CRISPR interference (CRISPRi) [426].

Intriguingly, HOIPIN-8 treatment also blocked necroptosis in polyclonal HOIP KO cell lines, indicating that HOIPIN-8 may have additional off-target effects. This is of great interest for future studies, since HOIPIN-8 is a widely used HOIP inhibitor that has been used in various studies addressing immune receptor-induced NF-κB and cell death signaling. Of note, HOIP inhibition with the mycotoxin gliotoxin also effectively blocked necroptosis and cell death could also be rescued in siRNA-mediated HOIP knockdown cells. Both HOIPIN-8 and gliotoxin target the catalytic center of HOIP [282, 286] and it remains to be established whether these LUBAC inhibitors additionally target other proteins that may affect the MLKL trafficking machinery or MLKL itself.

Furthermore, our data show that HOIPIN-8 only acts in human but not in murine cells, suggesting species-specific effects.

We identified FLOT1 and FLOT2 as novel putative targets of LUBAC-mediated M1 poly-Ub during necroptosis by performing UBAN-based pulldown of M1-ubiquitinated proteins from necroptotic cells. Interestingly, FLOTs reportedly regulate endocytosis and degradation of MLKL, thus counteracting necroptotic cell death [166]. Although interactions between FLOTs and MLKL have been demonstrated previously [166] our data suggest that enrichment of FLOTs in M1 poly-Ub pulldowns is likely not a result of an interaction with M1-ubiquitinated MLKL. However, since FLOTs are implicated in the regulation of protein trafficking [402] and NSA blocked FLOT1/2 enrichment in M1 poly-Ub pulldowns, it is tempting to speculate that there is a link between FLOTs and necroptosis-induced MLKL trafficking. Therefore, the characterization of MLKL trafficking pathways as well as the formation of MLKL hotspots at the plasma membrane in the context of FLOT deficiency or LUBAC deficiency could shed light on the underlying mechanisms. Whether FLOTs are directly ubiquitinated or interact with other proteins that are M1-ubiquitinated remains to be established, therefore, future studies should aim to identify possible ubiquitination sites within FLOT1 and FLOT2. Furthermore, additional experiments to analyze putative FLOT1/2-MLKL-M1 poly-Ub co-localization and interaction upon necroptosis induction would help to unravel the potential link between LUBAC/M1 poly-Ub and FLOTs during necroptosis.

Finally, by using primary hPOs, we established a novel platform for the investigation of necroptotic cell death which can be applied in future studies for cytokine profiling and immunostainings to assess the necroptotic pathway in near-physiological settings.

7 Deutsche Zusammenfassung

Bei der Nekroptose handelt es sich um eine Form des programmierten Zelltods, welche morphologisch dem nekrotischen Zelltod ähnelt, jedoch durch spezifische zelluläre Signalwege reguliert wird. Die Aktivierung des Nekroptose-Signalwegs führt zur Perforation der Plasmamembran, was die Ausschüttung sogenannter DAMPs (engl. *danger-associated molecular patterns*) nach sich zieht, und schließlich zum nekroptotischen Zelltod führt. Zudem produzieren nekroptotische Zellen verschiedene pro-inflammatorische Zytokine und Chemokine. Nekroptose spielt unter anderem eine Rolle bei inflammatorischen Erkrankungen, wie bei dem Systemischen inflammatorischen Response Syndrom, bei Ischämie-Reperfusionsschaden und bei chronisch entzündlichen Darmerkrankungen, sowie bei verschiedenen Krebserkrankungen.

Nekroptose kann über die Aktivierung unterschiedlicher Immunrezeptoren wie beispielsweise des TNF Rezeptors 1 (TNFR1) ausgelöst werden. Stimulation von TNFR1 durch dessen Ligand TNFα führt zur Formation des sogenannten TNFR1 Komplex I, bestehend aus den Proteinen TRADD, TRAF1/2 und RIPK1, welche die Ubiquitin E3 Ligasen cIAP1/2 rekrutieren, die wiederum einige Komponenten des Komplex I ubiquitinieren. Dies führt zur Rekrutierung des E3 Ubiquitin Ligase Komplex LUBAC (engl. *linear ubiquitin chain assembly complex*), welcher Rezeptor-assoziierte Proteine, beispielsweise RIPK1, sowie bereits vorhandene K63-Ubiquitinketten mit sogenanntem linearen bzw. M1-Ubiquitin modifiziert. Diese Modifizierung führt wiederum zur Rekrutierung der Proteine TAK1/TAB1/TAB3 sowie NEMO/IKKα/IKKβ, welche die Aktivierung der MAPK- und NF-κB Signalwege auslösen. Unter bestimmten Umständen, wenn cIAP1/2 und Caspasen blockiert oder herunterreguliert sind, kann die Aktivierung des TNFR1 die Auslösung von Nekroptose nach sich ziehen. Dies geschieht aufgrund der Destabilisierung des Komplex I, wenn dessen Komponenten weniger oder nicht mehr ubiquitiniert sind, und wird durch die Deubiquitinase CYLD begünstigt. Es kommt zur Auto-Phosphorylierung und Aktivierung von RIPK1, welches wiederum phosphorylierungsabhängig RIPK3 aktiviert. Aktiviertes RIPK3 bildet zusammen mit RIPK1 das sogenannte Nekrosom und rekrutiert und phosphoryliert die Pseudokinase MLKL an T357 und S358. Die Aktivierung des Nekroptose Effektors MLKL fördert dessen Konformationsänderung in die pro-nekroptotische Form, was

wahrscheinlich dessen Oligomerisierung initiiert und den anschließenden Transport zur Plasmamembran ermöglicht. An der Plasmamembran akkumuliert MLKL in sogenannten Hot Spots und induziert die Bildung von Membran-Poren, was letztendlich zum Zelltod führt.

Der Prozess der Ubiquitinierung stellt einen der wichtigsten post-translationalen Proteinmodifikationsmechanismen dar und wird durch sogenannte Ubiquitin E3 Ligasen, im Zusammenspiel mit E1 Ubiquitin-aktivierenden Enzymen sowie E2 Ubiquitin-konjugierenden Enzymen, induziert. Ubiquitinierung beschreibt die kovalente Binding von Ubiquitin an Zielsubstrate, was zur Mono-Ubiquitinierung oder Bildung von Poly-Ubiquitin-Ketten führen kann. Dabei kann Ubiquitin über sieben verschiedene Lysin-Reste (K6, K11, K27, K29, K33, K48 und K63) oder über das N-terminale primäre Amin (M1) verknüpft werden. Letzteres wird speziell durch den E3 Ligase Komplex LUBAC induziert, welcher aus der E3 Ubiquitin Ligase HOIP sowie den Proteinen HOIL-1 und Sharpin besteht. M1-Ubiquitin spielt eine wichtige Rolle bei der Regulation von Signalwegen, die durch die Aktivierung von Immunrezeptoren wie TNFR1 initiiert werden, und reguliert dabei die Zellantwort durch Kontrolle des zell-protektiven NF-κB (engl. *nuclear factor-kappa B*) und MAPK (engl. *mitogen-activated protein kinase*) Signalwegs. Entsprechend der Funktion von LUBAC in der Kontrolle pro-inflammatorischer Signalwege, zeigen Patienten sowie auch Mausmodelle mit Gen-Mutationen oder Verlust einer der LUBAC-Untereinheiten inflammatorische Symptome, die verschiedene Organe betreffen. M1-Ubiquitin kann von den Deubiquitinasen OTULIN und CYLD abgebaut werden. CYLD kann neben M1-Ubiquitin auch K63-Ubiquitin abbauen und spielt unter anderem eine Rolle in der Regulation des Ubiquitinierungsstatus von Komponenten des TNFR1 Komplexes. Sowohl CYLD als auch OTULIN können mit HOIP interagieren, jedoch bindet nur OTULIN direkt an HOIP, während CYLD mit HOIP über das Adapter-Protein SPATA2 interagiert. OTULIN ist die bislang einzige Deubiquitinase, welche ausschließlich M1-Ubiquitin abbauen kann. Ob OTULIN eine aktive Rolle in der Kontrolle von Immunrezeptor-induzierten Signalwegen spielt ist nach aktuellem Forschungsstand noch nicht geklärt. Neueste Studien zeigen jedoch, dass OTULIN der Auto-Ubiquitinierung von HOIP entgegenwirkt und damit dessen katalytische Aktivität reguliert. Obwohl noch nicht alle zellulären Zielproteine von OTULIN identifiziert wurden, führt ein Mangel an OTULIN, zum Beispiel durch Verlust des OTULIN-Gens,

zu einen markanten Anstieg der zellulärem M1-Ubiquitin-Level und zu Defekten bei der Aktivierung des NF-κB-Signalwegs, was in Patienten zum Krankheitsbild ORAS (engl. *OTULIN-dependent autoinflammatory syndrome*) führt.

In der vorliegenden Arbeit wurde die Rolle von LUBAC und M1-Ubiquitin im Kontext des TNFR1-vermittelten Signalwegs untersucht. Zunächst generierten wir mit Hilfe der CRISPR/Cas9-Technologie HT-29 (humane Kolonkarzinomzellen) und THP-1 (humane Monozyten) Zelllinien, bei denen die Gene für die Deubiquitinasen OTULIN und CYLD ausgeschaltet sind (engl. *knockout,* KO), um deren Funktionen im Kontext des TNFR1-vermittelten NF-κB Signalwegs sowie der Aktivierung von TNFR1-vermitteltem Zelltod zu analysieren. Wir nutzten dabei eine Kombination aus TNFα (T) und dem Smac-Mimetikum BV6 (B), um den TNFR1-induzierten apoptotischen Zelltod auszulösen, oder die Kombination aus T, B und dem Caspasen-Inhibitor zVAD.fmk (Z), um nekroptotischen Zelltod auszulösen. Trotz des starken Anstiegs von zellulärem M1-Ubiquitin, zeigten sowohl HT-29 als auch THP-1 OTULIN KO Zellen im Vergleich zu den Kontrollzellen keine markanten Veränderungen bezüglich der Aktivierung des NF-κB Signalwegs sowie der Zelltodlevel. Im Gegensatz dazu zeigten CYLD KO Zelllinien basal eine erhöhte Expression von NF-κB-induzierten Genen, sowie einen leicht verminderten TB- oder TBZ-induzierten Zelltod, was mit der Rolle von CYLD im TNFR1 Signalweg erklärt werden kann. Markante Beeinträchtigungen der TNFα-induzierten NF-κB Aktivierung waren dagegen in Zellen zu beobachten, in denen beide Gene für OTULIN und CYLD ausgeschaltet waren. Zudem konnten wir eine starke Zunahme von Zelltod in OTULIN/CYLD KO HT-29 Zellen beobachten, wenn diese mit TNFα behandelt wurden.

Die katalytische Aktivität von HOIP kann *in vitro* mit den Inhibitoren HOIPIN-8 und Gliotoxin geblockt werden. Um die Funktion des M1-Ubiquitins weiter zu charakterisieren, analysierten wir den TNFR1-induzierten Zelltod nach Behandlung der Zellen mit HOIPIN-8 oder Gliotoxin und konnten nachweisen, dass beide Inhibitoren TBZ-induzierten nekroptotischen Zelltod sowohl in HT-29 als auch in THP-1 Zellen zeitabhängig blockieren. Zudem konnten wir den Effekt von HOIPIN-8 in humanen, von adulten Stammzellen abgeleiteten, Pankreas-Organoiden reproduzieren. Die Organoid-Technologie stellt eine wichtige Brücke zwischen der 2D-Zellkultur und klassischen Tiermodellen dar, da sie die Untersuchung von Erkrankungen und Gewebehomöostase in physiologisch ähnlicher Umgebung erlaubt. Die Verwendung

von Organoiden zur Modellierung des nekroptotischen Zelltods stellt daher eine wichtige neue Plattform zur Erforschung von Nekroptose dar. Des Weiteren konnten wir den zyto-protektiven Effekt der LUBAC-Inhibition während der Nekroptose mittels RNA-Interferenz-vermittelter Blockade der HOIP Expression verifizieren, jedoch nicht in CRISPR/Cas9-vermittelten HOIP KO Zellen.

Um aufzuklären wie LUBAC-Inhibition die Nekroptose beeinflusst, wurde der nekroptotische Signalweg unter Behandlung mit HOIPIN-8 untersucht. Die Western Blot Analyse der M1-Ubiquitin-Level zeigte einen deutlichen Anstieg von M1-Ubiquitin nach Behandlung der Zellen mit TBZ, welcher höher war als bei Behandlung der Zellen mit TNFα oder TB und effektiv mit HOIPIN-8 blockiert werden konnte. Interessanterweise zeigte die Untersuchung der nekroptotischen Schlüsselproteine, dass HOIPIN-8 die nekroptotische Phosphorylierung von RIPK1, RIPK3 und MLKL nicht vermindert und keinen Einfluss auf die Formation des Nekrosoms hat. Zudem konnten wir mittels nicht-reduzierendem Western Blot keine Veränderung der Nekroptose-induzierten MLKL-Oligomerisierung feststellen, was darauf hindeutet, dass der zyto-protektive Effekt von HOIPIN-8 nicht auf eine Blockade des frühen nekroptotischen Signalwegs zurückzuführen ist. Nach dessen Oligomerisierung wird MLKL über Transportwege, die wahrscheinlich den Golgi-Apparat, die Mikrotubuli sowie Aktin und verschiedene bis dato unbekannte regulatorische und akzessorische Proteine involvieren, zur Plasmamembran transportiert. Die Akkumulation von aktiviertem MLKL an der Plasmamembran und damit die Zelltodinduktion kann durch verschiedene Mechanismen verhindert werden. Zum einen kann MLKL über Endozytose und anschließenden lysosomalen Abbau von der Plasmamembran entfernt werden, zum anderen wird MLKL über Exozytose in extrazellulären Vesikeln (Exosomen) in das umliegende Medium abgegeben. Um die Lokalisation von aktiviertem MLKL nach Nekroptose-Induktion unter Behandlung von HOIPIN-8 zu untersuchen, führten wir Zellfraktionierungsexperimente, Immunfluoreszenzfärbungen und Exosomen-Aufbereitungen durch. Wir konnten feststellen, dass LUBAC-Inhibition mit HOIPIN-8 die Akkumulation von aktiviertem MLKL in Membranfraktionen reduzierte und die Bildung von MLKL-Hot Spots an der Plasmamembran verhinderte. Zudem verminderte HOIPIN-8 die Abgabe von MLKL in Nekroptose-induzierten Exosomen. Zusammengefasst, zeigen diese Daten, dass HOIPIN-8 die Membranlokalisation von MLKL hemmt, ohne den vorangehenden Nekroptose-Signalweg zu beeinflussen.

Die oben genannten Effekte der LUBAC-Inhibition auf den TBZ-induzierten nekroptotischen Zelltod konnten nicht in murinen Zelllinien reproduziert werden, obwohl HOIPIN-8 sowohl humanes als auch murines HOIP blockiert. Dies könnte auf spezies-spezifische Unterschiede in der Regulation von Nekroptose zurückzuführen sein. Sowohl RIPK3 als auch MLKL sind Ziel zahlreicher regulatorischer Modifikationen wie Ubiquitinierung und Phosphorylierung, die die Aktivität und Kompartimentierung der beiden Proteine beeinflussen und sich in verschiedenen Spezies unterscheiden. Studien zeigen beispielsweise, dass murines und humanes RIPK3 und MLKL nicht den nekroptotischen Signalweg in Zellen der jeweiligen anderen Spezies komplettieren können, was auf divergente Aktivierungsmechanismen von MLKL zurückführbar ist. Entsprechende Unterschiede in der Regulation des Transports oder der Membranverfügbarkeit von humanem und murinem MLKL könnten daher den unterschiedlichen Effekten von HOIPIN-8 zugrunde liegen.

Nekroptose geht mit der Produktion und Ausschüttung pro-inflammatorischer DAMPs und Zytokine einher. Wir untersuchten daher den Effekt der LUBAC-Inhibition oder verminderter LUBAC-Expression auf die Produktion von Zytokinen, indem wir mittels MACE-Seq (engl. *massive analysis of cDNA ends-sequencing*) eine Transkriptom-Analyse durchführten, sowie mittels quantitativer RT-PCR die Transkription einzelner Gene analysierten. Wir konnten dabei feststellen, dass LUBAC-induziertes M1-Ubiquitin für die Nekroptose-induzierte Expression pro-inflammatorischer Mediatoren wie beispielsweise CXCL1, CXCL10, TNFα und ICAM1 essentiell ist. Weiterhin konnten wir zeigen, dass die Expression dieser Proteine durch den KO von MLKL oder durch die Inhibition von MLKL mit dem MLKL-Inhibitor Nekrosulfonamid (NSA) blockiert werden kann, was die bereits bekannte These bestätigt, dass die Nekroptose-induzierte Zytokin-Produktion MLKL-abhängig ist.

Des Weiteren konnten wir in der vorliegenden Studie FLOT1 und FLOT2 als zwei potentielle Zielproteine für die LUBAC-vermittelte M1-Ubiquitinierung während der Nekroptose identifizieren. Beide Proteine konnten mittels UBAN (engl. *Ubiquitin-binding in ABIN and NEMO*)-basierten M1-Ubiquitin-Pulldowns aus Lysaten von nekroptotischen Zellen angereichert werden, was wiederum mittels HOIPIN-8 Behandlung oder HOIP KO blockiert werden konnte. Zudem konnte die Anreicherung von FLOT1/2 durch die Inhibition des Nekroptose-Signalwegs mittels Inhibitoren wie NSA verhindert werden.

Die vorliegende Studie identifizierte die LUBAC-vermittelte M1-Ubiquitinierung als neuen Regulator TNFR1-induzierter Nekroptose. Wir konnten zeigen, dass LUBAC für die Nekroptose-induzierte und MLKL-abhängige Produktion pro-inflammatorischer Zytokine essentiell ist. Die Inhibition von LUBAC mittels HOIPIN-8 führte in humanen Zelllinien und primären humanen Pankreas-Organoiden zur zeitabhängigen Blockade des nekroptotischen Zelltods, jedoch nicht in murinen Zelllinien. Neben den neuen Erkenntnissen zur Regulation von Nekroptose, konnten wir mit der Verwendung von primären humanen Pankreas-Organoiden eine neue Plattform für die Untersuchung von Nekroptose etablieren.

8 References

1. Wajant, H., K. Pfizenmaier, and P. Scheurich, *Tumor necrosis factor signaling.* Cell Death Differ, 2003. **10**(1): p. 45-65.

2. Locksley, R.M., N. Killeen, and M.J. Lenardo, *The TNF and TNF receptor superfamilies: integrating mammalian biology.* Cell, 2001. **104**(4): p. 487-501.

3. Vandenabeele, P., et al., *Molecular mechanisms of necroptosis: an ordered cellular explosion.* Nat Rev Mol Cell Biol, 2010. **11**(10): p. 700-14.

4. Ashkenazi, A. and V.M. Dixit, *Death receptors: signaling and modulation.* Science, 1998. **281**(5381): p. 1305-8.

5. Vince, J.E., et al., *TRAF2 must bind to cellular inhibitors of apoptosis for tumor necrosis factor (tnf) to efficiently activate nf-kappab and to prevent tnf-induced apoptosis.* J Biol Chem, 2009. **284**(51): p. 35906-15.

6. Haas, T.L., et al., *Recruitment of the linear ubiquitin chain assembly complex stabilizes the TNF-R1 signaling complex and is required for TNF-mediated gene induction.* Mol Cell, 2009. **36**(5): p. 831-44.

7. Park, S.M., J.B. Yoon, and T.H. Lee, *Receptor interacting protein is ubiquitinated by cellular inhibitor of apoptosis proteins (c-IAP1 and c-IAP2) in vitro.* FEBS Lett, 2004. **566**(1-3): p. 151-6.

8. Bertrand, M.J., et al., *cIAP1 and cIAP2 facilitate cancer cell survival by functioning as E3 ligases that promote RIP1 ubiquitination.* Mol Cell, 2008. **30**(6): p. 689-700.

9. Mahoney, D.J., et al., *Both cIAP1 and cIAP2 regulate TNFalpha-mediated NF-kappaB activation.* Proc Natl Acad Sci U S A, 2008. **105**(33): p. 11778-83.

10. Varfolomeev, E., et al., *c-IAP1 and c-IAP2 are critical mediators of tumor necrosis factor alpha (TNFalpha)-induced NF-kappaB activation.* J Biol Chem, 2008. **283**(36): p. 24295-9.

11. Dynek, J.N., et al., *c-IAP1 and UbcH5 promote K11-linked polyubiquitination of RIP1 in TNF signalling.* EMBO J, 2010. **29**(24): p. 4198-209.

12. Gerlach, B., et al., *Linear ubiquitination prevents inflammation and regulates immune signalling.* Nature, 2011. **471**(7340): p. 591-6.

13. Emmerich, C.H., et al., *The linear ubiquitin chain assembly complex forms part of the TNF-R1 signalling complex and is required for effective TNF-induced gene induction and prevents TNF-induced apoptosis.* Adv Exp Med Biol, 2011. **691**: p. 115-26.

14. Rahighi, S., et al., *Specific recognition of linear ubiquitin chains by NEMO is important for NF-kappaB activation.* Cell, 2009. **136**(6): p. 1098-109.

15. Kanayama, A., et al., *TAB2 and TAB3 activate the NF-kappaB pathway through binding to polyubiquitin chains.* Mol Cell, 2004. **15**(4): p. 535-48.

16. Emmerich, C.H., et al., *Lys63/Met1-hybrid ubiquitin chains are commonly formed during the activation of innate immune signalling.* Biochem Biophys Res Commun, 2016. **474**(3): p. 452-461.

17. Emmerich, C.H., et al., *Activation of the canonical IKK complex by K63/M1-linked hybrid ubiquitin chains.* Proc Natl Acad Sci U S A, 2013. **110**(38): p. 15247-52.

18. Sabio, G. and R.J. Davis, *TNF and MAP kinase signalling pathways.* Semin Immunol, 2014. **26**(3): p. 237-45.

19. Zhang, J., et al., *An unexpected twist to the activation of IKKbeta: TAK1 primes IKKbeta for activation by autophosphorylation.* Biochem J, 2014. **461**(3): p. 531-7.

20. Hayden, M.S. and S. Ghosh, *Shared principles in NF-kappaB signaling.* Cell, 2008. **132**(3): p. 344-62.

21. Park, Y.H., M.S. Jeong, and S.B. Jang, *Death domain complex of the TNFR-1, TRADD, and RIP1 proteins for death-inducing signaling.* Biochem Biophys Res Commun, 2014. **443**(4): p. 1155-61.

22. Kischkel, F.C., et al., *Cytotoxicity-dependent APO-1 (Fas/CD95)-associated proteins form a death-inducing signaling complex (DISC) with the receptor.* EMBO J, 1995. **14**(22): p. 5579-88.

23. Walczak, H. and P.H. Krammer, *The CD95 (APO-1/Fas) and the TRAIL (APO-2L) apoptosis systems.* Exp Cell Res, 2000. **256**(1): p. 58-66.

24. Nunez, G., et al., *Caspases: the proteases of the apoptotic pathway.* Oncogene, 1998. **17**(25): p. 3237-45.

25. Micheau, O. and J. Tschopp, *Induction of TNF receptor I-mediated apoptosis via two sequential signaling complexes.* Cell, 2003. **114**(2): p. 181-90.

26. Kelliher, M.A., et al., *The death domain kinase RIP mediates the TNF-induced NF-kappaB signal.* Immunity, 1998. **8**(3): p. 297-303.

27. Wang, L., F. Du, and X. Wang, *TNF-alpha induces two distinct caspase-8 activation pathways.* Cell, 2008. **133**(4): p. 693-703.

28. Dondelinger, Y., et al., *RIPK3 contributes to TNFR1-mediated RIPK1 kinase-dependent apoptosis in conditions of cIAP1/2 depletion or TAK1 kinase inhibition.* Cell Death Differ, 2013. **20**(10): p. 1381-92.

29. Legarda-Addison, D., et al., *NEMO/IKKgamma regulates an early NF-kappaB-independent cell-death checkpoint during TNF signaling.* Cell Death Differ, 2009. **16**(9): p. 1279-88.

30. Yang, S., et al., *Pellino3 targets RIP1 and regulates the pro-apoptotic effects of TNF-alpha.* Nat Commun, 2013. **4**: p. 2583.

31. Riedl, S.J. and Y. Shi, *Molecular mechanisms of caspase regulation during apoptosis.* Nat Rev Mol Cell Biol, 2004. **5**(11): p. 897-907.

32. Kerr, J.F., A.H. Wyllie, and A.R. Currie, *Apoptosis: a basic biological phenomenon with wide-ranging implications in tissue kinetics.* Br J Cancer, 1972. **26**(4): p. 239-57.

33. Meier, P., A. Finch, and G. Evan, *Apoptosis in development.* Nature, 2000. **407**(6805): p. 796-801.

34. Brill, A., et al., *The role of apoptosis in normal and abnormal embryonic development.* J Assist Reprod Genet, 1999. **16**(10): p. 512-9.

35. Giovannetti, A., et al., *Apoptosis in the homeostasis of the immune system and in human immune mediated diseases.* Curr Pharm Des, 2008. **14**(3): p. 253-68.

36. Mattson, M.P., *Apoptosis in neurodegenerative disorders.* Nat Rev Mol Cell Biol, 2000. **1**(2): p. 120-9.

37. Hanahan, D. and R.A. Weinberg, *Hallmarks of cancer: the next generation.* Cell, 2011. **144**(5): p. 646-74.

38. Fulda, S. and K.M. Debatin, *Apoptosis signaling in tumor therapy.* Ann N Y Acad Sci, 2004. **1028**: p. 150-6.

39. Pasparakis, M. and P. Vandenabeele, *Necroptosis and its role in inflammation.* Nature, 2015. **517**(7534): p. 311-20.

40. Bertheloot, D., E. Latz, and B.S. Franklin, *Necroptosis, pyroptosis and apoptosis: an intricate game of cell death.* Cell Mol Immunol, 2021. **18**(5): p. 1106-1121.

41. Mompean, M., et al., *The Structure of the Necrosome RIPK1-RIPK3 Core, a Human Hetero-Amyloid Signaling Complex.* Cell, 2018. **173**(5): p. 1244-1253 e10.

42. Li, J., et al., *The RIP1/RIP3 necrosome forms a functional amyloid signaling complex required for programmed necrosis.* Cell, 2012. **150**(2): p. 339-50.

43. Cho, Y.S., et al., *Phosphorylation-driven assembly of the RIP1-RIP3 complex regulates programmed necrosis and virus-induced inflammation.* Cell, 2009. **137**(6): p. 1112-23.

44. Laster, S.M., J.G. Wood, and L.R. Gooding, *Tumor necrosis factor can induce both apoptic and necrotic forms of cell lysis.* J Immunol, 1988. **141**(8): p. 2629-34.

45. Holler, N., et al., *Fas triggers an alternative, caspase-8-independent cell death pathway using the kinase RIP as effector molecule.* Nat Immunol, 2000. **1**(6): p. 489-95.

46. Karl, I., et al., *TRAF2 inhibits TRAIL- and CD95L-induced apoptosis and necroptosis.* Cell Death Dis, 2014. **5**(10): p. e1444.

47. Jouan-Lanhouet, S., et al., *TRAIL induces necroptosis involving RIPK1/RIPK3-dependent PARP-1 activation.* Cell Death Differ, 2012. **19**(12): p. 2003-14.

48. Voigt, S., et al., *TRAIL-induced programmed necrosis as a novel approach to eliminate tumor cells.* BMC Cancer, 2014. **14**: p. 74.

49. Brault, M., et al., *Intracellular Nucleic Acid Sensing Triggers Necroptosis through Synergistic Type I IFN and TNF Signaling.* J Immunol, 2018. **200**(8): p. 2748-2756.

50. Schock, S.N., et al., *Induction of necroptotic cell death by viral activation of the RIG-I or STING pathway.* Cell Death Differ, 2017. **24**(4): p. 615-625.

51. Chen, D., et al., *PUMA amplifies necroptosis signaling by activating cytosolic DNA sensors.* Proc Natl Acad Sci U S A, 2018. **115**(15): p. 3930-3935.

52. He, S., et al., *Toll-like receptors activate programmed necrosis in macrophages through a receptor-interacting kinase-3-mediated pathway.* Proc Natl Acad Sci U S A, 2011. **108**(50): p. 20054-9.

53. Kaiser, W.J., et al., *Toll-like receptor 3-mediated necrosis via TRIF, RIP3, and MLKL.* J Biol Chem, 2013. **288**(43): p. 31268-79.

54. Lim, J., et al., *Autophagy regulates inflammatory programmed cell death via turnover of RHIM-domain proteins.* Elife, 2019. **8**.

55. Upton, J.W. and W.J. Kaiser, *DAI Another Way: Necroptotic Control of Viral Infection.* Cell Host Microbe, 2017. **21**(3): p. 290-293.

56. Upton, J.W., W.J. Kaiser, and E.S. Mocarski, *DAI/ZBP1/DLM-1 complexes with RIP3 to mediate virus-induced programmed necrosis that is targeted by murine cytomegalovirus vIRA.* Cell Host Microbe, 2012. **11**(3): p. 290-7.

57. He, S., et al., *Receptor interacting protein kinase-3 determines cellular necrotic response to TNF-alpha.* Cell, 2009. **137**(6): p. 1100-11.

58. Kaczmarek, A., P. Vandenabeele, and D.V. Krysko, *Necroptosis: the release of damage-associated molecular patterns and its physiological relevance.* Immunity, 2013. **38**(2): p. 209-23.

59. Zhu, K., et al., *Necroptosis promotes cell-autonomous activation of proinflammatory cytokine gene expression.* Cell Death Dis, 2018. **9**(5): p. 500.

60. Degterev, A., et al., *Chemical inhibitor of nonapoptotic cell death with therapeutic potential for ischemic brain injury.* Nat Chem Biol, 2005. **1**(2): p. 112-9.

61. Duprez, L., et al., *RIP kinase-dependent necrosis drives lethal systemic inflammatory response syndrome.* Immunity, 2011. **35**(6): p. 908-18.

62. Zelic, M., et al., *RIP kinase 1-dependent endothelial necroptosis underlies systemic inflammatory response syndrome.* J Clin Invest, 2018. **128**(5): p. 2064-2075.

63. Kondylis, V. and M. Pasparakis, *RIP Kinases in Liver Cell Death, Inflammation and Cancer.* Trends Mol Med, 2019. **25**(1): p. 47-63.

64. Pierdomenico, M., et al., *Necroptosis is active in children with inflammatory bowel disease and contributes to heighten intestinal inflammation.* Am J Gastroenterol, 2014. **109**(2): p. 279-87.

65. Ofengeim, D., et al., *Activation of necroptosis in multiple sclerosis.* Cell Rep, 2015. **10**(11): p. 1836-49.

66. He, L., et al., *Low expression of mixed lineage kinase domain-like protein is associated with poor prognosis in ovarian cancer patients.* Onco Targets Ther, 2013. **6**: p. 1539-43.

67. Ertao, Z., et al., *Prognostic value of mixed lineage kinase domain-like protein expression in the survival of patients with gastric caner.* Tumour Biol, 2016. **37**(10): p. 13679-13685.

68. Ruan, J., et al., *Mixed lineage kinase domain-like protein is a prognostic biomarker for cervical squamous cell cancer.* Int J Clin Exp Pathol, 2015. **8**(11): p. 15035-8.

69. Moriwaki, K., et al., *Differential roles of RIPK1 and RIPK3 in TNF-induced necroptosis and chemotherapeutic agent-induced cell death.* Cell Death Dis, 2015. **6**(2): p. e1636.

70. Nugues, A.L., et al., *RIP3 is downregulated in human myeloid leukemia cells and modulates apoptosis and caspase-mediated p65/RelA cleavage.* Cell Death Dis, 2014. **5**(8): p. e1384.

71. Krysko, O., et al., *Necroptotic cell death in anti-cancer therapy.* Immunol Rev, 2017. **280**(1): p. 207-219.

72. Gong, Y., et al., *The role of necroptosis in cancer biology and therapy.* Mol Cancer, 2019. **18**(1): p. 100.

73. Draber, P., et al., *LUBAC-Recruited CYLD and A20 Regulate Gene Activation and Cell Death by Exerting Opposing Effects on Linear Ubiquitin in Signaling Complexes.* Cell Rep, 2015. **13**(10): p. 2258-72.

74. Brummelkamp, T.R., et al., *Loss of the cylindromatosis tumour suppressor inhibits apoptosis by activating NF-kappaB.* Nature, 2003. **424**(6950): p. 797-801.

75. Kovalenko, A., et al., *The tumour suppressor CYLD negatively regulates NF-kappaB signalling by deubiquitination.* Nature, 2003. **424**(6950): p. 801-5.

76. Trompouki, E., et al., *CYLD is a deubiquitinating enzyme that negatively regulates NF-kappaB activation by TNFR family members.* Nature, 2003. **424**(6950): p. 793-6.

77. O'Donnell, M.A., et al., *Caspase 8 inhibits programmed necrosis by processing CYLD.* Nat Cell Biol, 2011. **13**(12): p. 1437-42.

78. Peltzer, N., M. Darding, and H. Walczak, *Holding RIPK1 on the Ubiquitin Leash in TNFR1 Signaling.* Trends Cell Biol, 2016. **26**(6): p. 445-461.

79. Petrie, E.J., P.E. Czabotar, and J.M. Murphy, *The Structural Basis of Necroptotic Cell Death Signaling.* Trends Biochem Sci, 2019. **44**(1): p. 53-63.

80. Hsu, H., et al., *TNF-dependent recruitment of the protein kinase RIP to the TNF receptor-1 signaling complex.* Immunity, 1996. **4**(4): p. 387-96.

81. Dannappel, M., et al., *RIPK1 maintains epithelial homeostasis by inhibiting apoptosis and necroptosis.* Nature, 2014. **513**(7516): p. 90-4.

82. Polykratis, A., et al., *Cutting edge: RIPK1 Kinase inactive mice are viable and protected from TNF-induced necroptosis in vivo.* J Immunol, 2014. **193**(4): p. 1539-1543.

83. Kaiser, W.J., et al., *RIP1 suppresses innate immune necrotic as well as apoptotic cell death during mammalian parturition.* Proc Natl Acad Sci U S A, 2014. **111**(21): p. 7753-8.

84. Berger, S.B., et al., *Cutting Edge: RIP1 kinase activity is dispensable for normal development but is a key regulator of inflammation in SHARPIN-deficient mice.* J Immunol, 2014. **192**(12): p. 5476-80.

85. Takahashi, N., et al., *RIPK1 ensures intestinal homeostasis by protecting the epithelium against apoptosis.* Nature, 2014. **513**(7516): p. 95-9.

86. Degterev, A., et al., *Identification of RIP1 kinase as a specific cellular target of necrostatins.* Nat Chem Biol, 2008. **4**(5): p. 313-21.

87. Zhang, Y., et al., *RIP1 autophosphorylation is promoted by mitochondrial ROS and is essential for RIP3 recruitment into necrosome.* Nat Commun, 2017. **8**: p. 14329.

88. Keusekotten, K., et al., *OTULIN antagonizes LUBAC signaling by specifically hydrolyzing Met1-linked polyubiquitin.* Cell, 2013. **153**(6): p. 1312-26.

89. de Almagro, M.C., et al., *Cellular IAP proteins and LUBAC differentially regulate necrosome-associated RIP1 ubiquitination.* Cell Death Dis, 2015. **6**: p. e1800.

90. Verhelst, K., et al., *A20 inhibits LUBAC-mediated NF-kappaB activation by binding linear polyubiquitin chains via its zinc finger 7.* EMBO J, 2012. **31**(19): p. 3845-55.

91. Tokunaga, F., et al., *Specific recognition of linear polyubiquitin by A20 zinc finger 7 is involved in NF-kappaB regulation.* EMBO J, 2012. **31**(19): p. 3856-70.

92. Dondelinger, Y., et al., *Serine 25 phosphorylation inhibits RIPK1 kinase-dependent cell death in models of infection and inflammation.* Nat Commun, 2019. **10**(1): p. 1729.

93. Duprez, L., et al., *Intermediate domain of receptor-interacting protein kinase 1 (RIPK1) determines switch between necroptosis and RIPK1 kinase-dependent apoptosis.* J Biol Chem, 2012. **287**(18): p. 14863-72.

94. Zhang, D., J. Lin, and J. Han, *Receptor-interacting protein (RIP) kinase family.* Cell Mol Immunol, 2010. **7**(4): p. 243-9.

95. Sun, X., et al., *Identification of a novel homotypic interaction motif required for the phosphorylation of receptor-interacting protein (RIP) by RIP3.* J Biol Chem, 2002. **277**(11): p. 9505-11.

96. Zhang, D.W., et al., *RIP3, an energy metabolism regulator that switches TNF-induced cell death from apoptosis to necrosis.* Science, 2009. **325**(5938): p. 332-6.

97. Wu, X.N., et al., *Distinct roles of RIP1-RIP3 hetero- and RIP3-RIP3 homo-interaction in mediating necroptosis.* Cell Death Differ, 2014. **21**(11): p. 1709-20.

98. Sun, L., et al., *Mixed lineage kinase domain-like protein mediates necrosis signaling downstream of RIP3 kinase.* Cell, 2012. **148**(1-2): p. 213-27.

99. Chen, W., et al., *Diverse sequence determinants control human and mouse receptor interacting protein 3 (RIP3) and mixed lineage kinase domain-like (MLKL) interaction in necroptotic signaling.* J Biol Chem, 2013. **288**(23): p. 16247-16261.

100. Xie, T., et al., *Structural insights into RIP3-mediated necroptotic signaling.* Cell Rep, 2013. **5**(1): p. 70-8.

101. Hildebrand, J.M., et al., *Activation of the pseudokinase MLKL unleashes the four-helix bundle domain to induce membrane localization and necroptotic cell death.* Proc Natl Acad Sci U S A, 2014. **111**(42): p. 15072-7.

102. Wang, H., et al., *Mixed lineage kinase domain-like protein MLKL causes necrotic membrane disruption upon phosphorylation by RIP3.* Mol Cell, 2014. **54**(1): p. 133-146.

103. Chen, X., et al., *Translocation of mixed lineage kinase domain-like protein to plasma membrane leads to necrotic cell death.* Cell Res, 2014. **24**(1): p. 105-21.

104. Tanzer, M.C., et al., *Evolutionary divergence of the necroptosis effector MLKL.* Cell Death Differ, 2016. **23**(7): p. 1185-97.

105. Dondelinger, Y., et al., *MLKL compromises plasma membrane integrity by binding to phosphatidylinositol phosphates.* Cell Rep, 2014. **7**(4): p. 971-81.

106. Petrie, E.J., J.M. Hildebrand, and J.M. Murphy, *Insane in the membrane: a structural perspective of MLKL function in necroptosis.* Immunol Cell Biol, 2017. **95**(2): p. 152-159.

107. Rodriguez, D.A., et al., *Characterization of RIPK3-mediated phosphorylation of the activation loop of MLKL during necroptosis.* Cell Death Differ, 2016. **23**(1): p. 76-88.

108. Grootjans, S., T. Vanden Berghe, and P. Vandenabeele, *Initiation and execution mechanisms of necroptosis: an overview.* Cell Death Differ, 2017. **24**(7): p. 1184-1195.

109. Murphy, J.M., et al., *The pseudokinase MLKL mediates necroptosis via a molecular switch mechanism.* Immunity, 2013. **39**(3): p. 443-53.

110. Petrie, E.J., et al., *Conformational switching of the pseudokinase domain promotes human MLKL tetramerization and cell death by necroptosis.* Nat Commun, 2018. **9**(1): p. 2422.

111. Rubbelke, M., et al., *Locking mixed-lineage kinase domain-like protein in its auto-inhibited state prevents necroptosis.* Proc Natl Acad Sci U S A, 2020. **117**(52): p. 33272-33281.

112. Davies, K.A., et al., *Distinct pseudokinase domain conformations underlie divergent activation mechanisms among vertebrate MLKL orthologues.* Nat Commun, 2020. **11**(1): p. 3060.

113. Quarato, G., et al., *Sequential Engagement of Distinct MLKL Phosphatidylinositol-Binding Sites Executes Necroptosis.* Mol Cell, 2016. **61**(4): p. 589-601.

114. Davies, K.A., et al., *The brace helices of MLKL mediate interdomain communication and oligomerisation to regulate cell death by necroptosis.* Cell Death Differ, 2018. **25**(9): p. 1567-1580.

115. Huang, D., et al., *The MLKL Channel in Necroptosis Is an Octamer Formed by Tetramers in a Dyadic Process.* Mol Cell Biol, 2017. **37**(5).

116. Liu, S., et al., *MLKL forms disulfide bond-dependent amyloid-like polymers to induce necroptosis.* Proc Natl Acad Sci U S A, 2017. **114**(36): p. E7450-E7459.

117. Samson, A.L., et al., *MLKL trafficking and accumulation at the plasma membrane control the kinetics and threshold for necroptosis.* Nat Commun, 2020. **11**(1): p. 3151.

118. Cai, Z., et al., *Plasma membrane translocation of trimerized MLKL protein is required for TNF-induced necroptosis.* Nat Cell Biol, 2014. **16**(1): p. 55-65.

119. Tanzer, M.C., et al., *Quantitative and Dynamic Catalogs of Proteins Released during Apoptotic and Necroptotic Cell Death.* Cell Rep, 2020. **30**(4): p. 1260-1270 e5.

120. Yatim, N., et al., *RIPK1 and NF-kappaB signaling in dying cells determines cross-priming of CD8(+) T cells.* Science, 2015. **350**(6258): p. 328-34.

121. Aaes, T.L., et al., *Vaccination with Necroptotic Cancer Cells Induces Efficient Anti-tumor Immunity.* Cell Rep, 2016. **15**(2): p. 274-87.

122. Murai, S., et al., *A FRET biosensor for necroptosis uncovers two different modes of the release of DAMPs.* Nat Commun, 2018. **9**(1): p. 4457.

123. Gong, Y.N., et al., *ESCRT-III Acts Downstream of MLKL to Regulate Necroptotic Cell Death and Its Consequences.* Cell, 2017. **169**(2): p. 286-300 e16.

124. Seo, J., et al., *Necroptosis molecular mechanisms: Recent findings regarding novel necroptosis regulators.* Exp Mol Med, 2021. **53**(6): p. 1007-1017.

125. Karlowitz, R. and S.J.L. van Wijk, *Surviving death: emerging concepts of RIPK3 and MLKL ubiquitination in the regulation of necroptosis.* FEBS J, 2021.

126. Samson, A.L., et al., *Location, location, location: A compartmentalized view of TNF-induced necroptotic signaling.* Sci Signal, 2021. **14**(668).

127. Kist, M., et al., *Impaired RIPK1 ubiquitination sensitizes mice to TNF toxicity and inflammatory cell death.* Cell Death Differ, 2021. **28**(3): p. 985-1000.

128. Seo, J., et al., *CHIP controls necroptosis through ubiquitylation- and lysosome-dependent degradation of RIPK3.* Nat Cell Biol, 2016. **18**(3): p. 291-302.

129. Seo, J., E.W. Lee, and J. Song, *New role of E3 ubiquitin ligase in the regulation of necroptosis.* BMB Rep, 2016. **49**(5): p. 247-8.

130. Feltham, R., et al., *Mind Bomb Regulates Cell Death during TNF Signaling by Suppressing RIPK1's Cytotoxic Potential.* Cell Rep, 2018. **23**(2): p. 470-484.

131. Li, X., et al., *Ubiquitination of RIPK1 regulates its activation mediated by TNFR1 and TLRs signaling in distinct manners.* Nat Commun, 2020. **11**(1): p. 6364.

132. Amin, P., et al., *Regulation of a distinct activated RIPK1 intermediate bridging complex I and complex II in TNFalpha-mediated apoptosis.* Proc Natl Acad Sci U S A, 2018. **115**(26): p. E5944-E5953.

133. de Almagro, M.C., et al., *Coordinated ubiquitination and phosphorylation of RIP1 regulates necroptotic cell death.* Cell Death Differ, 2017. **24**(1): p. 26-37.

134. Wang, H., et al., *PELI1 functions as a dual modulator of necroptosis and apoptosis by regulating ubiquitination of RIPK1 and mRNA levels of c-FLIP.* Proc Natl Acad Sci U S A, 2017. **114**(45): p. 11944-11949.

135. Jaco, I., et al., *MK2 Phosphorylates RIPK1 to Prevent TNF-Induced Cell Death.* Mol Cell, 2017. **66**(5): p. 698-710 e5.

136. Menon, M.B., et al., *p38(MAPK)/MK2-dependent phosphorylation controls cytotoxic RIPK1 signalling in inflammation and infection.* Nat Cell Biol, 2017. **19**(10): p. 1248-1259.

137. Dondelinger, Y., et al., *MK2 phosphorylation of RIPK1 regulates TNF-mediated cell death.* Nat Cell Biol, 2017. **19**(10): p. 1237-1247.

138. Dondelinger, Y., et al., *NF-kappaB-Independent Role of IKKalpha/IKKbeta in Preventing RIPK1 Kinase-Dependent Apoptotic and Necroptotic Cell Death during TNF Signaling.* Mol Cell, 2015. **60**(1): p. 63-76.

139. Geng, J., et al., *Regulation of RIPK1 activation by TAK1-mediated phosphorylation dictates apoptosis and necroptosis.* Nat Commun, 2017. **8**(1): p. 359.

140. Lafont, E., et al., *TBK1 and IKKepsilon prevent TNF-induced cell death by RIPK1 phosphorylation.* Nat Cell Biol, 2018. **20**(12): p. 1389-1399.

141. Xu, D., et al., *TBK1 Suppresses RIPK1-Driven Apoptosis and Inflammation during Development and in Aging.* Cell, 2018. **174**(6): p. 1477-1491 e19.

142. Choi, S.W., et al., *PELI1 Selectively Targets Kinase-Active RIP3 for Ubiquitylation-Dependent Proteasomal Degradation.* Mol Cell, 2018. **70**(5): p. 920-935 e7.

143. Lee, S.B., et al., *The AMPK-Parkin axis negatively regulates necroptosis and tumorigenesis by inhibiting the necrosome.* Nat Cell Biol, 2019. **21**(8): p. 940-951.

144. Mei, P., et al., *E3 ligase TRIM25 ubiquitinates RIP3 to inhibit TNF induced cell necrosis.* Cell Death Differ, 2021. **28**(10): p. 2888-2899.

145. Onizawa, M., et al., *The ubiquitin-modifying enzyme A20 restricts ubiquitination of the kinase RIPK3 and protects cells from necroptosis.* Nat Immunol, 2015. **16**(6): p. 618-27.

146. Roedig, J., et al., *USP22 controls necroptosis by regulating receptor-interacting protein kinase 3 ubiquitination.* EMBO Rep, 2021. **22**(2): p. e50163.

147. Lee, S.Y., et al., *Casein kinase-1gamma1 and 3 stimulate tumor necrosis factor-induced necroptosis through RIPK3.* Cell Death Dis, 2019. **10**(12): p. 923.

148. Hanna-Addams, S., et al., *CK1alpha, CK1delta, and CK1epsilon are necrosome components which phosphorylate serine 227 of human RIPK3 to activate necroptosis.* Proc Natl Acad Sci U S A, 2020. **117**(4): p. 1962-1970.

149. Chen, W., et al., *Ppm1b negatively regulates necroptosis through dephosphorylating Rip3.* Nat Cell Biol, 2015. **17**(4): p. 434-44.

150. Li, X., et al., *O-GlcNAc Transferase Suppresses Inflammation and Necroptosis by Targeting Receptor-Interacting Serine/Threonine-Protein Kinase 3.* Immunity, 2019. **50**(3): p. 576-590 e6.

151. Xie, Y., et al., *Inhibition of Aurora Kinase A Induces Necroptosis in Pancreatic Carcinoma.* Gastroenterology, 2017. **153**(5): p. 1429-1443 e5.

152. Seong, D., et al., *Identification of MYC as an antinecroptotic protein that stifles RIPK1-RIPK3 complex formation.* Proc Natl Acad Sci U S A, 2020. **117**(33): p. 19982-19993.

153. Li, D., et al., *A cytosolic heat shock protein 90 and cochaperone CDC37 complex is required for RIP3 activation during necroptosis.* Proc Natl Acad Sci U S A, 2015. **112**(16): p. 5017-22.

154. Petersen, S.L., et al., *TRAF2 is a biologically important necroptosis suppressor.* Cell Death Differ, 2015. **22**(11): p. 1846-57.

155. Shi, C.S. and J.H. Kehrl, *Bcl-2 regulates pyroptosis and necroptosis by targeting BH3-like domains in GSDMD and MLKL.* Cell Death Discov, 2019. **5**: p. 151.

156. Seo, J., et al., *Beclin 1 functions as a negative modulator of MLKL oligomerisation by integrating into the necrosome complex.* Cell Death Differ, 2020. **27**(11): p. 3065-3081.

157. Najafov, A., et al., *TAM Kinases Promote Necroptosis by Regulating Oligomerization of MLKL.* Mol Cell, 2019. **75**(3): p. 457-468 e4.

158. Zhao, X.M., et al., *Hsp90 modulates the stability of MLKL and is required for TNF-induced necroptosis.* Cell Death Dis, 2016. **7**(2): p. e2089.

159. Jacobsen, A.V., et al., *HSP90 activity is required for MLKL oligomerisation and membrane translocation and the induction of necroptotic cell death.* Cell Death Dis, 2016. **7**(1): p. e2051.

160. Johnston, A.N., et al., *Necroptosis-blocking compound NBC1 targets heat shock protein 70 to inhibit MLKL polymerization and necroptosis.* Proc Natl Acad Sci U S A, 2020. **117**(12): p. 6521-6530.

161. Garcia, L.R., et al., *Ubiquitylation of MLKL at lysine 219 positively regulates necroptosis-induced tissue injury and pathogen clearance.* Nat Commun, 2021. **12**(1): p. 3364.

162. Liu, Z., et al., *Oligomerization-driven MLKL ubiquitylation antagonizes necroptosis.* EMBO J, 2021. **40**(23): p. e103718.

163. Yoon, S., K. Bogdanov, and D. Wallach, *Site-specific ubiquitination of MLKL targets it to endosomes and targets Listeria and Yersinia to the lysosomes.* Cell Death Differ, 2022. **29**(2): p. 306-322.

164. Sai, K., et al., *Necroptosis mediators RIPK3 and MLKL suppress intracellular Listeria replication independently of host cell killing.* J Cell Biol, 2019. **218**(6): p. 1994-2005.

165. Yoon, S., et al., *MLKL, the Protein that Mediates Necroptosis, Also Regulates Endosomal Trafficking and Extracellular Vesicle Generation.* Immunity, 2017. **47**(1): p. 51-65 e7.

166. Fan, W., et al., *Flotillin-mediated endocytosis and ALIX-syntenin-1-mediated exocytosis protect the cell membrane from damage caused by necroptosis.* Sci Signal, 2019. **12**(583).

167. Frank, D., et al., *Activated MLKL attenuates autophagy following its translocation to intracellular membranes.* J Cell Sci, 2019. **132**(5).

168. Yoon, S., et al., *Necroptosis is preceded by nuclear translocation of the signaling proteins that induce it.* Cell Death Differ, 2016. **23**(2): p. 253-60.

169. Weber, K., et al., *Nuclear RIPK3 and MLKL contribute to cytosolic necrosome formation and necroptosis.* Commun Biol, 2018. **1**: p. 6.

170. Zargarian, S., et al., *Phosphatidylserine externalization, "necroptotic bodies" release, and phagocytosis during necroptosis.* PLoS Biol, 2017. **15**(6): p. e2002711.

171. Petrie, E.J., et al., *Identification of MLKL membrane translocation as a checkpoint in necroptotic cell death using Monobodies.* Proc Natl Acad Sci U S A, 2020. **117**(15): p. 8468-8475.

172. Gong, Y.N., et al., *Biological events and molecular signaling following MLKL activation during necroptosis.* Cell Cycle, 2017. **16**(19): p. 1748-1760.

173. Douanne, T., et al., *Pannexin-1 limits the production of proinflammatory cytokines during necroptosis.* EMBO Rep, 2019. **20**(10): p. e47840.

174. Chen, J., et al., *Interferon-gamma induces the cell surface exposure of phosphatidylserine by activating the protein MLKL in the absence of caspase-8 activity.* J Biol Chem, 2019. **294**(32): p. 11994-12006.

175. Bickel, P.E., et al., *Flotillin and epidermal surface antigen define a new family of caveolae-associated integral membrane proteins.* J Biol Chem, 1997. **272**(21): p. 13793-802.

176. Lang, D.M., et al., *Identification of reggie-1 and reggie-2 as plasmamembrane-associated proteins which cocluster with activated GPI-anchored cell adhesion molecules in non-caveolar micropatches in neurons.* J Neurobiol, 1998. **37**(4): p. 502-23.

177. Lingwood, D. and K. Simons, *Lipid rafts as a membrane-organizing principle.* Science, 2010. **327**(5961): p. 46-50.

178. Sezgin, E., et al., *The mystery of membrane organization: composition, regulation and roles of lipid rafts.* Nat Rev Mol Cell Biol, 2017. **18**(6): p. 361-374.

179. Morrow, I.C., et al., *Flotillin-1/reggie-2 traffics to surface raft domains via a novel golgi-independent pathway. Identification of a novel membrane targeting domain and a role for palmitoylation.* J Biol Chem, 2002. **277**(50): p. 48834-41.

180. Solis, G.P., et al., *Reggie/flotillin proteins are organized into stable tetramers in membrane microdomains.* Biochem J, 2007. **403**(2): p. 313-22.

181. Amaddii, M., et al., *Flotillin-1/reggie-2 protein plays dual role in activation of receptor-tyrosine kinase/mitogen-activated protein kinase signaling.* J Biol Chem, 2012. **287**(10): p. 7265-78.

182. Pust, S., et al., *Flotillins as regulators of ErbB2 levels in breast cancer.* Oncogene, 2013. **32**(29): p. 3443-51.

183. Langhorst, M.F., et al., *Linking membrane microdomains to the cytoskeleton: regulation of the lateral mobility of reggie-1/flotillin-2 by interaction with actin.* FEBS Lett, 2007. **581**(24): p. 4697-703.

184. Rossy, J., et al., *Flotillins interact with PSGL-1 in neutrophils and, upon stimulation, rapidly organize into membrane domains subsequently accumulating in the uropod.* PLoS One, 2009. **4**(4): p. e5403.

185. Affentranger, S., et al., *Dynamic reorganization of flotillins in chemokine-stimulated human T-lymphocytes.* BMC Cell Biol, 2011. **12**: p. 28.

186. Solis, G.P., et al., *Reggies/flotillins regulate E-cadherin-mediated cell contact formation by affecting EGFR trafficking.* Mol Biol Cell, 2012. **23**(10): p. 1812-25.

187. Guillaume, E., et al., *Flotillin microdomains stabilize cadherins at cell-cell junctions.* J Cell Sci, 2013. **126**(Pt 22): p. 5293-304.

188. Glebov, O.O., N.A. Bright, and B.J. Nichols, *Flotillin-1 defines a clathrin-independent endocytic pathway in mammalian cells.* Nat Cell Biol, 2006. **8**(1): p. 46-54.

189. Frick, M., et al., *Coassembly of flotillins induces formation of membrane microdomains, membrane curvature, and vesicle budding.* Curr Biol, 2007. **17**(13): p. 1151-6.

190. Meister, M. and R. Tikkanen, *Endocytic trafficking of membrane-bound cargo: a flotillin point of view.* Membranes (Basel), 2014. **4**(3): p. 356-71.

191. Komander, D. and M. Rape, *The ubiquitin code.* Annu Rev Biochem, 2012. **81**: p. 203-29.

192. Pickart, C.M., *Mechanisms underlying ubiquitination.* Annu Rev Biochem, 2001. **70**: p. 503-33.

193. Baker, R.T. and P.G. Board, *The human ubiquitin-52 amino acid fusion protein gene shares several structural features with mammalian ribosomal protein genes.* Nucleic Acids Res, 1991. **19**(5): p. 1035-40.

194. Redman, K.L. and M. Rechsteiner, *Identification of the long ubiquitin extension as ribosomal protein S27a.* Nature, 1989. **338**(6214): p. 438-40.

195. Schulman, B.A. and J.W. Harper, *Ubiquitin-like protein activation by E1 enzymes: the apex for downstream signalling pathways.* Nat Rev Mol Cell Biol, 2009. **10**(5): p. 319-31.

196. Ye, Y. and M. Rape, *Building ubiquitin chains: E2 enzymes at work.* Nat Rev Mol Cell Biol, 2009. **10**(11): p. 755-64.

197. Buetow, L. and D.T. Huang, *Structural insights into the catalysis and regulation of E3 ubiquitin ligases.* Nat Rev Mol Cell Biol, 2016. **17**(10): p. 626-42.

198. Vijay-Kumar, S., C.E. Bugg, and W.J. Cook, *Structure of ubiquitin refined at 1.8 A resolution.* J Mol Biol, 1987. **194**(3): p. 531-44.

199. Dikic, I., S. Wakatsuki, and K.J. Walters, *Ubiquitin-binding domains - from structures to functions.* Nat Rev Mol Cell Biol, 2009. **10**(10): p. 659-71.

200. Reyes-Turcu, F.E., et al., *The ubiquitin binding domain ZnF UBP recognizes the C-terminal diglycine motif of unanchored ubiquitin.* Cell, 2006. **124**(6): p. 1197-208.

201. Kamadurai, H.B., et al., *Insights into ubiquitin transfer cascades from a structure of a UbcH5B approximately ubiquitin-HECT(NEDD4L) complex.* Mol Cell, 2009. **36**(6): p. 1095-102.

202. Hu, M., et al., *Crystal structure of a UBP-family deubiquitinating enzyme in isolation and in complex with ubiquitin aldehyde.* Cell, 2002. **111**(7): p. 1041-54.

203. Sloper-Mould, K.E., et al., *Distinct functional surface regions on ubiquitin.* J Biol Chem, 2001. **276**(32): p. 30483-9.

204. Jin, L., et al., *Mechanism of ubiquitin-chain formation by the human anaphase-promoting complex.* Cell, 2008. **133**(4): p. 653-65.

205. Clague, M.J., C. Heride, and S. Urbe, *The demographics of the ubiquitin system.* Trends Cell Biol, 2015. **25**(7): p. 417-26.

206. Akutsu, M., I. Dikic, and A. Bremm, *Ubiquitin chain diversity at a glance.* J Cell Sci, 2016. **129**(5): p. 875-80.

207. Flotho, A. and F. Melchior, *Sumoylation: a regulatory protein modification in health and disease.* Annu Rev Biochem, 2013. **82**: p. 357-85.

208. Haas, A.L., et al., *Interferon induces a 15-kilodalton protein exhibiting marked homology to ubiquitin.* J Biol Chem, 1987. **262**(23): p. 11315-23.

209. Enchev, R.I., B.A. Schulman, and M. Peter, *Protein neddylation: beyond cullin-RING ligases.* Nat Rev Mol Cell Biol, 2015. **16**(1): p. 30-44.

210. Maghames, C.M., et al., *NEDDylation promotes nuclear protein aggregation and protects the Ubiquitin Proteasome System upon proteotoxic stress.* Nat Commun, 2018. **9**(1): p. 4376.

211. Guzzo, C.M., et al., *RNF4-dependent hybrid SUMO-ubiquitin chains are signals for RAP80 and thereby mediate the recruitment of BRCA1 to sites of DNA damage.* Sci Signal, 2012. **5**(253): p. ra88.

212. Ohtake, F., et al., *Ubiquitin acetylation inhibits polyubiquitin chain elongation.* EMBO Rep, 2015. **16**(2): p. 192-201.

213. Yan, F., et al., *Threonine ADP-Ribosylation of Ubiquitin by a Bacterial Effector Family Blocks Host Ubiquitination.* Mol Cell, 2020. **78**(4): p. 641-652 e9.

214. Yang, C.S., et al., *Ubiquitin Modification by the E3 Ligase/ADP-Ribosyltransferase Dtx3L/Parp9.* Mol Cell, 2017. **66**(4): p. 503-516 e5.

215. Qiu, J., et al., *Ubiquitination independent of E1 and E2 enzymes by bacterial effectors.* Nature, 2016. **533**(7601): p. 120-4.

216. Herhaus, L. and I. Dikic, *Expanding the ubiquitin code through post-translational modification.* EMBO Rep, 2015. **16**(9): p. 1071-83.

217. Swaney, D.L., et al., *Global analysis of phosphorylation and ubiquitylation cross-talk in protein degradation.* Nat Methods, 2013. **10**(7): p. 676-82.

218. Hornbeck, P.V., et al., *PhosphoSitePlus, 2014: mutations, PTMs and recalibrations.* Nucleic Acids Res, 2015. **43**(Database issue): p. D512-20.

219. Foot, N., T. Henshall, and S. Kumar, *Ubiquitination and the Regulation of Membrane Proteins.* Physiol Rev, 2017. **97**(1): p. 253-281.

220. Mevissen, T.E.T. and D. Komander, *Mechanisms of Deubiquitinase Specificity and Regulation.* Annu Rev Biochem, 2017. **86**: p. 159-192.

221. Husnjak, K. and I. Dikic, *Ubiquitin-binding proteins: decoders of ubiquitin-mediated cellular functions.* Annu Rev Biochem, 2012. **81**: p. 291-322.

222. Matsumoto, M.L., et al., *K11-linked polyubiquitination in cell cycle control revealed by a K11 linkage-specific antibody.* Mol Cell, 2010. **39**(3): p. 477-84.

223. Finley, D., *Recognition and processing of ubiquitin-protein conjugates by the proteasome.* Annu Rev Biochem, 2009. **78**: p. 477-513.

224. Chau, V., et al., *A multiubiquitin chain is confined to specific lysine in a targeted short-lived protein.* Science, 1989. **243**(4898): p. 1576-83.

225. Morris, J.R. and E. Solomon, *BRCA1 : BARD1 induces the formation of conjugated ubiquitin structures, dependent on K6 of ubiquitin, in cells during DNA replication and repair.* Hum Mol Genet, 2004. **13**(8): p. 807-17.

226. Nishikawa, H., et al., *Mass spectrometric and mutational analyses reveal Lys-6-linked polyubiquitin chains catalyzed by BRCA1-BARD1 ubiquitin ligase.* J Biol Chem, 2004. **279**(6): p. 3916-24.

227. Elia, A.E., et al., *Quantitative Proteomic Atlas of Ubiquitination and Acetylation in the DNA Damage Response.* Mol Cell, 2015. **59**(5): p. 867-81.

228. Gatti, M., et al., *RNF168 promotes noncanonical K27 ubiquitination to signal DNA damage.* Cell Rep, 2015. **10**(2): p. 226-38.

229. Wickliffe, K.E., et al., *K11-linked ubiquitin chains as novel regulators of cell division.* Trends Cell Biol, 2011. **21**(11): p. 656-63.

230. Fei, C., et al., *Smurf1-mediated Lys29-linked nonproteolytic polyubiquitination of axin negatively regulates Wnt/beta-catenin signaling.* Mol Cell Biol, 2013. **33**(20): p. 4095-105.

231. Al-Hakim, A.K., et al., *Control of AMPK-related kinases by USP9X and atypical Lys(29)/Lys(33)-linked polyubiquitin chains.* Biochem J, 2008. **411**(2): p. 249-60.

232. Huang, H., et al., *K33-linked polyubiquitination of T cell receptor-zeta regulates proteolysis-independent T cell signaling.* Immunity, 2010. **33**(1): p. 60-70.

233. Yuan, W.C., et al., *K33-Linked Polyubiquitination of Coronin 7 by Cul3-KLHL20 Ubiquitin E3 Ligase Regulates Protein Trafficking.* Mol Cell, 2014. **54**(4): p. 586-600.

234. Mukhopadhyay, D. and H. Riezman, *Proteasome-independent functions of ubiquitin in endocytosis and signaling.* Science, 2007. **315**(5809): p. 201-5.

235. Ikeda, F., et al., *SHARPIN forms a linear ubiquitin ligase complex regulating NF-kappaB activity and apoptosis.* Nature, 2011. **471**(7340): p. 637-41.

236. Boisson, B., et al., *Human HOIP and LUBAC deficiency underlies autoinflammation, immunodeficiency, amylopectinosis, and lymphangiectasia.* J Exp Med, 2015. **212**(6): p. 939-51.

237. Shimizu, Y., L. Taraborrelli, and H. Walczak, *Linear ubiquitination in immunity.* Immunol Rev, 2015. **266**(1): p. 190-207.

238. Chen, Z.J. and L.J. Sun, *Nonproteolytic functions of ubiquitin in cell signaling.* Mol Cell, 2009. **33**(3): p. 275-86.

239. Clague, M.J., S. Urbe, and D. Komander, *Breaking the chains: deubiquitylating enzyme specificity begets function.* Nat Rev Mol Cell Biol, 2019. **20**(6): p. 338-352.

240. Grou, C.P., et al., *The de novo synthesis of ubiquitin: identification of deubiquitinases acting on ubiquitin precursors.* Sci Rep, 2015. **5**: p. 12836.

241. Faesen, A.C., et al., *The differential modulation of USP activity by internal regulatory domains, interactors and eight ubiquitin chain types.* Chem Biol, 2011. **18**(12): p. 1550-61.

242. Sato, Y., et al., *Structures of CYLD USP with Met1- or Lys63-linked diubiquitin reveal mechanisms for dual specificity.* Nat Struct Mol Biol, 2015. **22**(3): p. 222-9.

243. Sato, Y., et al., *Structural basis for specific cleavage of Lys6-linked polyubiquitin chains by USP30.* Nat Struct Mol Biol, 2017. **24**(11): p. 911-919.

244. Gersch, M., et al., *Mechanism and regulation of the Lys6-selective deubiquitinase USP30.* Nat Struct Mol Biol, 2017. **24**(11): p. 920-930.

245. Cunningham, C.N., et al., *USP30 and parkin homeostatically regulate atypical ubiquitin chains on mitochondria.* Nat Cell Biol, 2015. **17**(2): p. 160-9.

246. Rivkin, E., et al., *The linear ubiquitin-specific deubiquitinase gumby regulates angiogenesis.* Nature, 2013. **498**(7454): p. 318-24.

247. Mevissen, T.E.T., et al., *Molecular basis of Lys11-polyubiquitin specificity in the deubiquitinase Cezanne.* Nature, 2016. **538**(7625): p. 402-405.

248. Bremm, A., S.M. Freund, and D. Komander, *Lys11-linked ubiquitin chains adopt compact conformations and are preferentially hydrolyzed by the deubiquitinase Cezanne.* Nat Struct Mol Biol, 2010. **17**(8): p. 939-47.

249. Cavadini, S., et al., *Cullin-RING ubiquitin E3 ligase regulation by the COP9 signalosome.* Nature, 2016. **531**(7596): p. 598-603.

250. Schulz, S., et al., *Ubiquitin-specific protease-like 1 (USPL1) is a SUMO isopeptidase with essential, non-catalytic functions.* EMBO Rep, 2012. **13**(10): p. 930-8.

251. Malakhov, M.P., et al., *UBP43 (USP18) specifically removes ISG15 from conjugated proteins.* J Biol Chem, 2002. **277**(12): p. 9976-81.

252. Kirisako, T., et al., *A ubiquitin ligase complex assembles linear polyubiquitin chains.* EMBO J, 2006. **25**(20): p. 4877-87.

253. Tokunaga, F., et al., *SHARPIN is a component of the NF-kappaB-activating linear ubiquitin chain assembly complex.* Nature, 2011. **471**(7340): p. 633-6.

254. Yamanaka, K., et al., *Identification of the ubiquitin-protein ligase that recognizes oxidized IRP2.* Nat Cell Biol, 2003. **5**(4): p. 336-40.

255. Fujita, H., et al., *Cooperative Domain Formation by Homologous Motifs in HOIL-1L and SHARPIN Plays A Crucial Role in LUBAC Stabilization.* Cell Rep, 2018. **23**(4): p. 1192-1204.

256. Schaeffer, V., et al., *Binding of OTULIN to the PUB domain of HOIP controls NF-kappaB signaling.* Mol Cell, 2014. **54**(3): p. 349-61.

257. Elliott, P.R., et al., *Molecular basis and regulation of OTULIN-LUBAC interaction.* Mol Cell, 2014. **54**(3): p. 335-48.

258. Elliott, P.R., et al., *SPATA2 Links CYLD to LUBAC, Activates CYLD, and Controls LUBAC Signaling.* Mol Cell, 2016. **63**(6): p. 990-1005.

259. Kupka, S., et al., *SPATA2-Mediated Binding of CYLD to HOIP Enables CYLD Recruitment to Signaling Complexes.* Cell Rep, 2016. **16**(9): p. 2271-80.

260. Schlicher, L., et al., *SPATA2 promotes CYLD activity and regulates TNF-induced NF-kappaB signaling and cell death.* EMBO Rep, 2016. **17**(10): p. 1485-1497.

261. Wagner, S.A., et al., *SPATA2 links CYLD to the TNF-alpha receptor signaling complex and modulates the receptor signaling outcomes.* EMBO J, 2016. **35**(17): p. 1868-84.

262. van Well, E.M., et al., *A protein quality control pathway regulated by linear ubiquitination.* EMBO J, 2019. **38**(9).

263. Fujita, H., et al., *Mechanism underlying IkappaB kinase activation mediated by the linear ubiquitin chain assembly complex.* Mol Cell Biol, 2014. **34**(7): p. 1322-35.

264. Sato, Y., et al., *Specific recognition of linear ubiquitin chains by the Npl4 zinc finger (NZF) domain of the HOIL-1L subunit of the linear ubiquitin chain assembly complex.* Proc Natl Acad Sci U S A, 2011. **108**(51): p. 20520-5.

265. Shimizu, S., et al., *Differential Involvement of the Npl4 Zinc Finger Domains of SHARPIN and HOIL-1L in Linear Ubiquitin Chain Assembly Complex-Mediated Cell Death Protection.* Mol Cell Biol, 2016. **36**(10): p. 1569-83.

266. Stieglitz, B., et al., *LUBAC synthesizes linear ubiquitin chains via a thioester intermediate.* EMBO Rep, 2012. **13**(9): p. 840-6.

267. Stieglitz, B., et al., *Structural basis for ligase-specific conjugation of linear ubiquitin chains by HOIP.* Nature, 2013. **503**(7476): p. 422-426.

268. Smit, J.J., et al., *The E3 ligase HOIP specifies linear ubiquitin chain assembly through its RING-IBR-RING domain and the unique LDD extension.* EMBO J, 2012. **31**(19): p. 3833-44.

269. Lechtenberg, B.C., et al., *Structure of a HOIP/E2~ubiquitin complex reveals RBR E3 ligase mechanism and regulation.* Nature, 2016. **529**(7587): p. 546-50.

270. Tokunaga, F., et al., *Involvement of linear polyubiquitylation of NEMO in NF-kappaB activation.* Nat Cell Biol, 2009. **11**(2): p. 123-32.

271. Smit, J.J., et al., *Target specificity of the E3 ligase LUBAC for ubiquitin and NEMO relies on different minimal requirements.* J Biol Chem, 2013. **288**(44): p. 31728-37.

272. Hrdinka, M. and M. Gyrd-Hansen, *The Met1-Linked Ubiquitin Machinery: Emerging Themes of (De)regulation.* Mol Cell, 2017. **68**(2): p. 265-280.

273. Boisson, B., et al., *Immunodeficiency, autoinflammation and amylopectinosis in humans with inherited HOIL-1 and LUBAC deficiency.* Nat Immunol, 2012. **13**(12): p. 1178-86.

274. Peltzer, N., et al., *HOIP deficiency causes embryonic lethality by aberrant TNFR1-mediated endothelial cell death.* Cell Rep, 2014. **9**(1): p. 153-165.

275. Lee, I.Y., et al., *MST1 Negatively Regulates TNFalpha-Induced NF-kappaB Signaling through Modulating LUBAC Activity.* Mol Cell, 2019. **73**(6): p. 1138-1149 e6.

276. Meschede, J., et al., *The parkin-coregulated gene product PACRG promotes TNF signaling by stabilizing LUBAC.* Sci Signal, 2020. **13**(617).

277. Heger, K., et al., *OTULIN limits cell death and inflammation by deubiquitinating LUBAC.* Nature, 2018. **559**(7712): p. 120-124.

278. Goto, E. and F. Tokunaga, *Decreased linear ubiquitination of NEMO and FADD on apoptosis with caspase-mediated cleavage of HOIP.* Biochem Biophys Res Commun, 2017. **485**(1): p. 152-159.

279. Joo, D., et al., *Regulation of Linear Ubiquitin Chain Assembly Complex by Caspase-Mediated Cleavage of RNF31.* Mol Cell Biol, 2016. **36**(24): p. 3010-3018.

280. Strickson, S., et al., *The anti-inflammatory drug BAY 11-7082 suppresses the MyD88-dependent signalling network by targeting the ubiquitin system.* Biochem J, 2013. **451**(3): p. 427-37.

281. De Cesare, V., et al., *The MALDI-TOF E2/E3 Ligase Assay as Universal Tool for Drug Discovery in the Ubiquitin Pathway.* Cell Chem Biol, 2018. **25**(9): p. 1117-1127 e4.

282. Sakamoto, H., et al., *Gliotoxin suppresses NF-kappaB activation by selectively inhibiting linear ubiquitin chain assembly complex (LUBAC).* ACS Chem Biol, 2015. **10**(3): p. 675-81.

283. Johansson, H., et al., *Fragment-Based Covalent Ligand Screening Enables Rapid Discovery of Inhibitors for the RBR E3 Ubiquitin Ligase HOIP.* J Am Chem Soc, 2019. **141**(6): p. 2703-2712.

284. Tsai, Y.I., et al., *Single-Domain Antibodies as Crystallization Chaperones to Enable Structure-Based Inhibitor Development for RBR E3 Ubiquitin Ligases.* Cell Chem Biol, 2020. **27**(1): p. 83-93 e9.

285. Katsuya, K., et al., *Small-molecule inhibitors of linear ubiquitin chain assembly complex (LUBAC), HOIPINs, suppress NF-kappaB signaling.* Biochem Biophys Res Commun, 2019. **509**(3): p. 700-706.

286. Oikawa, D., et al., *Molecular bases for HOIPINs-mediated inhibition of LUBAC and innate immune responses.* Commun Biol, 2020. **3**(1): p. 163.

287. Fiil, B.K. and M. Gyrd-Hansen, *The Met1-linked ubiquitin machinery in inflammation and infection.* Cell Death Differ, 2021. **28**(2): p. 557-569.

288. Oikawa, D., et al., *Linear Ubiquitin Code: Its Writer, Erasers, Decoders, Inhibitors, and Implications in Disorders.* Int J Mol Sci, 2020. **21**(9).

289. Komander, D., et al., *Molecular discrimination of structurally equivalent Lys 63-linked and linear polyubiquitin chains.* EMBO Rep, 2009. **10**(5): p. 466-73.

290. Damgaard, R.B., et al., *OTULIN deficiency in ORAS causes cell type-specific LUBAC degradation, dysregulated TNF signalling and cell death.* EMBO Mol Med, 2019. **11**(3).

291. Douglas, T. and M. Saleh, *Post-translational Modification of OTULIN Regulates Ubiquitin Dynamics and Cell Death.* Cell Rep, 2019. **29**(11): p. 3652-3663 e5.

292. Fiil, B.K., et al., *OTULIN restricts Met1-linked ubiquitination to control innate immune signaling.* Mol Cell, 2013. **50**(6): p. 818-830.

293. Hrdinka, M., et al., *CYLD Limits Lys63- and Met1-Linked Ubiquitin at Receptor Complexes to Regulate Innate Immune Signaling.* Cell Rep, 2016. **14**(12): p. 2846-58.

294. Damgaard, R.B., et al., *OTULIN protects the liver against cell death, inflammation, fibrosis, and cancer.* Cell Death Differ, 2020. **27**(5): p. 1457-1474.

295. Damgaard, R.B., et al., *The Deubiquitinase OTULIN Is an Essential Negative Regulator of Inflammation and Autoimmunity.* Cell, 2016. **166**(5): p. 1215-1230 e20.

296. Zhou, Q., et al., *Biallelic hypomorphic mutations in a linear deubiquitinase define otulipenia, an early-onset autoinflammatory disease.* Proc Natl Acad Sci U S A, 2016. **113**(36): p. 10127-32.

297. Takiuchi, T., et al., *Suppression of LUBAC-mediated linear ubiquitination by a specific interaction between LUBAC and the deubiquitinases CYLD and OTULIN.* Genes Cells, 2014. **19**(3): p. 254-72.

298. van Wijk, S.J.L., et al., *Linear ubiquitination of cytosolic Salmonella Typhimurium activates NF-kappaB and restricts bacterial proliferation.* Nat Microbiol, 2017. **2**: p. 17066.

299. Weinelt, N. and S.J.L. van Wijk, *Ubiquitin-dependent and -independent functions of OTULIN in cell fate control and beyond.* Cell Death Differ, 2021. **28**(2): p. 493-504.

300. Verboom, L., et al., *OTULIN Prevents Liver Inflammation and Hepatocellular Carcinoma by Inhibiting FADD- and RIPK1 Kinase-Mediated Hepatocyte Apoptosis.* Cell Rep, 2020. **30**(7): p. 2237-2247 e6.

301. Nabavi, M., et al., *Auto-inflammation in a Patient with a Novel Homozygous OTULIN Mutation.* J Clin Immunol, 2019. **39**(2): p. 138-141.

302. Zinngrebe, J., et al., *Compound heterozygous variants in OTULIN are associated with fulminant atypical late-onset ORAS.* EMBO Mol Med, 2022. **14**(3): p. e14901.

303. Chu, Y., et al., *LUBAC and OTULIN regulate autophagy initiation and maturation by mediating the linear ubiquitination and the stabilization of ATG13.* Autophagy, 2020: p. 1-16.

304. Wang, W., et al., *ABL1-dependent OTULIN phosphorylation promotes genotoxic Wnt/beta-catenin activation to enhance drug resistance in breast cancers.* Nat Commun, 2020. **11**(1): p. 3965.

305. Zuo, Y., et al., *Regulation of the linear ubiquitination of STAT1 controls antiviral interferon signaling.* Nat Commun, 2020. **11**(1): p. 1146.

306. Stangl, A., et al., *Regulation of the endosomal SNX27-retromer by OTULIN.* Nat Commun, 2019. **10**(1): p. 4320.

307. Griewahn, L., et al., *SPATA2 restricts OTULIN-dependent LUBAC activity independently of CYLD.* Cell Rep, 2023. **42**(1): p. 111961.

308. Kupka, S., et al., *Formation and removal of poly-ubiquitin chains in the regulation of tumor necrosis factor-induced gene activation and cell death.* FEBS J, 2016. **283**(14): p. 2626-39.

309. Dondelinger, Y., et al., *Poly-ubiquitination in TNFR1-mediated necroptosis.* Cell Mol Life Sci, 2016. **73**(11-12): p. 2165-76.

310. Wright, A., et al., *Regulation of early wave of germ cell apoptosis and spermatogenesis by deubiquitinating enzyme CYLD.* Dev Cell, 2007. **13**(5): p. 705-716.

311. Wagner, S., et al., *Ubiquitin binding mediates the NF-kappaB inhibitory potential of ABIN proteins.* Oncogene, 2008. **27**(26): p. 3739-45.

312. Verstrepen, L., I. Carpentier, and R. Beyaert, *The biology of A20-binding inhibitors of NF-kappaB activation (ABINs).* Adv Exp Med Biol, 2014. **809**: p. 13-31.

313. Zhu, G., et al., *Optineurin negatively regulates TNFalpha- induced NF-kappaB activation by competing with NEMO for ubiquitinated RIP.* Curr Biol, 2007. **17**(16): p. 1438-43.

314. Qiu, Y., et al., *Emerging views of OPTN (optineurin) function in the autophagic process associated with disease.* Autophagy, 2022. **18**(1): p. 73-85.

315. Ryan, T.A. and D.A. Tumbarello, *Optineurin: A Coordinator of Membrane-Associated Cargo Trafficking and Autophagy.* Front Immunol, 2018. **9**: p. 1024.

316. Outlioua, A., M. Pourcelot, and D. Arnoult, *The Role of Optineurin in Antiviral Type I Interferon Production.* Front Immunol, 2018. **9**: p. 853.

317. Damgaard, R.B., et al., *The ubiquitin ligase XIAP recruits LUBAC for NOD2 signaling in inflammation and innate immunity.* Mol Cell, 2012. **46**(6): p. 746-58.

318. Ea, C.K., et al., *Activation of IKK by TNFalpha requires site-specific ubiquitination of RIP1 and polyubiquitin binding by NEMO.* Mol Cell, 2006. **22**(2): p. 245-57.

319. Bertrand, M.J., et al., *Cellular inhibitors of apoptosis cIAP1 and cIAP2 are required for innate immunity signaling by the pattern recognition receptors NOD1 and NOD2.* Immunity, 2009. **30**(6): p. 789-801.

320. Tarantino, N., et al., *TNF and IL-1 exhibit distinct ubiquitin requirements for inducing NEMO-IKK supramolecular structures.* J Cell Biol, 2014. **204**(2): p. 231-45.

321. Kelsall, I.R., et al., *The E3 ligase HOIL-1 catalyses ester bond formation between ubiquitin and components of the Myddosome in mammalian cells.* Proc Natl Acad Sci U S A, 2019. **116**(27): p. 13293-13298.

322. Zak, D.E., et al., *Systems analysis identifies an essential role for SHANK-associated RH domain-interacting protein (SHARPIN) in macrophage Toll-like receptor 2 (TLR2) responses.* Proc Natl Acad Sci U S A, 2011. **108**(28): p. 11536-41.

323. Sasaki, Y., et al., *Defective immune responses in mice lacking LUBAC-mediated linear ubiquitination in B cells.* EMBO J, 2013. **32**(18): p. 2463-76.

324. Teh, C.E., et al., *Linear ubiquitin chain assembly complex coordinates late thymic T-cell differentiation and regulatory T-cell homeostasis.* Nat Commun, 2016. **7**: p. 13353.

325. Oda, H., et al., *Human LUBAC deficiency leads to autoinflammation and immunodeficiency by dysregulation in TNF-mediated cell death.* medRxiv, 2022: p. 2022.11.09.22281431.

326. Seymour, R.E., et al., *Spontaneous mutations in the mouse Sharpin gene result in multiorgan inflammation, immune system dysregulation and dermatitis.* Genes Immun, 2007. **8**(5): p. 416-21.

327. Rickard, J.A., et al., *TNFR1-dependent cell death drives inflammation in Sharpin-deficient mice.* Elife, 2014. **3**.

328. Kumari, S., et al., *Sharpin prevents skin inflammation by inhibiting TNFR1-induced keratinocyte apoptosis.* Elife, 2014. **3**.

329. Shimizu, Y., et al., *The Linear ubiquitin chain assembly complex acts as a liver tumor suppressor and inhibits hepatocyte apoptosis and hepatitis.* Hepatology, 2017. **65**(6): p. 1963-1978.

330. Taraborrelli, L., et al., *LUBAC prevents lethal dermatitis by inhibiting cell death induced by TNF, TRAIL and CD95L.* Nat Commun, 2018. **9**(1): p. 3910.

331. Peltzer, N., et al., *LUBAC is essential for embryogenesis by preventing cell death and enabling haematopoiesis.* Nature, 2018. **557**(7703): p. 112-117.

332. Zheng, D., T. Liwinski, and E. Elinav, *Inflammasome activation and regulation: toward a better understanding of complex mechanisms.* Cell Discov, 2020. **6**: p. 36.

333. Rodgers, M.A., et al., *The linear ubiquitin assembly complex (LUBAC) is essential for NLRP3 inflammasome activation.* J Exp Med, 2014. **211**(7): p. 1333-47.

334. Douglas, T. and M. Saleh, *Cross-regulation between LUBAC and caspase-1 modulates cell death and inflammation.* J Biol Chem, 2020. **295**(16): p. 5216-5228.

335. Noad, J., et al., *LUBAC-synthesized linear ubiquitin chains restrict cytosol-invading bacteria by activating autophagy and NF-kappaB.* Nat Microbiol, 2017. **2**: p. 17063.

336. Belgnaoui, S.M., et al., *Linear ubiquitination of NEMO negatively regulates the interferon antiviral response through disruption of the MAVS-TRAF3 complex.* Cell Host Microbe, 2012. **12**(2): p. 211-22.

337. Inn, K.S., et al., *Linear ubiquitin assembly complex negatively regulates RIG-I- and TRIM25-mediated type I interferon induction.* Mol Cell, 2011. **41**(3): p. 354-65.

338. HogenEsch, H., et al., *A spontaneous mutation characterized by chronic proliferative dermatitis in C57BL mice.* Am J Pathol, 1993. **143**(3): p. 972-82.

339. Liang, Y. and J.P. Sundberg, *SHARPIN regulates mitochondria-dependent apoptosis in keratinocytes.* J Dermatol Sci, 2011. **63**(3): p. 148-53.

340. Potter, C.S., et al., *Chronic proliferative dermatitis in Sharpin null mice: development of an autoinflammatory disease in the absence of B and T lymphocytes and IL4/IL13 signaling.* PLoS One, 2014. **9**(1): p. e85666.

341. HogenEsch, H., et al., *Increased expression of type 2 cytokines in chronic proliferative dermatitis (cpdm) mutant mice and resolution of inflammation following treatment with IL-12.* Eur J Immunol, 2001. **31**(3): p. 734-42.

342. HogenEsch, H., et al., *Absence of Peyer's patches and abnormal lymphoid architecture in chronic proliferative dermatitis (cpdm/cpdm) mice.* J Immunol, 1999. **162**(7): p. 3890-6.

343. Gijbels, M.J., et al., *Ultrastructure of epidermis of mice with chronic proliferative dermatitis.* Ultrastruct Pathol, 1995. **19**(2): p. 107-11.

344. Gijbels, M.J., et al., *Pathogenesis of skin lesions in mice with chronic proliferative dermatitis (cpdm/cpdm).* Am J Pathol, 1996. **148**(3): p. 941-50.

345. Nilsson, J., et al., *Polyglucosan body myopathy caused by defective ubiquitin ligase RBCK1.* Ann Neurol, 2013. **74**(6): p. 914-9.

346. Wang, K., et al., *Whole-genome DNA/RNA sequencing identifies truncating mutations in RBCK1 in a novel Mendelian disease with neuromuscular and cardiac involvement.* Genome Med, 2013. **5**(7): p. 67.

347. Oda, H., et al., *Second Case of HOIP Deficiency Expands Clinical Features and Defines Inflammatory Transcriptome Regulated by LUBAC.* Front Immunol, 2019. **10**: p. 479.

348. Knittel, G., et al., *Rewired NFkappaB signaling as a potentially actionable feature of activated B-cell-like diffuse large B-cell lymphoma.* Eur J Haematol, 2016. **97**(6): p. 499-510.

349. Yang, Y., et al., *Essential role of the linear ubiquitin chain assembly complex in lymphoma revealed by rare germline polymorphisms.* Cancer Discov, 2014. **4**(4): p. 480-93.

350. Dubois, S.M., et al., *A catalytic-independent role for the LUBAC in NF-kappaB activation upon antigen receptor engagement and in lymphoma cells.* Blood, 2014. **123**(14): p. 2199-203.

351. Yang, Y., et al., *Targeting Non-proteolytic Protein Ubiquitination for the Treatment of Diffuse Large B Cell Lymphoma.* Cancer Cell, 2016. **29**(4): p. 494-507.

352. Nakayama, Y., et al., *Linear Polyubiquitin Chain Modification of TDP-43-Positive Neuronal Cytoplasmic Inclusions in Amyotrophic Lateral Sclerosis.* J Neuropathol Exp Neurol, 2020. **79**(3): p. 256-265.

353. Weinlich, R., et al., *Necroptosis in development, inflammation and disease.* Nat Rev Mol Cell Biol, 2017. **18**(2): p. 127-136.

354. Sanjana, N.E., O. Shalem, and F. Zhang, *Improved vectors and genome-wide libraries for CRISPR screening.* Nat Methods, 2014. **11**(8): p. 783-784.

355. Doench, J.G., et al., *Optimized sgRNA design to maximize activity and minimize off-target effects of CRISPR-Cas9.* Nat Biotechnol, 2016. **34**(2): p. 184-191.

356. Schneider, C.A., W.S. Rasband, and K.W. Eliceiri, *NIH Image to ImageJ: 25 years of image analysis.* Nat Methods, 2012. **9**(7): p. 671-5.

357. Martin, M., *Cutadapt removes adapter sequences from high-throughput sequencing reads.* 2011, 2011. **17**(1): p. 3.

358. Dobin, A., et al., *STAR: ultrafast universal RNA-seq aligner.* Bioinformatics, 2013. **29**(1): p. 15-21.

359. Love, M.I., W. Huber, and S. Anders, *Moderated estimation of fold change and dispersion for RNA-seq data with DESeq2.* Genome Biol, 2014. **15**(12): p. 550.

360. Ramirez, F., et al., *deepTools2: a next generation web server for deep-sequencing data analysis.* Nucleic Acids Res, 2016. **44**(W1): p. W160-5.

361. Almeida, J.L., C.R. Hill, and K.D. Cole, *Mouse cell line authentication.* Cytotechnology, 2014. **66**(1): p. 133-47.

362. Broutier, L., et al., *Culture and establishment of self-renewing human and mouse adult liver and pancreas 3D organoids and their genetic manipulation.* Nat Protoc, 2016. **11**(9): p. 1724-43.

363. van Wijk, S.J., E. Fiskin, and I. Dikic, *Selective monitoring of ubiquitin signals with genetically encoded ubiquitin chain-specific sensors.* Nat Protoc, 2013. **8**(7): p. 1449-58.

364. Muller, S., et al., *APADB: a database for alternative polyadenylation and microRNA regulation events.* Database (Oxford), 2014. **2014**.

365. Weinelt, N., et al., *Species-specific LUBAC-mediated M1 ubiquitination regulates necroptosis by segregating the cellular distribution and fate of activated MLKL.* bioRxiv, 2022: p. 2022.12.08.519265.

366. Lork, M., K. Verhelst, and R. Beyaert, *CYLD, A20 and OTULIN deubiquitinases in NF-kappaB signaling and cell death: so similar, yet so different.* Cell Death Differ, 2017. **24**(7): p. 1172-1183.

367. Moquin, D.M., T. McQuade, and F.K. Chan, *CYLD deubiquitinates RIP1 in the TNFalpha-induced necrosome to facilitate kinase activation and programmed necrosis.* PLoS One, 2013. **8**(10): p. e76841.

368. Katsuya, K., et al., *High-Throughput Screening for Linear Ubiquitin Chain Assembly Complex (LUBAC) Selective Inhibitors Using Homogenous Time-Resolved Fluorescence (HTRF)-Based Assay System.* SLAS Discov, 2018. **23**(10): p. 1018-1029.

369. Eiraku, M. and Y. Sasai, *Self-formation of layered neural structures in three-dimensional culture of ES cells.* Curr Opin Neurobiol, 2012. **22**(5): p. 768-77.

370. Lancaster, M.A. and J.A. Knoblich, *Organogenesis in a dish: modeling development and disease using organoid technologies.* Science, 2014. **345**(6194): p. 1247125.

371. Fatehullah, A., S.H. Tan, and N. Barker, *Organoids as an in vitro model of human development and disease.* Nat Cell Biol, 2016. **18**(3): p. 246-54.

372. Boj, S.F., et al., *Organoid models of human and mouse ductal pancreatic cancer.* Cell, 2015. **160**(1-2): p. 324-38.

373. Dossena, M., et al., *Standardized GMP-compliant scalable production of human pancreas organoids.* Stem Cell Res Ther, 2020. **11**(1): p. 94.

374. Georgakopoulos, N., et al., *Long-term expansion, genomic stability and in vivo safety of adult human pancreas organoids.* BMC Dev Biol, 2020. **20**(1): p. 4.

375. Jung, N., et al., *Non-invasive analysis of pancreas organoids in synthetic hydrogels defines material-cell interactions and luminal composition.* Biomater Sci, 2021. **9**(16): p. 5415-5426.

376. Vanlangenakker, N., et al., *TNF-induced necroptosis in L929 cells is tightly regulated by multiple TNFR1 complex I and II members.* Cell Death Dis, 2011. **2**: p. e230.

377. Vietri, M., M. Radulovic, and H. Stenmark, *The many functions of ESCRTs.* Nat Rev Mol Cell Biol, 2020. **21**(1): p. 25-42.

378. Steiner, A., et al., *An Update on Autoinflammatory Diseases: Relopathies.* Curr Rheumatol Rep, 2018. **20**(7): p. 39.

379. Asaoka, T., et al., *Linear ubiquitination by LUBEL has a role in Drosophila heat stress response.* EMBO Rep, 2016. **17**(11): p. 1624-1640.

380. Aalto, A.L., et al., *M1-linked ubiquitination by LUBEL is required for inflammatory responses to oral infection in Drosophila.* Cell Death Differ, 2019. **26**(5): p. 860-876.

381. Miyashita, H., et al., *Crosstalk Between NDP52 and LUBAC in Innate Immune Responses, Cell Death, and Xenophagy.* Front Immunol, 2021. **12**: p. 635475.

382. Dondelinger, Y., et al., *An evolutionary perspective on the necroptotic pathway.* Trends Cell Biol, 2016. **26**(10): p. 721-732.

383. Garnish, S.E., et al., *Conformational interconversion of MLKL and disengagement from RIPK3 precede cell death by necroptosis.* Nat Commun, 2021. **12**(1): p. 2211.

384. Meng, Y., et al., *Human RIPK3 maintains MLKL in an inactive conformation prior to cell death by necroptosis.* Nat Commun, 2021. **12**(1): p. 6783.

385. Meng, Y., et al., *Human RIPK3 C-lobe phosphorylation is essential for necroptotic signaling.* Cell Death Dis, 2022. **13**(6): p. 565.

386. Murphy, J.M., *The Killer Pseudokinase Mixed Lineage Kinase Domain-Like Protein (MLKL).* Cold Spring Harb Perspect Biol, 2020. **12**(8).

387. Tanzer, M.C., et al., *Necroptosis signalling is tuned by phosphorylation of MLKL residues outside the pseudokinase domain activation loop.* Biochem J, 2015. **471**(2): p. 255-65.

388. Petrie, E.J., et al., *Viral MLKL Homologs Subvert Necroptotic Cell Death by Sequestering Cellular RIPK3.* Cell Rep, 2019. **28**(13): p. 3309-3319 e5.

389. Mahdi, L.K., et al., *Discovery of a Family of Mixed Lineage Kinase Domain-like Proteins in Plants and Their Role in Innate Immune Signaling.* Cell Host Microbe, 2020. **28**(6): p. 813-824 e6.

390. Bigenzahn, J.W., et al., *An Inducible Retroviral Expression System for Tandem Affinity Purification Mass-Spectrometry-Based Proteomics Identifies Mixed Lineage Kinase Domain-like Protein (MLKL) as an Heat Shock Protein 90 (HSP90) Client.* Mol Cell Proteomics, 2016. **15**(3): p. 1139-50.

391. Dovey, C.M., et al., *MLKL Requires the Inositol Phosphate Code to Execute Necroptosis.* Mol Cell, 2018. **70**(5): p. 936-948 e7.

392. McNamara, D.E., et al., *Direct Activation of Human MLKL by a Select Repertoire of Inositol Phosphate Metabolites.* Cell Chem Biol, 2019. **26**(6): p. 863-877 e7.

393. Reynoso, E., et al., *Thioredoxin-1 actively maintains the pseudokinase MLKL in a reduced state to suppress disulfide bond-dependent MLKL polymer formation and necroptosis.* J Biol Chem, 2017. **292**(42): p. 17514-17524.

394. Corro, C., L. Novellasdemunt, and V.S.W. Li, *A brief history of organoids.* Am J Physiol Cell Physiol, 2020. **319**(1): p. C151-C165.

395. Choi, M.E., et al., *Necroptosis: a crucial pathogenic mediator of human disease.* JCI Insight, 2019. **4**(15).

396. Li, S., et al., *Necroptosis in inflammatory bowel disease and other intestinal diseases.* World J Clin Cases, 2018. **6**(14): p. 745-752.

397. Murakami, Y., et al., *Programmed necrosis, not apoptosis, is a key mediator of cell loss and DAMP-mediated inflammation in dsRNA-induced retinal degeneration.* Cell Death Differ, 2014. **21**(2): p. 270-7.

398. Welz, P.S., et al., *FADD prevents RIP3-mediated epithelial cell necrosis and chronic intestinal inflammation.* Nature, 2011. **477**(7364): p. 330-4.

399. Bonnet, M.C., et al., *The adaptor protein FADD protects epidermal keratinocytes from necroptosis in vivo and prevents skin inflammation.* Immunity, 2011. **35**(4): p. 572-82.

400. Weinlich, R., et al., *Protective roles for caspase-8 and cFLIP in adult homeostasis.* Cell Rep, 2013. **5**(2): p. 340-8.

401. Wallach, D., et al., *Programmed necrosis in inflammation: Toward identification of the effector molecules.* Science, 2016. **352**(6281): p. aaf2154.

402. Kwiatkowska, K., et al., *Flotillins: At the Intersection of Protein S-Palmitoylation and Lipid-Mediated Signaling.* Int J Mol Sci, 2020. **21**(7).

403. Meister, M., et al., *Regulation of cargo transfer between ESCRT-0 and ESCRT-I complexes by flotillin-1 during endosomal sorting of ubiquitinated cargo.* Oncogenesis, 2017. **6**(6): p. e344.

404. Solis, G.P., et al., *Reggies/flotillins interact with Rab11a and SNX4 at the tubulovesicular recycling compartment and function in transferrin receptor and E-cadherin trafficking.* Mol Biol Cell, 2013. **24**(17): p. 2689-702.

405. Redpath, G.M.I., et al., *Flotillins promote T cell receptor sorting through a fast Rab5-Rab11 endocytic recycling axis.* Nat Commun, 2019. **10**(1): p. 4392.

406. Bodrikov, V., et al., *Reggie-1 and reggie-2 (flotillins) participate in Rab11a-dependent cargo trafficking, spine synapse formation and LTP-related AMPA receptor (GluA1) surface exposure in mouse hippocampal neurons.* Exp Neurol, 2017. **289**: p. 31-45.

407. John, B.A., et al., *Flotillins bind to the dileucine sorting motif of beta-site amyloid precursor protein-cleaving enzyme 1 and influence its endosomal sorting.* FEBS J, 2014. **281**(8): p. 2074-87.

408. Fork, C., et al., *Flotillin-1 facilitates toll-like receptor 3 signaling in human endothelial cells.* Basic Res Cardiol, 2014. **109**(6): p. 439.

409. Jang, D., et al., *Essential role of flotillin-1 palmitoylation in the intracellular localization and signaling function of IGF-1 receptor.* J Cell Sci, 2015. **128**(11): p. 2179-90.

410. Ludwig, A., et al., *Flotillin microdomains interact with the cortical cytoskeleton to control uropod formation and neutrophil recruitment.* J Cell Biol, 2010. **191**(4): p. 771-81.

411. Haglund, K., et al., *Recruitment of Pyk2 and Cbl to lipid rafts mediates signals important for actin reorganization in growing neurites.* J Cell Sci, 2004. **117**(Pt 12): p. 2557-68.

412. Strauss, K., et al., *Exosome secretion ameliorates lysosomal storage of cholesterol in Niemann-Pick type C disease.* J Biol Chem, 2010. **285**(34): p. 26279-88.

413. Phuyal, S., et al., *Regulation of exosome release by glycosphingolipids and flotillins.* FEBS J, 2014. **281**(9): p. 2214-27.

414. Mizuno, E., et al., *STAM proteins bind ubiquitinated proteins on the early endosome via the VHS domain and ubiquitin-interacting motif.* Mol Biol Cell, 2003. **14**(9): p. 3675-89.

415. Lohi, O. and V.P. Lehto, *VHS domain marks a group of proteins involved in endocytosis and vesicular trafficking.* FEBS Lett, 1998. **440**(3): p. 255-7.

416. Hirano, S., et al., *Double-sided ubiquitin binding of Hrs-UIM in endosomal protein sorting.* Nat Struct Mol Biol, 2006. **13**(3): p. 272-7.

417. Bache, K.G., et al., *STAM and Hrs are subunits of a multivalent ubiquitin-binding complex on early endosomes.* J Biol Chem, 2003. **278**(14): p. 12513-21.

418. Pornillos, O., et al., *Structure and functional interactions of the Tsg101 UEV domain.* EMBO J, 2002. **21**(10): p. 2397-406.

419. Sundquist, W.I., et al., *Ubiquitin recognition by the human TSG101 protein.* Mol Cell, 2004. **13**(6): p. 783-9.

420. Teo, H., D.B. Veprintsev, and R.L. Williams, *Structural insights into endosomal sorting complex required for transport (ESCRT-I) recognition of ubiquitinated proteins.* J Biol Chem, 2004. **279**(27): p. 28689-96.

421. Najjar, M., et al., *RIPK1 and RIPK3 Kinases Promote Cell-Death-Independent Inflammation by Toll-like Receptor 4.* Immunity, 2016. **45**(1): p. 46-59.

422. Conos, S.A., et al., *Active MLKL triggers the NLRP3 inflammasome in a cell-intrinsic manner.* Proc Natl Acad Sci U S A, 2017. **114**(6): p. E961-E969.

423. Wang, X., et al., *RNA viruses promote activation of the NLRP3 inflammasome through a RIP1-RIP3-DRP1 signaling pathway.* Nat Immunol, 2014. **15**(12): p. 1126-33.

424. Moriwaki, K., et al., *A RIPK3-caspase 8 complex mediates atypical pro-IL-1beta processing.* J Immunol, 2015. **194**(4): p. 1938-44.

425. Lawlor, K.E., et al., *RIPK3 promotes cell death and NLRP3 inflammasome activation in the absence of MLKL.* Nat Commun, 2015. **6**: p. 6282.

426. Qi, L.S., et al., *Repurposing CRISPR as an RNA-guided platform for sequence-specific control of gene expression.* Cell, 2013. **152**(5): p. 1173-83.

Erklärung

Ich erkläre hiermit, dass ich die vorgelegte Dissertation mit dem Titel „Novel functions of LUBAC-mediated M1 poly-ubiquitination in TNFR1-mediated necroptosis“ selbständig angefertigt und mich anderer Hilfsmittel als der in ihr angegebenen nicht bedient habe, insbesondere, dass alle Entlehnungen aus anderen Schriften mit Angabe der betreffenden Schrift gekennzeichnet sind. Alle Beiträge von Kollegen und Kolleginnen werden in der Arbeit explizit erwähnt und sind im Folgenden nochmals aufgeführt:

Figure 33. Loss of LUBAC function blocks necroptosis-induced and MLKL-dependent cytokine production.
Sonja Smith (Technische Assistentin): Durchführung der qPCR Analyse für CXCL1 in Figure 33E; eigener Beitrag: Durchführung der Experimente, Analyse und Aufarbeitung der qPCR Daten.

Figure 34. Loss of LUBAC function blocks necroptosis-induced CXCL1 release.
Sonja Smith (Technische Assistentin): Durchführung des ELISAs; eigener Beitrag: Durchführung der Experimente, Analyse und Aufarbeitung der ELISA Daten.

Das unten aufgeführte Material wurde im Rahmen von Forschungskooperationen erstellt:

Figure 17. HOIPIN-8 prevents BV6/Emricasan-induced necroptotic cell death in primary hPOs.
Figure 18. HOIPIN-8 prevents Birinapant/Emricasan-induced necroptotic cell death in primary hPOs.
Figure 19. HOIPIN-8 prevents BV6/zVAD.fmk-induced necroptotic cell death in primary hPOs.

Kaja Nicole Wächtershäuser und Francesco Pampaloni (Physical Biology Group, Buchmann Institute for Molecular Life Sciences (BMLS), Goethe University Frankfurt, Germany): Kultivierung der hPOs, Durchführung der Experimente, Analyse und Visualisierung der Daten; eigener Beitrag: Aufarbeitung der Abbildung.

Figure 32. Necroptosis induces an inflammatory cytokine profile which can be blocked by inhibition of LUBAC function with HOIPIN-8.
Geoffroy Andrieux, Tonmoy Das und Melanie Börries (Institute of Medical Bioinformatics and Systems Medicine, Medical Center-University of Freiburg, Faculty of Medicine, University of Freiburg, Germany): Analyse und Visualisierung der MACE-Seq Daten; eigener Beitrag: Durchführung der Experimente, Aufarbeitung der Abbildung.

Die folgenden Teile der Dissertation sind bereits in Teilen veröffentlich worden:

Aus „Ubiquitin-dependent and -independent functions of OTULIN in cell fate control and beyond" [299]

Vereinzelte Textpassagen aus folgenden Kapiteln:

2.4.2.1 OTULIN

6.3 The role of OTULIN and CYLD in TNFR1-mediated signaling

Teile von folgenden Abbildungen:

Figure 4. LUBAC-mediated M1 poly-Ub regulates immune receptor signaling.

Aus „Species-specific LUBAC-mediated M1 ubiquitination regulates necroptosis by segregating the cellular distribution and fate of activated MLKL" (bioRxiv 2022.12.08.519265; doi: https://doi.org/10.1101/2022.12.08.519265) [365]

Vereinzelte Textpassagen aus folgenden Kapiteln:

1 Abstract

2.2.3.3 Regulation of necroptosis by compartmentalization of MLKL

3 Aim of the study

4.2.3 Maintenance of primary organoids

4.2.4 Induction and imaging of necroptotic cell death in primary hPOs

4.2.11 Massive Analysis of cDNA Ends (MACE-seq)

5.2.1 The effect of LUBAC deficiency on necroptotic cell death

5.2.2 Necroptosis induces an inflammatory cytokine profile that is dependent on LUBAC function

5.2.3 FLOT1/2 are putative targets of LUBAC-mediated M1 poly-Ub during necroptosis

6.1 HOIPIN-8-mediated LUBAC inhibition blocks necroptosis in human but not in murine cells

6.2 Modelling necroptosis in primary human pancreatic organoids

6.4 LUBAC-mediated M1 poly-Ub controls necroptosis-dependent pro-inflammatory cytokine production

6.5 FLOTs and their potential role in LUBAC and M1 Ub-dependent regulation of necroptosis

Teile von folgenden Abbildungen:

Figure 10 HOIPIN-8 inhibits LUBAC-induced M1 poly-Ub and TNFα-induced NF-kB activation in HT-29 cells.

Figure 11 LUBAC inhibition with HOIPIN-8 or gliotoxin blocks TBZ-induced necroptosis in HT-29 and THP-1 cells.

Figure 12 TBZ-induced necroptosis results in increased M1 poly-Ub levels which can be prevented by LUBAC inhibition with HOIPIN-8.

Figure 13 siRNA-mediated HOIP knockdown blocks TBZ-induced cell death and M1 poly-Ub levels in HT-29 cells.

Figure 14 Loss of LUBAC function does not reduce TBZ-induced phosphorylation of RIPK1, RIPK3 and MLKL.

Figure 15 Treatment with HOIPIN-8 does not influence TBZ-induced necrosome formation and MLKL oligomerization.

Figure 16 TBZ-induced increases in M1 poly-Ub during necroptosis are not dependent on RIPK3 and MLKL.

Figure 17 HOIPIN-8 prevents BV6/Emricasan-induced necroptotic cell death in primary hPOs.

Ich versichere, die Grundsätze der guten wissenschaftlichen Praxis beachtet, und nicht die Hilfe einer kommerziellen Promotionsvermittlung in Anspruch genommen zu haben.

Frankfurt am Main, den